Characterisation of Tools for Studying Renal Mineral Ion Homeostasis and Drug-Induced Nephrotoxicity

Rebecca Martina Wadey (0954796)

PhD Thesis 2014

DECLARATION

This work has not been submitted in substance for any other degree or award at this or any other university or place of learning, nor is it being submitted concurrently in candidature for any degree or other award.

STATEMENT 1

This thesis is being submitted in partial fulfilment of the requirements for the degree of PhD.

STATEMENT 2

This thesis is the result of my own independent work/investigation, except where otherwise stated. Other sources are acknowledged by explicit references. The views expressed are my own.

STATEMENT 3

I hereby give consent for my thesis, if accepted, to be available for photocopying and for inter-library-loan, and for the title and summary to be made available to outside organisations.

Signed: R. M. Wadley **(candidate)**

Date: **06.02.2015**

Summary

The complex interplay between regulatory factors of kidney mineral ion homeostasis are difficult to investigate *in vivo*. In addition, preclinical drug safety testing is limited by lack of translational tools for screening novel drugs for nephrotoxicity. At Cardiff University, my PhD project aimed to characterise tools to address these needs. At AstraZeneca, the use of tissue biomarkers as tools for assessing kidney injury in retrospective studies where urine biomarker samples are not available, was evaluated.

To enable studies of mineral ion homeostasis, an *in vitro* human primary renal cell model was characterised. Cells expressed phenotypic marker proteins (E-, N-Cadherin) as well as proteins involved in mineral ion homeostasis (FGFR1-4, Klotho, NaP_i IIa, NCX1, PMCA1). They also exhibited morphological features and functional characteristics of renal cells *in vivo*. Data were presented as an oral abstract communication at the American Society of Nephology Meeting, 2013.

To enable studies of drug-induced nephrotoxicity, *in vitro* primary mouse and human renal cell models were characterised. A concentration-dependent increase in apoptosis was observed in mouse cells following 24-hour treatment with medium containing cisplatin, cyclosporin A and BEA. Following 24-hour treatment, the same nephrotoxins increased expression of the kidney injury biomarkers kidney injury molecule-1 (KIM-1) and osteopontin. Human cells responded to 24-hour treatment with medium containing cisplatin with expression of KIM-1, osteopontin and clusterin. Parallel use of such rodent and human models would revolutionise preclinical translational drug safety assessment.

Cisplatin-treated rats were used to evaluate the use of tissue biomarkers as tools in studies where urine biomarker samples are not available, such as retrospective studies in drug safety testing. Of the biomarkers investigated, KIM-1 and osteopontin showed greatest correlation with their corresponding urinary biomarkers. As such, they offer greatest utility as tissue biomarkers in retrospective studies. Data were published in Toxicologic Pathology (Wadey et al. 2013).

Acknowledgements

I really enjoyed my time as a PhD student, but it would not have been possible without the support of my funding bodies, supervisors, colleagues, friends and family.

I would like to begin by thanking the Biotechnology and Biological Sciences Research Council and AstraZeneca for funding my Industrial CASE Studentship, as well as Cardiff University for providing me with a place to study. I would also like to thank my two supervisors, Professor Daniela Riccardi and Doctor Sally Price, for welcoming me to their laboratories at Cardiff University and AstraZeneca and for providing me with guidance.

Thank you to all the patients at University Hospital Wales who kindly donated kidney samples, and to the staff, particularly Mrs Fiona Morgan, for processing these samples. Thank you also to Professor Jürg Biber for the NaP_i IIa antibody.

I would also like to say a special thank you to my colleagues Mrs Lydia Searchfield, Mr Joao Graça and Doctor Valentina Peta, Doctor Mark Pinches and Doctor Huw Jones, who have contributed to my work at various stages of my project. Thank you also to my other colleagues Tom, Sarah, Martin, Poly, Irene, Charlie, Rachel, Julia and Stuart for your friendship.

Finally, a special thank you to my parents Jo and Ray, my brother Owen, and my boyfriend Matt for the love and support you have given me throughout!

List of Abbreviations

$1,25(OH)_2D_3$	1,25-dihydroxyvitamin D_3
ADHR	Autosomal dominant hypophosphatemic rickets
αGST	Alpha glutathione S-transferase
AKI	Acute kidney injury
AKIN	Acute Kidney Injury Network
ALP	Alkaline phosphatase
AQP2	Aquaporin-2
AUC	Area under the curve
βGP	Beta-glycerophosphate
β_2MG	Beta 2-microglobulin
BUN	Blood urea nitrogen
BSA	Bovine serum albumin
Ca^{2+}_o	Extracellular free ionised calcium
CKD	Chronic kidney disease
CRT1	Copper transporter-1
CYP24A1	24-hydroxylase
CYP27B1	1α-hydrolase
DAB	3,3'-diaminobenzidine
EMEA	European Medicines Agency
ERK	Extracellular signal related kinase
FDA	Food and Drug Administration
FFPE	Formalin-fixed, paraffin-embedded
FGF23	Fibroblast growth factor 23
FGFr	Fibroblast growth factor receptor
GFR	Glomerular filtration rate
HEK	Human embryonic kidney
Ig	Immunoglobulin

IHC	Immunohistochemistry
iNOS	Inducible nitric oxide synthase
i.p.	Intraperitoneal
ISOM	Inner stripe of the outer medulla
JG	Joao Graça
KIM-1	Kidney injury molecule-1
LS	Lydia Searchfield
MAPK	Mitogen-activated protein kinase
MSD	MesoScale discovery
NCX1	Sodium-calcium exchanger-1
NaP_i IIa	Sodium-phosphate co-transporter type IIa
OCT	Organic cation transporter
OPN	Osteopontin
OSOM	Outer stripe of the outer medulla
PFA	Paraformaldehyde
PTHR1	Parathyroid hormone receptor 1
PMCA1	Plasma membrane Ca^{2+} ATPase
PRE	Phosphate responsive element
PSTC	Predictive Safety Testing Consortium
PTH	Parathyroid hormone
RIFLE	Risk, Injury, Failure, Loss of function, End-stage renal disease
RCC	Renal cell carcinoma
ROC	Receiver operating characteristic
SCr	Serum creatinine
TFF3	Trefoil factor-3
TIO	Tumour-induced osteomalacia
TMA	Tissue Microarray
TUNEL	Terminal deoxyribonucleotidyl transferase-mediated dUTP nick end labelling

VP	Valentina Peta
v/v	Volume per volume
w/v	Weight per volume

Table of Contents

CHAPTER 1

Characterisation of Primary Human Renal Cells as a Novel Tool for Studying Mineral Ion Homeostasis by the Kidney

1.1 Abstract

Mineral ion homeostasis involves the complex interplay between Ca and Pi regulating transporting mechanisms and their regulating hormones (*i.e.,* PTH, FGF23, Klotho and $1,25(OH)_2D_3$). However, complex interactions between FGF23, PTH, $1,25(OH)_2D_3$, P_i and extracellular free ionized calcium (Ca^{2+}) that regulate mineral ion homeostasis by the kidney are difficult to investigate in humans under normal physiological conditions, let alone under states of disordered mineral ion metabolism such as chronic kidney disease-mineral and bone disorder (CKD-MBD). As such, much of the data regarding mineral ion metabolism presented in the literature is gathered from observations in rodents, but a complete understanding of the cause-effect relationship is currently lacking. In this study, we performed a cross-species comparison of the expression patterns of FGFr1-4 and Klotho (key proteins involved in mineral ion metabolism) in human, rat and mouse kidneys. Differences in the expression patterns of FGFr1-4 were identified suggesting that rodent models may not be appropriate for studying mineral ion metabolism by the human kidney as differences in protein expression may indicate differences in mineral ion handling. As such, an *in vitro* co-culture of primary human proximal and distal tubule cells as a novel tool for studying mineral ion metabolism specifically by the human kidney was characterised. FGFr1-4 and Klotho, as well as other proteins involved in mineral ion metabolism by the kidney including NaP_i IIa, NCX1 and PMCA1, are expressed in culture. The cell model responds as expected to known physiological stimuli (FGF23-induced ERK phosphorylation) and we show that changes in protein expression and cellular localization occur when cells are cultured in P_i-free medium (NaP_i IIa and PMCA1 upregulation) or in the presence of P_i-containing medium supplemented with FGF23 (NCX1 translocation to the cell membrane). This chapter demonstrates the suitability of the primary kidney cell model, thereby enabling future studies of mineral ion metabolism by the human kidney under experimental conditions that mimic both physiological and pathophysiological scenarios.

1.2 Introduction

Inorganic Phosphorus

Inorganic phosphorus (P_i) is essential for normal physiological function. As well as being required for bone and tooth mineralisation, phospholipid bilayer membranes and nucleotides that form DNA and RNA, it is used as a cell signalling molecule and an energy source for metabolic processes (Jüppner 2011; Takeda et al. 2004). As such, the ability to detect and react to changes in the extracellular concentration of P_i is critical. In healthy individuals, P_i levels are maintained within the physiological range of 0.81 to 1.45mM (2.5 to 4.5 mg/dl) (S. Moe 2008) with reserves sequestered in bone and any excess is excreted by the kidney (Kirchner et al. 2008). The homeostatic mechanism controlling P_i levels is, however, complex. It involves several different factors including fibroblast growth factor-23 (FGF23), parathyroid hormone (PTH), 1,25-dihydroxyvitamin D_3 ($1,25(OH)_2D_3$; the active form of Vitamin D), Ca^{2+}, and P_i itself.

P_i Homeostasis and FGF23

Fibroblast growth factors (FGFs) are a family of structurally related glycoproteins that control many different biological activities (Beenken and Mohammadi 2009). Fibroblast growth factor-23 is a 30kDa member of the FGF family that acts within the homeostatic 'bone-parathyroid-kidney' axis to eliminate excess P_i from the body in the urine; it is a phosphaturic factor. Following an acute P_i loading event, such as after the consumption of a P_i-rich meal, FGF23 is secreted into the circulation by osteocytes (Bonewald and Wacker 2013). It is currently unclear how a change in serum P_i is sensed (Bergwitz and Jüppner 2011; Witteveen et al. 2012; Wolf 2010). Nevertheless, once FGF23 has been secreted into the circulation, it behaves like a hormone and exerts its homeostatic effect in its target organ, the kidney. FGF23 signals for the down-regulation of the proximal tubule brush border membrane sodium-dependent phosphate co-transporters, NaP_i IIa and NaP_i IIc (Gattineni et al. 2009). Downregulation of these phosphate-conserving proteins by FGF23 has been elegantly illustrated both *in vitro* using isolated, microperfused mouse proximal tubule segments (Baum et al. 2005) and *in vivo* using mice treated with recombinant FGF23 (Shimada et al. 2002). FGF23 also acts in the proximal tubule to suppress 1α-hydrolase (CYP27B1) activity and stimulate 24-hydroxylase

(CYP24A1) activity (Shimada et al. 2004b). Changing the dynamics of these enzymes negatively modulates the formation of $1,25(OH)_2D_3$ and, as such, prevents dietary P_i absorption in the gut via NaP_i IIb (Miyamoto et al. 2005). FGF23 therefore has two means of reducing serum P_i levels; firstly, by increasing its urinary excretion, and secondly, by reducing any further intestinal absorption. Figure 1.1 shows the regulation of hyperphosphatemia by FGF23.

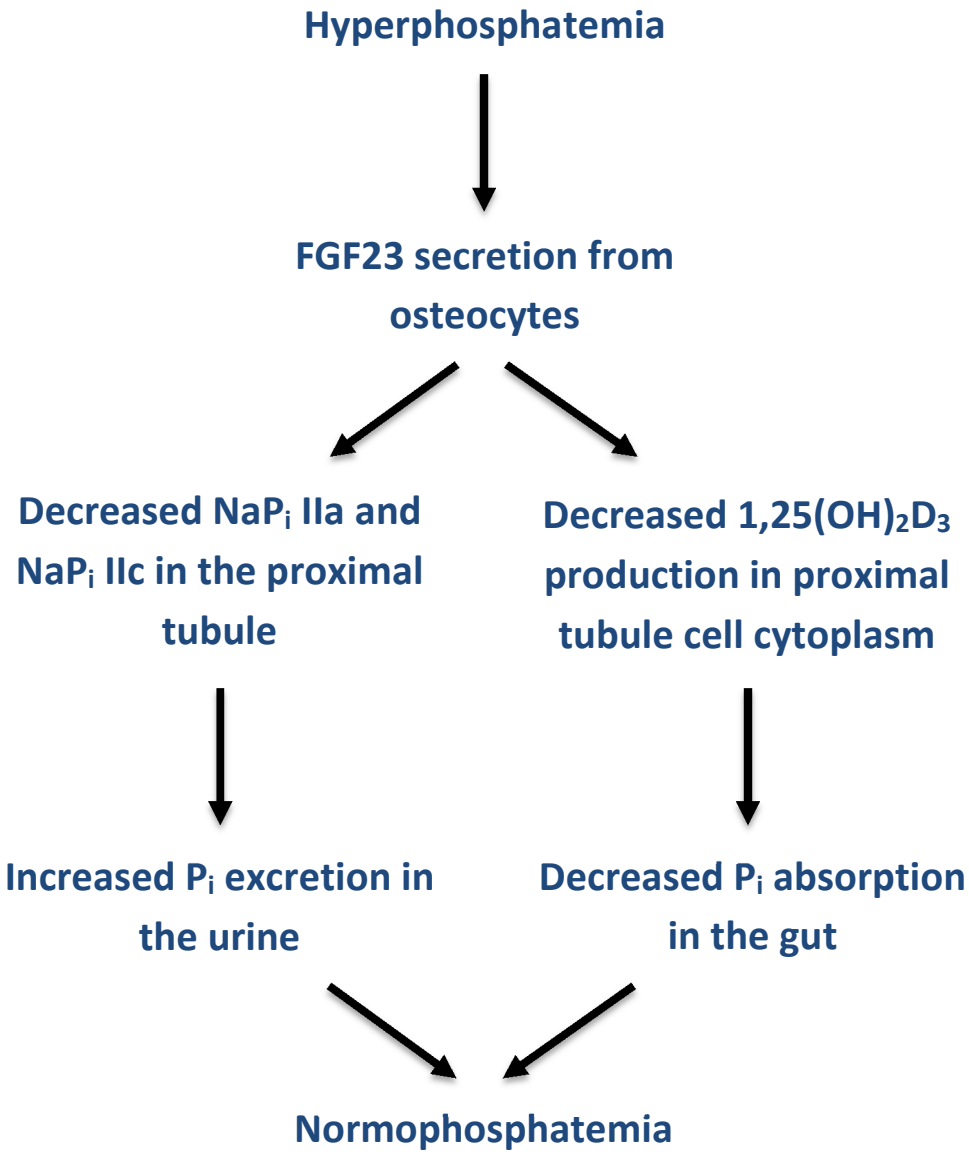

Figure 1.1. Regulation of Hyperphosphatemia by Fibroblast Growth Factor-23. Hyperphospatemia induces the secretion of the hormone fibroblast growth factor-23 (FGF23) from osteocytes (Bonewald and Wacker 2013). FGF23 circulates in the blood to act on its target organ, the kidney. Together with its cofactor, Klotho, FGF23 signals for the downregulation of the sodium-phosphate co-transporter types IIa and IIc (NaP_i IIa, NaP_i IIc) present on proximal tubule cell brush border membranes (Gattineni et al. 2009). Downregulation of NaP_i transporters prevents the reabsorbtion of P_i filtered at the glomerulus thereby increasing urinary P_i excretion (phosphaturia). In addition, FGF23 negatively modulates 1,25-dihydroxyvitamin D_3 ($1,25(OH)2D_3$) production in the proximal tubule by supressing and simulating the anabolic and catabolic activities of 1α-hydrolase and 25-hydroxylase respectively (Shimada et al. 2004b). Reduced circulating levels of $1,25(OH)2D_3$ results in the downregulation of the sodium-phosphate co-transporter type IIb (NaP_i IIb) in the gut which thereby prevents further P_i absorption into the blood (Miyamoto et al. 2005). In summary, FGF23 restores normophosphatemia during a state of hyperphosphatemia in two ways; firstly, by increasing urinary P_i excretion, and secondly, by reducing P_i absorption from the diet in the gut.

Structure and Localisation of Fibroblast Growth Factor Receptors in the Kidney

There are five fibroblast growth factor receptors (FGFr), four of which are highly conserved single-pass transmembrane receptors with extracellular immunoglobulin-like, ligand-binding domains, and an intracellular tyrosine kinase-linked domain (A. Brooks et al. 2012; Eswarakumar et al. 2005; Mohammadi et al. 2005; Powers et al. 2000). Based on current data gathered by immunohistochemistry, *in situ* hybridisation and polymerase chain reaction (PCR), FGFr1, FGFr2, FGFr3 and FGFr4 are expressed by kidney tubule epithelium. However, published data are discordant in terms of the localisation of each receptor along the nephron.

Previous studies have reported expression of FGFr1 in the proximal tubule in mouse (Andrukhova et al. 2012; Gattineni et al. 2009), and in the distal tubule in mouse (Andrukhova et al. 2012; Liu et al. 2008), rat (Cancilla et al. 2001) and human (Floege et al. 1999). FGFr1 has also been reported to be expressed in the kidney in humans with no specific location (Hughes 1997).

FGFr2 expression has been reported previously in both the proximal and distal tubules (Andrukhova et al. 2012) as well as the macula densa in mouse (Liu et al. 2008). In rats, it has been reported in the distal tubule (Cancilla et al. 2001), and in humans, it has been reported to be express in the kidney with no specific location (Hughes 1997).

Previous studies have localised FGFr3 in mouse kidney to the proximal (Andrukhova et al. 2012; Gattineni et al. 2009; Liu et al. 2008) and distal tubules (Andrukhova et al. 2012; Liu et al. 2008). In rat kidney, FGFr3 has been shown to be expressed in proximal tubule and distal tubule (Cancilla et al. 2001). In humans, expression of FGFr3 has been reported as minimal with no specific location (Hughes 1997).

Previous studies have localised FGFr4 in mouse kidney to the proximal (Andrukhova et al. 2012; Gattineni et al. 2009) and distal tubules (Andrukhova et al. 2012; Liu et al. 2008). Literature searches reveal little information regarding the expression pattern FGFr4 in rat (Horlick et al. 1992) and human (Fuhrmann et al. 1999; Hughes 1997) kidneys other than that they are expressed. A summary of FGFr1-4 expression patterns presented in current literature in human, rat and mouse kidneys is presented in Table 1.1.

Protein	Species	Method	Localisation
FGFr1	Human	IHC/ISH	DT[b], Kidney[d]
	Rat	IHC	G[c], Thin L[c], DT[c], CD[c]
	Mouse	IHC/ISH/PCR	PT[e], PT[f], DT[a], DT[f]
FGFr2	Human	IHC	Kidney[d]
	Rat	IHC	PT[c], DT[c]
	Mouse	IHC/PCR	PT[f], DT[f], MD[a]
FGFr3	Human	IHC	Kidney[d]
	Rat	IHC	PT[c], DT[c]
	Mouse	IHC/ISH/PCR	PT[a], PT[e], PT[f], DT[a], DT[f]
FGFr4	Human	IHC/PCR	Kidney[d], Kidney[g], Kidney[i]
	Rat	NB	Kidney[h]
	Mouse	IHC/ISH/PCR	PT[e], PT[f], DT[a], DT[f]

Table 1.1. Summary of the Localisation of Fibroblast Growth Factor Receptors (FGFr) 1-4 in Adult Human, Rat and Mouse Kidney Presented in Current Literature. Details regarding the localisation of FGFr1-4 human, rat and mouse kidney are detailed. The methods used to localise each receptor to a nephron segment in each study are also detailed. IHC = immunohistochemistry; ISH = *in situ* hybridisation; PCR = polymerase chain reaction; NB = Northern blot; CD = collecting duct; DT = distal tubule; G = glomerulus; MD = macula densa; PT = proximal tubule; Thin L = Thin Limb. ([a](Liu et al. 2008); [b](Floege et al. 1999); [c](Cancilla et al. 2001); [d](Hughes 1997); [e](Gattineni et al. 2009); [f](Andrukhova et al. 2012) [g](Fuhrmann et al. 1999), [h](Horlick et al. 1992), [i](Mutsaers et al. 2014)).

Lack of consistency between species could be due to true species differences, but it may also be a consequence of differences in methodology, or in antibody/probes used or metabolic/pathophysiological status. Each immunohistochemistry study, for example, used different methods of tissue fixation (Methyl Carnoy's solution (Floege et al. 1999), 10% neutral buffered-formalin (Floege et al. 1999; Hughes 1997), paraformaldehyde (Liu et al. 2008) and Bouin's fixative (Cancilla et al. 2001)) as well as different methods of heat-mediated or enzymatic antigen retrieval (no antigen retrieval (Floege et al. 1999), 0.01% protease XXIV at 37°C for 5-15 minutes (Hughes 1997), target retrieval solution at 95°C for 30 minutes (Liu et al. 2008) and 0.2% trypsin solution at room temperature for 30 minutes (Cancilla et al. 2001)). In addition to all these methodological differences, different antibodies were used across each of the studies, and as such, it is very difficult to draw any reliable conclusions when the results between each study are so different. Given the importance of FGF23 in maintaining serum P_i homeostasis, and the fact that animal models are often used to study it, it is surprising that to date there has been no cross-species comparison of FGFr localisation along the nephron using the same antibodies. Indeed, better understanding of FGFr localisation may help in elucidating which FGFr (or combination of FGFrs) FGF23 signals through.

Which FGFr is the receptor for FGF23?

The exact identity of the FGF23-specific FGFr is currently not known. Owing to the fact that the phosphaturic effects of FGF23 occur in the proximal tubule (Gattineni et al. 2009; Miyamoto et al. 2005), it may seem logical to hypothesize that the FGF23-specific FGFr also resides in the proximal tubule. However, data for and against this hypothesis are abundant.

Firstly, FGFr activation by FGF23 requires the presence of the cofactor, Klotho, a 130kDa type 1 single-pass transmembrane protein (Kurosu et al. 2006). Klotho was originally identified as an 'age suppressor' when mice with a defect in Klotho gene expression were shown to exhibit multiple ageing-like phenotypes including osteoporosis, arteriosclerosis, skin atrophy and infertility, and die prematurely at 2 months of age (Kuro-o et al. 1997). Deletion of Klotho specifically from the nephron results in an aging-like phenotype similar to that of systemic Klotho deletion (Lindberg et al. 2014). Klotho is essential for FGF23 signalling as it converts FGFr into a receptor specific for FGF23 (Urakawa et al. 2006).

Highlighting its requirement in this role are the facts that *Klotho*$^{-/-}$ mice have a similar phenotype to *Fgf23*$^{-/-}$ mice (Nakatani et al. 2009) and that monoclonal antibodies raised against Klotho inhibit FGF23 signalling in a dose-dependent manner (Urakawa et al. 2006).

Current opinion is that expression of Klotho (both mRNA and protein) is confined to the distal tubule (Farrow et al. 2009; Kato et al. 2000; S. Li et al. 2004). More recent data show Klotho mRNA and protein expression in the proximal tubule (Andrukhova et al. 2012; Hu et al. 2010). However, the subcellular localisation of Klotho in the proximal tubule between these two studies does not match; Andrukhova et al. (2012) report basolateral expression, whilst Hu et al. (2010) report apical, basolateral and cytoplasmic expression. In addition, whilst both groups identified much less Klotho mRNA in the proximal tubule compared to the distal tubule, Andrukhova et al. reported equal levels of protein expression with Hu et al. reporting much weaker protein expression in the proximal tubule compared to the distal tubule. As such, more localisation studies are needed to validate the presence or absence of Klotho in the proximal tubule.

If Klotho is not expressed in the proximal tubule, then 'how do signalling events linking Klotho-dependent FGF23 signalling in the distal tubule produce a physiological effect in the proximal tubule?' In order to answer that question, a distal-proximal paracrine signalling mechanism (Farrow et al. 2009) possibly involving peritubular capillaries (Hu et al. 2012), has been proposed. According to this model, Klotho is produced in the distal tubule and translocates to the proximal tubule. This view is supported by the fact that in addition to the 130kDa transmembrane-bound form, Klotho also exists as a 70kDa soluble protein, which is a product of alternative gene splicing or shedding of the extracellular domain of the transmembrane-bound form (Hu et al. 2012).

However, regardless of whether or not Klotho is expressed in the proximal tubule or translocates there following production in the distal tubule, there is important evidence supporting the fact that the FGF23-specific FGFr resides in the distal tubule; FGF23 induces signalling events in the distal tubule before changes in the proximal tubule are seen. Mice treated with recombinant FGF23 display ERK phosphorylation in distal tubules after 10 minutes followed by downregulation of NaP_i IIa protein (but not mRNA) in proximal tubules after 30-60 minutes (Farrow et al. 2010). *In vitro* studies have also shown the ability of FGF23 to activate ERK (Yamazaki et al. 2010) and as ERK is part of the

RAF/MEK/ERK pathway, it is also interesting to note that mice treated with inhibitors of MEK, have a similar phenotype to FGF23$^{-/-}$ or Klotho$^{-/-}$ mice (Diaz et al. 2012).

All that said, in terms of functional studies, FGFr1 appears to be the predominant receptor for the phosphaturic actions of FGF23 in mice with FGFr4 playing a lesser role (Gattineni et al. 2009). Indeed, a pull-down binding assay has shown that FGF23 binds specifically to splice variant FGFr1(IIIc) in the presence of Klotho (Urakawa et al. 2006). In addition, deletion of FGFr3 or FGFr4 was not shown to correct hypophosphatemia in *Hyp* mice (a mouse model of X-linked hypophosphatemia) and as such neither were considered to mediate the phosphaturic effects of FGF23 by these authors (Liu et al. 2008).

Studies of FGF23 under Pathophysiological Conditions Reveal Physiological Role

Much of the current understanding of FGF23 and P_i physiology has come from studying it under pathophysiological states. FGF23 was originally identified as a key player in phosphate metabolism when a mutated form was shown to be responsible for autosomal dominant hypophosphatemic rickets (ADHR) (White et al. 2000). ADHR is an inherited, gain-of-function disease whereby missense mutations in the *fgf23* gene prevent it from degradation by protease cleavage resulting in prolonged biological activity (Shimada et al. 2002; White et al. 2001). Since then, FGF23 has been shown to be central to a number of other diseases of phosphate metabolism.

X-linked hypophosphatemia (XLH) is an inherited phosphate-wasting disease. It is caused by an inactivating mutation in phosphate-regulating endopeptidase (PHEX) which, by an as yet unknown mechanism, results in increased FGF23 levels (Strom and Jüppner 2008). Tumour-induced osteomalacia (TIO) is an acquired disease of small and often benign FGF23-secreting mesenchymal tumours (Shimada et al. 2001). In similarity with ADHR and XLH patients, TIO patients have persistently high levels of FGF23 resulting in renal phosphate wasting, hypophosphatemia and impaired bone mineralisation (Chong et al. 2011; Shimada et al. 2001). FGF23 levels can however be restored towards normal and the disease treated by removal of the tumours (Fukumoto 2012).

The effects of raised FGF23 can be modelled in mice by constitutively overexpressing the *Fgf23* gene. Mice with raised FGF23 are phenotypically similar to patients with ADHR, XLH and TIO with regards to their renal phosphate-wasting, hypophosphatemia and

impaired bone mineralisation (Larsson et al. 2004; Shimada et al. 2004c). Pharmacological inhibition of FGFr (Wöhrle et al. 2013) and inhibition of FGF23 using FGF23 antibodies (Aono et al. 2009) restores normophosphatemia in these mice. These findings indicate that there is the potential for therapeutic treatment of such diseases in humans.

On the other hand, insufficient levels of circulating FGF23 can also produce problems. In humans, familial tumoral calcinosis (FTC) is an autosomal recessive disorder characterised by hyperphosphatemia and ectopic soft tissue calcifications (Benet-Pagès et al. 2005). It can be caused by mutations in FGF23 itself, the FGF23-glycosylating enzyme GALANT3 or the FGF23 cofactor Klotho (Lammoglia and Mericq 2009). In a similar manner to hypophosphatemic diseases, hyperphosphatemic diseases such as FTC can be modelled and studied in mice. *Fgf23* knockout mice develop hyperphosphatemia as a result of increased renal phosphate reabsorption via NaP_i IIa, have elevated $1,25(OH)_2D_3$ levels, and show excessive mineralisation of soft tissues such as the heart and kidney (Shimada et al. 2004a; Sitara et al. 2004; Sitara 2007).

FGF23 within the Bone-Parathyroid-Kidney Axis of P_i Homeostasis

FGF23 plays a key role in maintaining P_i balance, but it is just one part of the much wider 'bone-parathyroid-kidney' axis of P_i homeostasis in which P_i is also under the control of parathyroid hormone (PTH), $1,25(OH)_2D_3$ and Ca^{2+}, as well as P_i itself (Bergwitz and Jüppner 2010).

In addition to raising FGF23 levels via an unknown mechanism (Wolf 2010), an increase in P_i increases PTH by stabilising PTH mRNA (Moallem et al. 1998) and stimulating PTH secretion (Almaden et al. 1996; Estepa et al. 1999). The primary role of PTH is to increase Ca^{2+} levels by increasing bone resorption, kidney reabsorption and gut absorption when extracellular free ionised calcium (Ca^{2+}_o) levels fall below their normal physiological range of 1.1 - 1.3mM (4.4 - 5.4 mg/dL) (Peacock 2010). However, PTH also acts to both increase and decrease P_i levels simultaneously. It acts to increase P_i levels by stimulating the production of $1,25(OH)_2D_3$ (Kinoshita et al. 2005) thereby increasing NaP_i IIb mediated P_i absorption in the gut (Marks et al. 2006), and acts to decrease P_i levels via kidney parathyroid hormone receptor 1 (PTHR1)-mediated NaP_i IIa downregulation (Kempson et

al. 1995; Matsumoto et al. 2010) and lysosomal degradation (Keusch et al. 1998). PTH also stimulates the production of FGF23 both directly (Lavi-Moshayoff et al. 2010), and indirectly by increasing $1,25(OH)_2D_3$ (Kinoshita et al. 2005) which itself increases FGF23 levels (Liu et al. 2006). Whilst PTH increases FGF23 and $1,25(OH)_2D_3$ levels, they both exert negative feedback on PTH by inhibiting gene transcription and secretion (Ben-Dov et al. 2007; Demay et al. 1992). FGF23 decreases $1,25(OH)_2D_3$ (Clarke 2011; Shimada et al. 2004b).

As depicted below, P_i homeostasis is a balance of complex interacting reciprocal control mechanisms acting between FGF23, PTH, $1,25(OH)_2D_3$ and P_i itself. Figure 1.2 summarises the 'bone-kidney-parathyroid' axis of serum P_i homeostasis discussed above.

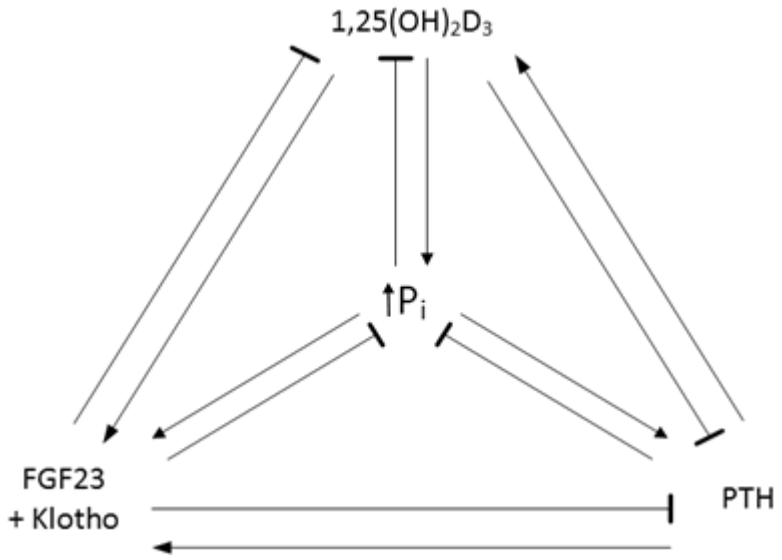

Figure 1.2. The 'Bone-Parathyroid-Kidney' Axis of Serum P_i Homeostasis. The 'bone-parathyroid-kidney' axis is a complex inter-relationship between P_i, FGF23, $1,25(OH)_2D_3$ and PTH that controls P_i homeostasis *in vivo*. Arrows inicate a positive influence (one factor increases the expression of another) and flat heads indicate a negative influence (one factor decreases the expression of another) between factors. An increase in serum P_i (hyperphosphatemia), increases serum FGF23 and serum PTH levels (Bergwitz and Jüppner 2010). PTH levels increase as a result of PTH mRNA stabilisation (Moallem et al. 1998) and stimulation of PTH secretion (Almaden et al. 1996; Estepa et al. 1999). PTH acts to both increase and decrease P_i levels simultaneously. It acts to increase P_i levels by stimulating the production of $1,25(OH)_2D_3$ (Kinoshita et al. 2005) thereby increasing NaP_i IIb mediated P_i absorption in the gut (Marks et al. 2006), and acts to decrease P_i levels via kidney parathyroid hormone receptor 1 (PTHR1)-mediated NaP_i IIa downregulation (Kempson et al. 1995; Matsumoto et al. 2010) and lysosomal degradation (Keusch et al. 1998), the result of which is phosphaturia. PTH also stimulates the production of FGF23 both directly (Lavi-Moshayoff et al. 2010), and indirectly by increasing $1,25(OH)_2D_3$ (Kinoshita et al. 2005) which itself increases FGF23 levels (Liu et al. 2006). Whilst PTH increases FGF23 and $1,25(OH)_2D_3$ levels, they both exert negative feedback on PTH by inhibiting gene transcription and secretion (Ben-Dov et al. 2007; Demay et al. 1992). FGF23 decreases serum $1,25(OH)_2D_3$ (Clarke 2011; Shimada et al. 2004b) leading to reduced P_i absorption in the gut via NaP_i IIb.

Chronic Kidney Disease-Mineral Bone Disorder, FGF23 and Klotho

In 2006, the Kidney Disease Improving Global Outcomes Foundation (KDIGO) coined the term 'Chronic Kidney Disease-Mineral Bone Disorder' (CKD-MBD) (S. Moe et al. 2006) in light of the fact that disordered mineral metabolism is a key feature of chronic kidney disease. CKD is a disease whereby glomerular filtration rate (GFR) declines over time and the kidneys lose their ability to excrete P_i (Kuro-o 2010). P_i retention is a target for therapeutic intervention because it is associated with an extremely increased risk of cardiovascular disease and mortality (Isakova et al. 2011; Quarles 2012). Controversies regarding the onset of the disease exist, particularly at the early stages when GFR has decreased, but P_i levels are normal.

Results from both the Chronic Renal Insufficiency Cohort (CRIC) longitudinal study (Isakova et al. 2011) and the Chronic Kidney Disease in Children observational study (Portale et al. 2014) show that increased FGF23 is the earliest detectable event following CKD onset. In early CKD, therefore, the rise in FGF23 followed by decrease in $1,25(OH)_2D_3$ and increase in PTH (Wolf 2010) maintain P_i levels within a normal physiological range (Gutierrez et al. 2005; Oliveira et al. 2010). However, over time, as renal function continues to deteriorate, these defence mechanisms are overwhelmed and hyperphosphatemia ensues (Shanahan et al. 2011).

A recent cross-sectional study (Pavik et al. 2013) confirmed a previous report (Koh et al. 2001) that levels of Klotho, the FGF23 receptor cofactor, decrease in early CKD. CKD may therefore be a state of renal resistance to FGF23, whereby Klotho deficiency causes FGF23 levels increase as a compensatory mechanism (Hu et al. 2011; Sakan et al. 2014; Six et al. 2014). As such, increased FGF23 and decreased Klotho have both been proposed as early biomarkers of disordered P_i metabolism/CKD onset (Fliser et al. 2007; Isakova et al. 2009; Wahl and Wolf 2012).

The full significance of FGF23 elevation in CKD remains to be fully elucidated (O. Moe and Kuro-O 2014). It appears that FGF23 may not just be a mere marker of disordered P_i metabolism but may also directly contribute to CKD pathophysiology. In CKD, FGF23 strongly and independently associates with cardiovascular events and all-cause mortality (Kendrick et al. 2011). Endothelial dysfunction and vascular stiffening (Mirza et al. 2009a),

atherosclerosis (Mirza et al. 2009b), vascular calcification (Desjardins et al. 2012) and left ventricular hypertrophy (Faul et al. 2011), are all associated with pathologically high levels of FGF23. As Klotho is not expressed in the heart (Faul et al. 2011), the effects of FGF23 outside the kidney and parathyroid gland are thought to be independent of Klotho. Indeed, there is evidence showing that FGF23 can bind, albeit with very low affinity, to FGFr in the absence of Klotho (Urakawa et al. 2006) and that Klotho-independent FGF23 signalling in the heart occurs via PLCγ rather than ERK (the classical Klotho-dependent FGF23 signalling pathway) to induce cardiomyocyte hypertrophy (Faul et al. 2011). It seems possible that the 1000-fold greater than normal FGF23 levels seen in CKD patients (Larsson et al. 2003), could have Klotho-independent effects.

FGFrs, Cancer and Ectopic Mineralisation

As previously mentioned, FGF23 is just one member of the FGF family (Beenken and Mohammadi 2009). Whilst FGF23 is involved in P_i homeostasis, other members play a role in regulating key cellular events such as cell proliferation, survival, differentiation and migration. Therefore, dysregulation of FGF/FGFr signalling is associated with many different developmental disorders and cancerous tumours (A. Brooks et al. 2012; Daniele et al. 2012; Dieci et al. 2013). As a consequence of this, FGF/FGFr signalling has become a target for therapeutic intervention in cancer, with *in vitro* and *in vivo* data highlighting the efficacy of inhibiting this pathway to preventing tumour growth (Dienstmann et al. 2014). However, because FGFs perform such a wide range of biological roles, broad FGFr inhibition has many unwanted side effects. One of the biggest complications pharmaceutical companies face in developing anti-cancer FGFr inhibitors has been hyperphosphatemia-mediated ectopic tissue mineralisation due to blockade of FGF23 phosphate homeostasis (Diaz et al. 2012; Turner and Grose 2010). Results from Phase I studies using AZD4547, a potent and selective inhibitor of FGFr1-3 (Gavine et al. 2012) and NVP-BGJ398, a pan FGFr inhibitor (Guagnano et al. 2011) both highlighted hyperphosphatemia as a common adverse event, with ectopic calcifications only minimised in the BJG398 trial with the aid of phosphate-binders (Dienstmann et al. 2014). Rather than balancing efficacy with unwanted side effects by using lower doses or using P_i lowering drugs as adjuncts, efforts to identify subtype selective FGFr inhibitors are ongoing.

1.3 Project Overview

The discovery of FGF23 as a key player in autosomal dominant hypophosphatemic rickets (White et al. 2000) drastically changed our understanding of P_i homeostasis. Presented previously is a summary detailing what is already known about FGF23 physiology and pathophysiology, and some of the major issues still facing the field have been highlighted. One of the biggest questions is 'which FGFr is the FGF23-specific FGFr?' Knowing the answer could revolutionise the treatment of both CKD-MBD and cancer. It is surprising, therefore, that to date, no cross-species comparison of FGFr localisation in the kidney has been carried out, especially given the fact that rodent species are used to model both CKD-MBD and cancer. If, based on current FGFr localisation studies, there are indeed differences in the expression patterns of FGFr along the nephron, then it begs the question, how good are rodent species as models for studying FGF23-mediated P_i homeostasis in humans? Differences in expression patterns and expression levels could indicate differences in P_i regulation between species. To negate species differences, it would be much better to adopt a human-specific *in vivo* model. However, due to the complex nature of the bone-parathyroid-kidney axis, studying it in humans *in vivo* is very difficult. The availability of an *in vitro* human kidney model through which the individual influence of FGF23, PTH, $1,25(OH)_2D_3$, Ca^{2+} and P_i itself has on P_i homeostasis would be greatly advantageous. Currently available human cell lines such as Human Embryonic Kidney (HEK)293 cells (Urakawa et al. 2006) and renal proximal tubule cells (RPTC) (Shalhoub et al. 2011) have been used for studying the actions of FGF23 *in vitro*. However, the phosphaturic action of FGF23 is thought to be a 'cross-talk' between proximal and distal tubule cells and a single cell type in culture does not enable such interactions. Co-cultures of primary human proximal and distal tubule cells have, however, been established by C. Brown et al. as a model for studying xenobiotic handling in the kidney (C. Brown et al. 2008). Another use of these cells is as a model for studying mineral ion homeostasis by the human kidney under defined conditions.

1.4 Aims

The aims of this study were:

1. To localise FGFr1, FGFr2, FGFr3 and FGFr4 in human, rat and mouse kidney tissue. The specific aims include:
    a. To perform sequence alignments for epitopes targeted by antibodies raised against FGFr1, FGFr2, FGFr3 and FGFr4 in each species to determine their species selectivity.
    b. To use immunohistochemistry to compare and contrast FGFr1, FGFr2, FGFr3 and FGFr4 expression patterns between species, and compare these findings against published literature.

2. To check the specificity of antibodies raised against Klotho, sodium-phosphate co-transporter IIa (NaP_i IIa), sodium-calcium exchanger 1 (NCX1) and plasma membrane calcium ATPase 1 (PMCA1) (other proteins also involved in mineral ion homeostasis by the kidney) by immunohistochemistry in human kidney.

3. To characterise an *in vitro* human primary co-culture of proximal and distal tubule cells as a novel model for studying mineral ion homeostasis by the human kidney. The specific aims include:
    a. Assess viability over time (using proliferation and apoptosis assays).
    b. Assess the maintenance of renal phenotype over time (using presence of E-Cadherin and N-Cadherin as markers of distal and proximal tubule cell phenotypes respectively).
    c. Assess cell morphology (including cobblestone appearance and proximal tubule cell brush border membranes).
    d. Assess the ability of *in vitro* renal cells to mimic *in vivo* renal cell responses to known physiological stimuli (including NaP_i IIa upregulation in response to no P_i, FGF23-induced ERK1/2 phosphorylation and MEK inhibitor-induced mineralisation).
    e. Assess the expression of key proteins in culture (FGFr1-4, Klotho, NaP_i IIa, NCX1 and PMCA1), and identify if FGF23 or P_i modulate their expression.

1.5 Materials and Methods

Antibody Epitope Sequence Alignments

Protein sequences for human, rat and mouse FGFr1, FGFr2, FGFr3 and FGFr4 were obtained from the UniProt database. Using Basic Local Alignment Search Tool (BLAST) the protein sequences for each protein from each species were aligned. The epitope (antigenic region) detected by each antibody for each of the proteins used in this study were selected and a comparison of similarities and differences in terms of sequence homology were made. The accession number used were: FGFr1 = Human (P11362), Rat (Q04589), Mouse (P16092); FGFr2 = Human (P21802), Rat (Q63238), Mouse (P21809); FGFr3 = Human (P22607), Rat (Q9JHX9), Mouse (Q61851); FGFr4 = Human (P22455), Rat (Q498D6), Mouse (Q03142). A list of the antibodies used in this study can be found in Table 1.2.

Obtaining Human, Rat and Mouse Kidney Tissue

Adult human kidney tissue for immunohistochemistry and cell culture was obtained from ethically-consented human kidneys surgically resected at The University Hospital Wales due to renal cell carcinoma (RCC) (Research Ethics Committee approval reference number: 07/WSE04/53) in collaboration with the Wales Cancer Bank. Macroscopically normal kidney cortex tissue was taken from a region separate to the carcinoma. Use of human kidney tissue was compliant the Human Tissue Act. Additional adult human kidney tissue for immunohistochemistry was sourced from Dr David Griffiths at The University Hospital Wales who had previously collected and prepared a human tissue microarray (TMA) of kidney cortex samples (both normal and diseased) (Searchfield et al. 2011). Adult human kidney cortex tissue for immunohistochemistry performed at AstraZeneca was obtained from the AstraZeneca Global Tissue Bank. Use of the tissue was compliant with the Human Tissue Act (HTA) as well as Global AstraZeneca Policy. Rat and mouse kidney tissue for immunohistochemistry was obtained from an adult male Han Wister rat (Harlan, UK) and an adult male C57Bl/6 mouse (Harlan, UK).

Immunohistochemistry

Cardiff: 4µm-thick formalin-fixed, paraffin-embedded sections of human kidney cortex were cut and air-dried onto strongly adhesive slides (Raymond A Lamb Limited, HistoBond E27.5HB), deparaffinised in xylene (Sigma, 534056) (2 x 5 minutes) and rehydrated using 100% (2 x 5 minutes) and 95% (1 x 5 minutes), 70% (1 x 5 minutes) ethanol (Sigma, 458600) and running tap water (1 x 5 minutes). Following pre-treatment (if required as per Table 1.2), tissue sections were incubated with 3% (v/v) H_2O_2 (Fisher Scientific, H/1750/15) in 1 x phosphate-buffered saline 0.05% (v/v) Tween-20 (Sigma, P5927) (PBST) (10 minutes) to quench endogenous peroxidase activity. Sections were washed with PBST (3 x 5 minutes). Non-specific binding of antibodies to tissue sections was prevented using serum-free protein block (Dako; X0909) (20 minutes). Individually diluted in antibody diluent (Dako, S2022), primary antibodies raised against FGFr1, FGFr2, FGFr3, FGFr4, Klotho, NaP_i IIa, NCX1, PMCA1, E-Cadherin and N-Cadherin (as per Table 1.2) were applied to tissue sections for 1 hour. Sections were washed with PBST (3 x 5 minutes). Immunoreactivity was detected and visualised using an anti-rabbit HRP polymer (Dako, K4065) (20 minutes) and liquid stable 3, 3' diaminobenzidine (DAB) (Dako; K3468) (1 minute) before sections were counterstained in haematoxylin (Sigma, HHS16) (1 minute). Sections were dehydrated using running water (1 x 5 minutes), 70% (1 x 5 minutes), 95% (1 x 5 minutes) and 100% (2 x 5 minutes) ethanol (Sigma, 458600), and then cleared in xylene (Sigma, 534056) (2 x 5 minutes). Slides were allowed to air dry before coverslips were mounted on slides using histomount (TAAB Labs, UK). Images were captured using a Mirax scanner (Zeiss, Germany) and Pannoramic Viewer software (3DHISTECH Kft, Hungary). For immunohistochemistry performed on human kidney cortex tissue microarray (TMA) samples, one section was used per antibody from which one image of the entire sample/field of view was captured. From this image, all proximal and distal tubules present were assessed for expression of the protein of interest. For immunohistochemistry performed on larger samples of human kidney cortex, one section was used per antibody. From these sections, images of 10 random fields of view were captured from which all proximal and distal tubules present were assessed for expression of the protein of interest.

AstraZeneca: 4μm-thick formalin-fixed, paraffin-embedded sections of human kidney cortex, or mouse and rat kidneys embedded in the transverse plane were cut and air-dried onto strongly adhesive slides (Leica Biosystems, Wetzlar, Germany). Sections were deparaffinised in xylene (Sigma, 33817) (2 x 5 minutes), and rehydrated using 100% (2 x 5 minutes) and 95% (1 x 5 minutes) ethanol (Sigma, 458600) followed by running tap water (1 x 5 minutes). Following pre-treatment (if required as per Table 1.2), all immunostaining was carried out at room temperature using a Labvision autostainer (Labvision, Fremont, USA). Sections were incubated with 3% H_2O_2 (Fisher Scientific, H/1750/15) 1 x Tris-buffered saline 0.05% Tween-20 (USB Corporation, 20605) (TBST) (10 minutes) to quench endogenous peroxidase activity. Sections were briefly rinsed with TBST before non-specific antibody binding was minimised using background blocker with casein (MP-966-P500; Menarini Diagnostics, Florence, Italy) (20 minutes). Individually diluted in 1X TBST, primary antibodies raised against FGFr1, FGFr2, FGFr3 and FGFr4 (as per Table 1.2) were applied to tissue sections for 1 hour. Sections were briefly rinsed with TBST before primary antibodies were conjugated with HRP using X-Cell Plus Universal Polymer HRP Kit (MP-XCP-U100, Menarini Diagnostics, Florence, Italy) (20 minutes). Sections were rinsed twice with TBST. Immunoreactivity was visualised using liquid stable 3, 3' diaminobenzidine (DAB) (MP-860-K25, Menarini Diagnostics, Florence, Italy) (10 minutes). Sections were rinsed twice with TBST and then counterstained using Carazzi's haematoxylin (Clin Tech Ltd, 642300) (1 minute). Sections were dehydrated using running tap water (1 x 5 minutes), 95% (1 x 5 minutes) and 100% (2 x 5 minutes) ethanol (Sigma, 458600), and then cleared in xylene (Sigma, 33817) (2 X 5 minutes). Sections were allowed to air dry before coverslips were mounted on the slides using histomount (TAAB Labs, Aldermaston, UK). Slides were scanned using a ScanScope scanner and images captured using ImageScope software (Aperio Technologies Incorporated, USA). For immunohistochemistry performed on human kidney cortex samples, one section was used per antibody. Form these sections, images of 10 random fields of view were captured from which all proximal and distal tubules present were assessed for expression of the proteins of interest. For immunohistochemistry performed on rat and mouse kidneys, one section per antibody was tested. In each case, 10 random fields of view of the kidney cortex were captured from which all proximal and distal tubules present were assessed for expression of the proteins of interest.

Protein	Supplier	IHC/IF Antigen Retrieval and Antibody Dilution	ICC Dilution
FGFr1	Abcam (ab71928)	Cardiff = 1:250 (H). AstraZeneca = Citrate 1:1000 (H, R & M)	1:200 (H)
FGFr2	Abcam (ab10648)	Cardiff = 1:500 (H). AstraZeneca = 1:1000 (H), 1:1500 (R), 1:2000 (M)	1:200 (H)
FGFr3	Abcam (ab10651)	Cardiff = 1:500 (H). AstraZeneca = 1:2000 (H, R & M)	1:100 (H)
FGFr4	Abcam (ab41948)	Cardiff = 1:250 (H). AstraZeneca = EDTA 1:500 (H, R &M)	1:100 (H)
Klotho	Abcam (ab75023)	Cardiff = 1:200 (H)	1:200 (H)
NaP_i IIa	Jürg Biber (Switzerland)	Cardiff = 1:500 (H)	1:200 (H)
NCX1	Abcam (ab2869)	Cardiff = 1:200 (H)	1:200 (H)
PMCA1	Abcam (ab3528)	Cardiff = 1:150 (H)	1:200 (H)
N-Cadherin	Abcam (ab12221)	Cardiff = 1:100 (FFPE) (H), 1:250 (Frozen) (H)	1:100 (H)
E-Cadherin	Abcam (ab1416)	Cardiff = 1:200 (FFPE) (H), 1:400 (Frozen) (H)	1:100 (H)

Table 1.2. Summary of antibodies used in the protein localisation study, and the human renal cell characterisation study. Details regarding the proteins investigated, the antibody suppliers and catalogue numbers, the antigen retrieval methods performed, antibody dilutions and antibody dilutions are provided. For the protein localisation study, work was done both at Cardiff University and AstraZeneca. The species in which the antibodies were tested are human (H), rat (R) and mouse (M). At AstraZeneca, citrate antigen retrieval (Citrate; Sigma, C1909) was performed at pH6 for 2 minutes at 110°C using a RHS-2 Rapid Histoprocessor (Milestone, Sorisole, Italy). Ethylenediaminetetraacetic acid (EDTA; Sigma, ED255) antigen retrieval was performed at pH8 for 2 minutes at 110°C using a RHS-2 Rapid Histoprocessor. FFPE = formalin-fixed, paraffin-embedded human kidney. Frozen = fresh frozen human kidney.

Human Renal Cell Isolation and Culture

Within 1 hour of removal from a patient, samples of macroscopically normal cortical tissue were dissected by a pathologist or biomedical scientist from the Wales Cancer Bank at the University Hospital Wales and transported to the host laboratory in isolation medium (RMPI 1640 medium with L-glutamine (VWR; 733-1708) containing 5% (v/v) FBS (GE Healthcare, UK), 2% (v/v) Pen/Strep (Invitrogen; 15140-122)) at 4°C. Under sterile conditions in a laminar flow hood (BIOQUELL, ABS1200CLS2-MK2), roughly $1cm^3$ pieces of freshly dissected cortical tissue were washed in phosphate-buffered saline pH 7.4 (PBS; Invitrogen, 10010-015) at 4°C. All metallic tools used were sterilised by autoclaving prior to use. Using metal tweezers and a disposable scalpel (Swann-Morton; 0501), cortical tissue was minced into a paste in 200µl 1X PBS pH 7.4 (Invitrogen; 10010-015) at 4°C. The resultant tissue paste was roughly divided into quarters. Using a sterile pipette tip with the top cut off, each quarter was placed in one of four 50ml polypropylene, conical bottom, tubes (Corning®, 430829) containing 37.5ml isolation medium (RMPI 1640 medium with L-glutamine (VWR; 733-1708) supplemented with 5% FBS (GE Healthcare, UK), 2% Pen/Strep (Invitrogen; 15140-122) and 0.67mg/ml collagenase type-IV (Worthington, LS004188)). (See method of collagenase type-IV preparation below). The four tubes were left at 4°C until the next day. Gentle agitation of the suspension inside the tubes to prevent settling of the tissue was achieved during this time using a cyclic rotator (VWR; 444-0502). Upon warming to 37°C for 15 minutes in a water bath the next day, tissue suspensions were vigorously agitated at 200 rotations/minute (rpm) in a shaking incubator (Jencons-PLS, Orbital incubator and shaker, 5150) for 2 hours at 37°C to enzymatically and mechanically dissociate the cells into a single cell suspension. To remove any remaining undigested tissue, the cell suspensions were filtered through a 40µm pore nylon strainer (BD Biosciences, UK; 352340) in to fresh 50ml tubes. To remove the collagenase and end the enzymatic digestion, cells were centrifuged twice at 150*g* for 7 minutes and each time re-suspended in fresh RMPI 1640 isolation medium (minus collagenase). The first time cells were re-suspended in 50ml RMPI 1640 isolation medium, and the second time, in 5ml RMPI 1640 isolation medium (minus collagenase). Cell suspensions were then loaded on top of discontinuous Percoll (GE Healthcare, GZ17089102) gradients made up of 1.04 and 1.07g/ml Percoll in isolation medium and 1X

PBS, respectively (See Percoll Gradient method below). Cells were then centrifuged at 1200*g* for 25 minutes in a swing out rotor (Eppendorf; Germany; 5720). A mixed population of proximal and distal tubule cells was aspirated from the intersection of the gradients and centrifuged twice at 150*g* for 7 minutes to remove excess Percoll. The first time, cells were re-suspended in 50ml RMPI 1640 isolation medium (minus collagenase), and the second time, cells were re-suspended in 5ml renal epithelial growth medium (REGM; Lonza, CC3191) containing the REGM SingleQuot kit supplements and growth factors, fetal calf serum (FCS), amphotericin B, epinephrine, human epidermal growth factor, hydrocortisone, insulin, transferrin and triiodothyronine (Lonza; CC4127). Rather than adding the gentamycin aliquot of the REGM SingleQuot kit supplements, 1% Penicillin (100units/ml)/Streptomycin (100µg/ml) (Invitrogen; 15140-122), was added to the culture medium. Gentamycin is a regularly used antibiotic in cell culture. However, it is also a nephrotoxin and it was thought that it may induce cell injury. As such a combination of Penicillin/Streptomycin was used. Once a bottle of Renal Epithelial Growth Medium containing the desired supplements was prepared, it was stored in darkness at 4°C, and used for up to one month.

For immunocytochemical assays, 100,000 cells were plated per 13mm Ø collagen type-IV (Sigma, C5533)-coated borosilicate glass coverslips (VWR, 631-0149) that were individually placed inside the wells of a 24-well tissue culture-treated plate (ThermoScientific, Nunclon™, 142475), or 0.4µm pore size polyethylene terephthalate (PET) transwells (VWR, 353180). 300,000 cells were plated in 35mm tissue culture-treated polypropylene plates (Falcon®, 353001). Cells were cultured in a humidified, 5% CO_2 incubator at 37°C (SANYO, MCO-18AIC). After warming to 37°C in a water bath, the cell culture medium was replaced on day 4, day 7, day 9 and day 14.

The cell culture protocol is based on that published by C. Brown et al., 2008.

For studies of protein regulation by P_i or FGF23, REGM was designated as P_i-containing medium as it inherently possessed $Na_2HP0_4 \bullet 7H_2O$ and $NaH_2P0_4 \bullet H_20$ at concentrations of 135mg/l and 62.50mg/l respectively, and P_i-free Dulbecco's Modified Eagle Medium (DMEM) (Invitrogen; 11971-025), with added REGM SingleQuot kit supplements and growth factors, was designated as P_i-free medium. Recombinant FGF23 (R&D systems,

2604-FG/CF) and recombinant Klotho (R&D systems, 1819-KL) plus heparin (Sigma, H3149) were added at working concentrations of 1µg/ml, 0.1µg/ml and 10µg/ml respectively. The glycosaminoglycan (GAG) heparin, was added as it is thought to enhance Klotho-dependent FGF23 activity by stabilising the FGF23-Klotho-FGFr complex (Urakawa et al. 2006). Concentrations of Klotho, heparin and FGF23 were based on those used in previous publications (Farrow et al. 2010; Goetz et al. 2010; Shalhoub et al. 2011; Smith et al. 2012).

Preparation of the Percoll Gradient for Isolating Primary Renal Cells

The Percoll gradient stock solution and gradients were prepared fresh on day of use under sterile conditions in a laminar flow tissue culture hood (BIOQUELL, ABS1200CLS2-MK2). For a roughly 1cm^3 sample of human kidney cortex, four Percoll gradients were prepared. The volumes required each of the gradient densities is described below. Into each 50ml polypropylene, conical bottom tube (Corning®, 430829), 7ml of the 1.07 density solution was added. With the 50ml tube at a 45° angle, 7ml of the 1.04 density solution was slowly pipetted down the inside of the tube, such that the 1.04 density solution sat on top of the 1.07 density solution. In a similar manner, 5ml of the cell suspension was then layered on top of the 1.04 density solution.

Percoll Stock Solution:

10X HBSS (Invitrogen; 14065-049)	4ml
Percoll (GE Healthcare; GZ17089102)	36ml

Percoll Gradient Density 1.04:

Percoll Stock Solution	10ml
RMPI 1640 Medium (VWR; 733-1708)	24ml

Percoll Gradient Density 1.07:

Percoll Stock Solution	20ml
1X PBS (Invitrogen; 10010-015)	16ml

Preparation of Collagenase Type-IV for Enzymatic Cell Isolation

The collagenase type-IV (Worthington, LS004188) for enzymatic cell digestion was prepared under sterile conditions in a laminar flow tissue culture hood (BIOQUELL, ABS1200CLS2-MK2). 25ml of RMPI 1640 isolation medium (Lonza, BE12-702F) was added to a 2.5g pot of collagenase type-IV (Worthington, LS004188) powder and repeatedly pipetted up and down to fully suspend to powder into a 100mg/ml stock solution. The stock solution was filter-sterilised though a 0.20µm pore size Minisart® syringe filter (Sartorius Stedium Biotech, Germany, 16534), after which 1ml aliquots were made in sterile 15ml tubes (Corning, 430791) and stored at -20°C. One aliquot was defrosted for use as and when required. To obtain the working concentration of collagenase type-IV (0.67mg/ml) needed for isolation of renal cells, 250µl of the 100mg/ml stock solution was added to 37.5ml RMPI 1650 isolation medium (Lonza, BE12-702F).

Preparation of Collagen-Coated Glass Coverslips for Cell Culture

13mm Ø borosilicate glass coverslips (VWR, 631-0149) were stored until required in copious 100% ethanol (Sigma, 458600). Under sterile conditions in a laminar flow hood (BIOQUELL, ABS1200CLS2-MK2), and using autoclave-sterilised metal tweezers, the 13mm Ø borosilicate glass coverslips (VWR, 631-0149) were individually placed into the wells of a 24-well tissue culture-treated plate (ThermoScientific, Nunclon™, 142475). During this process, coverslips were balanced at an angle against the side of each well to enable any ethanol on the coverslips to evaporate away. When all the ethanol had evaporated away (up to 1 hour later), the tissue culture plate containing the ethanol-sterilized coverslips, was further sterilized using the UV irradiation setting on the laminar flow tissue culture hood (BIOQUELL UK LTD, ABS1200CLS2-MK2) for 20 minutes.

All coverslips used for human renal cell cultures, were then coated with tissue culture grade collagen type–IV (Sigma, C5533). A 1mg/ml collagen stock solution was prepared from 5mg of lyophilized collagen type-IV powder in 5ml of 0.5M sterile acetic acid (Fisher Scientific, A/0360/PB17). The 1mg/ml stock solution was always prepared at least 24 hours in advance of requirement to allow for the collagen to completely dissolve, and was kept at 4°C. A working concentration of 0.1mg/ml collagen type-IV was prepared from the 1mg/ml stock solution using tissue culture grade distilled water (Invitrogen; 15230-

089). 200µl of 0.1mg/ml collagen type-IV solution was pipetted directly onto each 13mm Ø borosilicate glass coverslip (VWR, 631-0149) and left for 2 hours. After this time, the 0.1mg/ml collagen type-IV working concentration solution was removed, and the coverslips rinsed three times with sterile 1X PBS (Invitrogen, 10010-015) to remove any remaining traces of acetic acid. The final 1X PBS wash was left in the wells until just before renal cells were ready for plating.

Cell Proliferation Assay

The incorporation and immunofluorescent detection of 5-bromo-2'-deoxyuridine (BrdU), a thymidine analogue, into cellular DNA was used to investigate the percentage of cells undergoing proliferation, at day 5, day 8, day 10 and day 15 of culture. 5-bromo-2'-deoxyuridine (BrdU; Sigma, B5002) was added at a final concentration of 10µM to the culture medium 24 hours before cell fixation (*i.e.* on day 4, day 7, day 9 an day 14). Cells were removed from the incubator and transferred to the lab bench where the culture medium was then removed. Cells were fixed using 2% (w/v) paraformaldehyde (PFA; Sigma, 15,812-7) in 1X PBS pH 7.4 (10 minutes) at 4°C. 2% PFA stocks were pre-prepared and stored at -20°C. Aliquots were defrosted slowly on ice as and when required. Following fixation, cells were washed with 1X PBS pH 7.4 (3 X 5 minutes) at room temperature. Cells were permeabilised using 1X PBS pH 7.4 containing 0.05% (v/v) Tween-20 (Sigma, P5927) pH 7.4 (PBST) (5 minutes). Antigen retrieval was performed by incubating cells with 1N HCl (prepared from a 37% HCl stock solution (Sigma, 258148)) at 37°C (30 minutes) in a benchtop incubator (Techne Hybridiser, HB-1D). The antigen retrieval solution was removed and cells washed with PBST (3 X 5 minutes). Non-specific antibody binding sites were blocked using blocking buffer (1% (w/v) bovine serum albumin (BSA; Sigma, A7906), 3% (v/v) SeaBlock™ (EastCoast Bio, PP83-K1574) in PBST) at room temperature (1 hour). The blocking buffer was removed and cells incubated with an anti-BrdU primary antibody (mouse IgG; Abcam; ab8039) diluted 1:200 in blocking buffer (1 hour). To remove unbound antibodies, PBST washes were subsequently performed (3 X 5 minutes). Furthermore in darkness, Alexa Fluor® 594-conjugated secondary antibody diluted 1:400 in blocking buffer (goat anti-mouse IgG; Invitrogen; A11032) was applied to cells (1 hour). Again, to remove unbound antibodies, PBST washes performed (3 X 5 minutes). In order to identify all cell nuclei, cells were incubated

with 0.1µg/ml Hoechst 33342 (Invitrogen; H1399), a nucleic acid stain, diluted in blocking buffer (10 minutes). Cells underwent further PBST washes (3 X 5 minutes) to remove excess Hoechst 33342. Cells were briefly rinsed with distilled H_20, before excess H_20 was tapped off and coverslips mounted on slides using ProLong® Gold reagent (Invitrogen; P36930), a fluorescent anti-fade mounting medium. Slides were allowed to air-dry in darkness. Snapshots of slides were captured using a BX61 microscope (Olympus, Japan) and the percentage of proliferating cells out of the total number of cells was determined. A minimum of 500 cells at each time point were counted. Results were plotted graphically and analysed using Prism (GraphPad Software Inc., USA). To identify changes in proliferation over time, a one-way analysis of the variance (ANOVA) and a *post-hoc* Tukey multiple comparison test was performed. Results were deemed statistically significant when $p<0.05$ (*), $P<0.01$ (**) and $p<0.001$ (***). N=3, n=3.

Cell Apoptosis Assay

The percentage of human renal cells undergoing apoptotic cell death at day 5, day 8, day 10 and day 15 of culture, was determined using the DeadEnd™ Colorimetric Apoptosis Detection Kit (Promega, G7360). At each time point, cells were removed from the incubator and transferred to lab bench where the culture medium was then removed. Cells were fixed using 2% (w/v) paraformaldehyde (PFA; Sigma, 15,812-7) in 1X PBS pH 7.4 (10 minutes) at 4°C. 2% PFA stocks were pre-prepared and stored at -20°C. Aliquots were defrosted slowly on ice as and when required. Following fixation, cells were washed with 1X PBS pH 7.4 (3 X 5 minutes) at room temperature. Cells were then treated with the kit equilibration buffer (containing 200mM Potassium cacodylate, 25mM Tris-HCl, 0.2mM DTT, 0.25mg/ml BSA, 2.5mM cobalt chloride) at room temperature (5 minutes). Biotinylated nucleotides were incorporated at the 3'-OH end of fragmented, apoptotic DNA by recombinant terminal deoxynucleotidyl transferase (rTdT) at 37°C (1 hour). This rTDT reaction mix contained 1% (v/v) kit biotinylated nucleotide mix and 1% (v/v) kit rTdT enzyme in equilibration buffer. To terminate the TUNEL reaction, cells were then incubated with 2X saline sodium citrate (SSC) (15 minutes) at room temperature. 2X SSC was prepared by diluting the 20X SSC solution supplied with the kit 1:10 with deionised water before use. After cells were washed with 1X PBS pH 7.4 (3 X 5 minutes), endogenous peroxidases were quenched by treating cells with 0.3% (v/v) H_2O_2 (Fisher

Scientific, H/1750/15) (5 minutes). 1X PBST washes were subsequently repeated (3 X 5 minutes). Cells were incubated with kit streptavidin-HRP diluted 1:500 in 1X PBST (30 minutes). Following, further 1X PBST washes (3 X 5 minutes), immunoreactive sites were detected using the kit 3,3'-diaminobenzidine (DAB) (1 minute). The working concentration of DAB was achieved by diluting the 20X DAB Chromogen 1:20 in DAB substrate buffer. Cells were rinsed with distilled H_2O (3 X 5 minutes) and then counterstained with haematoxylin (Sigma, HHS16) (1 minute). Cells were dehydrated using 70%, 95%, 100% and 100% (v/v) ethanol (Sigma, 458600) (5 minutes each) and then cleared in xylene (Sigma, 534056) (2 X 5 minutes). Coverslips were allowed to air dry, and then mounted on glass slides using DPX mounting medium (Sigma, 44581). Images were captured using a DMRB microscope (Leica, Germany) and the number of apoptotic cells out of the total number of cells was determined. A minimum of 500 cells at each time point were counted. Results were plotted graphically and analysed using Prism (GraphPad Software Inc., USA). To identify changes in apoptosis over time, a one-way analysis of the variance (ANOVA) and a *post-hoc* Tukey multiple comparison test was performed. Results were deemed statistically significant when $p<0.05$ (*), $P<0.01$ (**) and $p<0.001$ (***). N=3, n=3.

Determination of the Percentage of Proximal to Distal Tubule Cell in Culture

Fluorescence activated cell sorting (FACS) analysis was used to determine the proportion of proximal and distal tubule cells at the point of isolation (*i.e.* at day 0), in addition to confirming that the cells isolated were indeed of proximal and distal tubule cell origin. Cells were fixed using 2% (v/v) paraformaldehyde (PFA, Sigma, 15,812-7) in PBS pH 7.4 (10 minutes). Following fixation, cells were spun in a benchtop centrifuge at 100*g* (Eppendorf, 5415D) (3 X 2 minutes) and each time resuspended in PBS pH 7.4. Non-specific binging sites were blocked using 5% (v/v) goat serum (Sigma, G9023) in PBS pH 7.4 for 1 hour. Cells were centrifuged at 100*g* (1 X 2 minutes) and then incubated with either anti-E-cadherin primary antibody (mouse IgG; 1:200 in blocking buffer; Abcam; ab1416) or anti N-cadherin primary antibody (rabbit IgG; 1:100 in blocking buffer; Abcam; ab12221) for 1 hour. To remove unbound antibodies, cells were centrifuged at 100*g* (3 X 2 minutes) and each time resuspended in PBS pH 7.4. Cells were then incubated with Alexa Fluor 488-conjugated secondary antibody (goat anti-mouse IgG; 1:1000 in blocking

buffer; Invitrogen; A11001) or Alexa Fluor 488-cojugated secondary antibody (goat anti-rabbit IgG; 1:1000 in blocking buffer; Invitrogen; A11034) for 1 hour. To remove unbound antibodies, cells were centrifuged at 100*g* (3 X 2 minutes). Throughout, cells were kept in darkness and all incubations were performed on ice. Following immunolabelling, cell suspensions were filtered through a 40µm pore nylon strainer (BD Biosciences, UK; 352340) and examined using a BD FACSCanto™ benchtop flow cytometer (BD Biosciences, UK) using BD FACSDiva™ software (BD Biosciences, UK). Gating of samples was based on size and granularity, and in order to standardise output, a minimum of 10,000 events were recorded per sample. Results were plotted graphically using Prism (GraphPad Software Inc., USA). N=3, n=3.

Immunofluorescent detection of E- and N-cadherin as phenotypic markers of distal and proximal tubule cells respectively was then used to assess the maintenance of distinct renal cell phenotypes after 5, 8, 10 and 15 days in culture. Cells were fixed using 2% (w/v) PFA in PBS (10 minutes) at 4°C and washed with PBS (3 x 5 minutes). Cells were permeabilised using PBST (5 minutes). Non-specific binding sites were blocked using 1% (w/v) BSA, 3% (v/v) SeaBlock™ (EastCoast Bio) PBST blocking buffer for 1 hour. Cells were incubated with anti-E-cadherin primary antibody (mouse IgG; 1:200 in blocking buffer; Abcam; ab1416) for 1 hour. Following PBST washes (3 x 5 minutes), and furthermore in darkness, Alexa Fluor 488-conjugated secondary antibody (goat anti-mouse IgG; 1:400 in blocking buffer; Invitrogen; A11001) was applied to cells for 1 hour. Cells were washed with PBST (3 x 5 minutes) before the process was repeated using anti N-cadherin primary antibody (rabbit IgG; 1:100 in blocking buffer; Abcam; ab12221) and Alexa Fluor 594-cojugated secondary antibody (goat anti-rabbit IgG; 1:400 in blocking buffer; Invitrogen; A11012). Cell nuclei were stained with 0.1µg/ml Hoechst (Invitrogen) in blocking buffer (10 minutes) before cells were washed with PBST (3 x 5 minutes). Coverslips were mounted on slides using Prolong Gold (Invitrogen; P36930) and allowed to dry overnight. Snapshots of slides were captured using a BX61 microscope (Olympus, Japan) and the percentage of proliferating cells out of the total number of cells was determined. A minimum of 500 cells at each time point were counted. Results were plotted graphically and analysed using Prism (GraphPad Software Inc., USA). N=3, n=3.

To identify any differences in the number of E-Cadherin positive cells versus the number of N-Cadherin positive cells over time (*i.e.* at day 0, 5, 8, 10 and 15), a two-way ANOVA and Bonferroni post-test was performed. Results were deemed statistically significant when $p<0.05$ (*), $P<0.01$ (**) and $p<0.001$ (***). N=3, n=3.

Identification of Proximal Tubule Microvilli by Electron Microscopy

After 5 days in culture, cells grown on 0.4µm pore size polyethylene terephthalate (PET) transwells (VWR, 353180) were rinsed with 1X PBS pH 7.4 (Invitrogen; 10010-015) (5 minutes) before fixation in 1% (w/v) glutaraldehyde (Agar Scientific, AGR1013) at 4°C (10 minutes). Cells were rinsed in ddH_2O (3 X 5 minutes), dehydrated using 50%, 70%, 90%, 100% and 100% ethanol (Sigma, 458600) (10 minutes each) and then treated with hexamethyldisilazane (TAAB Laboratories, H028) (HMDS; 3 x 5 minutes) to remove any remaining liquid from the sample, and then air dried. In the electron microscopy unit at Cardiff University, samples were attached to aluminium stubs (Elektron Technology, G301) with adhesive carbon tabs (Elektron Technology, G3347N), and then coated in gold (Elektron Technology, B7191) in a sputter coater (BioRad, SC500). Scanning electron microscopy was carried out by an electron microscopy technician at 5kV using a JEOL 840A scanning electron microscope (Samuel Roberts Nobel Microscopy Laboratory, USA). Images of proximal tubule cell brush border membranes were captured. N=2 (n=4, n=3).

Von Kossa's Mineral Deposition Assay

Von Kossa's mineralisation assay was used to assess the extent of mineral deposition by cultured renal cells over the culture time course. In von Kossa's mineralisation assay, silver cations react with phosphates and carbonates in calcium deposits and then reduced to black metallic silver by UV light. After 5, 8, 10 and 15 days in culture, cells were fixed using 2% (w/v) PFA in 1X PBS (10 minutes) at 4°C and washed with 1X PBS (3 x 5 minutes). Cells were incubated with 1% (w/v) silver nitrate (Sigma, S8157) under UV light (20 minutes) with any remaining unreacted silver ions subsequently removed by treatment with 5% (w/v) sodium thiosulphate (Sigma, S7026) (5 minutes). Cells were rinsed with distilled H_2O before 0.1% (w/v) Nuclear Fast Red (Acros Organics, 211980010) was used as a cellular counterstain (5 minutes). Following further H_2O rinses (3 x 5 minutes), cells were dehydrated using 70%, 95%, 100% and 100% ethanol (5 minutes each) and cleared

in xylene (Sigma, 534056) (2 X 5 minutes). Coverslips were mounted on slides using DPX mounting medium (Sigma). 2.5mM β-glycerophosphate (Sigma, G9422) was added to the culture medium 24 hours prior to cell fixation to induce mineralisation and act as a positive control. 10µM U0126 MEK inhibitor (Promega, V1121) was also added to the culture medium 24 hours prior to cell fixation to investigate the effect of inhibiting mineral ion regulation on mineral ion deposition. Images were captured using a DMRB microscope (Leica, Germany) from which the degree of mineralisation was determined by counting the number of cells that possess mineral deposits out of the total number of cells. A minimum of 500 cells at each time point for each condition were counted. Results were plotted graphically and analysed using Prism (GraphPad Software Inc.). To identify changes in the percentage of cells possessing mineral deposits in control and β-glycerophosphate-treated cells at each time point, a two-way analysis of the variance (ANOVA) and Bonferroni post-teat was performed. Results were deemed statistically significant when $p<0.05$ (*), $P<0.01$ (**) and $p<0.001$ (***). To identify differences in the number of cells possessing mineralisation over time for each condition, spearate one-way ANOVA and post-hoc Tukey multiple comparison tests were performed. Results were deemed statistically significant when $p<0.05$ (*), $P<0.01$ (**) and $p<0.001$ (***). For MEK inhibitor studies N=1, n=1, control and β-glycerophosphate studies N=3, n=3.

Preparation of Solutions for Von Kossa's Mineral Deposition Assay

1% Aqueous Silver Nitrate Solution:

1g Silver Nitrate (ACROS Organics, 197680250) in 100ml ddH_20. The solution was prepared in advance and stored in darkness at room temperature.

5% Sodium Thiosulphate Solution:

5g Sodium thiosulphate (Sigma, S-1648) in 100ml distilled H_2O. The solution was prepared in advance and stored at room temperature.

0.1% Nuclear Fast Red Solution:

0.1g Nuclear Fast Red (ACROS Organics, 211980010) and 5g Aluminium sulphate (Fisher Scientific, A/1840/60) in 100ml ddH_2O. The solution was prepared in advance and stored at room temperature. To prepare, both the aluminium sulphate and Nuclear Fast Red were added to the distilled H_20. In a glass beaker over a Bunsen burner, the solution was

slowly heated until boiling and then allowed to cool to room temperature. The solution was then filtered through filter paper (Whatman, 1001-150) and stored at room temperature until required.

Protein Regulation by P_i and FGF23 – Immunocytochemistry

Primary human renal cells were grown as described earlier to day 7 in regular growth medium (renal epithelial growth medium (REGM; Lonza, CC3191) containing the REGM SingleQuot kit supplements and growth factors (Lonza; CC4127). At this time, the medium was replaced with one of three different test media; *i.* regular growth medium (termed P_i-containing medium), *ii.* regular growth medium plus 1µg/ml FGF23, 0.1µg/ml Klotho and 10µg/ml heparin (termed P_i-containing medium plus FGF23) or *iii.* Dulbecco's Modified Eagle Medium (DMEM) (Invitrogen; 11971-025) with added REGM SingleQuot kit supplements and growth factors (Lonza; CC4127) (termed P_i-free medium). Following 24 hours in one of the three different media, cells at day 8 of culture were fixed using 2% (w/v) PFA (Sigma, 15,812-7) in 1 X PBS pH 7.4 (10 minutes) at 4°C, washed with 1 X PBS pH 7.4 (3 x 5 minutes) and permeabilised using 1X PBS pH 7.4 containing 0.05% (v/v) Tween-20 (Sigma, P5927) pH 7.4 (PBST). 0.3% (v/v) H_2O_2 (Fisher Scientific, H/1750/15) PBST pH 7.4 was used to quench endogenous peroxidase activity (5 minutes). A peroxidase Envsion^{TM} kit (Dako, Denmark; K5361) was used. Non-specific binding of the antibody to tissue sections was prevented using serum-free protein block (20 minutes). Individually diluted in antibody diluent (Dako, S2022) (as per Table 1.2), primary antibodies raised against FGFr1, FGFr2, FGFr3, FGFr4, Klotho, NaP_i IIa, NCX1 and PMCA1 were applied to cells for 1 hour. Excess antibodies were removed by washing cells with PBST (3 x 5 minutes). Cells were incubated for 30 minutes with anti-rabbit horseradish peroxidise (HRP)-conjugated polymer (Dako, K4065). PBST washes (3 x 5 minutes) were repeated to remove unbound antibodies and immunoreactive sites visualised using 3-3'-diaminobenzidine (DAB) chromogen substrate solution (Dako, K3468) (1 minute). Cells were briefly rinsed with distilled H_2O, counterstained with haematoxylin (Sigma, HH316) (1 minute), dehydrated using 70%, 95%, 100% and 100% ethanol (Sigma, 458600) (5 minutes each) and cleared in xylene (Sigma, 534056) (20 seconds). Coverslips were mounted on slides using DPX mounting medium (Sigma, 44581). Slides were scanned

using a Mirax scanner (Zeiss, Germany) and images captured using Panoramic Viewer software (3DHISTECH Kft, Hungary).

Detection of Vimentin

Vimentin is a filament protein expressed by dedifferentiated renal cells (Bonventre 2003; Hallman et al. 2008). To determine if primary human renal cells undergo dedifferentiation in culture over time, lysates were obtained from cells cultured or 5, 8, 10 and 15 days. On removal from the incubator, cells were briefly rinsed with 1X PBS before ice-cold RIPA buffer (Millipore; 20-188) was used to lyse cell membranes (10 minutes). The RIPA buffer was supplemented with a complete mini protease inhibitor cocktail tablet (Roche, 11836153001) to minimise protein degradation. Cell lysates were centrifuged (Sigma Laboratory Centrifuge SK18; SciQuip; UK) at 15000*g* for 10 minutes at 4°C, with the resultant supernatants aliquoted and stored at -80°C until prepared for Western blotting (protocol described below). The primary antibody used was anti-vimentin (rabbit IgG; 1:1000; abcam; ab92547) and the secondary antibody used was ImmunoPure goat anti-rabbit HRP-conjugated antibody (1:1000; Thermo Scientific; 31462). Human cortex lysate (prepared from a fresh human kidney sample from the Wales Cancer Bank) and recombinant human vimentin (abcam; ab73843) were used as positive controls. N=1, n=1.

ERK Activation by FGF23 – Western Blotting

Extracellular signal related kinase 1/2 (ERK1/2) is phosphorylated on residues thr^{202} and tyr^{204} following activation of FGFr by FGF23 (H. Li et al. 2011). To examine if this functional response is maintained *in vitro*, and whether this response could be blocked using a MEK inhibitor (MEK is upstream of ERK in FGF23 signalling pathway (Diaz et al. 2012)), an ERK activation assay was carried out. To equilibrate cells and reduce ERK activation to base line levels, cells were incubated for 30 minutes in a serum free physiological control buffer (20mM HEPES, 125mM NaCl, 4mM KCl, 0.5mM $CaCl_2$, 0.5mM $MgCl_2$, 5.5mM glucose, H_20, pH 7.4). The buffer was quickly removed and replaced with; *i.* control buffer, *ii.* control buffer plus 1µg/ml FGF23, 0.1µg/ml Klotho and 10µg/ml heparin, or *iii.* control buffer plus 1µg/ml FGF23, 0.1µg/ml Klotho, 10µg/ml heparin and 10µM U0126 MEK inhibitor. After 10 minutes at 37°C, experimental buffers were removed, cells were quickly rinsed with

1X PBS to enable protein extraction using radioimmunoprecipitation (RIPA) buffer (Millipore; 20-188) for 10 minutes on ice with gentle agitation. The RIPA buffer was supplemented with a complete mini protease inhibitor cocktail tablet (Roche, 11836153001) and a PhosSTOP tablet (Roche, 04906837001) to minimise both protein and phosphoprotein degradation. Cell lysates were centrifuged (Sigma Laboratory Centrifuge SK18; SciQuip; UK) at 15000*g* for 10 minutes at 4°C, with the resultant supernatants aliquoted and stored at -80°C until used for Western blotting (general Western blotting protocol described below). The primary antibody used was anti-active MAPK (rabbit IgG; 1:1000; Promega; V8031) and the secondary antibody used was ImmunoPure goat anti-rabbit HRP-conjugated antibody (1:5000; Thermo Scientific; 31462). To ensure equal loading, the Western blot membrane was stripped and re-probed using a primary antibody raised against Total-ERK (1:1000; mouse IgG; Santa Cruz; sc-135900) and an ImmunoPure goat anti-mouse HRP-conjugated antibody (1:5000; Thermo Scientific; 31446). N=1, n=1.

NaP_i IIa Regulation by P_i – Western Blotting

Following a 24 hour treatment with *i.* Pi-containing medium or *ii.* Pi-free medium, cells at day 8 of culture were quickly rinsed with 1X PBS to enable protein extraction using RIPA buffer (Millipore; 20-188) for 10 minutes on ice with gentle agitation. The RIPA buffer was supplemented with a complete mini protease inhibitor cocktail tablet (Roche, 11836153001) to minimise protein degradation. Cell lysates were centrifuged (Sigma Laboratory Centrifuge SK18; SciQuip; UK) at 15000*g* for 10 minutes at 4°C, with the resultant supernatants aliquoted and stored at -80°C until used for Western blotting (general Western blotting protocol described below). The NaP_i IIa primary antibody (rabbit IgG; 1:2000) used was a gift from Professor Jürg Biber, University of Zurich, Switzerland. The secondary antibody used was ImmunoPure goat anti-rabbit HRP-conjugated antibody (1:5000; Thermo Scientific; 31462). N=1, n=1.

General Western Blotting Protocol

The protein concentration of each sample was quantified using a colourimetric bicinchoninic acid (BCA) assay (Pierce, USA; 23227). Samples were mixed with 4X NuPage LDS sample buffer (Invitrogen; NP0007) and 10X NuPage reducing agent and heated at

70°C for 10 minutes. Samples of interest were loaded into separate lanes before separation by molecular weight was carried out by sodium dodecyl sulphate polyacrylamide gel electrophoresis for 35 minutes at 200V using NuPage Novex 10% Bis-Tris gels (Invitrogen; NP0301) using NuPage MES (Invitrogen; NP0002) SDS running buffer. Novex Sharp pre-stained protein standards (Invitrogen; LC5800) were used to estimate protein molecular weights. Resolved proteins were transferred to 0.2µm pore polyvinylidene fluoride (PVDF) membranes (BioRad; 162-0177) for 75 minutes at 40V. Successful transfer and equal protein loading was confirmed using 0.1% (w/v) Ponceau S (Sigma, P-3509) (1 minute). Non-specific antibody binding was reduced by incubating membranes in blocking buffer (5% non-fat dried milk (w/v) (Marvel Milk Powder) 1 X Tris (Sigma, RDD008)-buffered saline containing 0.05% Tween-20 (Sigma, P5927) (TBST)) overnight at 4°C. Membranes were exposed to a primary antibody diluted in blocking buffer for 1 hour at room temperature, before unbound antibodies were washed away with TBST (3 x 10 minutes). Membranes were subsequently incubated for 1 hour with a HRP-conjugated secondary antibody diluted in blocking buffer, before unbound antibodies were again washed away with TBST (3 x 10 minutes). Membranes were then incubated with enhanced chemiluminescence (ECL) detection reagents (VWR; RPN2232) before signals were subsequently developed on Amersham Hyperfilm ECL film (GE Healthcare; 28906838) or using a Gel Doc™ XR+ system (Bio-Rad Laboratories, Inc. USA).

1.6 Results

Human, Rat and Mouse Epitope Sequence Alignment for FGFr1, FGFr2, FGFr3 and FGFr4 Antibodies.

Sequence alignment was performed for the epitopes targeted by antibodies raised against each of FGFr1, FGFr2, FGFr3 and FGFr4 to determine how specific the selected antibodies were for each of the three different species.

FGFr1

The anti-FGFr1 antibody used was a rabbit polyclonal antibody. The datasheet from the supplier states that it reacts with human and rat FGFr1, and that it is expected to react with mouse FGFr1. It is raised against a synthetic peptide conjugated to KLH derived from within residues 350-450 of human FGFr1. Figure 1.3 shows that the epitope in rat differs from that of human by 1 amino acid (valine 396 in human FGFr1 is replaced with isoleucine 396 in rat FGFr1), and that the epitope in mouse differs by two amino acids (valine 391 and valine 396 in human FGFr1 are replaced with leucine 391 and isoleucine 396 in mouse FGFr1).

```
HUMAN 350   SHHSAWLTVLEALEERPAVMTSPLYLEIIIYCTGAFLISCMVGSVIVYKMK   400
      401   SGTKKSDFHSQMAVHKLAKSIPLRRQVTVSADSSASMNSGVLLVRPSRLS    450
RAT   350   SHHSAWLTVLEALEERPAVMTSPLYLEIIIYCTGAFLISCMVGSVIIYKMK   400
      401   SGTKKSDFHSQMAVHKLAKSIPLRRQVTVSADSSASMNSGVLLVRPSRLS    450
MOUSE 350   SHHSAWLTVLEALEERPAVMTSPLYLEIIIYCTGAFLISCMLGSVIIYKMK   400
      401   SGTKKSDFHSQMAVHKLAKSIPLRRQVTVSADSSASMNSGVLLVRPSRLS    450
```

Figure 1.3. FGFr1 Epitope Sequence Alignment. Sequence alignment reveals one difference in the amino acid sequence of the epitope detected by the FGFr1 antibody between human and rat, and two between that of human and mouse. Differences are highlighted in yellow. Valine 396 in human FGFr1 is replaced with isoleucine 396 in rat FGFr1, and valine 391 and valine 396 in human FGFr1 are replaced with leucine 391 and isoleucine 396 in mouse FGFr1. UniProt accession numbers used: Human (P11362), Rat (Q04589), Mouse (P16092). Sequence alignments performed by RW.

FGFr2

The anti-FGFr2 antibody used was a rabbit polyclonal antibody. The datasheet from the supplier states that it reacts with human, rat and mouse FGFr2. It was raised against a synthetic peptide corresponding to amino acids 362-374 of human FGFr2.

```
HUMAN       362 APGREKEITASPD 374
RAT         301 APVREKEITASPD 313
MOUSE       362 APVREKEITASPD 374
```

Figure 1.4. FGFr2 Epitope Sequence Alignment. Sequence alignment reveals one difference in the epitope detected by the antibody between human, and rat and mouse. Glycine 364 in human is replaced with valine 364 in rat mouse. A sequence identical to the mouse FGFr2 sequence exists between amino acids 301 and 313 of rat FGFr2. Like mouse, this sequence differs from that of human FGFr2 by one amino acid; glycine 364 in human is replaced with valine 303 in rat. Differences are highlighted in yellow. UniProt accession numbers used: Human (P21802), Rat (Q63238), Mouse (P21803). Sequence alignments performed by RW.

FGFr3

The anti-FGFr3 antibody used was a rabbit polyclonal antibody. The datasheet from the supplier states that it reacts with human FGFr3, but does not mention that of rat or mouse FGFr3. Raised against a 15 amino acid synthetic peptide corresponding to a region of human FGFr3, it detects an epitope beginning at alanine 359 and ending at valine 372. Figure 1.5 shows that the epitopes in rat and mouse FGFr3 differ from that of the epitope in human FGFr3 by two amino acids each.

```
HUMAN 359 AEEELVEADEAGSV 372

RAT   353 AEEELMEVDEAGSV 366

MOUSE 353 AEEELMETDEAGSV 366
```

Figure 1.5. FGFr3 Epitope Sequence Alignment. Sequence alignment reveals two differences in the epitope detected by the antibody between human, rat and mouse. Rat differs from human by two amino acids (valine 364 and alanine 366 in human FGFr3 are replaced methionine 364 and valine 366 in rat FGFr3). Mouse also differs from human by two amino acids (valine 364 and alanine 366 in human FGFr3 are replaced with methionine 364 and threonine 366 in mouse FGFr3). Differences are highlighted in yellow. UniProt accession numbers used: Human (P22607), Rat (Q9JHX9), Mouse (Q61851). Sequence alignments performed by RW.

FGFr4

The anti-FGFr4 antibody used was a rabbit polyclonal antibody. The datasheet from the supplier states that it reacts with human FGFr4, but does not mention rat or mouse FGFr4. Raised against a synthetic peptide corresponding to amino acids 100 to 200 of human FGFr4, it detects an epitope beginning at leucine 100 and ending at isoleucine 200. Figure 1.6 shows that the epitopes in rat and mouse FGFr4 differ from that of the epitope in human FGFr4 by several amino acids.

```
HUMAN  100    LCLARGSMIVLQNLTLITGDSLTSSNDDEDPKSHRDPSNRHSYPQQAPYWT
              HPQRMEKKLHAVPAGNTVKFRCPAAGNPTPTIRWLKDGQAFHGENRIGGI   200
RAT    97     LCLARGSMTVVHNLTLIMDDSLPSINN-EDPKTLSSSSSGHSYLQQAPYWT
              HPQRMEKKLHAVPAGNTVKFRCPAAGNPMPTIHWLKNGQAFHGENRIGGI   196
MOUSE  97     LCLARGSMTVVHNLTLLMDDSLTSISNDEDPKTLSSSSSGHVYPQQAPYWT
              HPQRMEKKLHAVPAGNTVKFRCPAAGNPMPTIHWLKDGQAFHGENRIGGI   196
```

Figure 1.6. FGFr4 Epitope Sequence Alignment. The epitope detected by the antibody falls between amino acids 100 and 200 of human FGFr4. Corresponding sequences differing by several amino acids is present in the rat and mouse FGFr4 sequences between amino acids 97 and 196. Differences are highlighted in yellow. UniProt accession numbers used: Human (P22455), Rat (Q498D6), Mouse (Q03142). Sequence alignments performed by RW.

FGFr1-4 Immunolocalisation in Human, Rat and Mouse Kidney Cortex

The immunolocalisation of FGFr1, FGFr2, FGFr3 and FGFr4 in formalin-fixed, paraffin-embedded (FFPE) adult human, rat and mouse kidney cortex are shown in representative images in Figures 1.7 – 1.10. A summary of the localisation patterns for each antibody across each species can be found in Tables 1.3-1.6. Figure 1.11 shows the immunolocalisation of Klotho, NaP_i IIa, NCX1 and PMCA1 in FFPE human kidney cortex, and confirms the specificity of these antibodies for use in the primary human cell characterisation work. A summary of the localisation patterns for each of these antibodies in human kidney cortex can be found in Table 1.7.

FGFr1

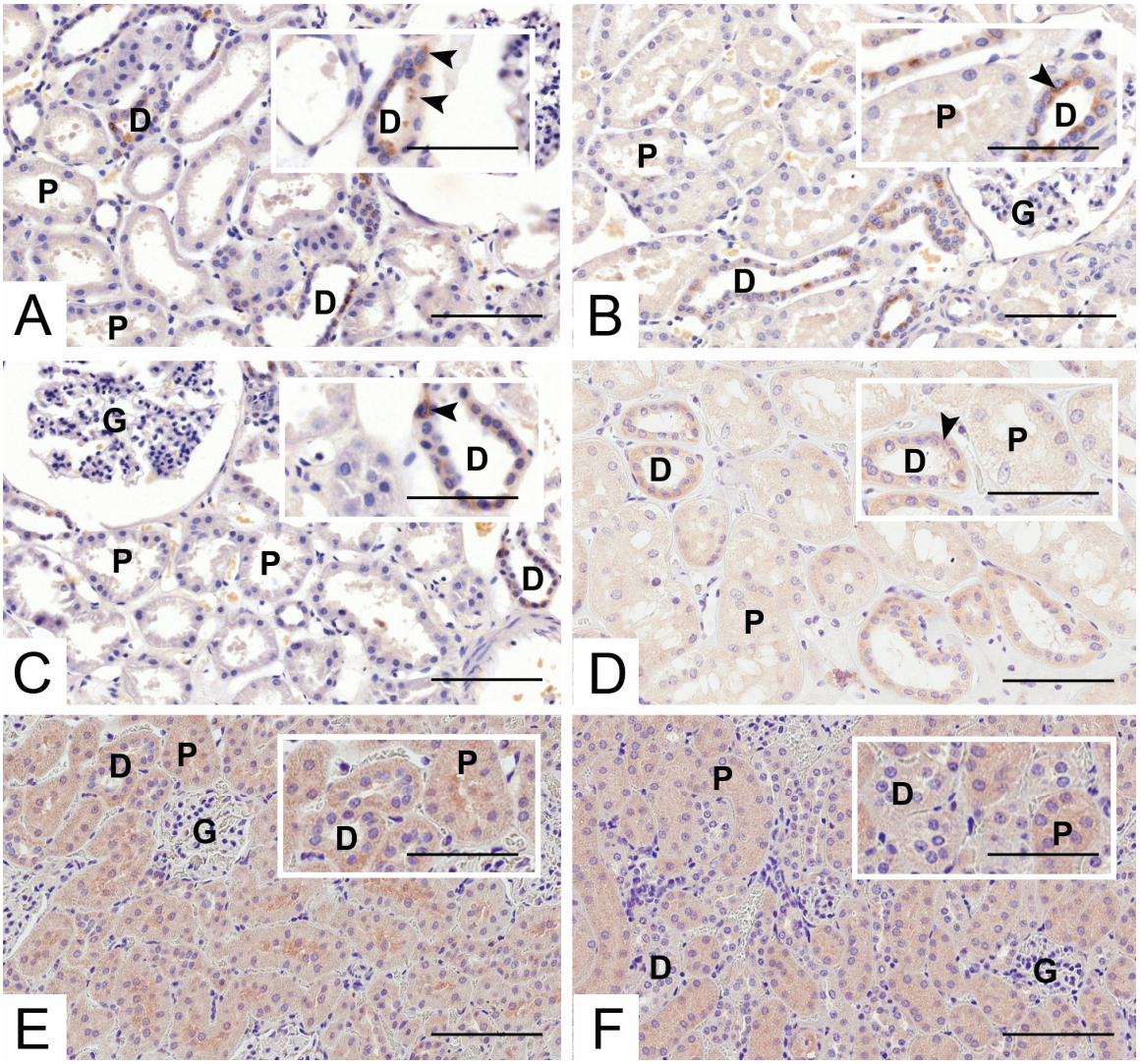

Figure 1.7. Immunolocalisation of FGFr1 in formalin-fixed, paraffin-embedded (A-D) Human, (E) Rat and (F) Mouse Kidney Cortex. (A-D) FGFr1 was localised in human kidney cortex samples to the distal tubule, where it appeared punctate pattern in a subset of cells (insert, arrows). N=4, n=4. (E) FGFr1 was localised in rat kidney cortex to both the proximal and distal tubule. N=1, n=1. (F) FGFr1 was localised in mouse kidney to the proximal tubule. N=1, n=1. In all cases, immunoreactivity for the protein of interest appears brown and the haematoxylin co-stain identifying cell nuclei appears blue. All images are representative of one section per sample. Human kidney cortex TMA images are representative of one field of view (A-C), with the larger human kidney cortex sample image (D) and rat (E) and mouse (F) kidney cortex images being representative of 10 fields of view. IHC performed by LS (A-C) and JG (D-F). Images captured by RW. Image analysis by RW. P = proximal tubule, D = distal tubule, G= glomerulus. Bars = 100µm. Insert Bars = 60 µm.

Receptor	Species	PT (% positive)	DT (% positive)
FGFr1	Human	0	100
	Human	0	100
	Human	0	100
	Human	0	100
FGFr1	Rat	100	100
FGFr1	Mouse	100	0

Table 1.3. Summary of the expression pattern of FGFr1 in formalin-fixed, paraffin-embedded human, rat and mouse kidney sections. In human kidney cortex samples, FGFr1 was expressed in 100% of distal tubules viewed (N=4, n=4; 19/19, 14/14, 17/17, 306/306) and 0% of proximal tubules viewed (N=4, n=4; 0/41, 0/46, 0/41, 0/559). In rat kidney cortex, FGFr1 immunoreactivity was detected in 100% of proximal tubules viewed (N=1, n=1; 303/303) and 100% of distal tubules viewed (N=1, n=1; 148/148). In mouse kidney cortex, FGFr1 immunoreactivity was detected in 100% of proximal tubules viewed (N=1, n=1; 476/476) and 0% of distal tubules viewed (N=1, n=1; 0/131). All data are representative of one section per sample. Values presented are representative of all proximal and distal tubules observed in human kidney cortex TMA sections obtained from one field of view, or representative of 10 fields of view in larger human kidney cortex sections and rat and mouse kidney cortex sections. Quantification performed by RW.

FGFr2

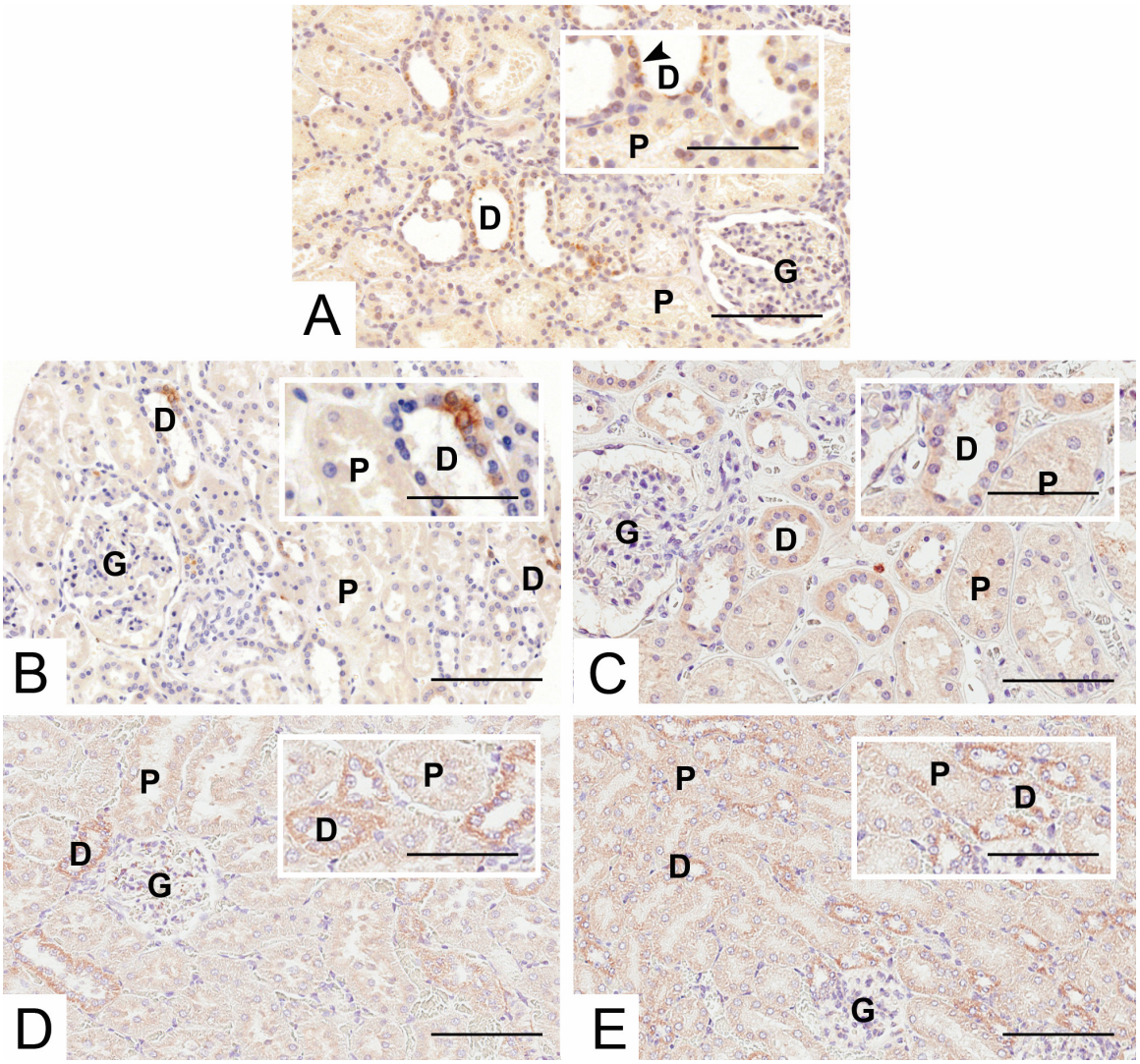

Figure 1.8. Immunolocalisation of FGFr2 in formalin-fixed, paraffin-embedded (A-C) Human, (D) Rat and (E) Mouse Kidney Cortex. (A) FGFr2 was localised in human kidney cortex to the distal tubule, where it appeared punctate in a subset of cells (insert, arrow). N=1, n=1. (B) FGFr2 was localised in human kidney cortex to the distal tubule, where it appeared punctate pattern in a subset of cells N=1, n=1. (C) FGFr2 was localised in human kidney cortex to the distal tubule. N=1, n=1. (D) FGFr2 was localised in rat kidney cortex to the distal tubule. N=1, n=1. (E) FGFr2 was localised in mouse kidney cortex to the distal tubule. N=1, n=1. In all cases, immunoreactivity for the protein of interest appears brown and the haematoxylin co-stain identifying cell nuclei appears blue. All images are representative of one section per sample. The human kidney cortex TMA image is representative of one field of view (B), with larger human kidney cortex sample images (A&C) and rat (E) and mouse (F) kidney cortex images being representative of 10 fields of view. IHC performed by LS (A&B) and JG (C-E). Images captured by RW. Image analysis performed by RW. P = proximal tubule, D = distal tubule, G = glomerulus. Bars = 100µm. Insert Bars = 60µm

Receptor	Species	PT (% positive)	DT (% positive)
	Human	0	100
FGFr2	Human	0	28
	Human	0	100
FGFr2	Rat	0	100
FGFr2	Mouse	0	100

Table 1.4. Summary of the expression pattern of FGFr2 in formalin-fixed, paraffin-embedded human, rat and mouse kidney sections. In human kidney cortex samples, FGFr2 immunoreactivity was detected in 100% of distal tubules viewed in human kidney in two samples (N=2, n=2; 128/128, 206/206) and 28% of distal tubules viewed in one sample (N=1, n=1; 8/20). In all samples, 0% of proximal tubules viewed were positive (N=3, n=3; 0/254, 0/33, 0/598). In rat kidney cortex, FGFr2 immunoreactivity was detected in 0% of proximal tubules viewed (N=1, n=1; 0/359) and 100% of distal tubules viewed (N=1, n=1; 180/180). In mouse kidney cortex, FGFr2 immunoreactivity was detected in 100% of distal tubules viewed (N=1, n=1; 211/211) and 0% of proximal tubules viewed (N=1, n=1; 0/506). All data are representative of one section per sample. Values presented are representative of all proximal and distal tubules observed in human kidney cortex TMA sections obtained from one field of view, or representative of 10 fields of view in larger human kidney cortex sections and rat and mouse kidney cortex sections. Quantification performed by RW.

FGFr3

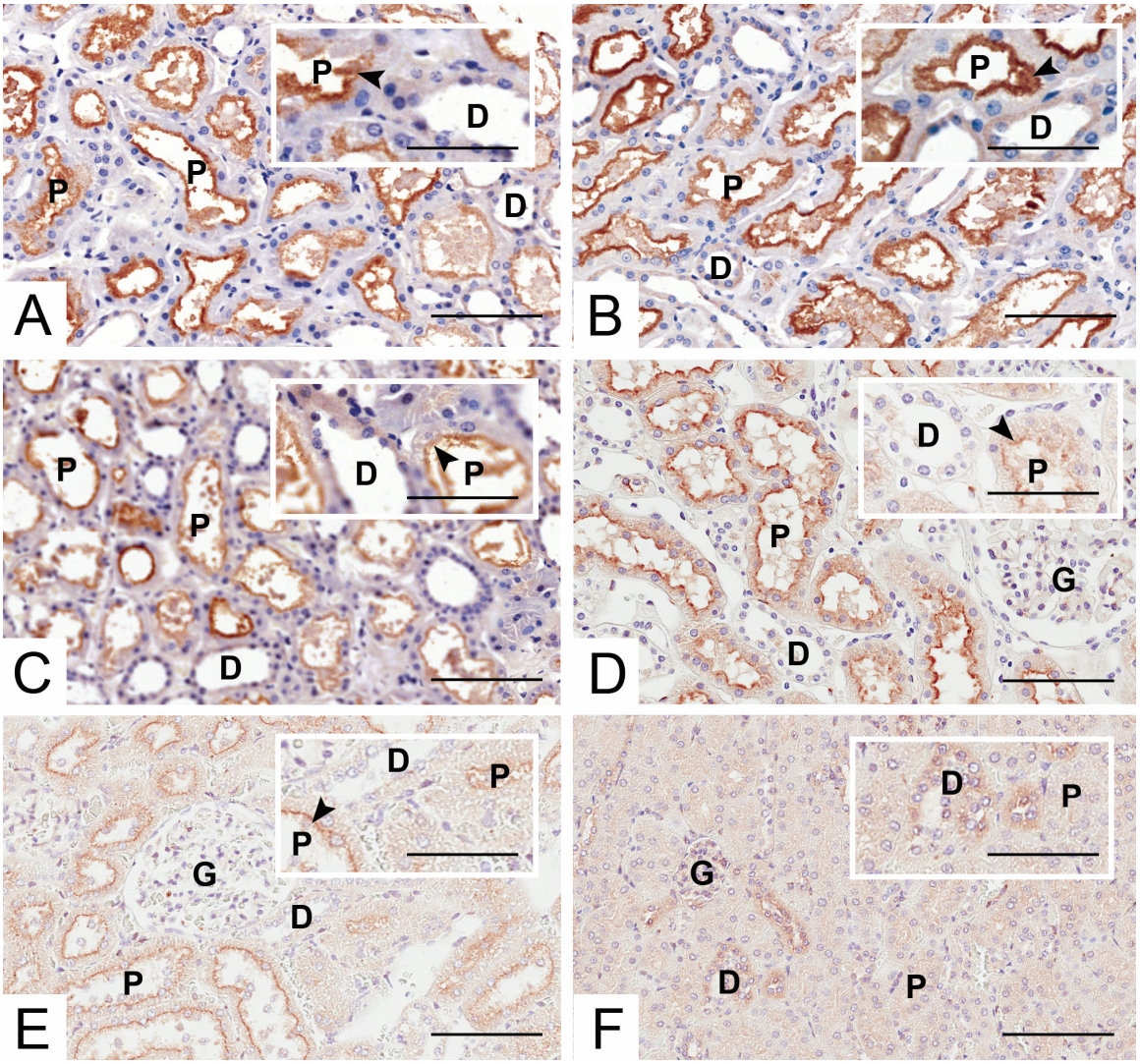

Figure 1.9. Immunolocalisation of FGFr3 in formalin-fixed, paraffin-embedded (A-D) Human, (E) Rat and (F) Mouse Kidney Cortex. (A) In human kidney cortex, FGFr3 was localised to proximal tubule brush border membranes (arrow head). Fainter immunoreactivity is also seen in distal tubule cell cytoplasm. N=1, n=1. (B) In human kidney cortex, FGFr3 was localised to proximal tubule brush border (arrow head). Fainter immunoreactivity is also seen in distal tubule cell cytoplasm. N=1, n=1. (C) In human kidney cortex, FGFr3 was localised to proximal tubule brush border membranes (arrow head). Fainter immunoreactivity is also seen in distal tubule cell cytoplasm. N=1, n=1. (D) In human kidney cortex, FGFr3 was localised to the proximal tubule brush border membrane (arrow). N=1, n=1. (E) In rat kidney cortex, FGFr3 was localised to proximal tubule brush border membranes (arrow). N=1, n=1. (F) In mouse kidney cortex, FGFr3 immunoreactivity was localised to the distal tubule cell cytoplasm. N=1, n=1. In all cases, immunoreactivity for the protein of interest appears brown and the haematoxylin co-stain identifying cell nuclei appears blue. All images are representative of one section per sample. Human kidney cortex TMA images are representative of one field of view (A-C), with the larger human kidney cortex sample (D) and rat (E) and mouse (F) kidney cortex samples being representative of 10 fields of view. IHC performed by LS (A-C) and JG (D-F). Images captured by RW. Image analysis performed by RW. P = proximal tubule, D = distal tubule, G= glomerulus. Bars = 100µm. Insert Bar = 60µm.

Receptor	Species	PT (% positive)	DT (% positive)
FGFr3	Human	100	100
	Human	100	100
	Human	100	100
	Human	100	0
FGFr3	Rat	100	0
FGFr3	Mouse	100	74.2

Table 1.5. Summary of the expression pattern of FGFr3 in formalin-fixed, paraffin-embedded human, rat and mouse kidney sections. FGFr3 was expressed in 100% of human proximal tubules viewed (N=4, n=4; 56/56, 50/50, 57/57, 663/663). FGFr3 was expressed in 100% of distal tubules in 3 out of 4 human kidneys (N=4, n=4; 23/23, 24/24, 32/32, 0/247). In rat kidney, FGFr3 was expressed 100% of proximal tubules (N=1, n=1; 1450/1450) and 0% of distal tubule cells (N=1, n=1; 0/363). In mouse kidney, FGFr3 was expressed 100% of proximal tubules (N=1, n=1; 673/673) and 74.2% of distal tubule cells (N=1, n=1; 161/217). Values presented are representative of all proximal and distal tubules observed in human kidney cortex TMA sections obtained from one field of view, or representative of 10 fields of view in larger human kidney cortex sections and rat and mouse kidney cortex sections. Quantification performed by RW.

FGFr4

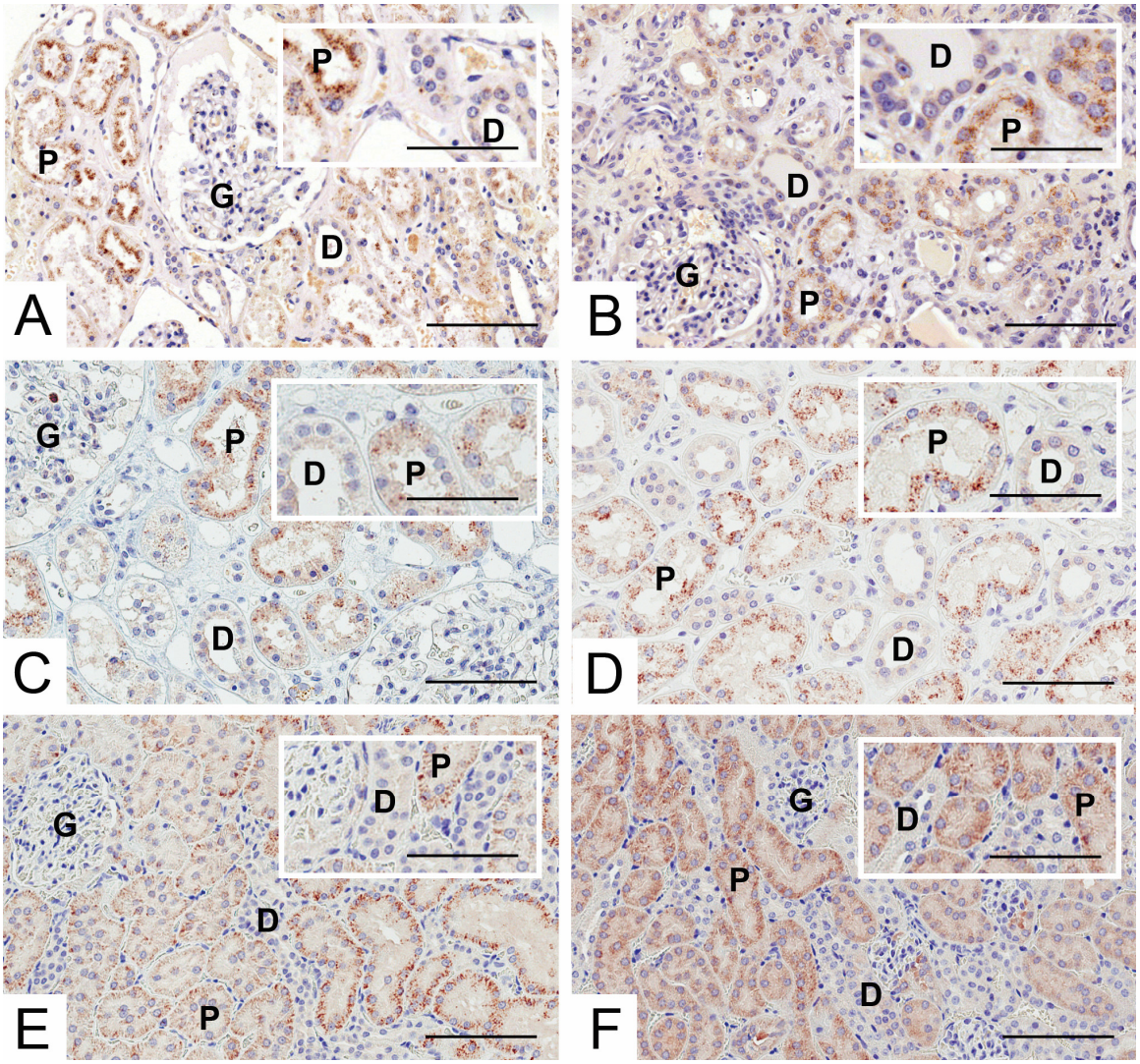

Figure 1.10. Immunolocalisation of FGFr4 in formalin-fixed, paraffin-embedded (A-D) Human, (E) Rat and (F) Mouse Kidney Cortex. (A) In human kidney cortex, FGFr4 was localised to proximal and distal tubule where it had a punctate appearance. N=1, n=1. (B) In human kidney cortex, FGFr4 was localised to proximal and distal tubule where it had a punctate appearance. N=1, n=1. (C) In human kidney cortex, FGFr4 was localised to proximal and distal tubule where it had a punctate appearance. N=1, n=1. (D) In human kidney cortex, FGFr4 was localised to proximal and distal tubule where it had a punctate appearance. N=1, n=1. (E) In rat kidney cortex, FGFr4 was localised to proximal tubule where it had a punctate appearance. N=1, n=1. (F) In mouse kidney cortex, FGFr4 was localised to proximal tubule where it had a punctate appearance. N=1, n=1. In all cases, immunoreactivity for the protein of interest appears brown and the haematoxylin co-stain identifying cell nuclei appears blue. All images are representative of one section per sample. The human kidney cortex TMA image is representative of one field of view (A), with larger human kidney cortex samples (B-D) and rat (E) and mouse (F) kidney cortex samples being representative of 10 fields of view. IHC performed by LS (A-C) and JG (D-F). Images captured by RW. Image analysis performed by RW. P = proximal tubule, D = distal tubule, G= glomerulus. Bars = 100µm. Insert bars = 60µm.

Receptor	Species	PT (% positive)	DT (% positive)
FGFr4	Human	100	100
	Human	100	100
	Human	100	100
	Human	100	100
FGFr4	Rat	100	0
FGFr4	Mouse	100	0

Table 1.6. Summary of the expression pattern of FGFr4 in formalin-fixed, paraffin-embedded human, rat and mouse kidney sections. FGFr4 was expressed in 100% of human proximal tubule viewed (N=4, n=4; 37/37, 167/167, 668/668, 562/562). FGFr4 was expressed in 100% of human distal tubules (N=4, n=4; 18/18, 71/71, 224/224, 190/190). In rat kidney, FGFr4 was expressed 100% of proximal tubules (N=1, n=1; 433/433) and 0% of distal tubule cells (N=1, n=1; 0/136). In mouse kidney, FGFr4 was expressed 100% of proximal tubules (N=1, n=1; 613/613) and 0% of distal tubule cells (N=1, n=1; 0/197). Values presented are representative of all proximal and distal tubules observed in human kidney cortex TMA sections obtained from one field of view, or representative of 10 fields of view in larger human kidney cortex sections and rat and mouse kidney cortex sections. Quantification performed by RW.

Klotho, NaP_i IIa, NCX1 and PMCA1 Immunolocalisation in Human Kidney Cortex

The expression patterns of Klotho, sodium/phosphate co-transporter type IIa (NaP_i IIa), sodium/calcium exchanger type 1 (NCX1) and plasma membrane calcium ATPase type 1 (PMCA1) in the kidney are well documented in the literature (Biber et al. 1996; Glendenning et al. 2000; Magyar et al. 2002; Murer et al. 2003; Palm et al. 2010). As such, to confirm the specificity of antibodies selected for use in the primary human renal cell characterisation work, immunohistochemistry was performed for each protein in FFPE human kidney sections. A non-commercially available antibody raised against human NaP_i IIa was used (the antibody was a gift from Professor Jürg Biber, University of Zurich, Switzerland). NaP_i IIa expression was specific to the proximal tubule (Figure 1.11C and 11.1D); 100% of proximal tubule cells were positive for NaP_i IIa and 100% of distal tubule cells were negative (Table 1.7). Commercially available antibodies were used for Klotho, NCX1 and PMCA1. Klotho exhibited both proximal and distal tubule expression (Figure 1.11A and 1.11B); 100% of proximal tubule cells were positive for Klotho and 100% of distal tubule cells were negative (Table 1.7). Expression was, however, stronger in the distal tubule as indicated by the darker brown immunoreactivity in those tubules. NCX1 and PMCA1 were both localised to the distal tubule. Both proteins exhibited strong basolateral distal tubule expression (Figure 1.11E and 1.11F, respectively). For both, 100% of proximal tubules were negative and 100% of distal convoluted tubule cells were positive (Table 1.7).

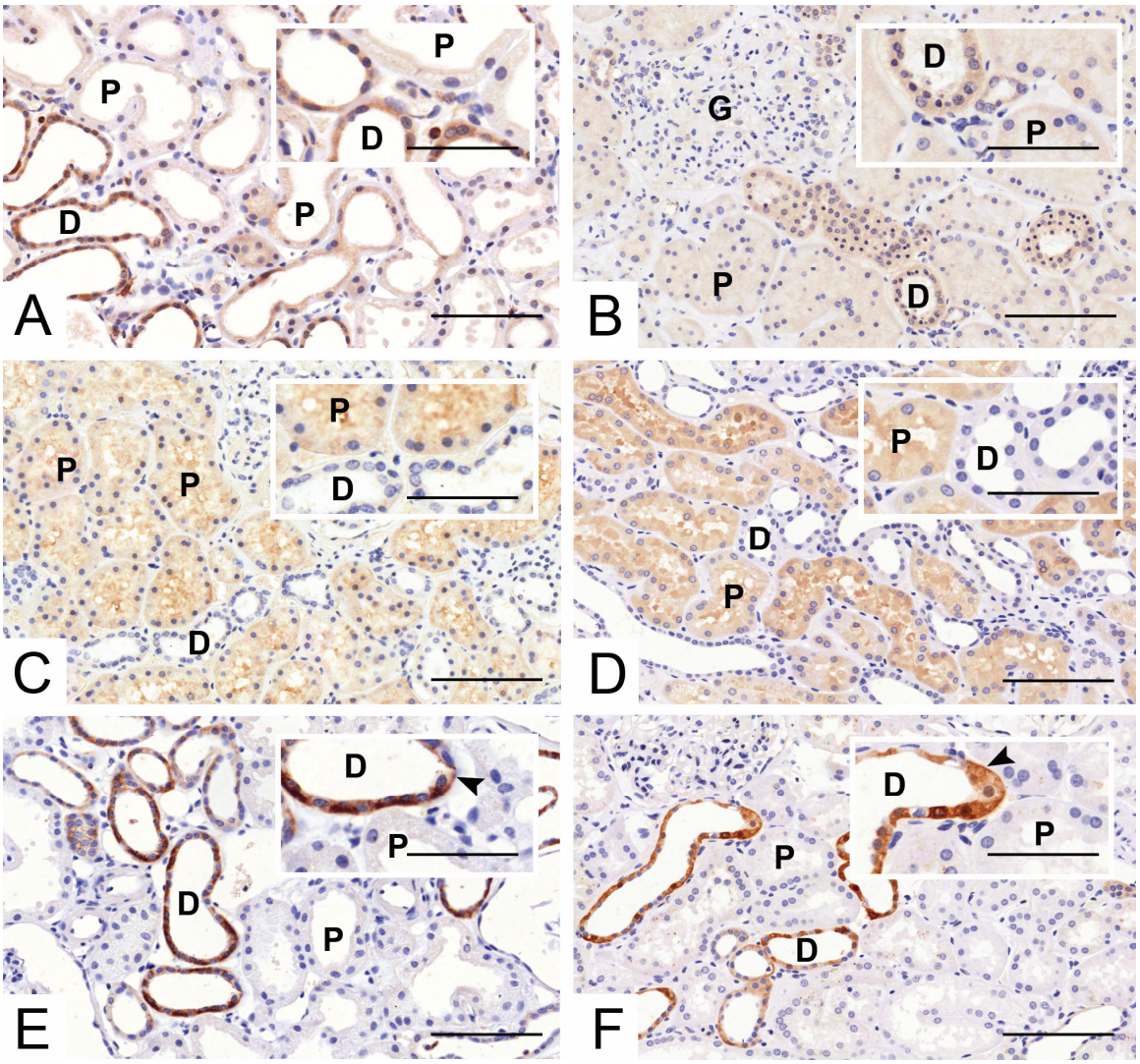

Figure 1.11. Immunolocalisation of Klotho, NaP_i IIa, NCX1 and PMCA1 in formalin-fixed, paraffin-embedded human kidney. (A&B) Klotho immunoreactivity was localised to the distal tubule and proximal tubule cell cytoplasm. In both samples, immunoreactivity was stronger in the distal tubule than the proximal tubule as evidenced by darker brown staining. N=2, n=2. (C&D) In both samples, NaP_i IIa immunoreactivity was localised to the proximal tubule. N=2, n=2. (E) NCX1 was localised to distal convoluted tubule cell cytoplasm and basolateral membrane (arrow head). N=1, n=1. (F) PMCA1 was localised to distal convoluted tubule cell cytoplasm and basolateral membrane (arrow head). N=1, n=1. In all cases, immunoreactivity for the protein of interest appears brown and the haematoxylin co-stain identifying cell nuclei appears blue. All images are representative of 10 fields of view of one section per sample. IHC performed by LS. Images captured by RW. Image analysis performed by RW. P = proximal tubule, D = distal tubule, G= glomerulus. Bars = 100µm. Insert bars = 60µm.

Protein	Species	PT (% positive)	DT (% positive)
Klotho	Human	100	100
	Human	100	100
NaP_i IIa	Human	100	0
	Human	100	0
NCX1	Human	0	100
PMCA1	Human	0	100

Table 1.7. Summary of the expression pattern of NaP_i IIa, NCX1 and PMCA1 in formalin-fixed, paraffin-embedded adult human kidney sections. Klotho was localised to 100% of human proximal (N=2, n=2; 242/242, 208/208) and distal (N=2, n=2; 145/145, 84/84) tubules viewed. NaP_i IIa was expressed in 100% of human proximal tubules viewed (N=2, n=2; 332/332, 283/283) and 0% of distal tubules viewed (N=2, n=2; 0/157, 0/94). NCX1 was expressed in 0% of proximal tubules viewed (N=1, n=1, 0/158) but was expressed in 100% of distal tubules viewed (N=1, n=1, 75/75). PMCA1 was expressed in 0% of proximal tubules viewed (N=1, n=1, 0/286), but was expressed in 100% of distal tubules viewed (N=1, n=1, 141/141). All data are representative of one section per sample. All values presented are representative of all proximal and distal tubules observed in human kidney cortex in 10 representative fields of view. Quantification performed by RW.

Proliferation and Apoptosis Viability Assays

The incorporation of 5-bromo-2'-deoxyuridine (BrdU) into actively proliferating cell nuclei, and terminal deoxyribonucleotidyl transferase-mediated dUTP nick end labelling (TUNEL) of apoptotic cell nuclei, was used to assess the overall viability of renal cells in culture over time.

A representative immunofluorescent image of BrdU incorporation into new DNA within proliferating cell nuclei is shown in Figure 1.12A. At day 5 of culture, the percentage of BrdU-positive cell nuclei was 12.93 ± 1.36% (mean ± SD; N=3, n=3) of total cell nuclei. By day 15, the percentage of BrdU-positive cell nuclei had significantly increased to 84.07 ± 4.99% (mean ± SD; N=3, n=3; $p < 0.001$ ***) compared to that at day 5, as determined using a one-way ANOVA and a post-hoc Tukey test (Figure 1.12C).

A representative light microscopy image of apoptotic cell nuclei in culture is shown in Figure 1.12B. At day 5 of culture, the percentage of cells undergoing apoptosis was 0.87 ± 0.12% (mean ± SD; N=3, n=3) of total cells. By day 15, the percentage of total cells undergoing apoptosis was not significantly different (1.20 ± 0.40%; mean ± SD; N=3, n=3; $P > 0.05$) to that at day 5, as determined using a one-way ANOVA and a post-hoc Tukey test (Figure 3.2D).

Overall, human renal cell viability was high throughout the culture time course as determined by high percentage of cells undergoing proliferation and a low percentage of cells undergoing apoptosis any each time point assessed.

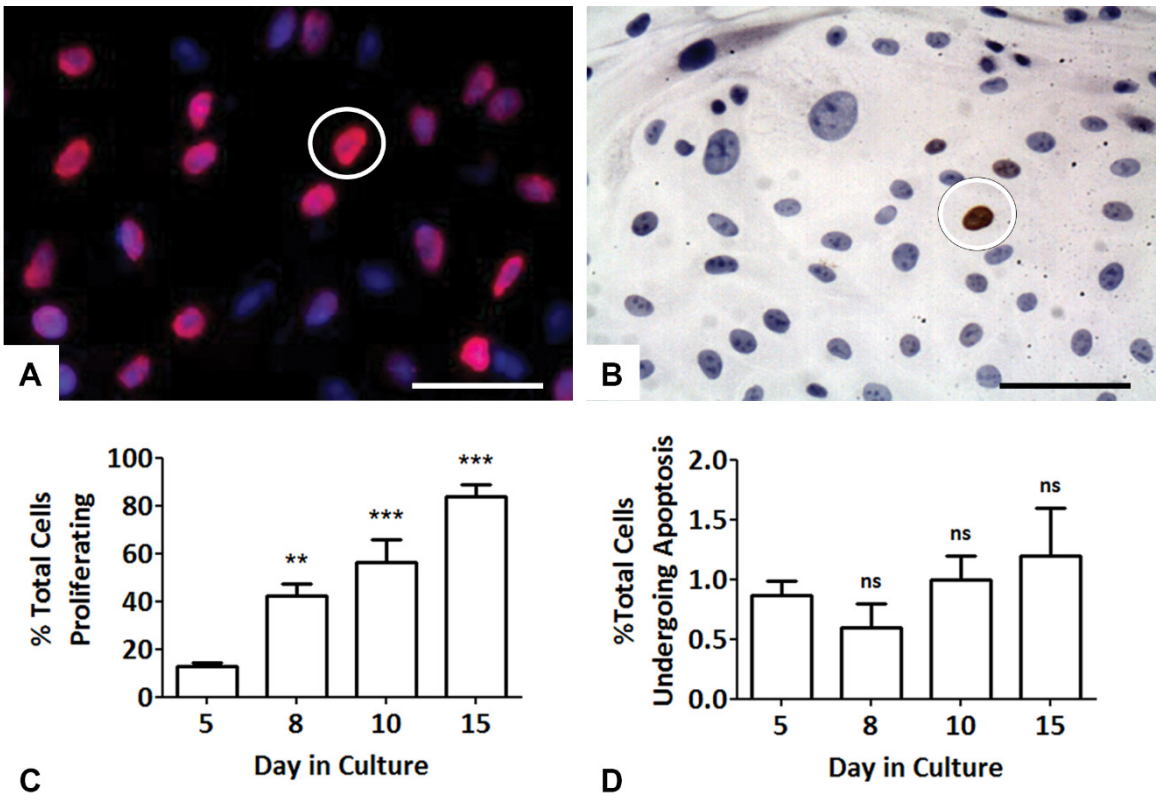

Figure 1.12. Assessment of primary human proximal and distal tubule cell co-culture viability using proliferation and apoptosis assays. (A) A representative image of proliferating cell nuclei after 8 days in culture. All cell nuclei are Hoechst positive (blue) and proliferating cell nuclei are also BrdU-positive (red; circled). Bar = 50µm. (B) A representative image of apoptotic TUNEL cell nuclei after 8 days in culture. All cell nuclei are haematoxylin positive (blue) and apoptotic cell nuclei also appear DAB positive (brown; circled). Bar = 50µm. (C) At day 5, 12.93 ± 1.36% (mean ± SD; N=3, n=3) of all cell nuclei were BrdU-positive. At day 8, there was a significant increase in BrdU-positive cell nuclei (42.28 ± 5.15%; mean ± SD; N=3, n=3; $p < 0.01$ **) compared to that at day 5. Significant increases in BrdU-positive cell nuclei were also seen at day 10 (56.57 ± 9.47%; mean ± SD; N=3, n=3; $p < 0.001$ ***) and day 15 (84.07 ± 4.99; mean ± SD; N=3, n=3; $p < 0.001$ ***) compared to day 5. Significant differences were identified using a one-way ANOVA and a post-hoc Tukey test. Random snapshots were taken such that a minimum of 100 total cells were counted at each time point per coverslip. (D) At day 5, 0.87 ± 0.12% (mean ± SD; N=3, n=3) of cells were apoptotic. At day 8, there was no significant difference in the percentage of apoptotic cells (0.60 ± 0.20%; mean ± SD; N=3, n=3; $p > 0.05$ ns) compared to that at day 5. No significant difference in the percentage of apoptotic cells was seen at day 10 (1.00 ± 0.20%; mean ± SD; N=3, n=3; $p > 0.05$ ns) nor at day 15 (1.20 ± 0.40%; mean ± SD; N=3, n=3; $p > 0.05$ ns) when compared to that at day 5. A one-way ANOVA and a post-hoc Tukey test was used to test for significant differences between time points. Random snapshots were taken such that a minimum of 500 total cells were counted per coverslip at each time point. Cell culture and assays performed by RW and LS. Counting of cell nuclei performed by LS. Statistical analysis performed by RW.

Maintenance of Phenotype and Morphology

Cadherins are calcium-dependent adhesion proteins (Prozialeck et al. 2004). N-Cadherin is the predominant cadherin in the proximal tubule whilst E-Cadherin is the predominant cadherin in the distal tubule (Prozialeck et al. 2004). In this study, immunohistochemistry on formalin-fixed, paraffin-embedded human kidney sections is in agreement with the literature; N-Cadherin was localised to the proximal tubule (Figure 1.13A) and E-Cadherin to distal tubule (Figure 13.3B). In the section stained for N-Cadherin, 100% of proximal tubules were positive, and 100% of distal tubules were negative (Figure 1.13A). In the section stained for E-Cadherin, 100% of proximal tubules were negative, and 100% of distal tubules positive (Figure 1.13B). Further confirmation of the antibody specificity for each tubule type was provided using dual immunofluorescence on a snap-frozen adult human kidney section (Figure 1.13C), where again, N-Cadherin was localised to the proximal tubule, and E-Cadherin to the distal tubule. As such, both antibodies were used to respectively identify the presence of primary human proximal and distal tubule cells in culture by dual immunofluorescence (Figure 1.13D). To confirm the presence of both cell types in culture over the culture time course, snapshots of dual immunofluorescent stainings were taken, and by counting cells individually (a minimum of 500 cells at each time point were counted), the percentage of proximal and distal tubule cells out of the total number of cells at day 5, day 8, day 10 and day 15 of culture was determined. Results are plotted graphically in Figure 1.13E. At day 0, the percentage of proximal and distal tubule cells was 57.9 ± 4.3 and 42.1 ± 4.3 (mean ± SD; N=3, n=3). After 5 days in culture, the percentage of proximal and distal tubule cells was 47.9 ± 4.8% and 52.1 ± 4.8% (mean ± SD; N=3, n=3), at day 8, it was 46.6 ± 2.7% and 53.4 ± 2.7% (mean ± SD; N=3, n=3), at day 10, it was 43.1 ± 3.4% and 56.9 ± 3.4% (mean ± SD; N=3, n=3), and at day 15 it was 40.7 ± 3.4% and 59.3 ± 3.4% (mean ± SD; N=3, n=3), respectively. A two-way ANOVA with Bonferroni post-test revealed a significant difference in the percentage of proximal and distal tubule cells at day 0 ($P<0.001$ ***), at day 10 ($P<0.01$ **) and at day 15 ($P<0.001$ ***). No significant difference in the two populations of cells were identified at day 5 or day 8.

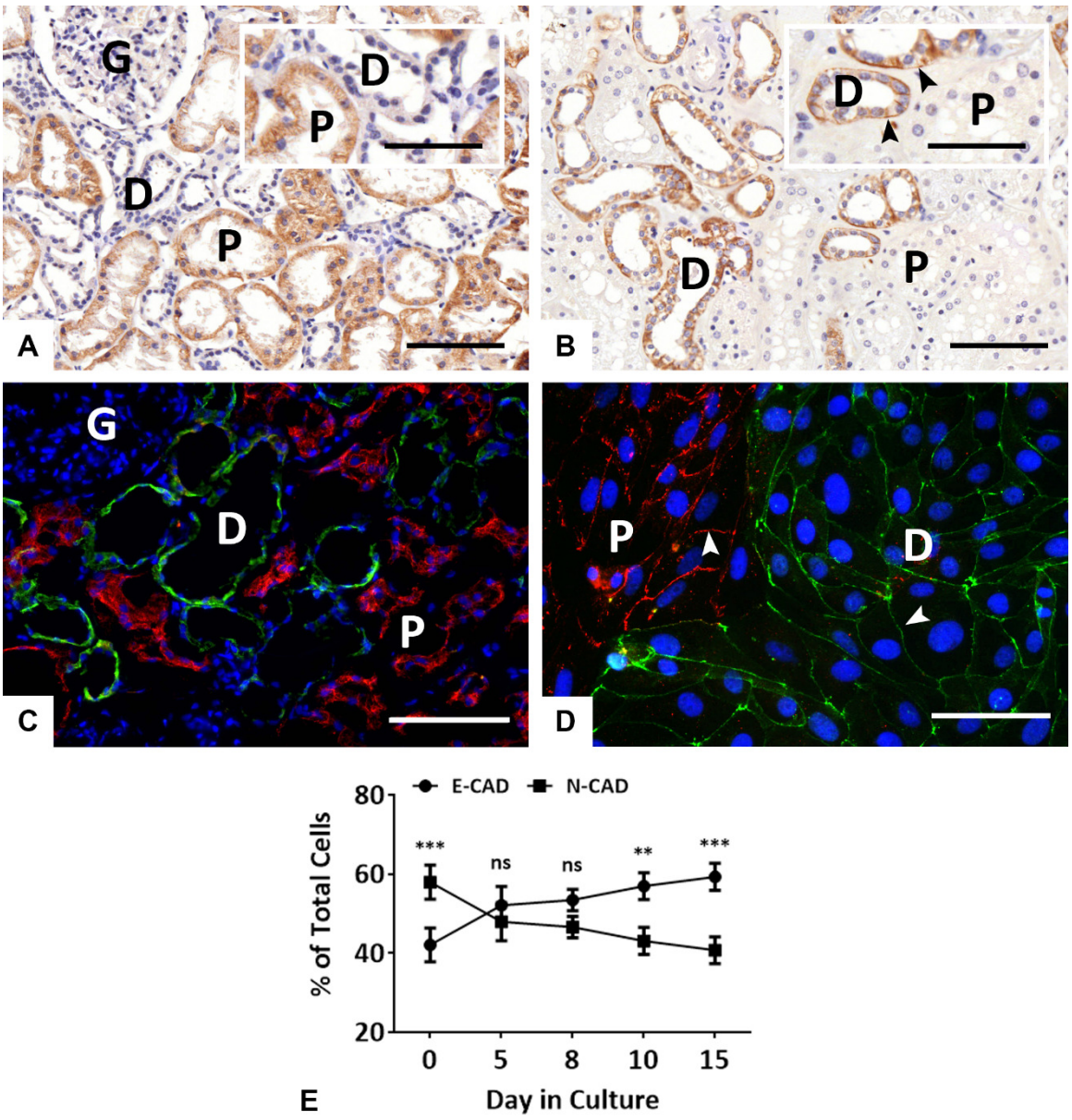

Figure 1.13. N-Cadherin and E-Cadherin Expression in FFPE human kidney cortex and primary human proximal and distal tubule cells. (A) In FFPE human kidney cortex, N-Cadherin was specifically localised to the proximal tubule. 100% of proximal tubules viewed were positive (N=1, n=1, 325/325) and 100% of distal tubules viewed were negative (N=1, n=1, 173/173). N-Cadherin appears brown and the haematoxylin co-stain identifying cell nuclei appears blue. Image presented is representative of five fields of view from one section. Bar = 100µm. Insert bar = 60µm. (B) In FFPE human kidney cortex, E-Cadherin was specifically localised to the distal tubule. 100% of distal tubules viewed were positive (N=1, n=1, 186/186) and 100% of proximal tubules viewed were negative (N=1, n=1, 278/278). E-Cadherin appears brown and the haematoxylin co-stain identifying cell nuclei appears blue. Note the clear cell membrane staining (arrow heads). Image presented is representative of five fields of view from one section. Bar = 100µm. Insert bar = 60µm. (C) In fresh frozen human kidney cortex, immunofluorescence localised N-Cadherin to the proximal tubule and E-Cadherin to the distal tubule. N-Cadherin appears red, E-Cadherin appears green, and the Hoechst co-stain identifying cell nuclei appears blue. Image presented is representative of five fields of view from one section. N=1, n=1. Bar = 200µm. (D) Dual immunofluorescence confirmed the presence of N-Cadherin-positive proximal tubule cells and E-Cadherin-positive distal tubule cells in primary human kidney cell culture. N-Cadherin appears red, E-Cadherin appears green, and the Hoechst co-stain identifying cell nuclei appears blue. Note the clear membrane staining (arrow heads). Bar = 20µm. (E) At day 0, the percentage of proximal and distal tubule cells was 57.9 ± 4.3 and 42.1 ± 4.3 (mean ± SD; N=3, n=3). At day 5, the percentage of proximal and distal tubule cells was 47.9 ± 4.8% and 52.1 ± 4.8% (mean ± SD; N=3, n=3), at day 8 it was 46.6 ± 2.7% and 53.4 ± 2.7% (mean ± SD; N=3, n=3), at day 10 it was 43.1 ± 3.4% and 56.9 ± 3.4% (mean ± SD; N=3, n=3), and at day 15 it was 40.7 ± 3.4% and 59.3 ± 3.4% (mean ± SD; N=3, n=3). A two-way ANOVA with a Bonferroni post-test revealed significant differences between the percentage of proximal and distal tubule cells at day 0 ($P<0.001$ ***), day 10 ($P<0.01$ **) and day 15 ($P<0.001$ ***). No significant difference in the two populations of cells was identified at day 5 or day 8 ($P>0.05$ ns). ns = not significant. P = proximal tubule. D = Distal tubule. IHC/IF performed by LS. Images captured by RW. Quantification of tubules performed by RW. Cell culture and assays performed by RW and LS. Quantification of E- and N-Cadherin positive cells performed by LS. Statistical analysis performed by RW.

Figures 1.14A and 1.14B show the typical morphological appearance of primary human renal cells cultured *in vitro*. Note the typical cobblestone morphology previously associated with cultured primary human renal cells (Wilmer et al. 2010). Scanning electron microscopy revealed the presence of microvilli, which are characteristic of the proximal tubule cells *in vivo,* on the cell membranes of day 5 proximal tubule cells grown on semi-permeable transwells (Figure 1.14C and 1.14D). Additionally, expression of vimentin, a filament protein expressed by dedifferentiated renal cells (Bonventre 2003; Hallman et al. 2008) was assessed. Although Western blotting of cell lysates prepared from cells cultured for 5, 8, 10 and 15 days did reveal the presence of vimentin, expression did not increase over time indicating that dedifferentiation did not occur (Figure 1.14E). Human kidney lysate and recombinant human vimentin were used as positive controls and confirm antibody specificity.

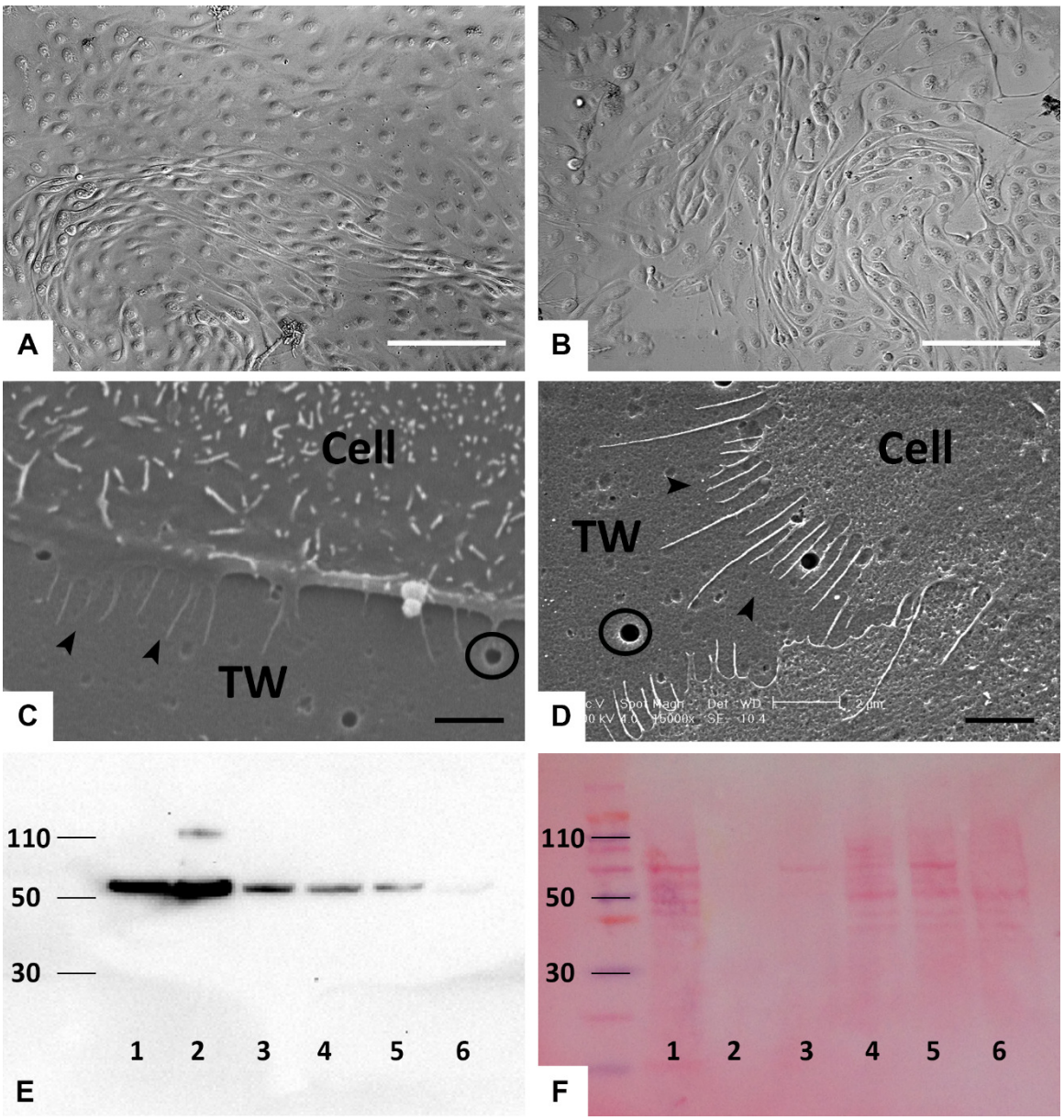

Figure 1.14. Maintenance of primary human renal cell morphology and differentiation in culture. (A&B) Light microscopy images of primary human renal cells displaying typical cobblestone morphology. N=1, n=1. Images presented are representative of 5 fields of view. (C&D) Scanning electron microscopy of day 5 cells grown on semi-permeable transwells shows the presence of microvilli (arrow heads) on a proximal tubule cell membranes. Arrows = microvilli. Circles = 0.4µm pores on the semi-permeable transwells. TW = transwell. Bars = 2µm. N=2 (n=3, n=4). Images presented are representative of 4 fields of view and 10 fields of view respectively. (E) Vimentin Western blot showing a decrease in the expression of vimentin in cell lysates over the culture time course (day 5 to day 15). Lane 1 – 5µg human cortex lysate; Lane 2 – 0.2µg recombinant human vimentin; Lane 3 – 1.25µg total protein from day 5 cells; Lane 4 – 5µg total protein from day 8 cells; Lane 5 – 5µg total protein from day 10 cells; Lane 6 – 5µg total protein from day 15 cells. The single band observed is at the expected molecular weight of 57kDa. N=1, n=1. (F) Ponceau S staining of the same Western blot membrane showing the protein loading in each lane. Cell culture, SEM and Western blot performed by RW.

ERK Activation and Mineralisation Assays

Acute (10 minute) treatment with buffer containing 1µg/ml FGF23 induced ERK activation in primary human renal cells at 8 days in culture, an effect that could be blocked by co-incubation with buffer also containing 10µg/ml of a commercially available MEK inhibitor (U1026) (Figure 1.15A). Western blotting of respective cell lysates shows a more intense phosphorylated-ERK (pERK) band in the lysate of cells treated with buffer containing 1µg/ml FGF23 compared to that of control cells (buffer alone) and cells treated with buffer containing 10µg/ml MEK inhibitor (U1026). Equal loading of protein in each lane was confirmed by stripping the membrane and re-probing for total-ERK (Figure 1.15A). As FGF23 signals though FGFr via the MAPK pathway (White et al. 2001), the fact that the cultured cells respond in the same fashion provides evidence that the cells functionally similar to those *in vivo*. Von Kossa's mineralisation assay revealed mineral deposition in primary human renal cells under control conditions (Figure 1.15K-N). Over time there was a gradual increase in mineral deposition as determined using a one-way ANOVA and post-hoc Tukey test; compared to cells at day 5 of which 4.4 ± 0.2% (mean±SD; N=3, n=3) possessed mineral deposits, 5.2 ± 0.4% (mean±SD; N=3, n=3; p> 0.05; ns) of day 8 cells had mineral deposits, 5.8 ± 0.4% (mean±SD; N=3, n=3; p< 0.01; **) of day 10 cells had mineral deposits, and 6.5 ± 0.3% (mean±SD; N=3, n=3; p> 0.01; ***) of day 15 cells had mineral deposits (Figure 1.15B). Von Kossa's mineralisation assay also revealed mineral deposition in primary human renal cells treated for 24 hours with medium containing 2.5mM βGP (a mineralising agent) (Figure 1.15C-F). Over time, a gradual increase in mineral deposition was identified a one-way ANOVA and post-hoc Tukey test; compared to cells at day 5 of which 13.9 ± 0.6% (mean±SD; N=3, n=3) possessed mineral deposits, 15.2 ± 0.4% (mean±SD; N=3, n=3; p> 0.05; ns) of day 8 cells had mineral deposits, 16.5 ± 0.4% (mean±SD; N=3, n=3; p< 0.01; **) of day 10 cells had mineral deposits, and 18.9 ± 0.5% (mean±SD; N=3, n=3; p> 0.01; ***) of day 15 cells had mineral deposits (Figure 1.15B). A two-way ANOVA and Bonferroni post-test, revealed a significant increase in mineral deposition between control and βGP-treated cells at each time point (N=3, n=3; P<0.01; ###) (Figure 1.15B). Von Kossa's mineralisation assay revealed mineral deposition in cells treated for 24 hours with medium containing 10µg/ml of a commercially available MEK inhibitor (Figure 1.15 G-J). The MEK inhibitor, increased mineralisation over time, and in comparison to time-matched controls (N=1, n=1) (Figure 1.15B).

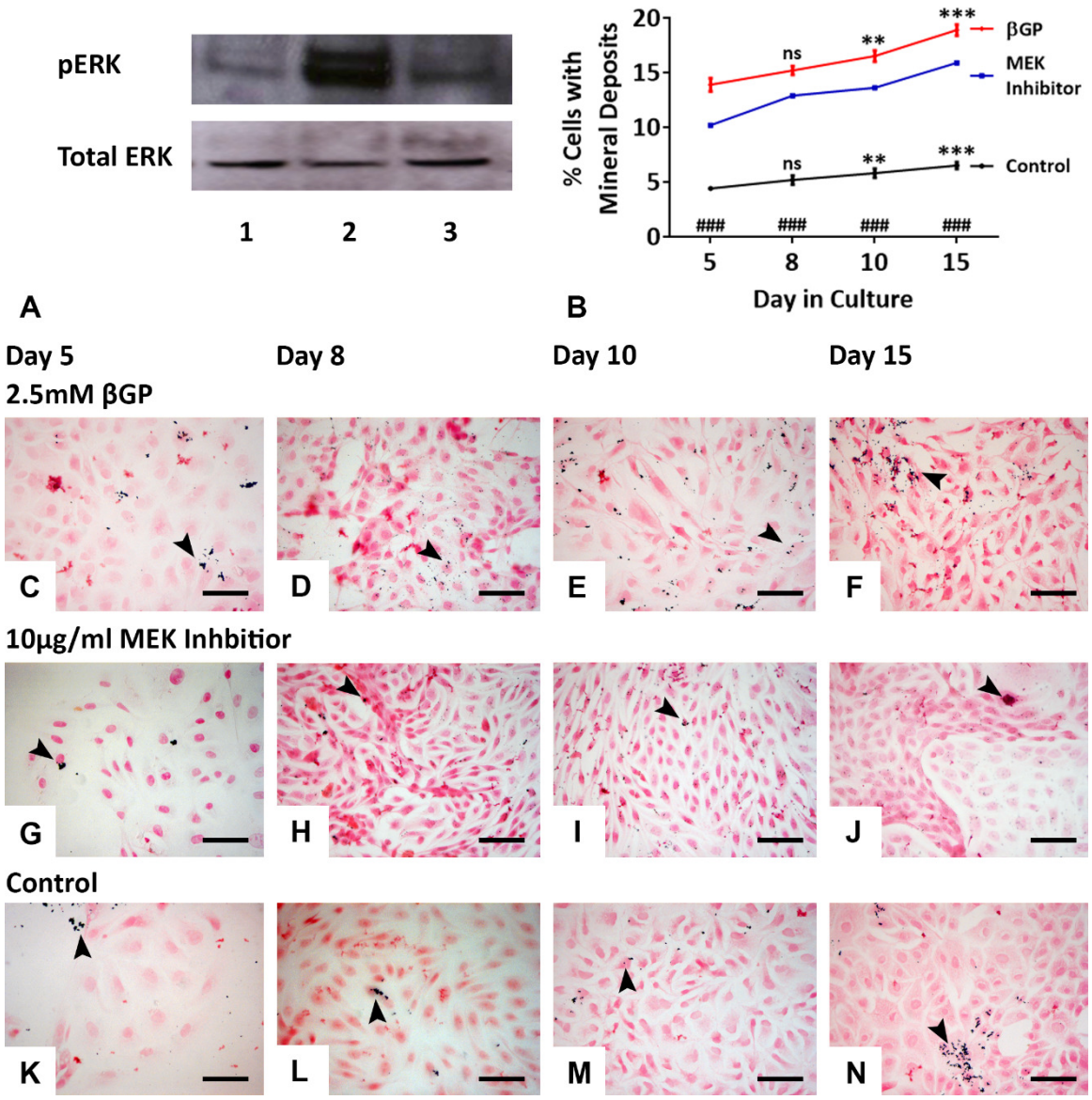

Figure 1.15. Functional characterisation of *in vitro* primary human renal cells. (A) Western blot shows that in comparison to cells treated with control buffer alone (lane 1), 10 minute treatment with buffer containing 1µg/ml FGF23 induced ERK activation (lane 2), a response that could be inhibited by co-incubation with buffer also containing 10 µg/ml of a commercially available MEK inhibitor (lane 3). 5µg total protein was loaded per lane. Total ERK bands confirm equal protein loading in each lane. (N=1, n=1). (B) Using a one-way ANOVA and post-hoc Tukey test, the number of cells with mineral deposits (as determined using von Kossa's mineralisation assay) increased from 4.4 ± 0.2% to 6.5 ± 0.3% (N=3, n=3; mean ± SD; $p<0.001$ ***) in cells treated with control medium from day 5 to day 15 of culture, respectively. Likewise, the number of cells with mineral deposits increased from 13.9 ± 0.6% to 18.9 ± 0.5% (N=3, n=3; mean ± SD; $p<0.001$ ***) in cells treated for 24 hours with medium containing 2.5mM βGP from day 5 to day 15 of culture, respectively. In cells treated for 24 hours with medium containing 10µg/ml MEK inhibitor, 10.2% of cells showed mineral deposits at day 5 compared to 15.9% of cells at day 15 (N=1, n=1). Using a two-way ANOVA and Bonferroni post-test, mineralisation was increased in βGP-treated cells compared to control cells at each time point assessed (N=3, n=3; $P<0.001$; ###). Images of mineral deposition (black dots; arrow heads) using von Kossa's mineralisation assay in (K-N) control cells, (G-J) 10µg/ml MEK inhibitor-treated cells, and (C-F) 2.5mM β-GP treated cells at day 5, 8, 10 and 15 days in culture, respectively. Images are representative of 5 random fields of view from which 500 cells were assessed. Bars = 50µm. Cell culture and assays performed by RW and LS. Western blot by LS. Quantification of mineral deposition performed by LS. Statistical analysis performed by RW.

Expression of FGFr1-4, Klotho, NaP_i IIa, NCX1 and PMCA1 in Cultured Cells

Using the same antibodies that were used in the earlier localisation study, the expression of FGFr1, FGFr2, FGFr3, FGFr4, Klotho, NaP_i IIa, NCX1 and PMCA1 were identified in day 8 primary human renal cells (Figure 1.16 and 1.17). Day 8 was chosen as the time point to investigate P_i- and FGF23-induced changes in protein expression, as it represented a time in culture when cells were neither too sparse nor too confluent (day 10 and day 15 cells were confluent and began to form domes and ridges *i.e.* they were not monolayers).

FGFr1-4 Immunocytochemistry

Fibroblast growth factor receptors 1-4 (FGFr1-4) were expressed by primary human renal cells cultured on collagen type-IV coated glass coverslips after 8 days culture under control conditions (Figure1.16A, D, G and J, respectively). Control culture conditions denote cells grown in P_i-containing medium. Whether P_i and FGF23 manipulations of the culture medium affect the expression of FGFr1-4, was investigated in cells at day 8 of culture in one of three treatment conditions. The three treatment conditions were; *i.* P_i-containing medium (control culture medium), *ii.* P_i-free medium, or *iii.* P_i-containing medium (control culture medium) plus FGF23. Figure 1.16 shows that for each receptor, expression was not regulated by removal of P_i from, nor the addition of FGF23 to the culture medium, compared to that of cells grown under normal conditions in P_i-containing medium; the immunocytochemical staining (the brown DAB colour) appears similar for each individual receptor across each of the treatment conditions.

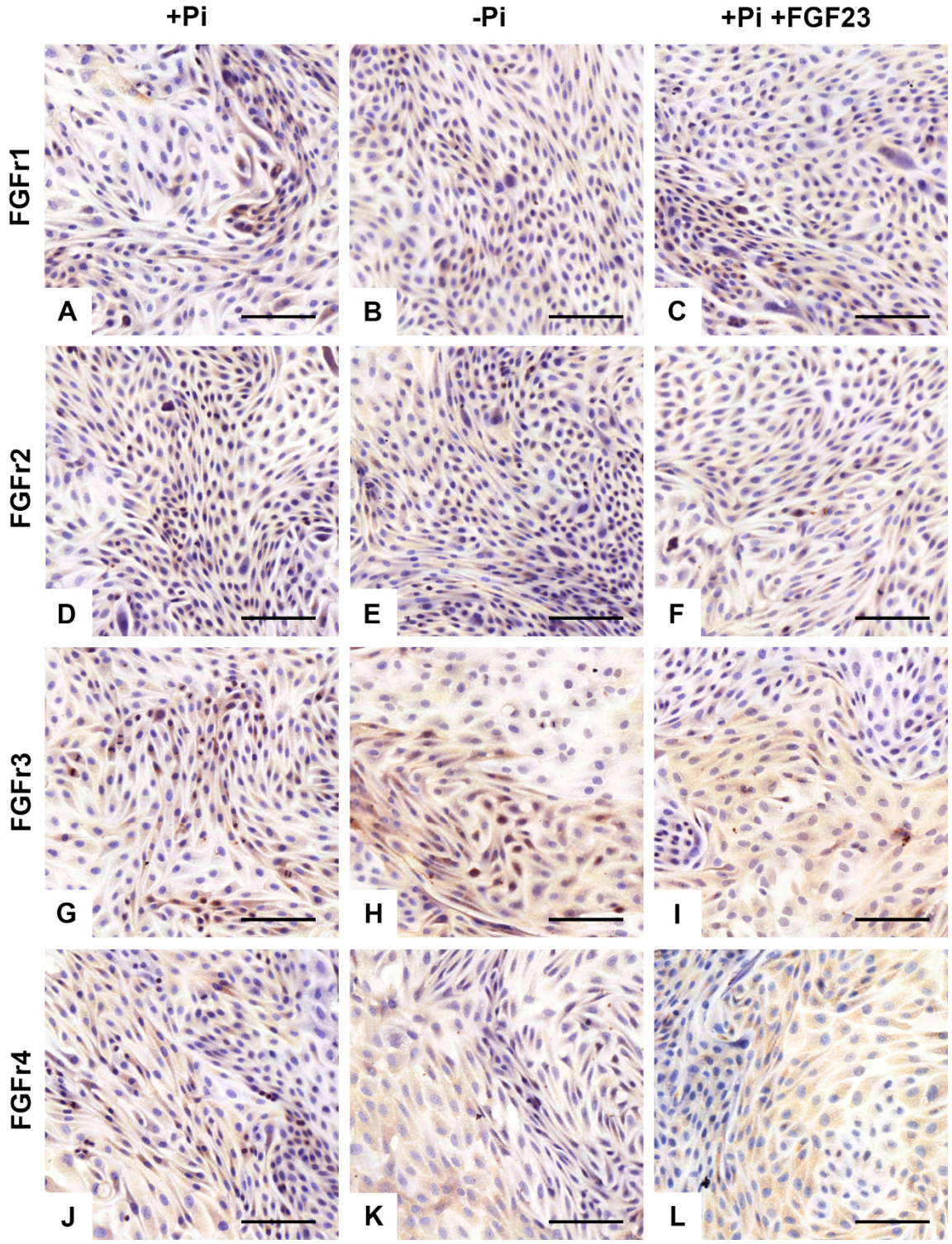

Figure 1.16. Expression of FGFr1-4 in day 8 primary human renal cells cultured for 24 hours in P_i-containing medium, P_i-free medium or P_i-containing medium plus FGF23, Klotho and heparin. (A, B, C) Immunoreactivity of FGFr1, (D, E, F) FGFr2, (G, H, I) FGFr3 and (J, K, L) FGFr4 in day 8 primary human renal cells cultured for 24 hours in (A, D, G, J) P_i-containing medium, (B, E, H, K) P_i-free medium and (C, F, I, L) P_i-containing medium plus 1µg/ml FGF23, 0.1µg/ml Klotho and 10µg/ml heparin. Immunoreactivity for the proteins of interest appears brown, and the haematoxylin co-stain identifying cell nuclei appears blue. No changes in protein expression were observed for each of the individual receptors in any condition. Images are representative of 5 fields of view, and of cells grown collagen type IV-coated glass coverslips. N=1, n=1 (FGFr1), N=1, n=1 (FGFr2), N=2, n=2 (FGFr3), N=2, n=2 (FGFr4). Bars = 150µm. Cell culture and assays performed by RW and LS.

Klotho, NaP_i IIa, NCX1 and PMCA1 Immunocytochemistry

Klotho and NaP_i IIa were expressed by primary human renal cells cultured normal on semi-permeable filter supports (transwells) after 8 days culture under control conditions (Figure 1.17A and 1.17D, respectively). NCX1 and PMCA1 were expressed by primary human renal cells cultured on collagen type-IV coated glass coverslips after 8 days culture under control conditions (Figure 1.17G and 1.17J, respectively). Normal culture conditions denote cells grown in P_i-containing medium. Whether P_i and FGF23 manipulations of the culture medium affect the expression of Klotho, NaP_i IIa, NCX1 and PMCA1, was investigated in cells at day 8 of culture in one of three treatment conditions. The three treatment conditions were; *i.* P_i-containing-medium (control culture medium), *ii.* P_i-free medium, or *iii.* P_i-containing (control culture medium) medium plus FGF23. No differences in Klotho immunoreactivity were observed in any of the conditions (Figure 1.17A-C). NaP_i IIa immunoreactivity was increased by culturing incubating cells in P_i-free medium (Figure 1.17E) compared to cells cultured in P_i-containing medium (Figure 1.17D). No difference was seen for NaP_i IIa following incubation with FGF23 (Figure 1.17F). NCX1 immunoreactivity was detected in the cell cytoplasm of cells cultured control P_i-containing medium (Figure 1.17G) and P_i-free medium (Figure 1.17H). Incubation with FGF23 induced NCX1 immunoreactivity at the cell membrane (Figure 1.17I). Compared to cells grown in P_i-containing medium (Figure 1.17J) and those grown in P_i-containing medium plus FGF23 (Figure 1.17L), PMCA1 immunoreactivity appeared to be upregulated in cells cultured in P_i-free medium (Figure 1.16K), where it was localised predominantly to the cell membrane. Expression was assessed by comparing the immunocytochemical staining (the brown DAB colour) across each of the treatment conditions.

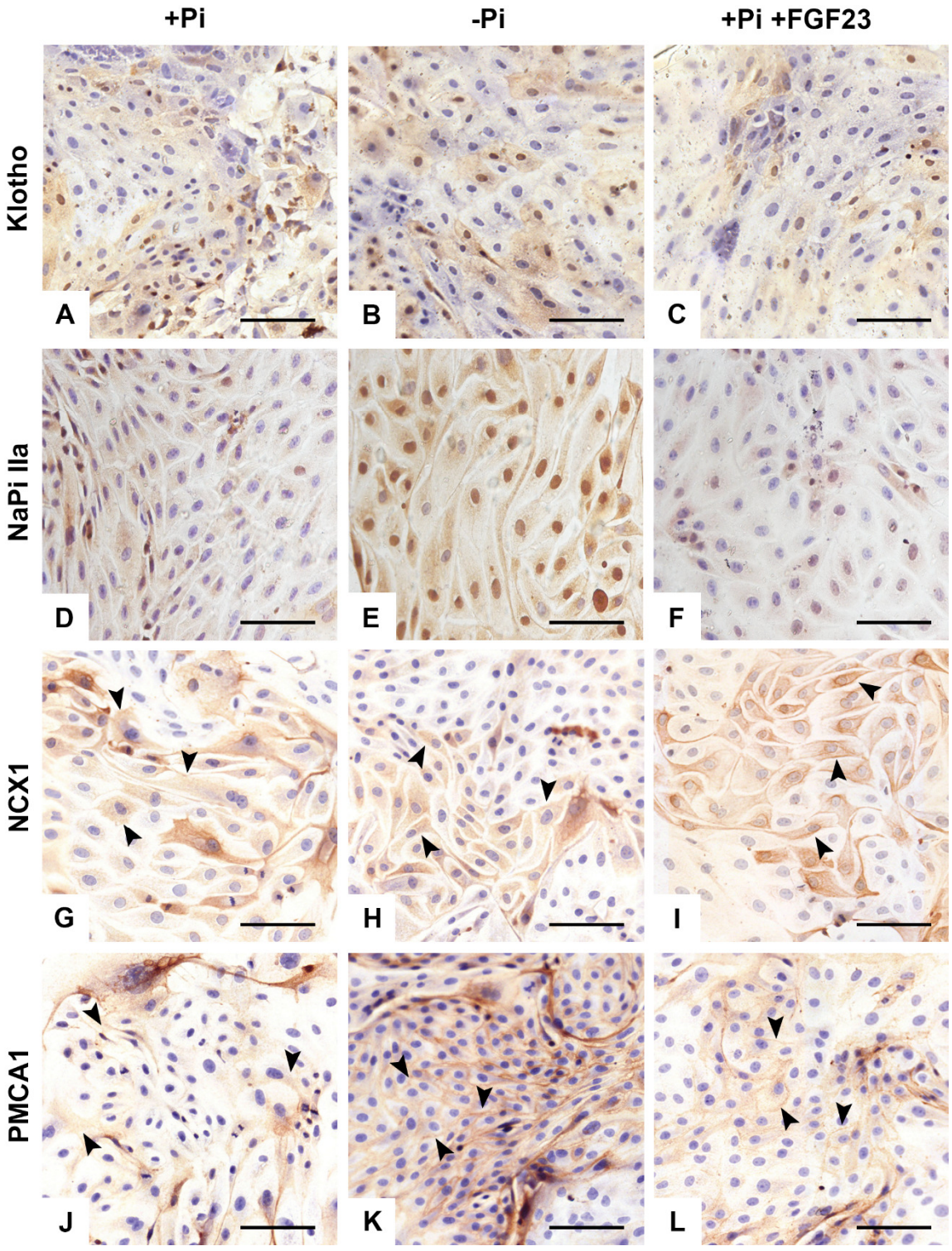

Figure 1.17. Expression of Klotho, NaP_i IIa, NCX1 and PMCA1 in day 8 primary human renal cells cultured for 24 hours in P_i-containing medium, P_i-free medium or P_i-containing medium plus FGF23, Klotho and heparin. Immunoreactivity of (A, B, C) Klotho, (D, E, F) NaP_i IIa, (G, H, I) NCX1 and (J, K, L) PMCA1 in day 8 cells cultured for 24 hours in (A, D, G, J) P_i-containing medium, (B, E, H, K) P_i-free medium and (C, F, I, L) P_i-containing medium plus 1µg/ml FGF23, 0.1µg/ml Klotho and 10µg/ml heparin. (A-C) No difference in Klotho immunoreactivity was observed across each of the treatment conditions. (D-F) NaP_i IIa immunoreactivity was increased in cells treated with P_i-free medium compared to the other treatment conditions. (G-I) NCX1 immunoreactivity was increased at the cell membrane in cells treated with medium containing FGF23 compared to the other treatment conditions (arrow heads). (J-L) PMCA1 immunoreactivity was increased at the cell membrane in cells treated with P_i–free medium compared to other treatment conditions (arrow heads). Immunoreactivity for the proteins of interest appears brown, and the haematoxylin co-stain identifying cell nuclei appears blue. Images are representative of cells grown on transwells (Klotho and NaP_i IIa) or collagen type IV-coated glass coverslips, (NCX1 and PMCA1), and are representative of 5 fields of view. N=1, n=1 (Klotho), N=3, n=3 (NaP_i IIa +P_i, -P_i), N=1, n=1 (NaP_i IIa +Pi+FGF23), N=1, n=1 (NCX1), N=1, n=1 (PMCA1). Bars = 100µm. Cell culture and assays performed by RW and LS.

NaP$_i$ IIa Immunoreactivity (Biological Replicates)

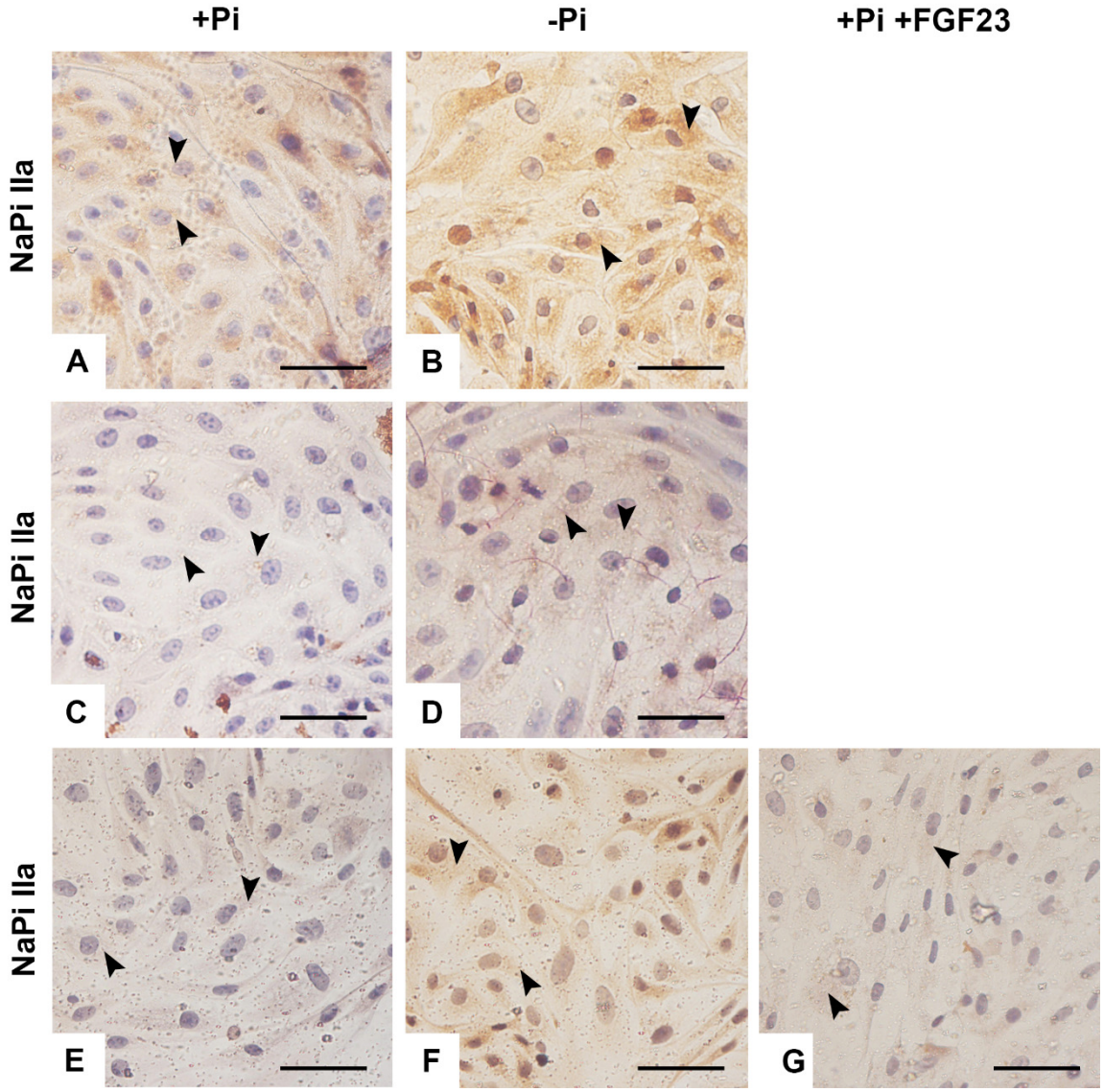

Figure 1.18. Modulation of NaP$_i$ IIa expression primary human renal cells at day 8 of culture in response to 24-hour treatment with P$_i$-containing medium, P$_i$-free medium or P$_i$-containing medium plus FGF23, Klotho and heparin. NaP$_i$ IIa immunoreactivity in P$_i$-containing medium (A, C, E), P$_i$-free medium (B, D, F) and P$_i$-containing medium plus 1µg/ml FGF23, 0.1µg/ml Klotho and 10µg/ml heparin. Compared to cells cultured in P$_i$-containing medium, NaP$_i$ IIa immunoreactivity within each biological sample is increased in cells treated with P$_i$-free medium (A vs B, C vs D, E vs F, respectively) (arrow heads). N=3, n=3 for P$_i$-containing and P$_i$-free conditions. N=1, n=1 for P$_i$-containing conditions plus FGF23. Images are representative of cells grown on transwells, and of 5 fields of view. NaP$_i$ IIa immunoreactivity appears brown, and the haematoxylin co-stain identifying cell nuclei appears blue. Bars = 50µm. Cell culture and assays performed by RW and LS.

NaP_i IIa Western Blotting

The increase in NaP_i IIa expression observed in primary human renal cells at day 8 of culture following 24-hour treatment with P_i–free medium compared to cells cultured in P_i-containing medium, was also detected by Western blotting of cell lysates (Figure 1.19).

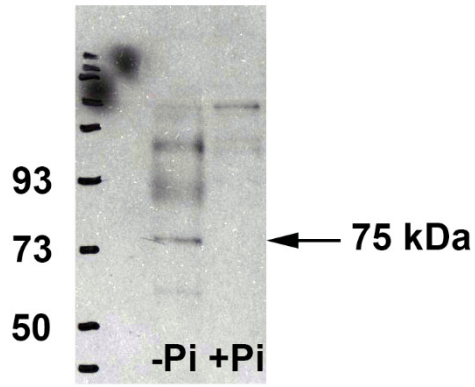

Figure 1.19. NaP_i IIa Western blot of primary human renal cell lysates obtained from cells at day 8 of culture following 24-hour treatment with P_i-containing medium or P_i-free medium. The Western blot shows a clear NaP_i IIa protein band in the cell lysate of cells cultured in P_i-free medium (-P_i) compared to that of cell cultured in P_i-containing medium (+P_i). The ~75kDa band corresponding to the expected molecular mass of NaP_i IIa protein based on its amino acid sequence is indicated with an arrow. 5µg total protein was loaded per lane. The anti-human NaP_i IIa primary antibody used was a gift from Professor Jürg Biber, University of Zurich, Switzerland. (N=1, n=1). Cell culture and assay performed by RW and LS. Western blot by LS.

In summary, immunocytochemistry confirmed the expression of eight key proteins involved in mineral ion metabolism by the kidney (FGFr1, FGFr2, FGFr3, FGFr4, NaP_i IIa, Klotho, NCX1 and PMCA1) in day 8 primary human renal cells. FGFr1, FGFr2, FGFr3, FGFr4, NCX1 and PMCA1 were expressed by day 8 cells cultured on collagen type IV-coated glass coverslips. NaP_i IIa and Klotho were expressed by day 8 cells cultured on semi-permeable filter supports (transwells). No changes in protein expression were observed for FGFr1, FGFr2, FGFr3, FGFr4 or Klotho when cultured in P_i-free medium or P_i-containing medium supplemented with FGF23 compared to that of cells cultured in P_i-containing medium alone. Expression of NaP_i IIa and PMCA1 increased following 24 hours of culture in P_i-free medium compared the expression of both proteins in control P_i-containing medium. Expression of NCX1 increased at the cell membrane following 24-hour culture in P_i-containing medium supplemented with FGF23 compared to the control P_i-containing medium alone. The increase in NaP_i IIa expression in P_i-free medium compared to P_i-containing medium was also detected by Western blotting of cell lysates.

1.7 Discussion

Soft tissue mineralisation owing to the blockade of FGF23-mediated P_i regulation, is a dose-limiting toxicity of novel anti-cancer FGFr inhibitors (Turner and Grose 2010). Rodents are one of the species used during the preclinical safety assessment of such drugs (non-human primates are also used), but how closely do they parallel the *in vivo* human situation? It is currently unknown which FGFr (or group of FGFrs) mediates the homeostatic effects of FGF23, and indeed therefore, which FGFr (or group of FGFrs) evokes ectopic mineral deposition when inhibited. In addition, rodents are frequently used to model chronic kidney disease-mineral bone disorder (CKD-MBD) (S. Moe et al. 2009; Shalhoub et al. 2012; Yang et al. 2010), but their utility for this application has not been directly assessed in terms of the similarity in FGFr localisation along the nephron. Previous data concerning the expression patterns of FGFr1-4 in adult human, rat and mouse kidneys are limited. As such, a comparison of the expression patterns of FGFr1-4 in adult human, rat and mouse kidneys, identifying similarities and/or differences between species in terms of nephron segments and subcellular compartments (*i.e.* apical membrane, basolateral membrane or cytoplasm), using the antibodies selected for use in the following cell characterisation, was performed.

FGFr1 was localized in adult human kidney to the distal tubule which is consistent with previous literature (Floege et al. 1999) and adds to other previous literature where it is merely reported as being expressed in the kidney (Hughes 1997). Using the same antibody, FGFr1 was detected in both proximal and distal tubule cytoplasm in rat. Previously, FGFr1 has been localized to the adult rat distal tubule but not the adult rat proximal tubule (Cancilla et al. 2001). The observation of FGFr1 immunoreactivity in the proximal tubule in adult mouse kidney in this study is consistent with previous reports (Andrukhova et al. 2012; Gattineni et al. 2009), with lack of distal tubule immunoreactivity in contrast to previous reports (Andrukhova et al. 2012; Liu et al. 2008).

FGFr2 was localised in adult human kidney to the distal tubule where it appeared in a punctate pattern, and was not observed in the proximal tubule. This adds to current literature where FGFr2 is merely reported as being expressed in the kidney at a low level with no specific localisation (Hughes 1997). In both adult rat and adult mouse kidney, FGFr2 was expressed in the distal tubule. This is in agreement with previous literature

(Andrukhova et al. 2012; Cancilla et al. 2001). However, no immunoreactivity was detected in the proximal tubule which contrasts with previous literature (Andrukhova et al. 2012; Cancilla et al. 2001).

FGFr3 was predominately localized in human kidney to the proximal tubule brush border membrane with fainter immunoreactivity in distal tubule cell cytoplasm (comparison within samples). This is in contrast to literature where FGFr3 has only been reported as being expressed at a low to no amount in the adult human kidney with no specific information regarding its specific localisation (Hughes 1997) but in line with a more recent literature where it was localized to both the proximal and distal tubule (but with no subcellular localisation *i.e.* at the brush border membrane) (Mutsaers et al. 2014). Using the same antibody, FGFr3 was also detected in adult rat kidney at the proximal tubule brush border membrane. However in contrast, no distal tubule staining was observed. FGFr3 has previously been reported to be expressed in both the proximal and distal tubule in adult rat kidney (Cancilla et al. 2001). In this study, mouse FGFr3 immunoreactivity was detected in the distal tubule cytoplasm, but not in the proximal tubule. Mouse FGFr3 has previously been reported to be expressed in both tubule types (Andrukhova et al. 2012; Cancilla et al. 2001; Liu et al. 2008).

FGFr4 was localised in adult human kidney to both the proximal and distal tubule cell cytoplasm, where it appeared in a punctate pattern, and within each sample, was more abundant in the proximal tubule. This adds to current literature where FGFr4 expression in adult human kidney has been reported as being expressed, but has not been localised to specific tubules (Fuhrmann et al. 1999; Hughes 1997; Mutsaers et al. 2014). In adult rat kidney, FGFr4 was localised only to the proximal tubule where it also appeared in a punctate pattern. Although FGFr4 has been reported as being expressed in adult rat kidney (Horlick et al. 1992), to the best of my knowledge, it has not been localised to specific tubules before. In adult mouse kidney, FGFr4 expression was localised to the cytoplasm of the proximal tubule only, where again it appeared in a punctate pattern. This result in agreement with previous reports of FGFr4 expression in mouse proximal tubules (Andrukhova et al. 2012; Gattineni et al. 2009) but in contrast with previous reports of FGFr4 expression mouse distal tubules (Andrukhova et al. 2012; Liu et al. 2008).

No cross-species comparison of FGFr1-4 localisation in adult human, rat and mouse kidney using the same antibodies has been reported in the literature to date. This study has highlighted that even when using the same antibodies (that are predicted to work in all three species), differences in expression patterns between species are seen. Additionally, this study has localised each FGFr1-4 to specific subcellular in the human kidney for the first time. Differences in FGFr expression patterns between species begs the question, how relevant are rodent models at modelling signalling through FGFrs in humans? Differences in expression patterns could indicate differences in the relative requirement or involvement of each receptor in each species. An *in vitro* human model, expressing FGFr1-4 and Klotho, as well as other proteins involved in mineral ion metabolism by the kidney (including NaP_i IIa, NCX1 and PMCA1) would be more appropriate for studying mineral ion metabolism specifically by human kidney cells.

Current opinion is that expression of Klotho (both mRNA and protein) is confined to the distal tubule (Farrow et al. 2009; Kato et al. 2000; S. Li et al. 2004). However, my studies shows that in humans, although strong Klotho immunoreactivity was indeed identified in the distal tubule, additional faint immunoreactivity was also identified in the proximal tubule. This result adds to the growing literature base indicating that Klotho is actually also expressed by the proximal tubule, albeit to a lesser extent (Andrukhova et al. 2012; Hu et al. 2010). In addition, in this study, NaP_i IIa was localised to the proximal tubule, and NCX1 and PMCA1 were both localised to the distal tubule of human kidney cortex tissue.

No currently available renal cell lines express all the key proteins involved in P_i homeostasis by the kidney, and as such, they cannot be accurately used to study P_i homeostasis by the kidney. Whilst it may possible to transfect cell lines from other species such as Madin-Darby Canine Kidney (MDCK) cells and Lilly Laboratories Culture-Pig Kidney (LLC-PK1) cells with 'missing' proteins, there are a number of associated problems. For example, transfecting MDCK cells with NaP_i IIa, results in protein expression on both apical and basolateral membranes (Quabius et al. 1996), an expression pattern not consistent with that found *in vivo* where expression is confined to apical membranes (Gattineni et al. 2009). In addition, MDCK strain 1 cells have a distal tubule background (Svennevig et al. 1995), and distal tubule cells do not express NaP_i IIa

naturally. Although human kidney cell lines also exist (e.g. human clear cell renal cell carcinoma (Caki-1) (Glube et al. 2007)) as do primary cultures of pure proximal tubule cells (Qi et al. 2007), such cell culture models are also not suitable. P_i homeostasis *in vivo* requires the presence of both distal and proximal tubule cells and using a single cell type model cannot, by nature, fulfil this requirement.

Therefore, the second part of this study was to characterise an *in vitro* primary human proximal and distal tubule cell co-culture model, based on a previously established model (C. Brown et al. 2008). The high viability of cells in culture was determined by the observation of high levels of proliferation and low levels of apoptosis. In the Brown et al. study, the ratio of proximal to distal tubule cells at the point of isolation was roughly 80% and 20% respectively, whereas in this study, it was roughly 60% and 40% respectively. Primary cultures are inherently associated with great variability owing to the different genetics, age and degrees of health of the patients from which the cells are obtained, and this could explain the differences seen. Interestingly, however, in addition to the fact that a greater proportion of distal to proximal tubule cells was obtained at the point of isolation, cells in this study also appeared to undergo a gradual 'distalisation' (in terms overall cell numbers, not phenotype) over time. This may be due to slight methodological differences between studies. In the Brown et al. study, cell phenotype was assessed when cells were grown on polycarbonate transwell filter supports, whilst in this study, it was assessed when cells were grown on collagen type IV-coated glass coverslips. Perhaps, proximal tubule cells adhere better to/detach less from transwells rather than coverslips, or preferentially grow better on transwells. In addition, α-Minimal Essential Medium (α-MEM; Life Technologies) modified according to Gibson-D'Ambrosio (Gibson-D'Ambrosio et al. 1987) supplemented with 10% fetal calf serum was used in the Brown et al. study, whereas Renal Epithelial Growth Medium (REGM; Lonza) was used in this study. Although the components of the culture medium used in this study are optimised for the specific culture of renal cells, they may have favoured the survival and growth of the distal tubule cell population over that of the proximal tubule cell population such that the percentage of proximal to distal tubule cells in culture changed over time. In any case, the presence of microvilli and the expression of N-cadherin (a proximal tubule marker protein) within the culture model together provide evidence that the 'distalisation' of the cell culture was

not a result of proximal tubule cell dedifferentiation. Primary renal cells also displayed a cobblestone morphology in culture comparable to that of primary renal cells reported by others (Wilmer et al. 2010). Further evidence indicating that cells in this model were not undergoing dedifferentiation was provided by the detection of no increase in vimentin (a marker of dedifferentiation (Hallman et al. 2008)) by Western blotting of cell lysates over time in culture.

Functional responses to known physiological stimuli were also assessed in the culture model. This first of these was FGF23-induced ERK phosphorylation. *In vivo* FGF23 signals the for the downregulation of NaP_i IIa through ERK; mice treated with recombinant FGF23 display ERK phosphorylation in distal tubules after 10 minutes followed by downregulation of NaP_i IIa protein in proximal tubules after 30-60 minutes (Farrow et al. 2010). *In vitro* studies have also shown the ability of FGF23 to phosphorylate ERK (Yamazaki et al. 2010), and as ERK is part of the RAF/MEK/ERK pathway, it is also interesting to note that mice treated with inhibitors of MEK, have a similar phenotype to $FGF23^{-/-}$ or $Klotho^{-/-}$ mice (Diaz et al. 2012) (*i.e.* MEK is required for downstream FGF23 signalling). In the current study, primary human renal cells displayed an increase in ERK phosphorylation following a 10 minute incubation with medium containing FGF23, a response that could be inhibited by co-incubation with medium containing a commercially available MEK inhibitor, thus confirming that cells in the model respond in a physiological manner.

The second functional assay was to screen cultured cells for their ability to undergo mineralisation. β-glycerophosphate (βGP) is a well-documented mineralising agent (Olesen et al. 2007; Shioi et al. 1995), and as such was used as a positive control. In the kidney, βGP is hydrolysed by alkaline phosphatase (ALP) whereupon inorganic phosphate (P_i) (which can be visualised using von Kossa's assay) is released (Prasad et al. 2005). Primary cultures of human renal cells exhibited βGP-induced mineralisation. *In vivo,* inhibiting MEK either directly or upstream with a pan-FGFr inhibitor has been shown to induce mineralisation of soft tissues such as the stomach mucosa, skeletal muscles and the kidney (Diaz et al. 2012; Yanochko et al. 2013). In the current study, primary human renal cells displayed an increase in mineral deposition following treatment with medium containing a MEK inhibitor compared to that of untreated cells. The ability to identify

mineral deposition in primary cultures in response to MEK (or FGFr) inhibition, suggests a potential use of this model in the preclinical screening of novel anti-cancer MEK or FGFr inhibitors for their likelihood to induce mineralisation in humans *in vivo*. Such data could be used alongside *in vivo* studies in preclinical species to guide compound selection for use in later clinical trials. For example, compounds that do not produce mineralisation in rodents *in vivo* nor in primary cultures of human renal cells *in vitro*, could progress to *in vivo* human studies.

The third functional test was to screen for NaP_i IIa upregulation under P_i-free conditions. Sodium-dependent phosphate transport by renal epithelial cells was first shown by Biber, Brown and Murer using cultured LLC-PK cells (Biber et al. 1983). Using the same cells, it was later shown that sodium-dependent phosphate transport could be regulated by phosphate (Caverzasio et al. 1984). NaP_i IIa upregulation under low P_i conditions is also a known *in vivo* phenomenon (rats fed a low P_i diet have significantly higher NaP_i IIa expression compared to rats fed a high P_i diet (Riccardi et al. 2000; Ritthaler et al. 1999). In this study, primary cultures of human renal cells displayed NaP_i IIa upregulation in response to culture in P_i-free medium by both immunocytochemistry and Western blotting of cell lysates, which again confirms their ability to respond to known physiological stimuli. Interestingly, the exact mechanism by which no/low P_i levels induce NaP_i IIa upregulation, is yet to be determined (Lanaspa et al. 2013). What is known, however, is that NaP_i IIa protein expression at the proximal tubule brush border membrane increases between 2 and 4 hours, before an increase in NaP_i IIa mRNA is detectable (Ritthaler et al. 1999) indicative of protein stores. Use of the cell model described in the current study has potential to be used for studying this aspect of P_i homeostasis. In addition, it would be useful to investigate whether NaP_i IIa is not merely expressed at the protein level, but is fully functional. This could be achieved in future studies by performing NaP_i IIa P_i uptake experiments akin to those performed by other groups (C. Brown et al. 2008; Wilmer et al. 2010).

Although NaP_i IIa is the most characterised proximal tubule P_i transporter, it is by no means the only proximal tubule P_i transporter; NaP_i IIc and two type III P_i transporters (PiT-1 and PiT-2) also exist (Lanaspa et al. 2013). NaP_i IIa is the predominant P_i transporter in mice, being responsible for the reabsorption of roughly 70% of filtered P_i (Iwaki et al.

2008). Interestingly, lack of NaP_i IIc in mice does not induce hyperphosphaturia or hypophosphatemia (Segawa et al. 2009), whilst in humans, however, lack of NaP_i IIc results in patients suffering hypophospatemic rickets (Bergwitz et al. 2006; Lorenz-Depiereux et al. 2006). As NaP_i IIc clearly plays a much more important role in P_i homeostasis in humans than in mice, it would be useful for future studies to investigate whether NaP_i IIc is also upregulated in primary human renal cells when cultured in P_i-free conditions, and proceed to use the model to study how exactly both are P_i upregulated when P_i levels are low.

Following viability and phenotypic assessment, the expression of key proteins known be involved in mineral ion homeostasis (FGFr1-4, NaP_i IIa, Klotho, NCX1 and PMCA1) was investigated in cells after 8 days in culture. FGFr1-4, NCX1 and PMCA1 were found to be expressed by primary human renal cells cultured on collagen type IV-coated glass coverslips. However, NaP_i IIa and Klotho were only expressed by cells at day 8 of culture when cultured on semi-permeable filter supports (transwells). This difference in protein expression between cells grown on collagen type IV-coated coverslips and transwells suggests that all future experiments be performed exclusively on transwells in an attempt to further recapitulate the *in vivo* renal proteome present with in the cell model more closely. Transwells have been reported to enhance cell polarisation (*i.e.* the presence of distinct apical and basolateral membranes) (C. Brown et al. 2008; Lash et al. 2006), and maintenance of cell polarisation could be a necessary requirement for the maintenance of Klotho and NaP_i IIa expression. Future studies using cells grown on transwells aim to provide additional confirmation of the utility of this model for studying mineral ion homeostasis by the kidney.

In this study, changes in the protein expression in response to FGF23 and P_i manipulations of the culture medium were observed for NCX1 and PMCA1. Whilst FGF23-treatment appeared to induce expression of NCX1 at the plasma membrane, lack of P_i in the culture medium appeared to induce PMCA1 expression at the plasma membrane. To the best of my knowledge, respective FGF23- and P_i-induced changes in NCX1 and PMCA1 expression have not been reported in previous published literature and are novel. These are exciting findings as they point towards previously unknown regulatory functions of FGF23 and P_i on these proteins and their involvement in mineral ion homeostasis. As above, future

studies aim to confirm these findings in cells grown on transwells, as well as show these changes quantitatively by image analysis using recently developed software (TissueGnostics, Medical & Biotech Solutions, Austria). Interestingly, FGF23 has recently been shown to modulate TRPV5 expression (Andrukhova et al. 2014). Like NCX1 and PMCA1 (Magyar et al. 2002), TRPV5 is expressed in the distal convoluted tubule (Hoenderop et al. 1999) where it too is involved in calcium reabsorption from the glomerular filtrate into the blood. Andrukhova et al. show both that TRPV5-transfected MDCK cells have increased membrane expression of TRPV5 in response to FGF23 treatment, and that FGF23 knockout mice have reduced membrane expression of TRPV5. Together, these data highlight a previously unknown function of FGF23 on renal calcium transport; that FGF23 positively modulates TRPV5 expression. The authors suggest that FGF23 can increase P_i excretion whilst simultaneously conserve extracellular Ca^{2+}. They point out, however, that this may have pathophysiological relevance in diseases such as chronic kidney disease. In this case, both elevated PTH and FGF23 levels can contribute to the calcium accumulation and vascular calcification observed in such patients. It would be interesting to observe the reported FGF23-induced increase in TRPV5 expression in that study in the primary human cells model characterised in this study. In addition, the observation of FGF23- and P_i-induced changes in NCX1 and PMCA1 changes *in vivo* would likewise validate the use of the cell model as a useful tool for studying mineral ion homeostasis by the kidney.

In the current study, the effects of FGF23 and P_i on the expression of FGFr1-4, Klotho, NaP_i IIa, NCX1 and PMCA1 proteins were assessed. However, the cell model could also be used to study the effects of $1,25(OH)_2D_3$, PTH and Ca^{2+} on these proteins. In addition, the effects of FGF23, $1,25(OH)_2D_3$, PTH, Ca^{2+} and P_i itself on the expression of other proteins known to be involved in mineral ion metabolism by the kidney such as the Pit-2 (Villa-Bellosta et al. 2009), Calcium-Sensing Receptor (CaSR) (Riccardi et al. 2000), Calbindin D28 (Cal28) (Zheng et al. 2004) and Transient Receptor Potential Cation Channel Subfamily V Member 5 (TrpV5) (Topala et al. 2009). In the current study, an attempt was made to assess the production of $1,25(OH)_2D_3$ by proximal tubule cells in the presence of FGF23 and the absence of P_i. No data were generated using an commercially available assay (1,25-Dihydroxy Vitamin D enzyme-linked immunosorbant assay (EIA) from

Immunodiagnostic Systems, UK) and this was likely due to the fact that it was optimised for serum and plasma samples, and cell lysates were used in the is this study. It will not be possible to investigate $1,25(OH)_2D_3$ directly in cultured human renal cells until more applicable assays become available. However, $1,25(OH)_2D_3$ production/degradation could be looked at indirectly by assessing the expression patterns of 1α-hydrolase and 25-hydroxylase by immunocytochemistry or Western blotting of cell lysates.

In summary, this study localised FGFr1-4 and Klotho to formalin-fixed, paraffin-embedded human kidney nephron segments adding important information to the field of mineral ion metabolism by the human kidney to that currently available in the literature. In addition, an *in vitro* mixed population of primary human proximal and distal tubule cells as a novel tool for studying mineral ion metabolism specifically by the human kidney was characterised. Cells were shown to possess high proliferation and low apoptosis indicating high viability, and maintained differentiated as evidenced by maintenance of expression of phenotypic marker proteins, morphology and functional responses to known stimuli (FGF23-induced ERK phosphorylation, MEK inhibitor-induced mineralisation and modulation of NaP_i IIa expression by P_i). Future studies aim to confirm these findings using cells grown on transwells. Overall, this model has the potential to be used for studies of mineral ion homeostasis specifically by the human kidney, as well as a tool to guide pharmaceutical drug development.

CHAPTER 2

Tissue Expression and Correlation of a Panel of Urinary Biomarkers Following Cisplatin-Induced Kidney Injury in Rats

2.1 Abstract

In recent years there has been a large effort to identify and validate urinary biomarkers of nephrotoxicity as non-invasive measurements with greater sensitivity and specificity than traditional biomarkers such as serum creatinine and blood urea nitrogen. In this study, cisplatin-treated rats were used to evaluate the possible use of tissue biomarkers in studies where urine samples are not available, such as retrospective studies in drug safety testing, by correlating tissue biomarker levels with urinary biomarker levels. In other words, the aim of this study was to correlate tissue and urine expression of the same biomarkers, such that identification of one, could indicate the presence of the other.

Six novel acute kidney injury biomarkers were investigated, and all except one (β_2-microglobulin) showed a significant increase (KIM-1, osteopontin and clusterin) or decrease (αGST and trefoil factor-3) in tissue expression 5 days after 1.0mg/kg or 2.5mg/kg cisplatin treatment. After eight days, these changes persisted, except those seen for αGST which no longer showed significant differences compared to control animals, despite more severe histopathology. All of the biomarkers, except β_2-microglobulin, showed utility as tissue biomarkers but KIM-1 and osteopontin were the best at predicting proximal tubule necrosis (as shown by the area under the curves from receiver operating characteristic curves). Kidney KIM-1 and OPN measurements also correlated closely with their corresponding urinary biomarker measurements, indicating that these urinary markers are sensitive and specific for tissue injury.

Future studies are needed to determine the wider application of tissue and urinary KIM-1 and osteopontin for detecting renal toxicity following the administration of other nephrotoxicants.

2.2 Introduction

Acute Kidney Injury Overview

Each human kidney contains roughly 1.25 million functional units called nephrons which together filter 150 – 180 litres of plasma per day and process it in order to regulate body fluid, electrolyte, and pH balance, as well as metabolise and eliminate waste products in the urine (Bonventre et al. 2010). Acute kidney injury (AKI) is a common condition with many aetiologies including tubulo-interstitial inflammation and edema, ischaemia, and drug-induced toxicity (Vaidya et al. 2008). It is characterised by a decrease in the ability of the kidney to carry out its physiological functions, and as such, is associated with a decrease in urine output (oliguria or anuria) and a build-up of waste products of metabolism such as creatinine and urea in the blood (azotaemia) (Bellomo et al. 2012; Kellum 2008). However, due to the large functional reserve of the kidney, these changes are only observed once the reserve has been depleted (De Loor et al. 2013). As a result, the term 'acute kidney injury' has largely replaced the term 'acute renal failure' (ARF) to highlight the fact that injury can occur long before functional impairment/failure is seen (Van Biesen et al. 2006). Acute kidney injury is a massive problem both in preclinical and clinical settings (Vaidya et al. 2008).

Diagnosing Acute Kidney Injury

Creatinine is a by-product of muscle metabolism and in healthy individuals is excreted by the kidney at a fairly constant rate. Measurements of creatinine in the blood (serum creatinine; SCr) can therefore be used to indirectly estimate glomerular filtration rate (GFR), which is an index of overall kidney function (Inker et al. 2012). In healthy males, SCr is between 0.7 – 1.3mg/dL (Charney et al. 2005) and GFR is between 90 – 120 ml/min/1.73cm^2 (Harris and Stribling 2007). A decline in GFR, reflected by a rise in SCr, indicates impaired kidney function/kidney injury. In addition, decreased urine output can indicate AKI (Legrand and Payen 2011).

A decade ago, while these pathological changes in serum creatinine and urine output were well known, roughly 30 different definitions of acute kidney injury, based on the degree by which each must change in order for a diagnosis to be made, were present in

the literature (Bellomo et al. 2001; Kellum et al. 2002). This meant that there was a large variation in the reported incidence of acute kidney injury and its associated mortality rate (Hoste et al. 2006). In 2004, the lack of a universally agreed definition of acute kidney injury led The Acute Dialysis Quality Initiative (ADQI) Group to introduce the Risk (R), Injury (I), Failure (F), Loss (L) of function, End stage renal disease (E) (also known as RIFLE) criteria in a bid to standardise its diagnosis (Bellomo et al. 2004). Each stage (R, I, F, L and E) described the degree by which serum creatinine or urine output should change for a diagnosis of AKI at a certain stage to be made. In 2007, the Acute Kidney Injury Network (AKIN) Group modified the RIFLE criteria adding that a diagnosis of AKI be made when even small changes in serum creatinine (≥ 0.3mg/dl) are seen within 48 hours. This amendment reflected studies showing that even small increases in serum creatinine are associated with an increased risk of mortality. These criteria were termed the Acute Kidney Injury Network (AKIN) criteria (Mehta et al. 2007). In 2012, building on both the RIFLE and AKIN criteria, the Kidney Disease: Improving Global Outcomes (KDIGO) organisation then released the clinical practise guidelines for diagnosing AKI (doi:10.1038/kisup.2012.7). Table 2.1 summarizes the KDIGO criteria for diagnosing AKI.

Stage	**Serum Creatinine Criteria**	**Urine Output Criteria**
1	Increase in SCr ≥ 0.3mg/dL in 48 hr **OR** 1.5- to 1.9-fold increase from baseline	< 0.5ml/kg/hr for > 6hr
2	2- to 2.9-fold increase from baseline	< 0.5ml/kg/hr for > 12hr
3	SCr ≥ 4.0mg/dL with acute increase of ≥ 0.5mg/dL **OR** 3-fold increase from baseline	< 0.3ml/kg/hr for 24hr **OR** anuria for 12hr

Table 2.1. Kidney Disease: Improving Global Outcomes (KDIGO) organisation clinical practise guidelines for diagnosing acute kidney injury. Detailed are the clinical practise guidelines for diagnosing different stages (stage 1-3 (stages of severity)) of acute kidney injury (AKI) based on measurements of serum creatinine (Scr) and urine output, as recommended by the Kidney Disease: Improving Global Outcomes organisation. Adapted from (doi:10.1038/kisup.2012.7).

As mentioned previously, it is recognised that even a small rise in serum creatinine is associated with increased risk of mortality (Chertow et al. 2005; Waikar and Bonventre 2009; H. Wang et al. 2012), and indeed, the greater the rise in serum creatinine, the greater the risk of mortality (Weisbord et al. 2006). The main reason for this, is that serum creatinine is neither specific nor sensitive enough to detect kidney injury early. In terms of specificity, serum creatinine is influenced by factors independent of renal function including age, gender, muscle mass, activity level and hydration state (Baxmann et al. 2008). In terms of sensitivity, serum creatinine is a late marker of kidney injury; levels can remain (up to a point) within a normal range following injury (Baxmann et al. 2008; de Geus et al. 2012) because the kidneys possess an extensive renal functional reserve (Ferguson et al. 2008; Parikh and Devarajan 2008). A further limitation of using creatinine as a tool for assessing renal function is that in addition to being passively filtered at the glomerulus, it is actively secreted from peritubular capillaries into the kidney filtrate by proximal tubule cell organic cation transporter 2 (OCT2) (Ciarimboli et al. 2012; Urakami et al. 2004). As such, clearance of creatinine in the urine (another measure of kidney function) overestimates glomerular filtration rate (GFR) by as much as 20% (Legrand and Payen 2011). In addition, inhibition of OCT2 by some xenobiotics, inhibits creatinine secretion and increases serum creatinine levels independently of reduced kidney function (Ciarimboli et al. 2012; Lepist et al. 2014).

In a similar manner, issues arise when diagnosing acute kidney injury (AKI) based on decreased urine output; a decrease in urine output can simply be a physiological response to maintain body volume during dehydration. Measurements of blood urea nitrogen (BUN) are also used clinically to assess kidney function. BUN is a measure of the nitrogen present in blood that comes from the waste product urea, and in healthy males is roughly 8 – 21 mg/dL (Charney et al. 2005). Blood urea nitrogen is increased in kidney injury, and like serum creatinine and urine output, can be affected by factors independent of kidney injury such as the consumption of a protein-rich meal or dehydration (Edelstein 2008).

It is evident that the current markers (serum creatinine and urine output) used to assess renal function and diagnose acute kidney injury are limited. Although criteria such as the KDIGO criteria have standardised and improved the diagnosis AKI, the fact is that they are still based on measurements of serum creatinine and urine output. Biomarkers with

higher sensitivity and specificity than serum creatinine and urine output are required if the detection, monitoring and prevention of acute kidney is to be improved even further.

Drug-Induced Acute Kidney Injury: A Preclinical and Clinical Problem

The kidney is one of the main organs involved in excretion of drugs and drug metabolites from the body, and also has drug metabolising capacity itself. It is not surprising, therefore, that drug-induced toxicity giving rise to acute kidney injury arises more frequently there than in many other organs. Indeed, drug-induced acute kidney injury is a big problem for both preclinical drug development and clinical therapeutics. One of the main reasons that compounds are dropped from development is due to the discovery of drug-induced toxic side effects (Kola and Landis 2004). As such, pharmaceutical companies aim to identify such compounds early during development in order to prevent late stage attrition, with associated loss of time, energy and investment (Bonventre et al. 2010). The gold-standard for determining whether a novel compound does or does not induce acute kidney injury in preclinical species, is histopathological observation following termination (Bonventre et al. 2010). In the clinic, drug-induced acute kidney injury contributes to 8-60% of all cases of acute kidney injury, depending on patient population studied (Schetz et al. 2005). Halting the progression of acute kidney injury is important as it is considered a serious risk factor for progression to end-stage renal disease (ESRD) (Gammelager et al. 2013), and is associated with an increased risk of death (Chertow et al. 2005; H. Wang et al. 2012). While histopathological observation is also the gold-standard for diagnosing acute kidney injury in humans, it requires an invasive biopsy, and as such, is only used in rare instances (Bonventre et al. 2010). Rather, despite their limitations, increases in serum creatinine (SCr) and blood urea nitrogen (BUN) are used alongside urinalysis (Star 1998).

Drug Metabolism and Excretion in the Kidney: Cisplatin

A common route of drug excretion from the body is in urine produced by the kidney. Many drugs (and drug metabolites) undergo elimination via passive filtration at the glomerulus and/or paracellular or transcellular secretion. During proximal tubule transcellular secretion, drugs pass from the peritubular capillaries through proximal tubule cell basolateral and apical membranes and into the glomerular filtrate (Khurana

2005). Cisplatin (*cis*-diammine-dichloro-platinum (II)), is chemotherapeutic drug used for treating solid tumours including those of the head, neck, lung, testis, ovary and breast (Blanchard 2012; Miller et al. 2010) is excreted from the body by both glomerular filtration and proximal tubule transcellular secretion (Blanchard 2012; Yao et al. 2007). During the process of transcellular secretion, it is transported across the proximal tubule basolateral membrane via organic cation transporter-2 (OCT2) (Ciarimboli et al. 2005) and copper transporter-1 (CTR1) (Ishida et al. 2002; Lin et al. 2002). Efflux of cisplatin at the apical membrane is mediated by multidrug and toxin extrusion 1 (MATE1) (Nakamura et al. 2010).

Cisplatin has a notorious dose-limiting nephrotoxic side effect (Blanchard 2012) which is thought to be a result of its biotransformation (metabolism) into a more toxic metabolite. Indeed, few drugs are excreted by the body unchanged; most undergo biotransformation into metabolites via phase I metabolism (which includes, for example, hydroxylation, reduction or oxidation reactions) or phase II metabolism (which includes, for example, methylation, acetylation, glucuronidation or sulfation reactions) (Moscovitz and Aleksunes 2013). Cisplatin is thought to undergo biotransformation (metabolism) in the kidney to a glutathione-conjugate, to a cysteinyl-glycine-conjugate, to a cysteine-conjugate and finally to a reactive thiol (Miller et al. 2010; Townsend et al. 2003). In addition, sensitivity to cisplatin appears to correlate with mitochondrial density (Qian et al. 2005) and proximal tubule cells have high density of mitochondria (Hall et al. 2008). Toxicity is also thought to be a result of a change in mitochondrial membrane potential, mitochondrial fragmentation, and subsequent release of apoptotic factors (C. Brooks et al. 2009). Despite its toxic side effects, cisplatin continues to have widespread clinical use as an effective anti-cancer agent in the clinic. In preclinical studies, cisplatin nephrotoxicity can be exploited as a reliable method for inducing renal injury in rodent models to study biomarkers of drug-induced toxicity.

Cisplatin's Therapeutic Mechanism

To exert its cytotoxic therapeutic actions, cisplatin forms interstrand and intrastrand cross-links between DNA purine bases (Oliver et al. 2010). In highly proliferative cancer cells, this prevents DNA replication and arrests tumour growth (Harder and Rosenberg 1970; Harder et al. 1976), and additionally results in the activation of signal transduction pathways involving ATM- and Rad3-related protein (ATR), p53, p57, mitogen-activated protein kinase (MAPK) and which induce cellular apoptosis (Siddik 2003).

Kidney Injury Biomarkers

As a result of the lack of sensitivity and specificity of SCr, BUN and urine output for diagnosing AKI, large collaborations between pharmaceutical and biotechnology industries, regulatory bodies such as the U.S. Food and Drug Administration (FDA) and the European Medicines Agency (EMA 2010) and academia (Bonventre et al. 2010), have led to the discovery of many novel diagnostic biomarkers of AKI. A biomarker, as defined by the Biomarkers Definitions Working Group, is 'a characteristic that is objectively measured and evaluated as an indicator of normal biological processes, pathogenic processes, or pharmacologic responses to therapeutic intervention' (Group. 2001). Before qualification for use by regulatory authorities, novel biomarkers require extensive characterisation to validate them in terms of their full capacity. The Predictive Safety Testing Consortium (PSTC) Working Group propose that ideal biomarkers must:

1. Detect injury early (*i.e.* before changes in SCr, urine output and/or BUN are seen, and even before histopathological changes are seen)
2. Localise the site of injury (*i.e.* is the injury confined to the proximal or distal tubule only, or it is affecting the whole nephron?)
3. Reflect the degree/extent of injury
4. Be applicable to many species (translational) so that they can be used both to guide drug development during preclinical safety testing and assist with patient management in clinical settings
5. Be easily accessible in tissue/fluids (Bonventre et al. 2010).

Urinary biomarkers are of particular interest because urine is readily accessible; no invasive kidney biopsy, or needle puncture is required. In addition, repeated urinary measurements can be made from patients thereby enabling the onset (when known) of, progression of, and recovery from injury to be tracked over time.

In terms of drug-induced AKI, biomarkers are required not only for improving the safety assessment of novel compounds in preclinical and clinical settings, but for monitoring kidney injury associated with drugs already marketed for human use (e.g. cisplatin).

When assessing the diagnostic power of a novel biomarker to identify AKI, Receiver Operating Characteristic (ROC) Analyses are performed and ROC Curves created. A ROC curve is a graphical plot of the true positive rate (sensitivity) versus the false positive rate (1 – specificity) for a variable (*i.e.* a biomarker) against a classifier (*i.e.* AKI) (Cook 2010). The area under the curve (AUC) indicates how sensitive and specific a biomarker is at correctly identifying AKI. For example, a biomarker with an AUC of 0.5 is essentially random, whilst a biomarker with an AUC of 1.0 would correctly identify AKI 100% of the time (perfect ability). The area under the curve can be used to compare the ability of a number of different biomarkers against each other as well as against current standards such as SCr (Warnock and Peck 2010).

Highlighted below are of some of the most promising tissue and urinary biomarkers of drug induced-AKI, some of which have already been qualified for use in certain settings by the FDA and EMEA (Dieterle et al. 2010b).

Kidney injury molecule-1

Kidney injury molecule-1 (KIM-1) is a type 1 membrane-spanning protein with a six cysteine immunoglobulin (Ig)-like domain and a single mucin domain (Han et al. 2002; Ichimura et al. 1998). It is also known as T-cell immunoglobulin mucin domains-1 (TIM-1) and hepatitis A virus receptor 1 (HAVCR-1) (Waanders et al. 2010). KIM-1 mRNA and protein are either undetectable (van Timmeren et al. 2006) or present at extremely low levels (Ichimura et al. 2004) in healthy kidneys but are massively upregulated following ischaemia (Ichimura et al. 1998), nephrotoxicity (Chiusolo et al. 2010; Ichimura et al. 2004) and protein overload nephropathy (van Timmeren et al. 2006). It is an especially good biomarker because it is expressed *de novo* in the kidney in response to injury.

Expressed in dedifferentiated, proliferating epithelial cells found within regenerating tubules (Ichimura et al. 1998), the KIM-1 ectodomain is shed into the kidney filtrate (urine) in a metalloproteinase-dependent manner (Bailly et al. 2002; Han et al. 2002) where it is thought to modulate the immune response and repair process after injury (Bonventre and Yang 2010). Its presence in urine means that it can serve as a non-invasive urinary biomarker of AKI; urinary levels can be monitored before injury, during injury and during recovery when the initial onset of injury is known. As such, it was qualified by the FDA and EMA in 2009 as a sensitive and specific urinary biomarker of drug-induced AKI for use in preclinical studies and on case-by-case phase 1 and phase 2 clinical trials using the KIM-1 urine dipstick test, RenaStick (Vaidya et al. 2009). KIM-1 is also a good biomarker for predicting kidney transplant rejection (Jin et al. 2013).

Osteopontin

Osteopontin (OPN) is a highly phosphorylated glycoprotein component of the mineralised extracellular matrices of both bone and teeth (Sodek et al. 2000). However, it is also widely expressed by other tissues including lung, liver, bladder, pancreas and kidney (Xie et al. 2001b). In healthy kidneys, expression of OPN is localised to the loop of Henle and the distal tubule (Hudkins et al. 1999; Xie et al. 2001a), where it is secreted into the urine to prevent the nucleation, growth and precipitation of minerals such as calcium oxalate monohydrate thereby preventing the formation of urinary stones (Asplin et al. 1998; Wesson et al. 2003). Upregulation of osteopontin in the kidney occurs following ischemia/reperfusion (Persy et al. 1999), nephrotoxicity (Verstrepen et al. 2001) and protein overload proteinuria (Eddy and Giachelli 1995) and is thought to be renoprotective. For example, following 30 minutes of ischemia, OPN -/- mice exhibit more severe kidney injury in association with greater inducible nitric oxide synthase (iNOS) expression compared to that of wild type mice (Noiri et al. 1999). As such, one of the ways OPN may be renoprotective is by reducing oxidative stress. Indeed, it has recently also been shown that ischemia/reperfusion induced kidney injury in rats is attenuated by inhibition of iNOS (P. Wang et al. 2013).

Alpha glutathione S-transferase

Glutathione S-transferases are small, cytosolic enzymes involved in detoxification, steroid hormone synthesis and aromatic amino acid catabolism (Hayes and Pulford 1995; Hayes

et al. 2005). The alpha isoform (alpha glutathione S-transferase; αGST) is highly and constitutively expressed throughout the proximal tubule and urinary levels are highest in people with well-preserved renal function (Branten et al. 2000). Increased urinary excretion of αGST is associated with proximal tubule brush border damage and decreased tissue expression (Branten et al. 2000). The time course of this increase is thought to be short; once the available αGST has been shed into the urine, no further shedding is possible (Endre and Pickering 2013).

Clusterin

Clusterin is a glycosylated protein with anti-apoptotic and pro-survival actions (Dieterle et al. 2010a). Although it is constitutively expressed by almost all mammalian tissues and is a major protein component of physiological fluids (Jones and Jomary 2002), it is only expressed in the kidney under pathophysiological conditions. Its relatively high molecular weight (75-80Kda) prevents it undergoing glomerular filtration under physiological conditions and therefore its presence in urine is indicative of kidney injury (Dieterle et al. 2010a; Silkensen et al. 1997). *De novo* gene expression of clusterin in the kidney can be induced by ischemia/reperfusion injury (W. Zhou et al. 2010) and drug nephrotoxicity (Betton et al. 2012; Kharasch et al. 2006; Vinken et al. 2012). As such, urinary clusterin has been formally qualified by the EMEA and FDA as a proximal tubule injury biomarker (Dieterle et al. 2010a). Clusterin is thought to play a role in renal regeneration following injury (Gobé et al. 1995).

Trefoil factor-3

Trefoil factor-3 (TFF3) is a small molecular weight peptide hormone secreted by mucous producing cells and epithelial tissues (Madsen et al. 2007). In the kidney it is expressed in collecting ducts of the outer stripe of the outer medulla and it is thought to play a protective role, although its exact function is as yet unknown (Astor et al. 2011). TFF3 urinary levels decrease following drug-induced acute kidney injury (Yu et al. 2010).

Beta 2-microglobulin

Beta 2-microglobulin (β_2MG) is the light chain component of major histocompatibility (MHC) class 1 molecules present on the cell membranes of most nucleated cells (Musialik 1989). It is freely filtered by the glomerulus and almost completely reabsorbed by proximal tubular cells (Miyata et al. 1998) such that only 0.3% of filtered β_2MG is excreted

in urine (Dieterle et al. 2010a). In the kidney, it is localised to the sub-apical endosomes of the proximal tubule that process it (Dieterle et al. 2010a). Levels of β_2MG in the urine can be increased in different ways depending on the type of kidney injury. When treated with toxins primarily affecting the glomerulus, for example, leakage of high molecular weight proteins into the filtrate compete with β_2MG for uptake in the proximal tubule (Thielemans et al. 1994). The problem associated with the use of β_2MG which thereby limits its use as a non-invasive urinary biomarker is, however, the fact that it degrades in urine samples at 37°C, pH6 (Davey and Gosling 1982).

2.3 Project Overview

Despite significant progress in identifying, validating and utilising urinary biomarkers, there is still little information for many of these on how they perform in tissue-based assays. For pharmaceutical companies, tissue-based assays offer the advantage that they can be carried out on retrospective samples from drug safety testing studies (or other relevant studies), where samples are usually formalin-fixed, paraffin-embedded and may be archived for long periods of time. As it is important that urinary biomarkers of kidney injury reflect the expression of the same biomarkers in kidney tissue, tissue-based assays offer the advantage that they can confirm that a protein detected in urine has indeed originated from the kidney (and not been filtered at the glomerulus, for example). Furthermore, when used alongside standard histopathology, tissue-based immunohistochemistry assays can be used to localise biomarkers to specific sites within the kidney and/or relate them to particular types of injury. Immunohistochemistry assays can therefore provide complimentary information to the urinary assays using corresponding antibodies.

2.4 Aims

This study was a retrospective study using formalin-fixed paraffin embedded kidney samples and urine samples collected as part of an earlier study at AstraZeneca where the nephrotoxic drug cisplatin was used to induce kidney injury in rats (Pinches et al. 2012b; Pinches et al. 2012a; Pinches et al. 2012c).

The aims of this study were:

1. To investigate changes in tissue biomarkers of kidney injury in a cisplatin-treated rat model of nephrotoxicity using positive pixel analysis
2. To determine the ability of tissue biomarkers to correlate with standard histopathology by constructing receiver operating characteristic curves
3. To determine the ability of tissue biomarkers to correlate with the same biomarkers in urine (where available).

KIM-1, osteopontin, αGST, clusterin, TFF3 and β_2MG were selected for investigation, all of which are becoming widely used as urinary biomarkers of nephrotoxicity (Bandele et al. 2013; Dieterle et al. 2010a; Tonomura et al. 2010; Yu et al. 2010; Y. Zhou et al. 2008).

2.5 Materials and Methods

In vivo Study Design

The *in vivo* study (from which immunohistochemistry data in the current study was generated), was carried out at AstraZeneca, UK, according to the Animals (Scientific Procedures) Act (1986) and AstraZeneca Standard Operating Procedures (SOPs). A total of 80, ten-week-old, male, Han Wistar rats were used (Harlan, UK) in the study. A maximum of 5 animals were housed per cage, and animals were subject to a 12 hour light/dark cycle with temperature and humidity maintained between 19°C and 23°C, and 40% and 70% respectively. Unlimited access to RM1 (E) SQC food pellets and water was provided, except during the 6 hour urine collection periods when food was temporarily withdrawn.

Animals were randomised into 10 different experimental groups with 5 animals per each vehicle-treated group and 10 animals per each cisplatin-treated group. Cisplatin (Sigma, UK) was formulated in a 0.9% (w/v) sodium chloride vehicle solution. On day 1, all animals received a single intra-peritoneal (i.p.) dose of the vehicle solution or 0.1mg/kg (low dose), 1.0mg/kg (mid dose) or 2.5mg/kg (high dose) of cisplatin. The different doses of cisplatin used in the study were based on earlier dose-finding exploratory studies at AstraZeneca. Animals were then either maintained for 5 days (all groups), 8 days (all groups) or 22 days (control and high dose groups only). Individual 6 hour metabowl urine collections were made 4 days before dosing and 2, 4, 7 and 21 days after dosing, and individual 18 hour metabowl urine collections were made 3 days before dosing and 3, 5, 8, 15 and 22 days after dosing. Urine samples were stored at -80°C until analysed. Following the appropriate duration of study for each group, animals were killed by administration of halothane. The kidneys were removed, fixed for 48 hours in 10% neutral-buffered formalin (NBF) and embedded in paraffin. Table 2.2 outlines the study plan.

Novel immunohistochemistry biomarker data in the current study was generated using the formalin-fixed, paraffin-embedded kidneys collected as described above.

Group	Animals/Group	Dose (mg/kg)	Urine Collection Day	Necropsy Day
1	5	0	-4 (-3), 2 (3) and 4, (5)	5
2	10	0.1	-4 (-3), 2 (3) and 4, (5)	5
3	10	1.0	-4 (-3), 2 (3) and 4, (5)	5
4	10	2.5	-4 (-3), 2 (3) and 4, (5)	5
5	5	0	-4 (-3), 2 (3), 4 (5) and 7 (8)	8
6	10	0.1	-4 (-3), 2 (3), 4 (5) and 7 (8)	8
7	10	1.0	-4 (-3), 2 (3), 4 (5) and 7 (8)	8
8	10	2.5	-4 (-3), 2 (3), 4 (5) and 7 (8)	8
9	5	0	-4 (-3), 2 (3), 4 (5), 7 (8), 14 (15) and 21 (22)	22
10	10	2.5	-4 (-3), 2 (3), 4 (5), 7 (8), 14 (15) and 21 (22)	22

Table 2.2. *In Vivo* Cisplatin Study Design. Details regarding the group number, the number of animals per group, the dose (mg/kg) of cisplatin that animals in each group received via intraperitoneal inject on day 1, the days that urine collections were made for each group, and the day animals were killed by administration of halothane and subsequently necropsied, is presented. Ten different groups of animals were used in this study (groups 1-10), with 5 animals in each group treated with 0mg/kg cisplatin, and 10 animals in each group treated with 0.1mg/kg, 1.0mg/kg and 2.5mg/kg cisplatin. A total of 85 animals were used in the study. Urine samples were collected from animals in each group for 6 hours (or 18 hours) at the days indicated. Animals in each group were culled 5, 8 or 22 days post treatment, at which point kidney tissue from each animal was fixed in 10% neutral buffered formalin for 24 hours and processed into paraffin blocks. This table is adapted from Pinches et al. 2012.

Histopathology

For each of the animals in the study (N=85), 4µm-thick kidney sections in the transverse plane were cut and air-dried onto strongly adhesive slides (Leica, Germany). Sections were deparaffinised in xylene (Sigma, 33817) (2 x 3 minutes) and rehydrated to water using 100% (1 x 2 minutes) and 70% (1 x 2 minutes) ethanol (Sigma, 458600). Sections were incubated in haematoxylin (Clin-Tech Ltd, 642300) (6 minutes), washed in running tap water (2 minutes), dipped in 0.2% acid water, washed in running tap water (2 minutes), incubated in Scott's Tap Water (1 minute) and then washed again in running water (2 minutes). Sections were incubated in eosin (Thermo Scientific, 6766008) (3 minutes) and then dehydrated using 70% (20 seconds) and 100% (15 seconds) and then cleared in xylene (Sigma, 33817) (3 x 1 minute). Coverslips were mounted on slides using histomount (TAAB Labs, Aldermaston, UK). Slides were examined by light microscopy and histopathological assessments made based on the following pathology scoring system for proximal tubule necrosis: 0 = no necrosis, 1 = minimal necrosis, 2 = mild necrosis, 3 = moderate necrosis and 4 = severe necrosis. Histopathological assessments of proximal tubule necrosis were made by a pathologist (Dr Huw Jones) in the pathology group at AstraZeneca, UK.

Immunohistochemistry

In the present study, tissue biomarker data for all control animals (N=5 0mg/kg cisplatin at day 5, N=5 0mg/kg cisplatin at day 8, N=5 0mg/kg cisplatin at day 22), and the first five animals from each of the cisplatin-dosed groups (N=5 animals treated with 0.1mg/kg cisplatin at day 5 and day 8, N=5 animals treated with 1.0mg/kg cisplatin at day 5 and day 8, N=5 animals treated with 2.5mg/kg cisplatin at day 5, day 8 and day 22) was generated using immunohistochemistry (N=50 animals in total). Six tissue biomarkers (KIM-1, OPN, αGST, clusterin, TFF3 and β_2MG) were investigated in this study. Therefore, 6 formalin-fixed, paraffin-embedded kidney tissue sections were required per animal so that one section could be used per biomarker for immunohistochemistry.

For immunohistochemistry, antigen retrieval pre-treatments and antibody dilutions were optimised for use on formalin-fixed, paraffin-embedded control (for OPN, αGST, TFF3 and β_2MG) or 2.5mg/kg cisplatin-treated (for KIM-1 and clusterin) rat kidney sections, before

use in the current study. Control rat kidney was used to optimise the immunohistochemical staining of OPN, αGST, TFF3 and β_2MG, as these proteins are expressed in healthy kidney tissue. Kidney tissue from a 2.5mg/kg cisplatin-treated rat was used to optimise the immunohistochemical staining for KIM-1 and clusterin, as there is little to no expression of these proteins in healthy kidney tissue.

Four μm-thick formalin-fixed, paraffin-embedded rat kidney sections in the transverse plane were cut and air-dried onto strongly adhesive slides (Leica, Germany), deparaffinised in xylene (Sigma, 33817) (2 X 5 minutes) and rehydrated to water using 100% (2 x 5 minutes) and 95% (1 x 5 minutes) ethanol (Sigma, 458600). Antigen retrieval pre-treatment was performed for osteopontin and αGST (Ethylenediaminetetraacetic acid (EDTA; Sigma, ED255) pH8 for 2 minutes at 110°C) and TFF3 and β_2MG (citrate (Sigma, C1090) pH6 for 2 minutes at 110°C) using a RHS-2 Rapid Histoprocessor (Milestone, Sorisole, Italy). No antigen retrieval was required to detect either KIM-1 or clusterin. Following antigen retrieval (if required), sections were rinsed in running tap water (10 minutes). All immunostaining was carried out at room temperature using a Labvision autostainer (Labvision, Fremont, USA). Incubation with 3% H_2O_2 (Fisher Scientific, H/1750/15) 1 x phosphate-buffered saline 0.05% Tween-20 (USB Corporation, 20605) (PBST) (10 minutes) was used to quench endogenous peroxidase activity before non-specific antibody binding was minimised using background blocker with casein (MP-966-P500; Biocare LLC, Concord, USA) (20 minutes). Sections were incubated for 1 hour with antibodies raised against KIM-1 (goat IgG; 1:400; AF3689, R & D Systems, USA), osteopontin (rabbit IgG; 1:100; 18628, IBL Co., Ltd, Japan), αGST (rabbit IgG; 1:1000; B-3025, Argutus Medical, Dublin, Ireland), clusterin (goat IgG; 1:100; AF2937, R & D Systems, USA), TFF3 (rabbit IgG; 1:300; bs_0503, BIOSS Inc., USA) and β_2MG (rabbit IgG; 1:200; LS-b331, Lifespan Biosciences, USA) individually diluted in 1X Tris-buffered saline 0.05% Tween-20 (USB Corporation, 20605) (TBST). To remove unbound primary antibodies, sections were briefly rinsed twice with TBST. The X-Cell Plus Universal Polymer HRP Kit (MP-XCP-U100, Biocare LLC) and X-Cell Plus Goat HRP-Polymer Kit (MP-GHRP-K100, Biocare LLC) were used to conjugate HRP to rabbit and goat primary antibodies respectively (20 minutes). To remove unbound secondary antibodies, sections were briefly rinsed twice with TBST. Immunoreactivity was visualised using liquid stable

3, 3' diaminobenzidine (DAB) (MP-860-K25, Biocare LLC) (10 minutes). Sections were briefly rinsed twice with TBST, and running tap water (5 minutes). Sections were counterstained using Carazzi's haematoxylin (Clin Tech Ltd, UK) (1 minute), dehydrated in graded ethanol (Sigma, 458600) (100% (2 x 5 minutes) and 95% (1 x 5 minutes)), and then cleared in xylene (Sigma, 33817) (2 X 5 minutes). Sections were allowed to air dry before coverslips were mounted on the slides using histomount (TAAB Labs, Aldermaston, UK). Rabbit and goat isotype controls (Dako, Denmark) were used as negative controls. A summary of the antibody supplier, dilutions and antigen retrieval methods used is summarized in Table 2.3. Immunohistochemistry for each biomarker (KIM-1, OPN, αGST, clusterin, TFF3 and β_2MG) was performed on one section from five animals at each dose (0mg/kg cisplatin, 0.1mg/kg cisplatin, 1.0mg/kg cisplatin and 2.5mg/kg cisplatin) and time point (day 5, day 8 and day 22).

Antibody	Supplier	Antigen Retrieval	Dilution
KIM-1	R & D Systems (AF3689)	No Antigen Retrieval	1:400
OPN	IBL Co. Limited (18628)	EDTA pH8 for 2 minutes at 110°C	1:100
αGST	Argutus Media (B_3025)	EDTA pH8 for 2 minutes at 110°C	1:1000
Clusterin	R & D Systems (AF2937)	No Antigen Retrieval	1:100
TFF3	BIOSS Inc. (bs_0503)	Citrate pH6 for 2 minutes at 110°C	1:300
β_2MG	LifeSpan Biosciences (LS-B331)	Citrate pH6 for 2 minutes at 110°C	1:200

Table 2.3. Summary of the antibodies, antibody suppliers, antigen retrieval methods and antibody dilutions used in this study. Antigen retrieval pre-treatments and antibody dilutions were optimised for use in the current study on formalin-fixed, paraffin-embedded control (for OPN, αGST, TFF3 and β_2MG) or 2.5mg/kg cisplatin-treated (for KIM-1 and clusterin) rat kidney tissue beforehand. EDTA = Ethylenediaminetetraacetic acid.

Image Analysis

Image analysis was performed for the immunohistochemistry tissue biomarker data generated for all control animals (N=5 0mg/kg cisplatin at day 5, N=5 0mg/kg cisplatin at day 8, N=5 0mg/kg cisplatin at day 22), and the first five animals from each of the cisplatin-dosed groups (N=5 animals treated with 0.1mg/kg cisplatin at day 5 and day 8, N=5 animals treated with 1.0mg/kg cisplatin at day 5 and day 8, N=5 animals treated with 2.5mg/kg cisplatin at day 5, day 8 and day 22) (N=50 animals in total).

Following immunohistochemistry, images of the rat kidney sections were captured using a ScanScope Scanner and ImageScope software (Aperio Technologies Incorporated, Vista, USA). Using the ImageScope Software, thresholds were set to detect DAB positivity (the brown staining indicating immunoreactivity for the biomarker of interest) in the kidney images. The images were subsequently analysed to determine the proportion of DAB-positive pixels (*i.e.* biomarker positive pixels) relative to the total number of pixels. The Arc sine transformation (Snedecor and Cochran 1989) was applied prior to significance testing. This transformation was insufficient to achieve homogeneity of variance across the control and cisplatin-treated groups. Therefore, one-sided, 2-sample t-tests assuming unequal variances were performed at the 5% significance level, to test for increases or decreases in cisplatin-treated groups compared to day-matched vehicle controls. Differences were deemed statistically significant (at the 5% level) when $P < 0.05$. Multiple pairwise t-test comparisons between control and time-matched cisplatin-treated animals were made rather than ANOVAs, as for ANOVA to be valid, the variances between each group must be approximately the same. Pairwise t-tests allow for unequal variances in each group to be compared.

Construction of Receiver Operator Characteristic Curves

Receiver operating characteristic curves are plots of the false positive rate (1-specificity) of a test on the x-axis and the true positive rate (sensitivity) of a test on the y-axis for different test values as the boundary between a positive and negative prediction. In this study, a false positive is considered the probability of a biomarker predicting proximal tubule necrosis when in fact there is no pathology, and a true positive is considered the probability of a biomarker predicting proximal tubule necrosis when indeed there is

proximal tubule necrosis. A diagonal line though the centre of a ROC plot represents 'no discrimination.' A biomarker with that curve would have no ability to correctly predict proximal tubule necrosis beyond that of chance. The area under curve (AUC) for this ROC plot is 0.5. As such, biomarkers with high sensitivity and specificity, have curves that are close to the left and top of the plot, where the AUC is 1.0. The greater the AUC of a ROC curve (*i.e.* the closer it is to 1.0), the greater the overall accuracy of a biomarker for predicting proximal tubule necrosis.

Using the immunohistochemistry biomarker data generated by positive pixel image analysis by myself, and the histopathology data generated by the pathologist Dr Huw Jones in the pathology group at AstraZeneca, UK, receiver operating characteristic (ROC) curves, to examine the ability of each biomarker studied (KIM-1, OPN, αGST, clusterin, TFF3 and β_2MG) to correctly predict proximal tubule necrosis (a key feature of cisplatin-induced kidney injury), were created with the assistance of clinical scientist Dr Mark Pinches, AstraZeneca, UK. Using an Analyse-it software package (Leeds, UK), a ROC curve was constructed and the AUC determined for each biomarker based on the method described by (DeLong et al. 1988).

To determine if the AUC for each of the biomarkers was significantly different from that of the other biomarkers, the AUC curve for each biomarker was contrasted with that of each of the others. This was again performed with the assistance of Dr Mark Pinches, AstraZeneca, UK. Using an Analyse-it software package (Leeds, UK), each ROC curve was compared against each of the other ROC curves based on the method described by (DeLong et al. 1988). Differences were deemed to be significant when $p < 0.05$ (*).

Urinary Biomarker Analysis: KIM1, OPN and αGST

Urinary biomarker analysis for KIM1, OPN and αGST was performed by the clinical pathology group at AstraZeneca, UK. Methods and data regarding these measurements has previously been published (Pinches *et al.,* 2012). Briefly, urinary biomarkers were assessed using a multiplex electrochemiluminescence-based MesoScale Discovery (MSD) Sector Imager 6000 instrument (MSD, Gaithersburg, MD, USA). Analysis was conducted using two plate options; αGST was assessed using the Argutus acute kidney injury (AKI) Test assay kit (MSD, Gaithersburg, MD, USA) according to the manufacturer's instructions

and KIM-1 and OPN were assessed with the kidney injury panel 1 assay kit (MSD; Gaithersburg, MD, USA). Urinary creatinine concentrations in each sample were measured on a Roche Modular P analyser (Roche Diagnostics, UK) using the Roche Diagnostics Jaffe reaction assay kit (Roche Diagnostics, UK). The Jaffe reaction is a quantitative, colorimetric test for creatinine. Under alkaline conditions, creatinine and picric acid form an orange-red coloured complex, the optical-density of which, can be read and used to determine the creatinine concentration (Wyss and Kaddurah-Daouk 2000). Urinary levels of each of the biomarkers in each sample were normalised against the corresponding urinary creatinine levels.

Correlation between Tissue and Urinary Biomarkers

In this study, urinary biomarker data (for KIM-1, OPN and αGST) generated from control and cisplatin-treated animals at day 5 and day 8 were correlated with the corresponding tissue biomarker data (for KIM-1, OPN and αGST) for each individual animal. N=5 animals for each time point (day 5 and day 8) and dose (0mg/kg, 0.1mg/kg, 1.0mg/kg and 2.5mg/kg) cisplatin. The correlation between tissue biomarker data (generated by myself) and urinary biomarker data (generated by the clinical pathology group at AstraZeneca) was determined by clinical scientist Dr Mark Pinches, AstraZeneca. Correlations between tissue biomarker expression (variable 1) and urinary biomarker expression (variable 2) were performed using a standard Pearson's correlation method using TIBCO Spotfire® software (Boston, MA, USA). Scatter plots to visualise the correlation between the two variables were constructed also using TIBCO Spotfire® software. Pearson's correlation is a test to measure the association between two variables (Pernet et al. 2012); r = +1 (positive correlation), r = 0 (no correlation) and r = -1 (negative correlation). In this study, positive correlation denotes a situation where an increase in the biomarker level in tissue expression is mirrored by an increase in the biomarker level in the urine.

2.6 Results

Images presented in Figures 2.1 – 2.7 contain data relating to day 5 vehicle control (0mg/kg cisplatin)-treated rats, and day 5, day 8 and day 22 high-dose (2.5mg/kg) cisplatin -treated rats. Only high-dose images are presented as greater differences were seen in this group than in lower dose groups. No differences were seen in biomarker expression between vehicle control groups at any time point, and so for simplicity, only day 5 images are shown.

Histopathology

Representative H&E images of kidneys from vehicle-treated and 2.5mg/kg cisplatin-treated rats are shown in Figure 2.1. No major abnormalities in kidneys were observed from control animals at any time point (Figure 2.1A & B). The majority of the effects of cisplatin were seen in the S3 segment of the proximal tubule in the outer stripe of the outer medulla (OSOM) and appeared in a temporal and dose-dependent manner. At 5 days, animals dosed with 2.5mg/kg cisplatin showed high incidence of severe tubular necrosis and nuclear pleomorphism (Figure 2.1C & D). Similar histopathological features were observed after 8 days in animals treated with 2.5mg/kg cisplatin (Figure 2.1E and 2.1F). However, at 8 days most animals also displayed necrotic S3 proximal tubules, tubular proteinaceous contents and necrotic cell debris. Distal tubules and collecting ducts were basophilic which is indicative of regeneration. By day 22, there was recovery from most of the histological findings (Figure 2.1G & H). At corresponding time points, animals dosed with 1.0mg/kg cisplatin showed a similar incidence but reduced severity of tissue damage by comparison with that seen in animals dosed with 2.5mg/kg. Pathological findings in animals dosed with 0.1mg/kg cisplatin were of low incidence and severity.

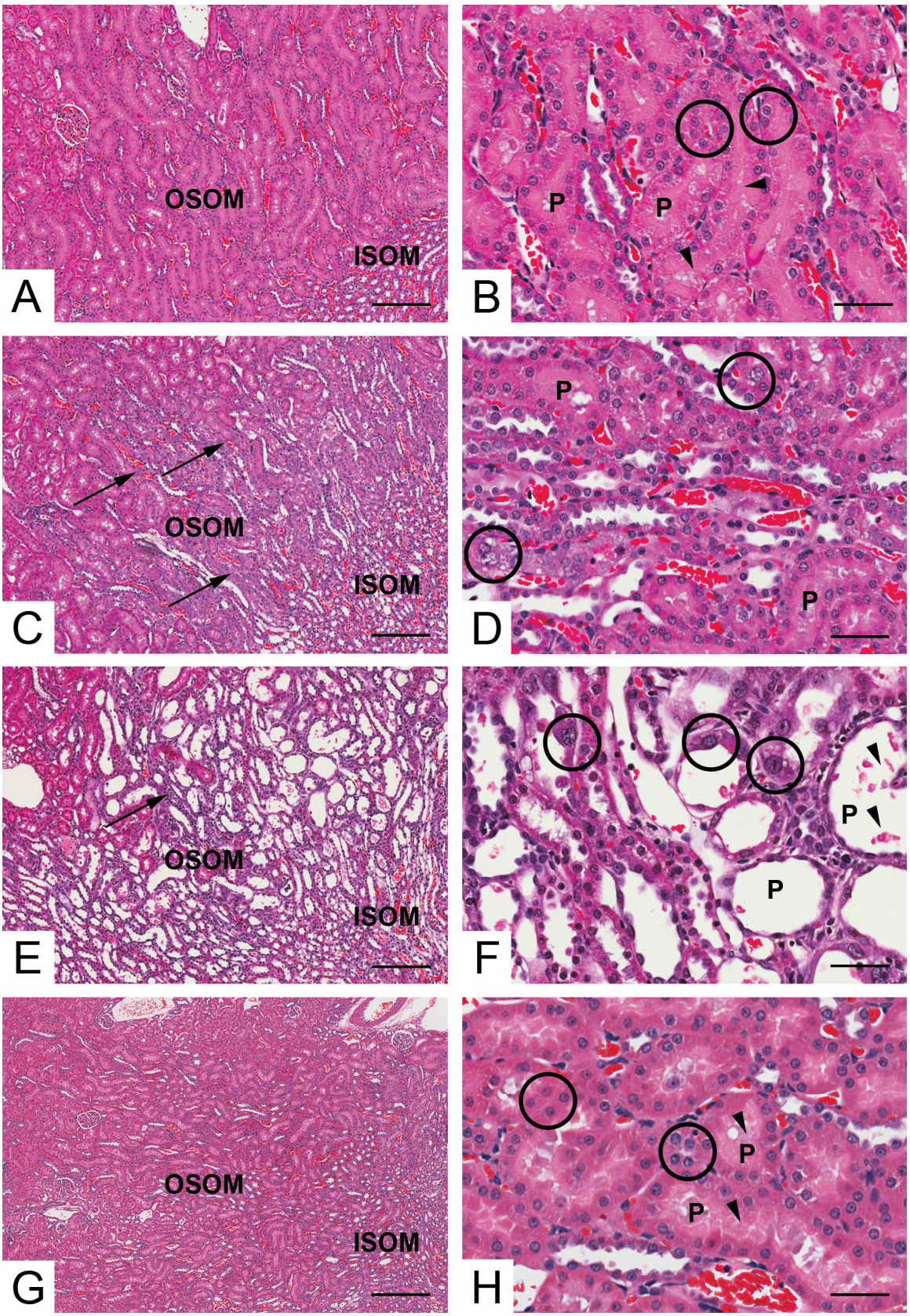

Figure 2.1. Representative H&E images of kidneys from rats treated with a single intra-peritoneal dose of a vehicle (A and B) or 2.5mg/kg cisplatin after 5 days (C and D), 8 days (E and F) and 22 days (G and H). Images are of kidneys sectioned in the transverse plane, and display the outer stripe of the outer medulla (OSOM), in the region of the

segment 3 (S3) proximal tubules, the region where the main nephrotoxic effect of cisplatin are observed. (A & B) Control rat kidney proximal tubules appear normal; brush border membranes are intact (arrow heads) and cell nuclei appear uniform in size and shape (circles). (C & D) Five days post cisplatin-treatment, S3 (also known as the pars recta or the straight) proximal tubules showed signs of tubular necrosis as indicated by nuclear pleomorphism (size variation; circles) and mild basophilia (cells appear more purple than pink) (arrows). (E & F) At day 8, cellular necrosis and nuclear pleomorphism had increased in severity and incidence (circles). Intraluminal cellular casts were also present in some tubules (arrow heads). (G & H) At day 22, much of the histopathology had reversed; nuclei were more uniform in size and shape (circles) and brush border membranes were present (arrow heads). One section per animal was stained for H&E. The entire section was observed by light microscopy before histopathological assessments were made. Images are representative of N=5, n=5 animals for vehicle-treated animals (0mg/kg cisplatin) and N=10, n=10 for cisplatin-treated animals (2.5mg/kg cisplatin). Bars = 250µm (A, C, E and G), 25µm (B, D, F and H).

KIM-1 Immunoreactivity

KIM-1 immunoreactivity was absent in control animal kidneys except for a few kidneys where faint immunoreactivity was identified in isolated tubules (Figure 2.2A). Five days after treatment with 2.5mg/kg cisplatin, KIM-1 immunoreactivity was detected in the S3 proximal tubule brush border membranes (arrow heads) in the outer stripe of the outer medulla (OSOM) on the border with the inner stripe of the outer medulla (ISOM) (Figure 2.2B). Positive pixel analysis identified a significant increase in KIM-1 immunoreactivity in rats dosed with 2.5mg/kg cisplatin compared to vehicle controls (Table 2.4). Eight days after treatment with 2.5mg/kg cisplatin, the distribution of immunoreactivity extended throughout the OSOM with KIM-1 immunoreactivity present on proximal tubule cell apical membranes (arrows) (Figure 2.2C). Some intraluminal proteinaceous contents and casts also stained positive (circled). At day 22, very little KIM-1 immunoreactivity was present and there were no statistically significant difference in the amount of immunoreactivity detected compared to that of control (Figure 2.2D). This finding was consistent with recovery from kidney injury, as seen by H&E pathology (Figure 2.1).

KIM-1 Immunoreactivity

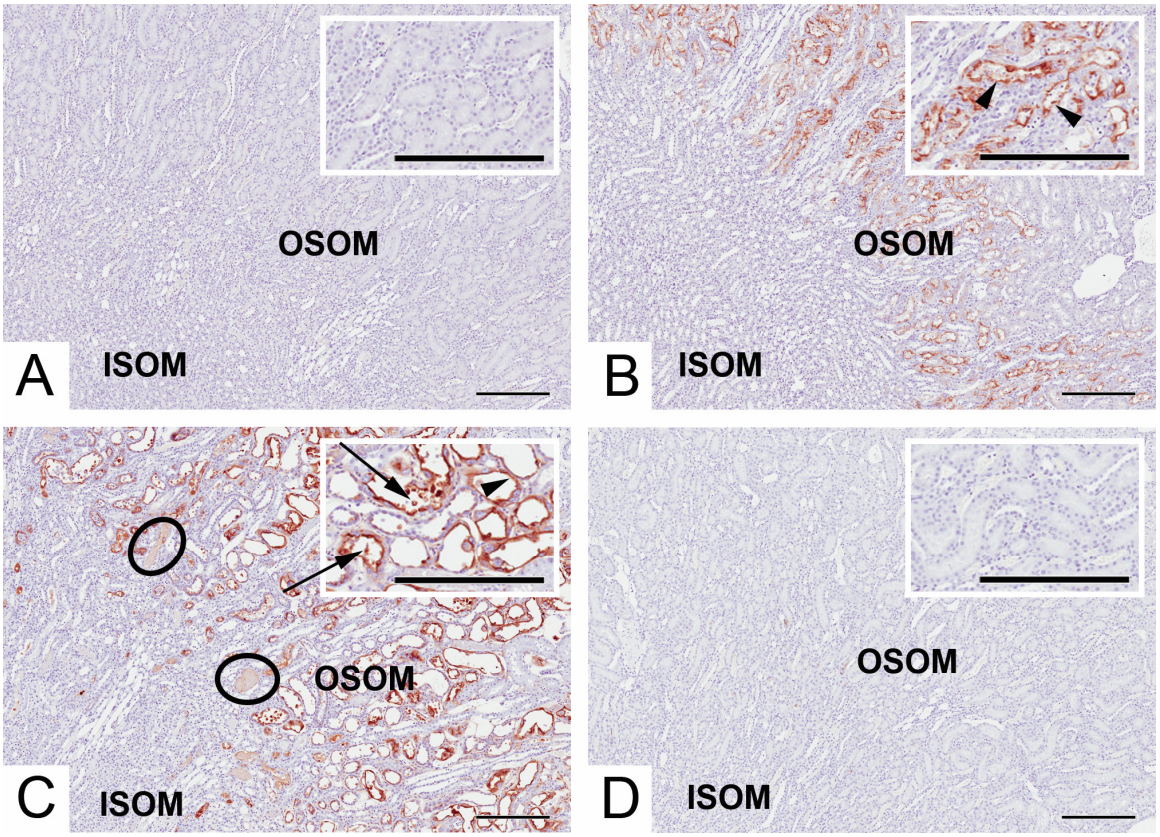

Figure 2.2. KIM-1 immunoreactivity in the kidneys of rats treated with a single intra-peritoneal dose of (A) a vehicle or 2.5mg/kg cisplatin after (B) 5 days, (C) 8 days and (D) 22 days. Images taken at the region of the S3 proximal tubules, in the outer stripe of the outer medulla (OSOM), the region where the nephrotoxic effects of cisplatin occur. (A) Extremely minimal KIM-1 immunoreactivity was detected in control kidneys. (B) At day 5, KIM-1 was detected in the brush border membranes of S3 proximal tubules (arrow heads) in the outer stripe of the outer medulla (OSOM) on the border with the inner stripe of the outer medulla (ISOM) (C) At day 8, KIM-1 immunoreactivity was detected on the apical membranes of S3 proximal tubules in the OSOM (arrow head). Some luminal debris (arrows) and proteinaceous content (circled) also stained positive. (D) By day 22, minimal KIM-1 immunoreactivity remained. KIM-1 immunoreactivity appears brown and the haematoxylin co-stain appears blue. Images representative of N=5, n=5 animals for each time point assessed. Bars = 250µm.

Osteopontin Immunoreactivity

In control rat kidneys, osteopontin was identified throughout the cytoplasm of cells in the thin limb of the loop of Henle (Figure 2.3A). At day 5, additional expression was seen in the thick ascending limbs of the loops of Henle, and there was an overall significant increase in osteopontin immunoreactivity the kidneys of rats dosed with 2.5mg/kg cisplatin compared to time-matched vehicle controls (Figure 2.3B; Table 2.4). At day 8, immunoreactivity for osteopontin was also present in S3 proximal tubules in rats treated with 2.5mg/kg cisplatin, and immunoreactivity remained significantly increased compared to time-matched vehicle controls (Figure 2.3C; Table 2.4). By day 22, immunoreactivity for osteopontin was comparable to that of control rat kidneys; expression was localised to the thin limb of the loop of Henle; no significant difference in immunoreactivity was detected compared to time-matched vehicle controls (Figure 2.3D; Table 2.4). This finding was consistent with recovery from kidney injury, as seen by H&E pathology (Figure 2.1).

Osteopontin Immunoreactivity

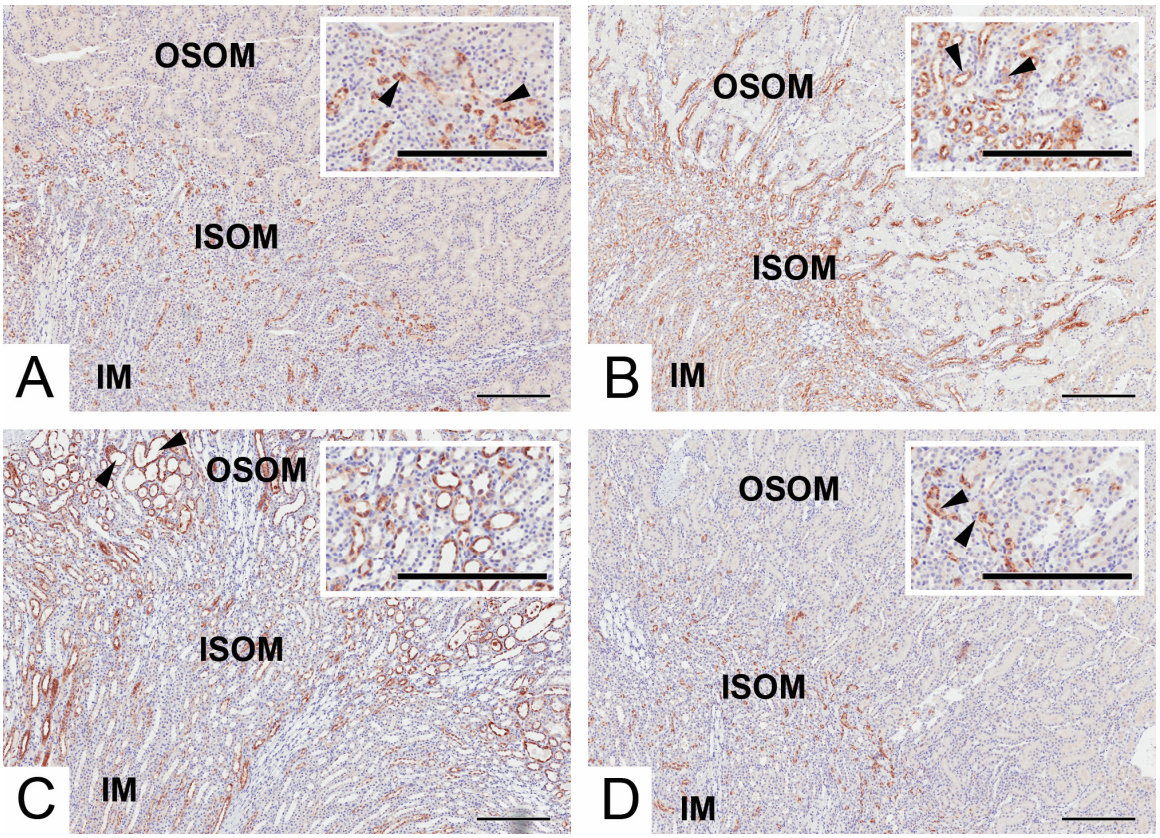

Figure 2.3. Osteopontin immunoreactivity in the kidneys of rats treated with a single intra-peritoneal dose of a (A) vehicle or 2.5mg/kg cisplatin after (B) 5 days, (C) 8 days and (D) 22 days. Images taken at the region of the S3 proximal tubules, in the outer stripe of the outer medulla (OSOM), the region where the nephrotoxic effects of cisplatin occur. (A) In control animals, osteopontin was confined to the thin limbs of the loop of Henle (arrow heads); staining was localised to the inner stripe of the outer medulla (ISOM) and the inner medulla (IM). (B) At day 5, thick and thin ascending limbs were positive for osteopontin (arrows heads). (C) At day 8, osteopontin was detected also detected in the S3 proximal tubule (arrow heads). (D) At day 22, osteopontin immunoreactivity was comparable to that of controls, where it was expressed in the thin limbs of the loop of Henle (arrow heads). Osteopontin immunoreactivity appears brown and the haematoxylin co-stain appears blue. Images representative of N=5, n=5 animals for each time point assessed. Bars = 250µm.

αGST Immunoreactivity

In control rat kidneys, αGST immunoreactivity was present in the cytoplasm of proximal tubules (Figure 2.4A). At day 5, there was a decrease in αGST immunoreactivity in S3 proximal tubules, where immunoreactivity also appeared to be of less uniform. The decrease in immunoreactivity in animals treated with 2.5mg/kg cisplatin was significant when compared to that of vehicle-treated time-matched controls (Figure 2.4B; Table 2.4). At day 8, immunoreactivity for αGST was very faint or absent in S3 proximal tubules in rats treated with 2.5mg/kg cisplatin and remained significantly different compared to time-matched vehicle controls (Figure 2.4C; Table 2.4). No significant changes in staining intensity were detected in lower dose groups at this time point suggestive of recovery from injury (Figure 2.4D; Table 2.4) consistent with recovery from kidney injury, as seen by H&E pathology (Figure 2.1).

αGST Immunoreactivity

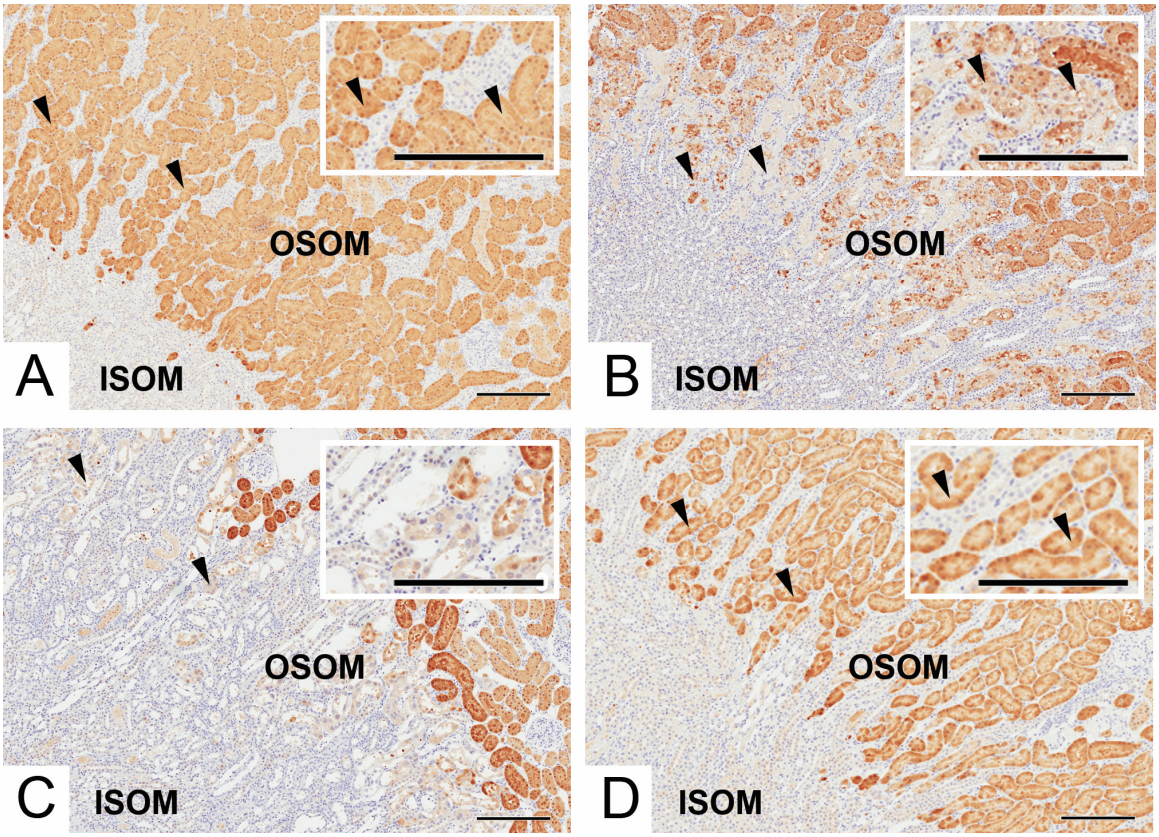

Figure 2.4. αGST immunoreactivity in the kidneys of rats treated with a single intra-peritoneal dose of (A) a vehicle or 2.5mg/kg cisplatin after (B) 5 days, (C) 8 days or (D) after 8 days when treated with 1.0mg/kg cisplatin. Images taken at the region of the S3 proximal tubules, in the outer stripe of the outer medulla (OSOM), the region where the nephrotoxic effects of cisplatin occur. (A) In control animals, αGST immunoreactivity was present and of uniform intensity in proximal tubules of the cortex and outer stripe of the outer medulla (OSOM) (arrow heads). (B) At day 5, αGST immunoreactivity was reduced in the S3 proximal tubules and was of much less uniform staining intensity (arrow heads). (C) At day 8, there was little αGST immunoreactivity in S3 proximal tubules (arrow heads). (D) By day 8, recovery of immunoreactivity comparable to that in control animals had occurred in rats treated with 1.0mg/kg cisplatin (arrow heads). aGST immunoreactivity appears brown and the haematoxylin co-stain appears blue. Images representative of N=5, n=5 animals for each time point assessed. Bars = 250µm.

Clusterin Immunoreactivity

Clusterin immunoreactivity was absent in control animals at every time point (Figure 2.5A). In cisplatin-treated animals at day 5, clusterin was localised to S3 proximal tubule brush border membranes in the OSOM on the border with ISOM (Figure 2.5B). Positive pixel analysis identified a significant increase in immunoreactivity in rats dosed with 1.0mg/kg compared to vehicle-treated controls (Table 2.4). At day 8, minimal immunoreactivity was identified in proximal tubule cells, but intraluminal cellular casts stained very strongly, as did intraluminal proteinaceous contents (Figure 2.5C). At this time point, the staining intensity was only significantly increased compared to controls with the highest dose of cisplatin (2.5mg/kg). By day 22, the amount of clusterin immunoreactivity was reduced compared to days 5 and 8 but there remained a significantly higher amount of staining compared to time-matched control animals (Figure 2.5D).

Clusterin Immunoreactivity

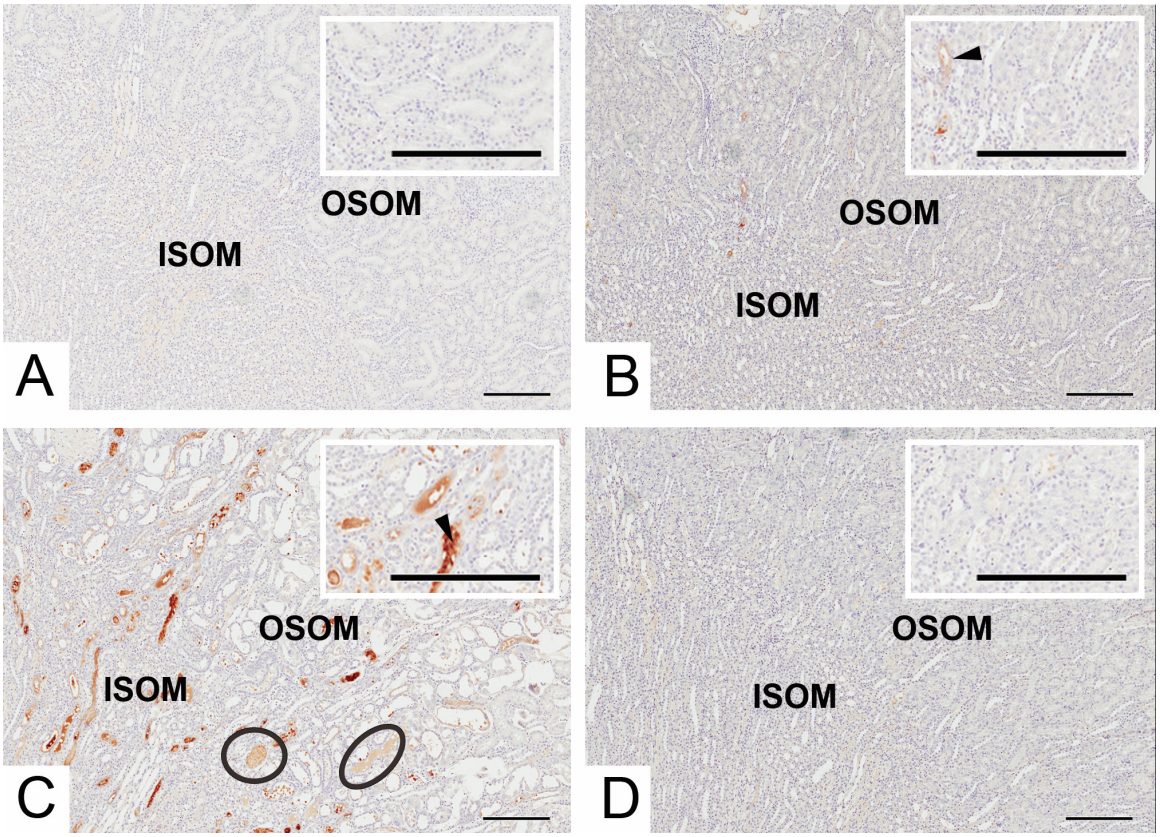

Figure 2.5. Clusterin immunoreactivity in the kidneys of rats treated with a single intra-peritoneal dose of (A) a vehicle or 2.5mg/kg cisplatin after (B) 5 days, (C) 8 days and (D) 22 days. Images taken at the region of the S3 proximal tubules, in the outer stripe of the outer medulla (OSOM), the region where the nephrotoxic effects of cisplatin occur. (A) In vehicle-treated animals, no clusterin immunoreactivity was detected. (B) At day 5, very minimal clusterin immunoreactivity was detected, but that which was detected, was localised to S3 proximal tubule brush border membranes in the OSOM on the border with ISOM. (C) At day 8, intraluminal cellular casts stained very strongly (arrow head), as did intraluminal proteinaceous contents (circled). (D) At day 22, the amount of clusterin immunoreactivity was reduced. Clusterin immunoreactivity appears brown and the haematoxylin co-stain appears blue. Images representative of N=5, n=5 animals for each time point assessed. Bars = 250µm.

TTF3 Immunoreactivity

In control animals, immunoreactivity for TFF3 was detected in S3 proximal tubules in the outer stipe of the outer medulla (OSOM) and thick ascending limbs of the loop of Henle in the inner stripe of the outer medulla (ISOM) and OSOM (Figure 2.6A). At day 5, immunoreactivity in the S3 proximal tubules was decreased in animals treated with 2.5mg/kg cisplatin Positive pixel analysis identified a significant decrease in TFF3 immunoreactivity in this dose group compared to time-matched vehicle controls (Figure 2.6B; Table 2.4). TFF3 remained significantly lower in these high dose animals at both 8 and 22 days when compared to time-matched vehicle controls (Figures 2.6C and 2.6D; Table 2.4). Significant decreases in TFF3 immunoreactivity were also detected in the 0.1mg/kg and 1mg/kg cisplatin-treated animals at day 8 (but not at day 5 or day 22) (Table 2.4).

TFF3 Immunoreactivity

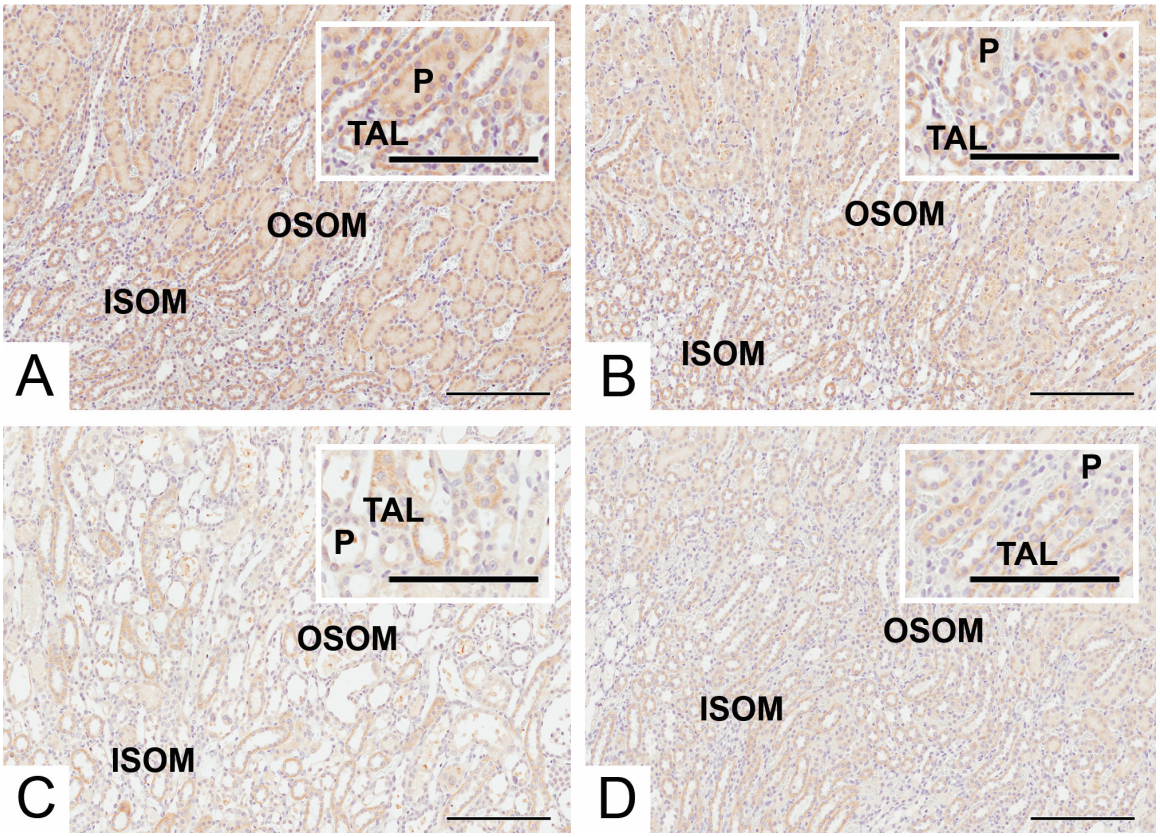

Figure 2.6. TFF3 immunoreactivity in the kidneys of rats treated with a single intra-peritoneal dose of a (A) vehicle or 2.5mg/kg cisplatin after (B) 5 days, (C) 8 days and (D) 22 days. Images taken at the region of the S3 proximal tubules, in the outer stripe of the outer medulla (OSOM), the region where the nephrotoxic effects of cisplatin occur. (A) TFF3 immunoreactivity was detected in S3 proximal tubules in the OSOM, and in thick ascending limbs in the ISOM and OSOM. (B) At day 5, immunoreactivity in the S3 proximal tubules was decreased, and remained lower at both 8 (C) and 22 (D) days. TFF3 immunoreactivity appears brown and the haematoxylin co-stain appears blue. Images representative of N=5, n=5 animals for each time point assessed. P = S3 proximal tubule, TAL = thick ascending limb. Bars = 200µm.

β_2MG Immunoreactivity

In control animals, β_2MG immunoreactivity was localised to S1 proximal tubular cells in the kidney cortex, and was distributed within subapical membrane vesicles as determined by its punctate appearance (Figure 2.7A). Although immunoreactivity appeared fainter (lighter brown immunoreactivity) positive pixel image analysis identified no change in number of pixels staining positive for β_2MG at day 5 in rats dosed with 2.5mg/kg cisplatin compared to vehicle controls (Figure 2.7B; Table 2.4). However, at day 8, a significant decrease in β_2MG immunoreactivity was identified in the 2.5mg/kg cisplatin-treated group (Figure 2.7C; Table 2.4). At day 22, staining appeared similar to that found in control animals with no significant change in immunoreactivity identified when compared to time-matched vehicle controls (Figure 2.7D). No changes were detected in lower dose groups at any time point.

B_2MG Immunoreactivity

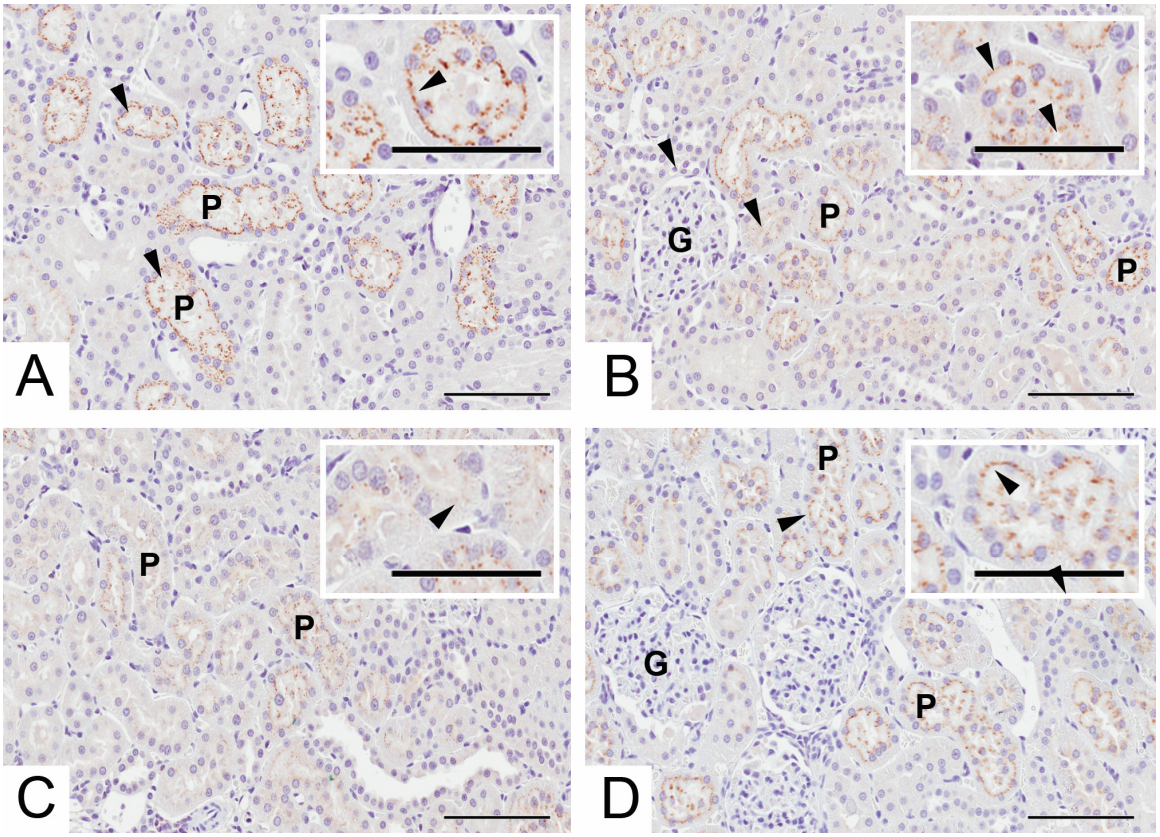

Figure 2.7. β_2MG immunoreactivity images of the kidney cortex of rats treated with a single intra-peritoneal dose of (A) a vehicle or 2.5mg/kg cisplatin after (B) 5 days, (C) 8 days and (D) 22 days. Images taken at the region of the S1 proximal tubules in the outer cortex, the region where β_2MG immunoreactivity is present in healthy rat kidneys. (A) In vehicle-treated animals, β_2MG immunoreactivity was localised to S1 proximal tubule cells in the kidney cortex, where it was specifically localised to S1 subapical membrane vesicles (as evidenced by its punctate pattern) (arrow heads). β_2MG immunoreactivity at days 5 (B) and 8 (C) appears fainter than in vehicle-treated animals, although a similar subapical membrane distribution is observed (arrow heads). (D) At day 22, immunoreactivity for β_2MG has recovered and is comparable to that of vehicle-treated animals (arrow heads). B_2MG immunoreactivity appears brown and the haematoxylin co-stain appears blue. Images representative of N=5, n=5 animals for each time point assessed. G = glomerulus. P = S1 proximal tubule. Bars = 100µm.

Biomarker	Day 5 (mg/kg)				Day 8 (mg/kg)				Day 22 (mg/kg)	
	0	0.1	1.0	2.5	0	0.1	1.0	2.5	0	2.5
KIM-1		ns	ns	***		ns	*	*		ns
	0.029 ±0.0084	0.019 ±0.0032	0.101 ±0.1108	0.191 ±0.0488	0.022 ±0.0049	0.017 ±0.0029	0.060 ±0.0373	0.224 ±0.1281	0.016 ±0.00034	0.014 ±0.0025
OPN		ns	ns	***		ns	ns	**		ns
	0.001 ±0.0007	0.001 ±0.0004	0.005 ±0.0055	0.012 ±0.0053	0.001 ±0.0001	0.001 ±0.0001	0.002 ±0.0013	0.016 ±0.0090	0.002 ±0.0006	0.001 ±0.0003
αGST		ns	*	**		ns	ns	*		
	0.749 ±0.0235	0.750 ±0.0213	0.652 ±0.0361	0.651 ±0.0444	0.636 ±0.0451	0.695 ±0.0392	0.703 ±0.0391	0.562 ±0.0321	-	-
Clusterin		ns	*	*		ns	ns	*		**
	0.00002 ±0.00001	0.00003 ±0.00002	0.00003 ±0.00001	0.00013 ±0.00011	0.00004 ±0.00002	0.00005 ±0.00003	0.00005 ±0.00004	0.0008 ±0.0008	0.00002 ±0.00001	0.00005 ±0.00002
TFF3		ns	ns	**		*	*	**		**
	0.778 ±0.0283	0.751 ±0.0483	0.732 ±0.0557	0.615 ±0.1034	0.773 ±0.0326	0.698 ±0.0695	0.675 ±0.0985	0.507 ±0.1335	0.671 ±0.0784	0.533 ±0.0432
β_2MG		ns	ns	ns		ns	ns	*		ns
	0.127 ±0.0426	0.104 ±0.0216	0.104 ±0.0178	0.119 ±0.0161	0.109 ±0.0347	0.092 ±0.0159	0.095 ±0.0122	0.072 ±0.0144	0.081 ±0.0033	0.076 ±0.103
KIM-1 (urine)		ns	***	***		ns	***	***		*
	-6	-2	2350	3308	-8	-7	370	4933	-25	55
OPN (urine)		ns	***	***		ns	**	***		***
	-8	-33	513	1197	9	52	328	972	-2	154
αGST (urine)		ns	***	***		ns	ns	ns		ns
	21	-40	206	9970	-49	-36	-31	-52	-23	-66

Table 2.4. Legend overleaf.

Table 2.4. Mean values for positive pixel quantification of immunohistochemistry (KIM-1, OPN, αGST, clusterin, TFF3 and β_2MG) and urinary (KIM-1, OPN, and αGST) biomarker measurements in rats dosed with 0, 0.1, 1.0, or 2.5 mg/kg cisplatin over time (day 5, day 8 and day 22). N=5, n=5 (mean±SD) for each biomarker at each time point and dose for immunohistochemistry (where one section per animal per biomarker was analysed), N=5, n=5 (mean) for control animal urinary measurements and N=10, n=10 for each cisplatin-treated animal urinary measurement. Pairwise one-sided, 2-sample t-tests assuming unequal variances were performed at the 5% significance level, to test for increases or decreases in cisplatin-treated groups compared to day-matched vehicle controls. Urinary data were generated in a previous study and are normalized to urinary creatinine (ng/mmol creatinine) (Pinches et al. 2012c). **ns** = not significant, $P < 0.05$ *; $P < 0.01$ **; $P < 0.001$ ***.

Receiver Operating Characteristic (ROC) Curve Analysis

Receiver Operating Characteristic (ROC) curves were constructed (Figure 2.8) to determine how sensitive and specific each of the biomarkers were for detecting proximal tubule necrosis (the primary histopathological change observed following cisplatin treatment (Figure 2.1)). Figure 2.1 shows that KIM-1 has the largest area under the ROC curve when cisplatin-induced proximal tubule necrosis was used as the classifier.

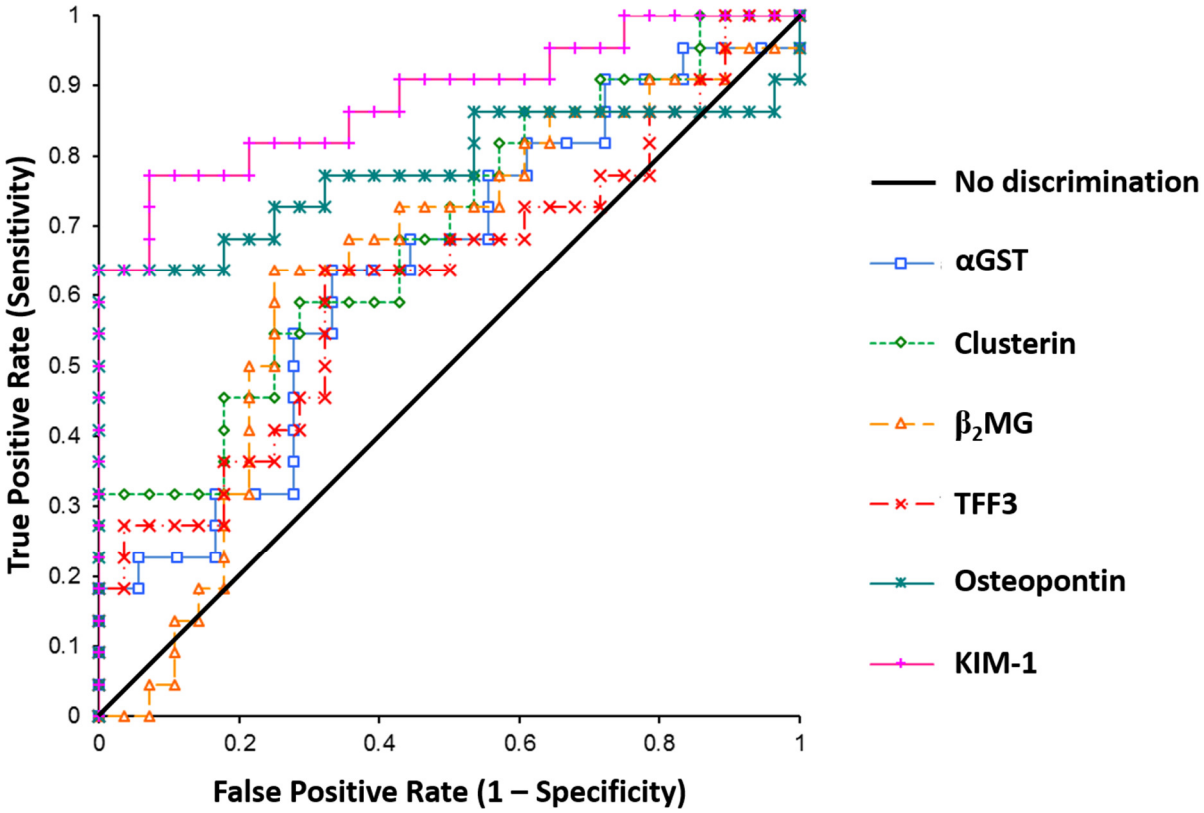

Figure 2.8. ROC curves showing biomarker discrimination (sensitivity and specificity) for detecting cisplatin-induced proximal tubule necrosis in rats, using the presence or absence of this pathology as a classifier. Immunohistochemistry data were generated from 50 animals per biomarker (where 28 animals did not have proximal tubule necrosis, and 22 animals did have proximal tubule necrosis as determined by histopathological assessment by Dr Huw Jones, AstraZeneca, UK). Data presented relates to all doses (0, 0.1, 1.0 and 2.5mg/kg cisplatin) and all time points (day 5, day 8 and day 22). The diagonal line though the centre of the ROC plot represents 'no discrimination.' A biomarker with this ROC curve would have no ability to correctly predict proximal tubule necrosis beyond that of chance. The plot reveals KIM-1 (pink curve) to have the largest area under the curve (AUC). ROC curves were generated using the (DeLong et al. 1988) method by Dr Mark Pinches, AstraZeneca.

Biomarker	Area Under Curve	95% Confidence Interval
KIM-1	0.88	0.78 – 0.98
OPN	0.78	0.63 – 0.94
αGST	0.64	0.47 – 0.82
clusterin	0.64	0.54 – 0.84
TFF3	0.62	0.46 – 0.79
β_2MG	0.69	0.48 - 0.80

Table 2.5. Area under the receiver operator characteristic curve values for rats treated with a single intraperitoneal dose of 0, 0.1, 1.0 or 2.5 mg/kg cisplatin and then killed after 5, 8 or 22 days. Immunohistochemistry data were generated from 50 animals per biomarker (where 28 animals did not have proximal tubule necrosis, and 22 animals did have proximal tubule necrosis as determined by histopathological assessment by Dr Huw Jones, AstraZeneca, UK). Data presented relates to all doses (0, 0.1, 1.0 and 2.5mg/kg cisplatin) and all time points (day 5, day 8 and day 22). The table shows that KIM-1, OPN and clusterin have an area under the curve ± 95% confidence intervals that do not cross the 0.5 'no discrimination' point indicating that these biomarkers perform better than chance alone.

To determine if the area under the curve for each of the biomarkers was significantly different from that of each of the others, pairwise comparisons were made using the method described by (DeLong et al. 1988), with the assistance of Dr Mark Pinches, AstraZeneca, UK (Table 2.6). KIM-1 had the largest area under the ROC curve. Significant differences between the AUCs for KIM-1 vs αGST, KIM-1 vs clusterin, Kim-1 vs TFF3 and KIM-1 vs β_2MG were identified, indicating that KIM-1 is better than these biomarkers at predicting proximal tubule necrosis. No significant difference was seen for KIM-1 vs OPN.

Comparison	Difference	95% CI	SE	P value
KIM-1 v OPN	-0.10	-0.24 to 0.04	0.073	0.1770
KIM-1 v aGST	-0.24	-0.40 to -0.08	0.081	0.0030 *
KIM-1 v Clus	-0.19	-0.34 to -0.05	0.075	0.0104 *
KIM-1 v TFF3	-0.26	-0.43 to 0.09	0.087	0.0032 *
KIM-1 v B_2MG	-0.24	0.43 to -0.05	0.098	0.0147 *
OPN v aGST	-0.14	0.33 to 0.05	0.096	0.1423
OPN v Clus	-0.09	-0.23 to 0.04	0.070	0.1836
OPN v TFF3	-0.16	-0.36 to 0.04	0.101	0.1167
OPN v B_2MG	-0.14	-0.36 to 0.08	0.110	0.2056
aGST v Clus	-0.05	-0.21 to 0.11	0.083	0.5581
aGST v TFF3	0.02	-0.20 to 0.23	0.110	0.8700
aGST v B_2MG	0.00	-0.27 to 0.27	0.140	0.9917
Clus v TFF3	0.07	-0.12 to 0.25	0.095	0.4843
Clus v B_2MG	0.05	-0.19 to 0.28	0.119	0.6936
TFF3 v B_2MG	0.02	-0.26 to 0.30	0.142	0.8909

Table 2.6. Comparisons of the AUC for each biomarker against that of each of the other biomarkers. The table details all pairs of biomarker AUCs compared, the difference in the AUC between pair, the 95% confidence interval (CI), the standard error (SE) and the p values. Differences were deemed statistically significant when $p < 0.05$ (*). Comparisons were made using the method described by (DeLong et al. 1988), using Analyse-it Software by Dr Mark Pinches (AstraZeneca, UK). Data were generated from 50 animals per biomarker (where 28 animals displayed no proximal tubule necrosis, and 22 animals possessed proximal tubule necrosis as determined by histopathological assessment).

Correlation of Tissue and Urinary Biomarkers

For three of the tissue biomarkers investigated (KIM-1, OPN and αGST), urinary biomarker data from the same animals has already been published (Pinches *et al.,* 2012). In order to determine whether tissue biomarkers can provide the same information as urinary biomarkers when urine samples are not available (such as in retrospective studies), the immunohistochemistry tissue biomarker data were correlated with urine biomarker for each animal, for all dose groups at day 5 and day 8. Figure 2.9 shows the relationships between the tissue biomarker data and the urinary biomarker data, using the urine collection taken on the same day the animals were terminated. For both KIM-1 and osteopontin, the immunohistochemistry biomarker data positively correlated with the urinary biomarker data (R^2 = 0.883 and 0.560, respectively). For αGST, there was no correlation between the two sets of data. No urinary data were available to make similar correlations for clusterin, TFF3, or β_2MG.

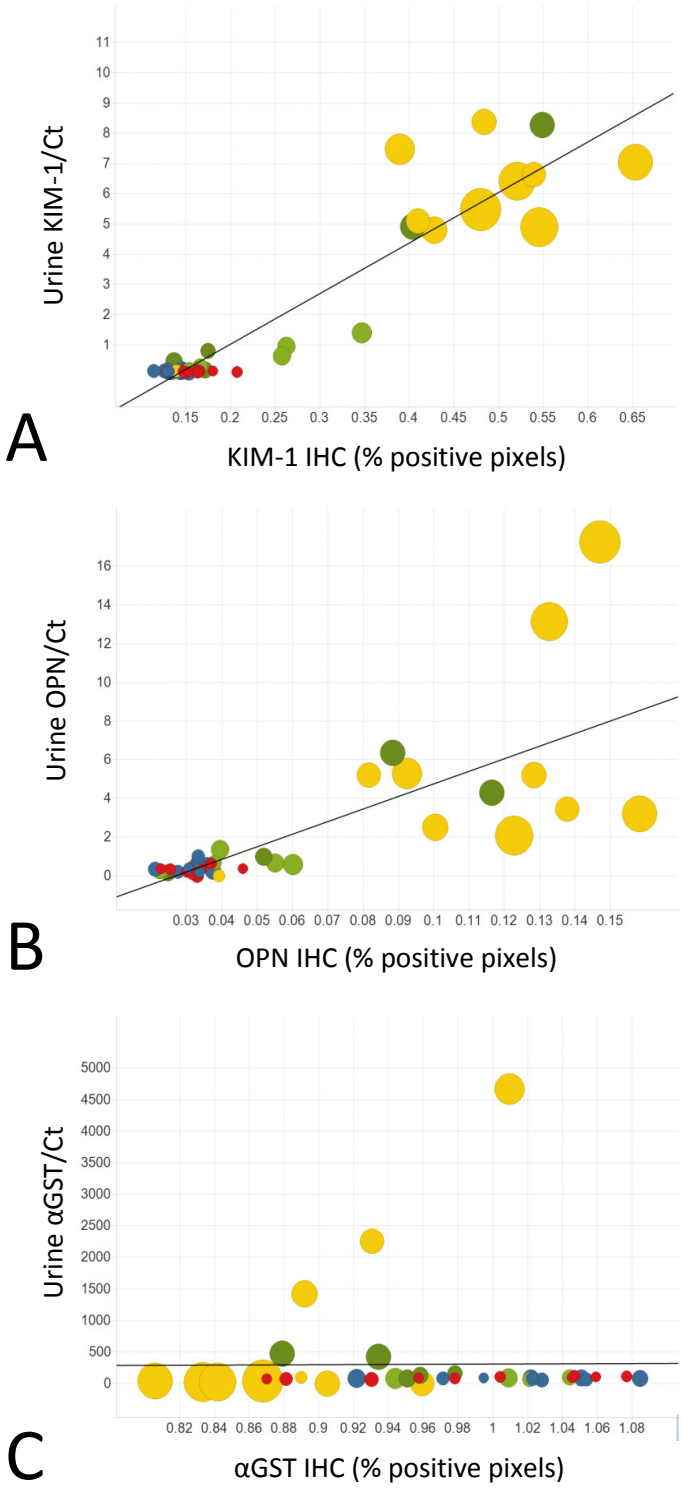

Figure 2.9. Correlation of urinary biomarker data with immunohistochemistry data for (A) KIM-1, (B) OPN, and (C) αGST following cisplatin-treatment. Urinary biomarker data represents the values measured on the same day (day 5 and day 8) that tissues were taken for immunohistochemistry. Urinary biomarker data are normalised to creatinine (Ct) and were generated in a previous study (Pinches *et al.,* 2012). Red circles represent animals treated with 0mg/kg cisplatin, blue circles = 0.1mg/kg cisplatin, green circles = 1.0mg/kg cisplatin and yellow circles = 2.5mg/kg cisplatin. Circle size is directly proportional to the severity of the pathology, which was graded (by Dr Huw Jones, AstraZeneca, UK) 0-4 for proximal tubule necrosis: 0 = no necrosis, 1 = minimal, 2 = mild, 3 = moderate, or 4 = severe KIM-1 = kidney injury molecule-1, OPN= osteopontin, αGST = alpha-glutathione S-transferase. N=5, n=5 animals for each time point and dose.

2.7 Discussion

In this study, a cisplatin model of nephrotoxicity was used to examine several renal injury biomarkers (KIM-1, osteopontin, αGST, clusterin, TFF3 and β_2MG) in rat kidney tissue and correlate the expression of these with measurements of the same biomarkers in the urine (where possible). The aim was to determine the utility of tissue biomarkers, which would allow biomarker analysis from retrospective studies in the drug discovery process, reducing the need for additional animal studies and resource. Whether the tissue data could provide additional information that may complement assessment of nephrotoxicity made using urinary biomarkers, and whether these can be used to provide the spatio-temporal description of the drug-induced damage/regeneration process, was also assessed.

In agreement with other groups (de Borst et al. 2007; Vinken et al. 2012), very low levels of KIM-1 immunoreactivity in some control rat kidneys was detected; a finding likely to reflect low levels of naturally occurring tubular injury/regeneration. In animals dosed with cisplatin, all animals that exhibited KIM-1 positive immunoreactivity also showed histopathological changes. However, as there was no significant difference in KIM-1 immunoreactivity in the low dose group, when minimal histopathological changes were observed (over no pathology in control animals), it indicates that KIM-1 immunoreactivity in tissue was not as sensitive as standard histopathology. The AUCs from ROC curves indicated that KIM-1 was the most predictive of the tissue biomarkers for proximal tubule necrosis (the predominant feature of the histopathology); it had had the highest AUC for all the tissue biomarkers investigated, and its 95% confidence intervals were above the 'no discrimination' point of 0.5 indicating that it predicts proximal tubule necrosis better than chance alone. Significant differences in group means for tissue KIM-1 were observed in the same dose groups that have previously reported significant changes in urinary KIM-1 (Pinches et al. 2012b). However, some animals showed increases in urinary KIM-1 in the mid-dose cisplatin group, when no increases in tissue KIM-1 were observed. This finding was in line with a previous study that demonstrated occasional increases in urinary KIM-1 before nephrotoxic changes were evident by histopathological evaluation (Hoffmann et al. 2010). The authors of this study did not propose that biomarker responses preceded the tubule damage, rather that the changes may be associated with

a few damaged tubules not evident in the particular histopathological section examined. However, in general, a high level of correlation between tissue and urinary KIM-1 was observed using a Pearson's correlation method, suggesting that tissue KIM-1 can be used as a predictive biomarker for cisplatin-induced nephrotoxicity, in the absence of urine samples.

Osteopontin expression was restricted to the loop of Henle in control rats, in agreement with previous observations (Hudkins et al. 1999; Persy et al. 1999). Similar to other animal models of nephrotoxicity, cisplatin-induced nephrotoxicity induced expression of osteopontin in other parts of the kidney (Xie et al. 2001a). The AUC from the ROC curve indicated that osteopontin was also a good predictor of proximal tubule necrosis, as the 95% confidence interval for OPN fell above the 'no discrimination' point of 0.5. Furthermore, there was a good correlation between urinary osteopontin levels and kidney tissue expression, but as with KIM-1, it was the standard histopathology that indicated the earliest signs of nephrotoxicity. Osteopontin is expressed in a variety of tissues including bone and many epithelial tissues (L. Brown et al. 1992; Denhardt and Guo 1993), and is also normally detectable in urine (Hedgepeth et al. 2001). Whilst non-renal sources of intact osteopontin would be too large to be filtered at the glomerulus, it is possible that osteopontin fragments from non-renal sources may become detectable in urine. Therefore parallel detection of osteopontin in both kidney and urine offers the advantage of confirming that any urinary changes seen are as a consequence of changes occurring in the tissue.

Clusterin expression was not detectable in control rat kidneys but expression within the proximal tubules became evident following treatment with cisplatin, consistent with previous reports (Ishii et al. 2007; Silkensen et al. 1997). Whilst the ROC curves for clusterin showed some discrimination for predicting proximal tubule necrosis, the AUC was less than that for KIM-1 or osteopontin. The 95% confidence interval for the clusterin was however, above the 'no discrimination' point of 0.5 suggesting that it does have utility for predicting proximal tubule necrosis.

In accordance with its role as a cytosolic protein in proximal tubule cells (Bauchet et al. 2011; Branten et al. 2000; Searchfield et al. 2011), αGST immunoreactivity was observed

throughout the proximal tubule in control rat kidney. αGST was significantly decreased in mid- and high-dose animals five days after cisplatin treatment but, by eight days, there was only a significant decrease with the high dose group. The AUC from the ROC curve for αGST suggested that this biomarker was not as good as other biomarkers at predicting proximal tubule necrosis as its 95% confidence interval crossed the 0.5 'no discrimination' point. There was also poor correlation between the tissue and urinary αGST measurements. Studies with other nephrotoxins looking at urinary αGST have also shown a poor correlation between proximal tubule necrosis and αGST (Kharasch et al. 1998; Prozialeck et al. 2009). Despite these findings, tissue and urinary αGST measurements have been shown to outperform serum creatinine as a biomarker for cisplatin induced nephrotoxicity (Pinches et al. 2012b).

TFF3 expression was detected in S3 proximal tubules in the OSOM, tubules in the ISOM and inner medulla, consistent with *in situ* hybridisation studies for mRNA in rats (Yu et al. 2010). Its expression was however more widespread than that shown by histochemistry using a trefoil peptide motif in a beta-galactosidase fusion protein, where expression was restricted to the collecting ducts of rat kidney (Chinery et al. 1993). This observation may reflect the different sensitivity of the techniques used. The AUC from the ROC curve showed that TFF3 was able to detect proximal tubule damage but was not as good as other biomarkers, as its 95% confidence interval crossed the 'no discrimination' point of 0.5. A decrease in TFF3 immunoreactivity was observed in cisplatin-treated kidneys, similar to that observed with other nephrotoxins, and is most likely a result of a gene regulatory response to tubular toxicity (Yu et al. 2010). In this study, TFF3 was the only biomarker to show significant change following low dose cisplatin at eight days. This suggests that kidney levels of TFF3 may be useful in detecting low levels of chronic (long-term) kidney damage and it would be interesting to study this further. TFF3 is also highly expressed in the gastrointestinal tract (Chinery et al. 1993; Suemori et al. 1991) and is small enough to be filtered at the glomerulus. Therefore immunohistochemistry may be useful in confirming that changes in urinary TFF3 originate from the kidney.

β_2MG was expressed in the S1 segment of the proximal tubules in control rats but is expressed throughout the body and is freely filtered at the glomerulus. Following filtration it is almost completely reabsorbed so under normal conditions it is not present

in the urine. However, both glomerular and tubular toxicity have been shown to impair this process resulting in increases of up to several hundred fold in urine. Consistent with this finding, no changes in β_2MG by immunohistochemistry were observed except 8 days after a high dose of cisplatin. This is probably the result of extensive necrosis and associated loss of protein from the tubules. The AUC from the ROC curve reflects this; there is some association with proximal tubule necrosis but the sensitivity and specificity of this biomarker is less than other biomarkers investigated. The 95% confidence interval for β_2MG also crossed the 'no discrimination' point of 0.5. Whilst urinary β_2MG appears to show utility as a biomarker of nephrotoxicity, tissue β_2MG is less sensitive and therefore should not be used for measurements in the absence of urine samples.

One of the key features of novel biomarkers is that they identify injury before changes in histopathology are seen. In this preclinical, retrospective study, the earliest samples available were obtained 5 days post cisplatin treatment, a time point when histopathological changes were clearly visible. Repeating the experiment to include earlier time points (e.g. days 1 – 5) or even earlier (e.g. 12 hours) would be useful in assessing the ability of the biomarkers to indicate injury before changes in histopathology are seen. Although this is important for drug discovery, it is especially important in the clinic where urinary biomarkers that can be identified in the urine before histopathological injury occurs enables clinicians to intervene (e.g. by lowering drug dose or using a different drug) and reduce the likelihood of AKI progression. A further limitation of this study was the sample size. A larger sample size might enable statistically significant differences between the performance of different biomarkers (as determined by the AUC from ROC curves) to become apparent.

In any case, future studies are also needed to determine the wider application of these biomarkers for detecting renal toxicity following the administration of other nephrotoxicants. In addition, their utility as broad-spectrum biomarkers of nephrotoxicity, biomarkers of nephrotoxicity specific to certain tubules or certain classes of drugs, or indeed biomarkers of other types of renal injury, needs addressing. Many other novel protein biomarkers of acute kidney injury exist (aquaporin-2, neutrophil gelatinase-associated lipocalin (NGAL), cystatin C, Fetuin A and liver-type fatty acid binding protein (LFABP) (Vaidya et al. 2008)) and could also be investigated.

In summary, this study investigated changes in tissue biomarkers of kidney injury in a cisplatin-treated rat model. The biomarkers investigated were KIM-1, osteopontin, αGST, clusterin, TFF3 and β_2MG. Out of the biomarkers investigated, KIM-1 and osteopontin were most predictive of proximal tubule necrosis (as determined AUC ROC analysis) and showed correlation with their corresponding urinary biomarkers. As such, KIM-1 and osteopontin offer greater utility as tissue biomarkers in retrospective studies when urine samples are not available.

CHAPTER 3

Characterisation of *In Vitro* and *Ex Vivo* Models as Tools for Studying Drug-Induced Nephrotoxicity

3.1 Abstract

The kidney is a major organ of drug-induced toxicity. Lack of translational preclinical models for predicting nephrotoxicity specifically in humans means that it is often detected at late stages of drug development, with significant delays in delivering safe drugs to the market. The availability of better rodent models for use in parallel with human models would improve translational drug safety assessment. In this study, two models were selected for characterisation as potential tools to meet this need; *ex vivo* kidney slices and *in vitro* primary renal cells.

Ex vivo rat kidney slice viability (determined by ATP content) was significantly reduced after 24 hours in culture under control conditions compared to the that immediately following slicing (1.04±0.07 vs 0.57±0.05 nmoles ATP/mg wet weight respectively (mean±SEM; $p < 0.01$ **; N=3, n=3)). In addition, histopathological changes indicative of loss of cell viability (nuclear condensation, loss of proximal tubule brush border membranes, cell sloughing into the tubule lumen) were observed in control slices after 1 and 24 hours in culture (N=3, n=3). Together, these data suggest that kidney slices are a valuable model only for acute studies. Future optimisation studies aim to improve slice viability in order to fully assess this model.

In contrast, *in vitro* primary mouse cells exhibited high viability (determined by high proliferation (N=3, n=3) and low apoptosis (N=3, n=3)) for up to 15 days in culture. After 8 days in culture, cells displayed a concentration-dependent increase in apoptosis in response to 24-hour treatment with medium containing the known nephrotoxins cisplatin (1, 3, 5µM), cyclosporin A (1, 3, 5µM) and BEA (3, 10, 30µM), compared to cells treated with control medium (N=3, n=3). In addition, cells exhibited concentration-dependent loss of cell adhesion to the tissue culture plate in response to treatment with cisplatin (1, 3, 10µM), cyclosporin A (1, 3, 10µM) and BEA (1, 3, 30µM) (N=3, n=3). When compared to time-matched control cells, 24-hour treatment with medium containing 10µM cisplatin, 10µM cyclosporin A and 30µM BEA induced the expression of the kidney injury biomarkers, kidney-injury molecule-1 (KIM-1) and osteopontin, but not that of clusterin (N=3, n=3). Compared to control cells of which 3.24 ± 0.05% were KIM-1 positive, treatment with cisplatin, cyclosporin A and BEA increased the number of KIM-1 positive cells to 79.21 ± 5.68% ($p < 0.001$ ***), 44.02 ± 5.73% ($p < 0.001$ ***) and 48.83 ±

4.89 ($p < 0.001$ ***), respectively. Compared to control cells of which 13.82 ± 2.28% were osteopontin-positive, treatment with cisplatin, cyclosporin A and BEA increased the number of osteopontin-positive cells to 71.91 ± 8.23% ($p < 0.001$ ***), 41.76 ± 1.92% ($p < 0.001$ ***) and 35.14 ± 2.47% ($p < 0.01$ **), respectively (results expressed as mean±SD and significance determined by one-way ANOVA and post-hoc Tukey test).

Primary human renal cells also exhibited high viability (high proliferation/low apoptosis) for up to 15 days in culture (N=3, n=3 for both). After 8 days in culture, 24-hour treatment with medium containing 25µM cisplatin induced expression of KIM-1, osteopontin and clusterin when compared to cells treated with control medium (N=1, n=1). Exposure to cisplatin increased the expression of all tested biomarkers, from 0% to 98% (KIM-1), from 57% to 95% (osteopontin) and from 4% to 41% (clusterin).

Differences in the expression of clusterin in response to nephrotoxin-treatment in human and mouse models not only highlight species differences, but reinforces the idea that use human models would not only improve studies of drug-induced toxicity specifically in humans, but when used alongside rodent models, would revolutionise preclinical, translational drug safety assessment.

3.2 Introduction

Nephrotoxicity

Drug toxicity is a leading cause of drug attrition from the development pipeline (Liebler and Guengerich 2005). An essential part of preclinical development is having appropriate models to predict the safety of a novel compound before administration to humans. A number of different preclinical animal models including rat, dog and monkey, are used to do this (Martignoni et al. 2006). Although very valuable, differences in drug handling between species means that toxicity in animals does not reliably predict toxicity in humans, nor safety in animals reliably predict safety in humans. This is evidenced by the fact that nephrotoxicity accounts for only 2% of all drug failures during preclinical studies but jumps to 19% of all failures in Phase III clinical studies (Redfern et al. 2010). In fact, results from the International Life Sciences Institute (ILSI) workshop, which set out to better understand the concordance of drug toxicity in humans with that of preclinical species, revealed that *in vivo* rat studies correctly predict toxicity in humans only 43% of the time (Olson et al. 2000). Improving translational (animal to human) safety assessment by reducing the rate of false positives and false negatives will respectively prevent drugs that are toxic to humans, but not animals reaching clinical trials, and drugs that are safe in humans but not animals, being mistakenly dropped from development. As such, to improve safety assessment and bridge-the-translational-gap, human models need to be used alongside animal models.

Assessing Nephrotoxicity Using Conventional *In Vitro* Cell Models

Currently, there are a number of different *in vitro* renal cell models that could potentially be used for regulatory toxicology studies during preclinical drug development for predicting toxicity in humans. However, most are inherently limited for use for this application.

With regard to the species from which the cells are derived, cell lines such as Madin Darby Canine Kidney cells (MDCK; (Ludwig et al. 2004)), Opossum Kidney cells (OK; (Y. Kim et al. 2005)), Lilly Laboratories Cell-Porcine Kidney-1 cells (LLC-PK1; (Pingle et al. 2004)) and Normal Rat Kidney Epithelial cells (NRK-52E; (Rached et al. 2008)), all of which have

previously been used for studying drug-induced toxicity, are of animal origin, and as such, are not acceptable models for human studies simply due to the fact they are not human.

With regard to cell lines derived from humans, a number exist, but their utility is somewhat limited. Human Embryonic Kidney (HEK)293 cells, for example, possess the neuronal markers neurofilament-M and neurofilament-L (NF-M and NF-L) and α-internexin (Shaw et al. 2002), and are actually believed to have derived form a neuronal population that were amongst the renal cells when targeted for immortalisation (Shaw et al. 2002; Tiong et al. 2014). Their lack of real renal epithelial cell phenotype instantly renders them of little use during preclinical drug nephrotoxicity studies.

Human Kidney (HK)2 is a human papilloma virus (HPV)-immortalised cell line derived from adult proximal tubule cells. It expresses a variety of proximal tubule brush border membrane enzymes including acid and alkaline phosphatases (ALP), gamma glutamyltranspeptidase (GGT) and leucine aminopeptidase (LAP) (Ryan et al. 1994), as well as the proximal tubule drug transporters monocarboxylate transporter 1 (MCT1) and organic anion transporter polypeptide 4C1 (OATP4C1) (Jenkinson et al. 2012). However, HK2 cells do not express other key drug transporters including organic anion uptake transporters 1 and 3 (OAT1 and OAT3), organic cation uptake transporter 2 (OCT2) (Jenkinson et al. 2012; Tiong et al. 2014). If used in preclinical drug safety assessment, the lack of such transporters may result in a potentially nephrotoxic compound not being taken up by the cells and its nephrotoxicity not being seen. Indeed, these results indicate that HK2 cells do not fully recapitulate all the features of proximal tubule cells *in vivo* and as such are not a good model for studying nephrotoxicity *in vitro*. This is exemplified by a recent study in which treatment with the nephrotoxin cisplatin induced apoptosis and expression of the known injury biomarker KIM-1 (both features of cisplatin toxicity), but not the expression of clusterin (another known biomarker of cisplatin toxicity) (Sohn et al. 2013). Even more recently, HK2 cells have also been used to identify novel biomarkers of cisplatin-induced renal injury (pyruvate kinase M1/M2 isoform M2 (PKM2) and eukaryotic translation elongation factor 1 gamma (EF-1γ)) (S. Kim et al. 2014), but again, results like this must be interpreted with caution.

Conditionally immortalised proximal tubule epithelial cell (ciPTEC) lines have been developed and characterised in terms of functional influx and efflux transporters from both human kidney tissue and proximal tubules cells present in urine (Jansen et al. 2014; Wilmer et al. 2010). ciPTEC isolated from exfoliated renal cells present in mid-stream urine, cells underwent immortalisation with the temperature-sensitive mutant U19tsA58 of SV40 large T antigen (SV40T) and the catalytic subunit of human telomerase (hTERT). Cells proliferate at the permissive temperature of 33°C under the control of SV40T, while at 37°C, SV40T expression decreases to minimise the effect of transfection on cellular functions. At this point, cells exhibit proximal tubule cell morphology (presence of microvilli), functional NaP_i IIa, OCT2 and MDR1, and expression of MRP4. Although further characterisation in terms of protein expression and function are needed, ciPTECs are the most promising immortalised renal cell model for use in nephrotoxicity studies, an application already being explored as part of the National Centre for the Replacement, Refinement and Reduction of Animals in Research (NC3Rs) CRACK-IT Nephrotube Challenge (https://www.crackit.org.uk/challenge-15-nephrotube). The major limitation of using these ciPTECs from urine, however, is that although they are collected from healthy volunteers, only 10% of urine samples contain viable primary cells for subsequent immortalisation (Wilmer et al. 2010). The authors state that whilst obtaining cells from urine is not ideal (it can be argued that cell damage could have led to their detachment from the basement membrane and subsequent sloughing into the urine), it is useful source of human material for *in vitro* research, especially in circumstances when obtaining tissue is not possible (*i.e.* invasive biopsy versus non-invasive collection of cells from urine).

In addition to the aforementioned immortal and conditionally immortal cell lines, stem cell-derived proximal tubule-like cells (PTLC) have been generated and undergone initial characterisation as a tool for identifying nephrotoxic compounds *in vitro* (Y. Li et al. 2014). Drug-induced kidney injury (DIKI) is associated with increased pro-inflammatory cytokines; cisplatin-induced AKI, for example, is associated with increased interleukin (IL)-1β, IL-6 and IL-18 (Faubel et al. 2007). Using stem cell-derived PTLC, Li et al., (2014) showed the combination of IL-6 and IL-8 as a readout to be highly predictive of DIKI injury (as determined by an area under a receiver operating characteristic curve of 0.80).

Although promising, such results must interpreted with caution because the stem cell-derived PTLC used in the study do not express key drug transporters at the same level as the primary human proximal tubule cells also assessed in the study; they express OAT2 and OAT3, proton-coupled peptide transporter (PCPT) and MDR1 in at least 3-fold less quantities than the primary human proximal tubule cells used (Y. Li et al. 2014), which may affect drug uptake and subsequent intracellular events.

An alternative to the use of cell lines is the use of primary cells. Although primary cells are more difficult to culture and are inherently associated with a degree inter-donor variability, they do offer a more physiologically relevant model. In this respect, primary cultures of proximal tubule cells, and co-cultures of proximal and distal tubule cells, have already undergone extensive characterisation as a models for drug transport studies (C. Brown et al. 2008; Verhulst et al. 2008) and studies of mineral ion homeostasis (see Chapter 1 of this thesis). When grown on semi-permeable filter supports (transwells), primary cells maintain apical-basolateral polarity as well as expression of endogenous plasma membrane drug transporters at the mRNA, protein and functional level for up to 10 days (C. Brown et al. 2008). Figure 3.1 highlights the expression of a range of drug transporters present on *in vitro* proximal tubule cell membranes at the mRNA, protein and functional level, compared to the same transporters found *in vivo*.

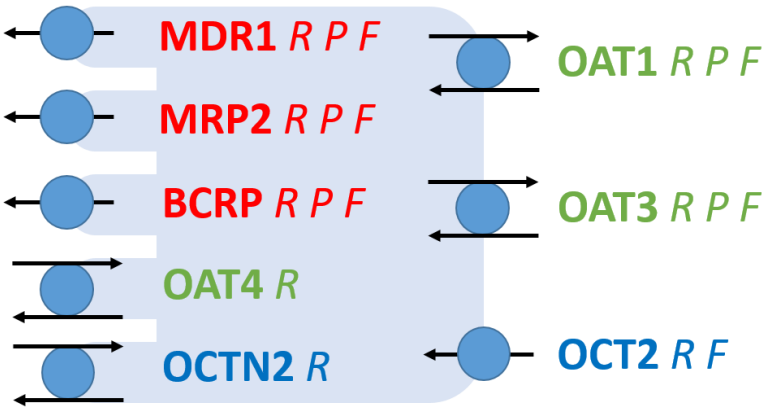

Figure 3.1. Expression of proximal tubule cell drug transporters *in vitro*. All transporters are expressed on human proximal tubule cell membranes *in vivo*. Image created from data published by (C. Brown et al. 2008). The same transporters were identified on primary human proximal tubule cell membranes *in vitro* in terms of mRNA expression (R), protein expression (P), and/or functional expression (F). ATP-binding cassette (ABC) transporters multidrug resistance protein 1 (MDR1), multidrug resistance protein 2 (MRP2) and breast cancer resistance protein (BCRP) appear in red, organic anion transporters (OAT) OAT1, OAT3 and OAT4 appear in green, and organic cation transporters (OCT) OCT2 and OCTN2 appear in blue. Figure created from data published by (C. Brown et al. 2008).

The above cell model (aProximate^{TM}) is commercially available under contract service from Newcastle University/SOLVO Biotechnology. One of the major advantages of this model over other primary proximal tubule cell models, such that from the contract research organisation (CRO) Fluofarma, is that the cells are cultured immediately after isolation; they are never frozen. Maintenance of drug transporter expression makes the aProximate^{TM} cell model a powerful tool for studying renal drug handing, drug-transporter interactions as well as drug-induced nephrotoxicity.

Whilst primary cultures offer greater utility than other discussed *in vitro* cell culture models currently available, like all *in vitro* cell culture models, they do not possess the 3D architecture of the *in vivo* tissue or organ of interest. The kidney is a complex organ made up of many different types of cells and cell-cell and cell-matrix interactions, all of which are important for maintaining correct cell phenotype and function (Astashkina et al. 2012).

Loss of Cell Adhesion as a Drug-Induced Effect

Roughly 6 X 10^4 cells are shed into the urine from the entire urinary tract system in healthy male, human, adults every 24 hours, and out of this total number, roughly 13% are viable living as determined by Trypan blue exclusion (Lang et al. 2013). The viable cell component of urine has been used in the development of conditionally immortalised human proximal tubule epithelial cells (ciPTEC) (Jansen et al. 2014; Wilmer et al. 2010) from healthy volunteers, primary human proximal tubule cells from healthy volunteers (Rahmoune et al. 2005), as well as well as urine-derived stem cells from healthy volunteers (Lang et al. 2013). This non-invasive method of isolating renal cells is particularly useful when biopsies of human kidney tissue (from which one could also isolate renal cells) is not possible (Rahmoune et al. 2005). The reason as to why viable renal cells might be present in the in urine is unclear but, it has been proposed to be the result of sublethal cell injury resulting in loss of cell adhesion from the basement membrane, causing the subsequent detachment into the tubular lumen (Prozialeck et al. 2007). The fact that viable cells are shed into the urine in healthy volunteers does, however, indicate that it is a normal *in vivo* physiological phenomenon.

In response to treatment with nephrotoxic drugs, there is an increase in renal epithelial cell detachment from the basement membrane (cell sloughing). The sloughing of cells into the tubular lumen is a well-documented *in vivo* phenomenon of treatment with, for example, the known nephrotoxin, cisplatin (Aleksunes et al. 2008; Huang et al. 2001; Wadey et al. 2013). Remaining epithelial cells repopulate denuded basement membranes enabling subsequent tubular regeneration *i.e.* reformation of the tubular epithelial barrier (Prozialeck et al. 2007).

Akin to the sloughing of renal cells from the basement membrane *in vivo*, cells grown *in vitro* display a similar detachment phenomenon from the tissue culture plate in response to treatment with nephrotoxins. In response to treatment with cisplatin, *in vitro* primary cultures of porcine proximal tubule cells have been shown to detach from the tissue culture substrate (collagen-coated coverslips) and subsequently float in the tissue culture medium (Kruidering et al. 1998). The authors of this paper quantified the number of detached cells as a percentage of the total cells *i.e.* the sum of the floating and attached cells. They propose that sublethal concentrations of cisplatin can induce cytoskeletal

changes which thereby affect cell adhesion and induce cell detachment. Cell detachment from the tissue culture substrate in response to cisplatin-treatment has also been shown by other groups (Del Bello et al. 2001; Mueller et al. 2003), in addition to other nephrotoxins including cyclosporin A (Slattery et al. 2005).

Assessing Nephrotoxicity Using Other Culture Methods

As kidney injury is one of the most frequent adverse events reported during drug development (Jang et al. 2013), there is great interest in models that closely recapitulate the microenvironment and/or structure of the kidney *in vivo*, thereby inducing a more *in vivo*-like phenotype, in order to guide drug development and improve the rate of late stage drug attrition. As such, alternative models to standard 2D culture models are under development.

Microfluidic Kidney Models

Microfluidics is a form of cell culture involving the flow (rather than the conventional static presence) of medium over cells in culture (Mehling and Tay 2014). In recent years, the use of *in vitro* microfluidic cell culture has become more popular owing largely to recognition of the fact that more physiologically relevant results can be obtained when *in vivo* cellular microenvironments are more accurately modelled.

In 2013, a paper was published detailing the characterisation of a microfluidic human primary proximal tubule on-a-chip model (Jang et al. 2013). Cultured on extracellular matrix-coated semi-permeable filter supports (transwells) to enhance cell polarity, primary proximal tubule cells were subjected to microfluidic apical sheer stress mimicking the *in vivo* luminal flow of filtrate through the nephron. Cells were shown to exhibit morphological features (apical-basolateral cell polarity and brush border membranes) and functional responses (alkaline phosphatase activity, glucose uptake and MDR1-mediated calcein-acetoxymethyl-ester (calcein-AM) extrusion) typical of proximal tubule cells *in vivo*. Highlighting the benefit of using a microfluidic model, enhanced cell recovery from cisplatin-induced injury (as determined by the number of viable cells remaining attached to transwells 4 days after cisplatin treatment) was observed in comparison to the same cells cultured in the same conditions but without apical sheer stress.

Bioengineered 3D Human Kidney Tissue

In 2013, DesRochers et al. described the development and characterisation of a bioengineered 3D human kidney tissue model for nephrotoxicity studies (DesRochers et al. 2013). Human kidney epithelial cells were isolated from patients, immortalised by serial passaging with hTERT-enriched culture medium, and identified to be of proximal tubule cell origin as a result of a number of different functional tests (PTH-induced increase in cAMP, γ-glutamyl transpeptidase (GGT) activity and sodium-dependent glucose uptake). When cultured in a 1:1 mix of Matrigel and rat tail collagen type-1 in 12-well semi-permeable transwells, 3D cell constructs (interconnected tubules) were identified after 2 weeks. Levels of the biomarkers kidney injury molecule-1 (KIM-1) and neutrophil gelatinase-associated lipocalin (NGAL) were then assessed in response to treatment with the nephrotoxins cisplatin, gentamicin and doxorubicin. In response to cisplatin, expression of both KIM-1 and NGAL were increased compared to control, akin to the *in vivo* response to cisplatin (Gaspari et al. 2010; Vaidya et al. 2010). However, although in contrast to well-documented effects *in vivo* (Kai et al. 2013; Vaidya et al. 2010; Zhang et al. 2008; Y. Zhou et al. 2008), gentamycin and doxorubicin both failed to increase levels of KIM-1 and NGAL above that of control. As such, although this model does appear to better recapitulate the *in vivo* 3D structure of the proximal tubule, it is limited by the fact it is based on the use of immortalized cells which do not always fully recapitulate the full functionality of renal cells *in vivo*. Further optimisation is required to validate it in terms of its true capacity as a useful tool for studying drug-induced nephrotoxicity, and predicting drug-induced toxicity in humans.

Kidney Slice Models

Precision-cut tissue slices have been used to study wide range of soft organs including lung (Bourke et al. 2005), liver and intestine (de Graaf et al. 2010), brain (Loryan et al. 2013) and kidney (Crawford et al. 2012; Peppiatt-Wildman et al. 2012) in an *ex vivo* set-up. The main advantage of using tissue slices for studying organ function is that the 3D structure of the organ is preserved, which by supporting the correct cell-cell and cell-matrix interactions, is likely to enable more physiologically relevant interactions between cells to occur (Vickers and Fisher 2004). As such, precision-cut *ex vivo* kidney tissue slices have previously been used for a wide range of studies including those relating to vasa recta properties and function (Crawford et al. 2012), intracellular calcium signalling

(Peppiatt-Wildman et al. 2012) and studying mechanisms of drug toxicity (Vickers et al. 2004).

Cisplatin, Cyclosporin A and BEA

The proximal tubule is of particular interest for studies of nephrotoxicity because active clearance, reabsorption, intracellular concentration and local interstitial accumulation of drugs occurs primarily in this region of the kidney (Jang et al. 2013). However, owing to the expression different transporters, metabolic characteristics and oxygen tensions within the kidney, segment-specific sensitivity to drugs is displayed (Bonventre et al. 2010). Three drugs used experimentally to induce segment-specific nephrotoxicity are cisplatin (a proximal tubule nephrotoxin), cyclosporin A (a distal tubule nephrotoxin) and 2-bromoethylamine hydrobromide (BEA) (a collecting duct nephrotoxin).

Cisplatin

Cisplatin is a clinically used anti-cancer drug with a notorious dose-limiting nephrotoxicity (Blanchard 2012). However, it has been used for inducing renal injury in rodents in order to investigate biomarkers of drug-induced acute kidney injury (Pinches et al. 2012b). Its kidney-specific toxicity is thought to arise from its uptake in to the cytoplasm of proximal tubule cells via the organic cation transporter 2 (OCT2) and copper transporter 1 (CTR1) (Ciarimboli et al. 2005; Ishida et al. 2002), and its subsequent biotransformation into a more toxic metabolite (Townsend et al. 2003). Experimentally, cisplatin has been used *in vitro* at 25-50µM in primary mouse proximal tubule cells (Cilenti et al. 2005), 50-500µM in primary porcine renal cells (Kruidering et al. 1997), 100µM in primary human renal cells (Jang et al. 2013), and in *ex vivo* tissue slices as 40-100µM (rat) and 80-500µM (human) (Vickers et al. 2004). It has also been used in other cell types at 1-20µM (Arantes-Rodrigues et al. 2013).

Cyclosporin A

Cyclosporin A is a clinically used immunosuppressant used to prevent organ transplant rejection but is associated with a dose-limiting nephrotoxic side effect (Busauschina et al. 2004). It is thought to induce ischemic renal injury as a result of afferent arteriole vasoconstriction (Busauschina et al. 2004), in addition to inducing tubular acidosis by inhibiting the distal tubule H^+ pump (Tsuruoka et al. 2003). Experimentally, it has been

used *in vitro* at 5µM in HEK 293 cells (Lamoureux et al. 2012), and in LLC-PK1 cells at concentrations of up to 42µM (Lally et al. 1999) and 83µM (Healy et al. 1998).

2-bromoethylamine hydrobromide

2-bromoethylamine hydrobromide (BEA) is a collecting duct nephrotoxin that induces renal papillary necrosis (RPN) in a dose-dependent manner (Bach et al. 1983). Although not used clinically, it is a good tool for inducing RPN in animal models in order to mimic the type of injury induced by analgesics such as aspirin, and non-steroidal anti-inflammatory drugs such as ibuprofen, in humans (Atta and Whelton 1997; Brix 2002). It is used experimentally in rodents to induce RPN rather than aspirin or ibuprofen itself, as it can induce injury within 24 hours of a single dose (Powell et al. 1991). It has been used studying novel biomarkers of nephrotoxicity in *in vivo* models (Hildebrand et al. 1999; S. A. Price et al. 2010).

3.3 Project Overview

The kidney is a major organ of drug-induced toxicity. Lack of relevant preclinical models for predicting nephrotoxicity specifically in humans means that it is often detected at late stages of drug development. This is evidenced by the fact that nephrotoxicity accounts for only 2% of all drug failures during preclinical animal studies but jumps to 19% of all failures in Phase III clinical human studies (Redfern et al. 2010). Characterisation of *ex vivo/in vitro* rodent models for use alongside *ex vivo/in vitro* human models would improve translational drug safety assessment; such models would reduce the risk of drugs that are toxic to humans but not animals (false negatives) reaching clinical trials, and drugs that are safe in humans but not animals (false positives) being mistakenly dropped from development.

Precision-cut slices of kidney tissue are a physiologically relevant *ex vivo* model owing to the maintenance of correct cell-cell and cell-matrix interactions; they represent a model possessing the 3-dimentional cellular complexity of the kidney *in vivo*. *Ex vivo* kidney slices have been previously explored as a tool for studying mechanisms of drug-induced kidney injury (Vickers et al. 2004). However, little information regarding changes in *ex vivo* kidney slice injury biomarker expression profiles following treatment with known nephrotoxins is available.

In terms of conventional *in vitro* models, primary cultures of renal cells are the most physiologically relevant. *In vitro* primary cultures of human renal cells have been shown to possess the full complement and expression level of drug transporters *in vivo* (C. Brown et al. 2008). However, there is little information regarding the ability of *in vitro* primary renal cells to respond to treatment with known nephrotoxins with changes in kidney injury biomarker expression.

3.4 Aims

The aims of this study were:

1. To characterise an *ex vivo* rat kidney slice model as a tool for studying drug-induced nephrotoxicity. The specific aims were:
   a. Assess slice viability over time using an ATP-content assay and by histomorphology.
   b. Assess slice viability over time in response to treatment with medium containing the known nephrotoxins cisplatin, cyclosporin A and BEA using an ATP-content assay.
   c. Assess changes in kidney injury biomarker expression following treatment with the known nephrotoxins cisplatin, cyclosporin A and BEA.

2. To characterise an *in vitro* primary mouse renal cell model as a tool for studying drug-induced nephrotoxicity. The specific aims were:
   a. Assess cell viability under control conditions over time in culture using proliferation and apoptosis assays.
   b. Assess concentration-dependent drug-induced apoptosis following treatment with medium containing cisplatin, cyclosporin A and BEA.
   c. Assess concentration-dependent cell detachment from the tissue culture plate following treatment with medium containing cisplatin, cyclosporin A and BEA.
   d. Assess changes in kidney injury biomarker (KIM-1, osteopontin and clusterin) expression following treatment medium containing cisplatin, cyclosporin A and BEA.

3. To characterise an *in vitro* primary human renal cell model as a tool for studying drug-induced nephrotoxicity. The specific aims were:
   a. Assess changes in kidney injury biomarker (KIM-1, osteopontin and clusterin) expression following treatment with medium containing cisplatin.

3.5 Materials and Methods

Mouse Kidney Cell Culture

One- to 3-month-old male C57Bl/6 mice were killed by schedule 1 cervical dislocation following UK Home Office approval and carried out in accordance with the Animals (Scientific Procedures) Act 1986. All metallic tools used were sterilised by autoclaving prior to use. Using scissors, sprung scissors and tweezers, kidneys were excised from mice and placed in 4°C 1X phosphate-buffered saline, pH 7.4 (PBS; Invitrogen, 10010-015) in a 35mm tissue culture-treated polypropylene plate (Falcon®, 353001). Kidneys were placed in 1X PBS (Invitrogen, 10010-015) to wash away any blood. Furthermore under sterile conditions in a laminar flow hood, fatty tissue surrounding the kidneys was removed using tweezers and sprung scissors. Next, the kidneys were decapsulated and transferred to another 35mm tissue culture-treated polypropylene plate (Falcon®, 353001) containing 1X PBS pH7.4 (Invitrogen, 10010-015) at 4°C for a second wash. Using tweezers to hold the kidneys still, a disposable sterile scalpel (Swann-Morton; 0501) was used to separate kidney cortical tissue from the rest of the kidney. Cortical tissue pieces were transferred to another 35mm tissue culture-treated polypropylene plate (Falcon®, 353001), where they were minced into a paste in 200µl 1X PBS pH 7.4 (Invitrogen, 10010-015) at 4°C. The resultant tissue paste was divided in half and using a sterile pipette tip with the top cut off, each half was placed in one of two 50ml polypropylene, conical bottom, tubes (Corning®, 430829) containing 37.5ml isolation medium (RMPI 1640 medium with L-glutamine (VWR; 733-1708) supplemented with 5% FBS (GE Healthcare, UK), 2% Pen/Strep (Invitrogen; 15140-122) and 0.67mg/ml collagenase type-IV (Worthington, LS004188)). (See method of collagenase type-IV preparation below). The two tubes were left at 4°C until the next day. Gentle agitation of the suspension inside the tubes to prevent settling of the tissue was achieved during this time using a cyclic rotator (VWR; 444-0502). Upon warming to 37°C for 15 minutes in a water bath the next day, tissue suspensions were vigorously agitated at 200 rotations/minute in a shaking incubator (Jencons-PLS, Orbital incubator and shaker, 5150) for 2 hours at 37°C to enzymatically and mechanically dissociate the cells into a single cell suspension. To remove any remaining undigested tissue, the cell suspensions were filtered through a 40µm pore nylon strainer (BD Biosciences, UK; 352340) in to fresh 50ml tubes

polypropylene, conical bottom, tubes (Corning®, 430829). To remove the collagenase and end the enzymatic digestion, cells were centrifuged twice at 150*g* for 7 minutes and each time re-suspended in fresh isolation medium (minus the collagenase). The first time cells were re-suspended in 50ml isolation medium, and the second time, in 5ml isolation medium. Cell suspensions were then loaded on top of discontinuous Percoll (GE Healthcare, GZ17089102) gradients made up of 1.04 and 1.07g/ml Percoll in isolation medium and 1X PBS, respectively (See Percoll Gradient method below). Cells were then centrifuged at 1200*g* for 25 minutes in a swing out rotor (Eppendorf; Germany; 5720). Cells were aspirated from the intersection of the gradients and centrifuged twice at 150*g* for 7 minutes to remove excess Percoll. The first time, cells were re-suspended in 50ml isolation medium (minus collagenase), and the second time, cells were re-suspended in 5ml renal epithelial growth medium (REGM; Lonza, CC3191) containing the REGM SingleQuot kit supplements and growth factors, fetal calf serum (FCS), amphotericin B, epinephrine, human epidermal growth factor, hydrocortisone, insulin, transferrin and triiodothyronine (Lonza; CC4127). Rather than adding the gentamycin aliquot of the REGM SingleQuot kit supplements, 1% Penicillin (100units/ml)/Streptomycin (100µg/ml) (Invitrogen; 15140-122), was added to the culture medium. Gentamycin is a regularly used antibiotic in cell culture. However, it is also a nephrotoxin and it was thought that it may induce cell injury. As such, a combination of Penicillin/Streptomycin was used. Once a bottle of Renal Epithelial Growth Medium containing the desired supplements was prepared, it was stored in darkness at 4°C, and used for up to one month.

For viability (proliferation and apoptosis) and immunocytochemical assays, 100,000 cells were plated per 13mm Ø collagen type-IV (Sigma, C5533)-coated borosilicate glass coverslips (VWR, 631-0149) that were individually placed inside the wells of a 24-well tissue culture-treated plate (ThermoScientific, Nunclon™, 142475). For drug-induced cell-detachment assays, 300,000 cells were plated in 35mm tissue culture-treated polypropylene plates (Falcon®, 353001). Cells were cultured in a humidified, 5% CO_2 incubator at 37°C (SANYO, MCO-18AIC). After warming to 37°C in a water bath, the cell culture medium was replaced on day 4, day 7, day 9 and day 14 of culture.

The cell culture protocol is based on that published by C. Brown et al., 2008.

Human Kidney Cell Culture

Human kidney tissue was obtained from ethically-consented human kidneys surgically resected due to renal cell carcinoma (RCC) (Research Ethics Committee approval reference number: 07/WSE04/53). Within 1 hour of removal, samples of macroscopically normal cortical tissue were dissected by a pathologist, and the specimens transported to the laboratory in isolation medium (RMPI 1640 medium with L-glutamine (VWR; 733-1708) containing 5% (v/v) fetal bovine serum (FBS; GE Healthcare, UK), 2% (v/v) Pen/Strep (Invitrogen; 15140-122)) at 4°C. Under sterile conditions in a laminar flow hood, roughly 1cm^3 pieces of freshly dissected cortical tissue were washed in phosphate-buffered saline pH 7.4 (PBS; Invitrogen, 10010-015) at 4°C. All metallic tools used were sterilised by autoclaving prior to use. Using metal tweezers and a disposable scalpel (Swann-Morton; 0501), cortical tissue was minced into a paste in 200µl 1X PBS pH 7.4 (Invitrogen; 10010-015) at 4°C. The resultant tissue paste was roughly divided into quarters. Using a sterile pipette tip with the top cut off, each quarter was placed in one of four 50ml polypropylene, conical bottom, tubes (Corning®, 430829) containing 37.5ml isolation medium (RMPI 1640 medium with L-glutamine (VWR; 733-1708) supplemented with 5% FBS (GE Healthcare, UK), 2% Pen/Strep (Invitrogen; 15140-122) and 0.67mg/ml collagenase type-IV (Worthington, LS004188)). (See method of collagenase type-IV preparation below). The four Falcon tubes were left at 4°C until the next day. Gentle agitation of the suspension inside the tubes to prevent settling of the tissue was achieved during this time using a cyclic rotator (VWR; 444-0502). Upon warming to 37°C for 15 minutes in a water bath the next day, tissue suspensions were vigorously agitated at 200 rotations/minute in a shaking incubator (Jencons-PLS, Orbital incubator and shaker, 5150) for 2 hours at 37°C to enzymatically and mechanically dissociate the cells into a single cell suspension. To remove any remaining undigested tissue, the cell suspensions were filtered through a 40µm pore nylon strainer (BD Biosciences, UK; 352340) in to fresh 50ml tubes. To remove the collagenase and end the enzymatic digestion, cells were centrifuged twice at 150*g* for 7 minutes and each time re-suspended in fresh RMPI 1640 isolation medium (minus the collagenase). The first time cells were re-suspended in 50ml RMPI 1640 isolation medium, and the second time, in 5ml RMPI 1640 isolation medium. Cell suspensions were then loaded on top of discontinuous Percoll (GE Healthcare, GZ17089102) gradients made up of 1.04 and 1.07g/ml Percoll in isolation medium and 1X

PBS, respectively (See Percoll Gradient method below). Cells were then centrifuged at 1200*g* for 25 minutes in a swing out rotor (Eppendorf; Germany; 5720). A mixed population of proximal and distal tubule cells was aspirated from the intersection of the gradients and centrifuged twice at 150*g* for 7 minutes to remove excess Percoll. The first time, cells were re-suspended in 50ml RMPI 1640 isolation medium (minus collagenase), and the second time, cells were re-suspended in 5ml renal epithelial growth medium (REGM; Lonza, CC3191) containing the REGM SingleQuot kit supplements and growth factors, fetal calf serum (FCS), amphotericin B, epinephrine, human epidermal growth factor, hydrocortisone, insulin, transferrin and triiodothyronine (Lonza; CC4127). Rather than adding the gentamycin aliquot of the REGM SingleQuot kit supplements, 1% Penicillin (100units/ml)/Streptomycin (100µg/ml) (Invitrogen; 15140-122), was added to the culture medium. Gentamycin is a regularly used antibiotic in cell culture. However, it is also a nephrotoxin and it was thought that it may induce cell injury. As such a combination of Penicillin/Streptomycin was used. Once a bottle of Renal Epithelial Growth Medium containing the desired supplements was prepared, it was stored in darkness at 4°C, and used for up to one month.

For immunocytochemical assays, 100,000 cells were plated per 13mm Ø collagen type-IV (Sigma, C5533)-coated borosilicate glass coverslips (VWR, 631-0149) that were individually placed inside the wells of a 24-well tissue culture-treated plate (ThermoScientific, Nunclon^{TM}, 142475). Cells were cultured in a humidified, 5% CO_2 incubator at 37°C (SANYO, MCO-18AIC). After warming to 37°C in a water bath, the cell culture medium was replaced on day 4 and day 7 (experiments performed at day 8).

The cell culture protocol is based on that published by C. Brown et al., 2008.

Preparation of the Percoll Gradient for Isolating Primary Renal Cells

The Percoll gradient stock solution and gradients were prepared fresh on day of use under sterile conditions in a laminar flow tissue culture hood (BIOQUELL, ABS1200CLS2-MK2). For two mouse kidney cortex samples (one animal) two Percoll gradients were prepared. For a roughly 1cm^3 sample of human kidney cortex, four Percoll gradients were prepared. The volumes required in each case is respectively described below. Into each 50ml polypropylene, conical bottom tube (Corning®, 430829), 7ml of the 1.07 density solution was added. With the 50ml tube at a 45° angle, 7ml of the 1.04 density solution was then slowly pipetted down the inside of the tube, such that the 1.04 density solution sat on top of the 1.07 density solution. In a similar manner, 5ml of the cell suspension was then layered on top of the 1.04 density solution.

Percoll Stock Solution:

10X HBSS (Invitrogen; 14065-049)	2ml	(Mouse)	4ml	(Human)
Percoll (GE Healthcare; GZ17089102)	18ml	(Mouse)	36ml	(Human)

Percoll Gradient Density 1.04:

Percoll Stock Solution	5ml	(Mouse)	10ml	(Human)
RMPI 1640 Medium (VWR; 733-1708)	12ml	(Mouse)	24ml	(Human)

Percoll Gradient Density 1.07:

Percoll Stock Solution	10ml	(Mouse)	20ml	(Human)
1X PBS (Invitrogen; 10010-015)	8ml	(Mouse)	16ml	(Human)

Preparation of Collagenase Type-IV for Enzymatic Cell Isolation

The collagenase type-IV for enzymatic cell digestion was prepared under sterile conditions in a laminar flow tissue culture hood (BIOQUELL, ABS1200CLS2-MK2). 25ml of RMPI 1640 isolation medium (Lonza, BE12-702F) was added to a 2.5g pot of collagenase type-IV (Worthington, LS004188) powder and repeatedly pipetted up and down to fully suspend to powder into a 100mg/ml stock solution. The stock solution was filter-sterilised though a 0.20µm pore size Minisart® syringe filter (Sartorius Stedium Biotech, Germany, 16534), after which 1ml aliquots were made in sterile 15ml tubes (Corning, 430791) and stored at -20°C. One aliquot was defrosted for use as and when required. To obtain the working concentration of collagenase type-IV (0.67mg/ml) needed for isolation of renal cells, 250µl of the 100mg/ml stock solution was added to 37.5ml RMPI 1650 isolation medium (Lonza, BE12-702F).

Preparation of glass coverslips for cell culture

13mm Ø borosilicate glass coverslips (VWR, 631-0149) were stored until required in copious 100% ethanol (Sigma, 458600). Under sterile conditions in a laminar flow hood (BIOQUELL, ABS1200CLS2-MK2), and using autoclave-sterilised metal tweezers, the 13mm Ø borosilicate glass coverslips (VWR, 631-0149) were individually placed into the wells of a 24-well tissue culture-treated plate (ThermoScientific, Nunclon™, 142475). During this process, coverslips were balanced at an angle against the side of each well to enable any ethanol on the coverslips to evaporate away. When all the ethanol had evaporated away (up to 1 hour later), the tissue culture plate containing the ethanol-sterilized coverslips, was further sterilized using the UV irradiation setting on the laminar flow tissue culture hood (BIOQUELL UK LTD, ABS1200CLS2-MK2) for 20 minutes.

All coverslips used for both mouse and human renal cell cultures, were then coated with tissue culture grade collagen type–IV (Sigma, C5533). A 1mg/ml collagen stock solution was prepared from 5g of lyophilized collagen type-IV powder in 5ml of 0.5M sterile acetic acid (Fisher Scientific, A/0360/PB17). The 1mg/ml stock solution was always prepared at least 24 hours in advance of requirement to allow for the collagen to completely dissolve, and was kept at 4°C. A working concentration of 0.1mg/ml collagen type-IV was prepared from the 1mg/ml stock solution using tissue culture grade distilled water (Invitrogen;

15230-089). 200µl of 0.1mg/ml collagen type-IV solution was pipetted directly onto each 13mm Ø borosilicate glass coverslip (VWR, 631-0149) and left for 2 hours. After this time, the 0.1mg/ml collagen type-IV working concentration solution was removed, and the coverslips rinsed three times with sterile 1X PBS (Invitrogen, 10010-015) to remove any remaining traces of acetic acid. The final 1X PBS wash was left in the wells until just before renal cells were ready for plating.

Proliferation Assay

The incorporation and immunofluorescent detection of 5-bromo-2'-deoxyuridine (BrdU), a thymidine analogue, into cellular DNA was used to investigate the percentage of mouse renal cells undergoing proliferation, at day 5, day 8, day 10 and day 15 of culture. 5-bromo-2'-deoxyuridine (BrdU; Sigma, B5002) was added at a final concentration of 10µM to the culture medium 24 hours before cell fixation (*i.e.* on day 4, day 7, day 9 an day 14 of culture). Cells were removed from the incubator and transferred to lab bench where the culture medium was then removed. Cells were fixed using 2% (w/v) paraformaldehyde (PFA; Sigma, 15,812-7) in 1X PBS pH 7.4 (10 minutes) at 4°C. 2% PFA stocks were pre-prepared and stored at -20°C. Aliquots were defrosted slowly on ice as and when required. Following fixation, cells were washed with 1X PBS pH 7.4 (3 X 5 minutes) at room temperature. Cells were permeabilised using 1X PBS pH 7.4 containing 0.05% (v/v) Tween-20 (Sigma, P5927) pH 7.4 (PBST) (5 minutes). Antigen retrieval was performed by incubating cells with 1N HCl (prepared from a 37% HCl stock solution (Sigma, 258148)) at 37°C (30 minutes) in a benchtop incubator (Techne hybridiser, HB-1D). The antigen retrieval solution was removed and cells washed with PBST (3 X 5 minutes). Non-specific antibody binding sites were blocked using blocking buffer (1% (w/v) bovine serum albumin (BSA; Sigma, A7906), 3% (v/v) SeaBlock™ (EastCoast Bio, PP83-K1574) in PBST) at room temperature (1 hour). The blocking buffer was removed and cells incubated with an anti-BrdU primary antibody (mouse IgG; Abcam; ab8039) diluted 1:200 in blocking buffer (1 hour). To remove unbound antibodies, PBST washes were subsequently performed (3 X 5 minutes). Furthermore in darkness, Alexa Fluor® 594-conjugated secondary antibody diluted 1:400 in blocking buffer (goat anti-mouse IgG; Invitrogen; A11032) was applied to cells (1 hour). Again, to remove unbound antibodies, PBST washes performed (3 X 5 minutes). In order to identify all cell nuclei,

cells were incubated with 0.1µg/ml Hoechst 33342 (Invitrogen; H1399), a nucleic acid stain, diluted in blocking buffer (10 minutes). Cells underwent further PBST washes (3 X 5 minutes) to remove excess Hoechst 33342. Cells were briefly rinsed with distilled H_20, before excess H_20 was tapped off and coverslips mounted on slides using ProLong® Gold reagent (Invitrogen; P36930), a fluorescent anti-fade mounting medium. Slides were allowed to air-dry in darkness. Random snapshots of slides were captured using a BX61 microscope (Olympus, Japan) and the percentage of proliferating cells out of the total number of cells was determined. Between 200 and 600 total cells were counted at each time point. Using Microsoft EXCEL, the percentage of proliferating cell nuclei out of the total number of cell nuclei was determined. Results were plotted graphically using Prism (GraphPad Software Inc., USA). To identify changes in proliferation over time, a one-way analysis of the variance (ANOVA) and a post-hoc Tukey test was performed. Results were deemed statistically significant when $p<0.05$ (*), $P<0.01$ (**) and $p<0.001$ (***). N=3, n=3 for all time points assessed.

Apoptosis Assay

The percentage of mouse renal cells undergoing apoptotic cell death at day 5, day 8, day 10 and day 15 of culture, was determined using the DeadEnd™ Colorimetric Apoptosis Detection Kit (Promega, G7360). At each time point, cells were removed from the incubator and transferred to lab bench where the culture medium was then removed. Cells were fixed using 2% (w/v) paraformaldehyde (PFA; Sigma, 15,812-7) in 1X PBS pH 7.4 (10 minutes) at 4°C. 2% PFA stocks were pre-prepared and stored at -20°C. Aliquots were defrosted slowly on ice as and when required. Following fixation, cells were washed with 1X PBS pH 7.4 (3 X 5 minutes) at room temperature. Cells were then treated with the kit equilibration buffer (containing 200mM Potassium cacodylate, 25mM Tris-HCl, 0.2mM DTT, 0.25mg/ml BSA, 2.5mM cobalt chloride) at room temperature (5 minutes). Biotinylated nucleotides were incorporated at the 3'-OH end of fragmented, apoptotic DNA by recombinant terminal deoxynucleotidyl transferase (rTdT) at 37°C (1 hour). This rTDT reaction mix contained 1% (v/v) kit biotinylated nucleotide mix and 1% (v/v) kit rTDT enzyme in equilibration buffer. To terminate the TUNEL reaction, cells were then incubated with 2X saline sodium citrate (SSC) (15 minutes) at room temperature. 2X SSC was prepared by diluting the 20X SSC solution supplied with the kit 1:10 with deionised

water before use. After cells were washed with 1X PBS pH 7.4 (3 X 5 minutes), endogenous peroxidases were quenched by treating cells with 0.3% (v/v) H_2O_2 (Fisher Scientific, H/1750/15) (5 minutes). 1X PBST washes were subsequently repeated (3 X 5 minutes). Cells were incubated with kit streptavidin-HRP diluted 1:500 in 1X PBST (30 minutes). Following, further 1X PBST washes (3 X 5 minutes), immunoreactive sites were detected using the kit 3,3'-diaminobenzidine (DAB) (1 minute). The working concentration of DAB was achieved by diluting the 20X DAB Chromogen 1:20 in DAB substrate buffer. Cells were rinsed with distilled H_2O (3 X 5 minutes) and then counterstained with haematoxylin (Sigma, HHS16) (1 minute). Cells were dehydrated using 70%, 95%, 100% and 100% (v/v) ethanol (Sigma, 458600) (5 minutes each) and then cleared in xylene (Sigma, 534056) (2 X 5 minutes). Coverslips were allowed to air dry, and then mounted on glass slides using DPX mounting medium (Sigma, 44581). Images were captured using a DMRB light microscope (Leica, Germany) from which a minimum of 100 total cells at day 5 were counted, and between 200 and 600 cells were counted at days 8, 10 and 15. Using Microsoft EXCEL the percentage of apoptotic cell nuclei out of the total number of cell nuclei was determined. Results were plotted graphically using Prism (GraphPad Software Inc., USA). To identify changes in apoptosis over time, a one-way analysis of the variance (ANOVA) and a post-hoc Tukey multiple comparison test was performed. Results were deemed statistically significant when $p<0.05$ (*), $P<0.01$ (**) and $p<0.001$ (***). N=3, n=3 for all time point assessed.

Concentration-Dependent, Drug-Induced Apoptosis

To assess concentration-dependent drug-induced apoptosis in primary mouse renal cells following treatment with control medium (vehicle control; medium), or medium containing cisplatin (1, 3, 5µM), cyclosporin A (1, 3, 5µM) or BEA (3, 10, 30µM), a similar protocol to that described above was used. The DeadEnd™ Fluormetric Apoptosis Detection Kit (Promega, G3250) was used. Following 24-hour treatment as described, cells at day 8 of culture were fixed using 2% (w/v) paraformaldehyde (PFA; Sigma, 15,812-7) in 1X PBS pH 7.4 (10 minutes) at 4°C. Following fixation, cells were washed with 1X PBST pH 7.4 (3 X 5 minutes) at room temperature (5 minutes). Fluorescein-conjugated nucleotides were incorporated at the 3'-OH end of fragmented, apoptotic DNA by recombinant terminal deoxynucleotidyl transferase (rTDT) at 37°C (1 hour). To terminate

the TUNEL reaction, cells were then incubated with 2X saline sodium citrate (SSC) (15 minutes) at room temperature. 2X SSC was prepared in advance by diluting the 20X SSC solution supplied with the kit 1:10 with deionised water. After, cells were washed with 1X PBST pH 7.4 (3 X 5 minutes). In order to identify all cell nuclei, cells were then incubated with 0.1µg/ml Hoechst 33342 (Invitrogen; H1399), diluted in 1X PBST (10 minutes), and the washed with 1X PBST (3 X 5 minutes). Cells were briefly rinsed with distilled H_20, before excess H_20 was tapped off and coverslips mounted on slides using ProLong® Gold reagent (Invitrogen; P36930), a fluorescent anti-fade mounting medium. Random snapshots were captured using a BX61 microscope (Olympus, Japan) from which 100 to 150 total cell nuclei were counted per coverslip. Using Microsoft EXCEL the percentage of apoptotic cell nuclei out of the total number of cell nuclei was determined. Results were plotted graphically using Prism (GraphPad Software Inc., USA). To identify changes in apoptosis, a one-way analysis of the variance (ANOVA) and a post-hoc Tukey multiple comparison test was performed. Results were deemed statistically significant when $p<0.05$ (*), $P<0.01$ (**) and $p<0.001$ (***). N=3, n=3 for all treatments.

Concentration-Dependent, Drug-Induced Loss of Cell Adhesion

Primary mouse renal cells were cultured in individual 35mm tissue culture-treated polypropylene plates (Falcon®, 353001), as per the method described above. On day 7, the control medium (REGM; Lonza, CC3191) was replaced with control medium (vechicle control; medium) or medium containing cisplatin (Calbiochem; 232120) at final concentrations of 1, 3 and 10µM, cyclosporin A (Sigma; 30024) at final concentrations of 1, 3 and 10µM, or BEA (Sigma; B65705) at final concentrations of 1, 3 and 30µM. Cells were then returned to the incubator for 24 hours. On day 8 of culture, 1ml medium was removed from each of the conditions and placed in a 1.5ml Eppendorf, and gently mixed by inverting. Using a haemocytometer number of cells floating in the control and drug-treated cell media, was determined. On completion, the control cells still attached to the cultured dish were enzymatically dissociated in 1ml of 0.05% Trypsin-EDTA (Invitrogen; 25300-054) at 37°C for 10 minutes. In a similar manner using the haemocytometer, the number of control cells that had remained attached to the tissue culture dish was counted. Using Microsoft EXCEL the number of floating cells in each of the control and drug-treated media, was made as a percentage of the total number of control cells *i.e.*

the combined total floating plus attached. These data were graphically plotted using Prism 5 (GraphPad Software; USA). To identify changes the number of floating cells between conditions, a one-way analysis of the variance (ANOVA) and post-hoc TUKEY test was performed. Results were deemed statistically significant when $p<0.05$ (*), $P<0.01$ (**) and $p<0.001$ (***). N=3, n=3 for all treatments.

Mouse Cell Biomarker Immunocytochemistry

At day 8 in culture, after 24 hours in control medium (vehicle control; medium), medium containing 10µM cisplatin (Calbiochem; 232120), 10µM cyclosporin A (Sigma; 30024) or 30µM BEA (Sigma; B65705), cells were fixed using 2% (w/v) paraformaldehyde (PFA; Sigma; 15,812-7) at 4°C. 2% PFA solutions were prepared in advance and frozen as 10ml aliquots in sterile 15ml tubes (Corning, 430791) at -20°C until required. Following fixation, cells were washed with 1X PBS pH 7.4 (3 X 5 minutes) and then permeabilised using 1X PBS, 0.05% Tween-20 (Sigma, P5927) pH 7.4 (PBST) (5 minutes). Freshly prepared 0.3% (v/v) H_2O_2 (Fisher Scientific, H/1750/15) PBST was used to quench endogenous peroxidase activity (5 minutes). Cells were then washed with 1X PBST (3 X 5 minutes). Non-specific binding sites were blocked using freshly prepared 1% (w/v) bovine serum albumin (BSA; Sigma, A7906), 3% (v/v) SeaBlock™ (EastCoast Bio, PP83-K1574) PBST blocking buffer (1 hour). Thereafter, cells were incubated with anti-KIM-1 (goat IgG; 1:200; R&D Systems; AF3689), anti-OPN (rabbit IgG; 1:200; IBL Co., Ltd, Japan; IBL-18628), or anti-clusterin (rabbit IgG; 1:200; Novus Biologicals; USA; NBP-19637) primary antibodies diluted in blocking buffer (1 hour). Unbound antibodies were removed by washing cells with PBST (3 X 5 minutes). Cells were incubated for 30 minutes with anti-rabbit (1:500; Thermo Scientific; 31462) or anti-goat (1:500; Thermo Scientific; 31402) horseradish peroxidise (HRP)-conjugated secondary antibodies, respectively. PBST washes (3 X 5 minutes) were repeated and immunoreactive sites subsequently visualised using 3-3'-diaminobenzidine (DAB) chromogen substrate solution (Dako; Denmark; K3468). Cells were rinsed with distilled H_2O, counterstained with haematoxylin (Sigma, HHS16) (1 minute), dehydrated using 70%, 95%, 100% and 100% ethanol (Sigma, 458600) (5 minutes each) and cleared in xylene (Sigma, 534056) (20 seconds), and allowed to air dry. Coverslips were mounted on glass slides using DPX mounting medium (Sigma, 44581) and images were captured using a DMRB light microscope (Leica, Germany). For each

coverslip, 5 random fields of view (snapshots) were captured. To determine the proportion of cells staining positive for each of the biomarkers out of the total cell number, cell counts from these images were made. A minimum of 500 cells per coverslip were counted. Using Microsoft EXCEL, the percentage of cells positive for each of the biomarkers out of the total number of cells was determined. These data were graphically plotted and analysed using Prism 5 (GraphPad Software; USA). To identify an increase in the number of cells staining positive for each of the biomarkers in control or drug-treated conditions, a one-way analysis of the variance (ANOVA) and a post-hoc TUKEY test was performed. Results were deemed statistically significant when $p<0.05$ (*), $P<0.01$ (**) and $p<0.001$ (***). N=3, n=3 for each treatment and biomarker.

Human Cell Biomarker Immunocytochemistry

At day 8 in culture, following 24-hour treatment in control medium (vehicle control; medium) or medium containing 25µM cisplatin (Calbiochem; 232120), human renal cells grown on collagen-type IV (Sigma, C5533)-coated 13mm Ø borosilicate glass coverslips (VWR, 631-0149) were fixed using 2% (w/v) paraformaldehyde (PFA; Sigma; 15,812-7) at 4°C. 2% PFA solutions were prepared in advance and frozen as 10ml aliquots in 15ml Falcon tubes at -20°C until required. Following fixation, cells were washed with 1X PBS pH 7.4 (3 X 5 minutes) and then permeabilised using 1X PBS, 0.05% Tween-20 (Sigma, P5927) pH 7.4 (PBST) (5 minutes). Freshly prepared 0.3% (v/v) H_2O_2 (Fisher Scientific, H/1750/15) PBST was used to quench endogenous peroxidase activity (5 minutes). Cells were then washed with 1X PBST (3 X 5 minutes). Non-specific binding sites were blocked using freshly prepared 1% (w/v) bovine serum albumin (BSA; Sigma, A7906), 3% (v/v) SeaBlock™ (EastCoast Bio, PP83-K1574) PBST blocking buffer (1 hour). Thereafter, cells were incubated with anti-KIM-1 (goat IgG; 1:200; R&D Systems; AF3689), anti-OPN (rabbit IgG; 1:200; IBL Co., Ltd, Japan; IBL-18628), or anti-clusterin (rabbit IgG; 1:200; Novus Biologicals; USA; NBP-19637) primary antibodies diluted in blocking buffer (1 hour). Unbound antibodies were removed by washing cells with PBST (3 X 5 minutes). Cells were subsequently incubated for 30 minutes with anti-rabbit (1:500; Thermo Scientific; 31462) or anti-goat (1:500; Thermo Scientific; 31402) horseradish peroxidise (HRP)-conjugated secondary antibodies, respectively. PBST washes (3 X 5 minutes) were repeated and immunoreactive sites subsequently visualised using 3-3'-diaminobenzidine (DAB)

chromogen substrate solution (Dako; Denmark; K3468). Cells were rinsed with distilled H_2O, counterstained with haematoxylin (Sigma, HHS16) (1 minute), dehydrated using 70%, 95%, 100% and 100% ethanol (Sigma, 458600) (5 minutes each) and cleared in xylene (Sigma, 534056) (20 seconds). Coverslips were mounted on glass slides using DPX mounting medium (Sigma, 44581). Slides were scanned using a Mirax Scanner (Zeiss, Germany) and images captured using Panoramic Viewer Software (3DHISTECH Kft, Hungary). Five random fields of view (snapshots) per coverslip were captured. To determine the proportion of cells staining positive for each of the biomarkers out of the total cell number, cell counts from these images were made. A minimum of 500 cells per coverslip were counted. Using Microsoft EXCEL, the percentage of cells positive for each of the biomarkers out of the total number of cells was determined. These data were graphically plotted using Prism 5 (GraphPad Software; USA). N=1, n=1 for each treatment and biomarker.

Rat Kidney Slice Culture

One- to 3-month-old male Han Wistar rats were killed by CO_2 inhalation following UK Home Office approval and carried out in accordance with the Animals (Scientific Procedures) Act 1986. All metallic tools used were sterilised by autoclaving prior to use. Using scissors and tweezers, kidneys were excised and rinsed with 1X phosphate buffered saline (PBS; Invitrogen, 10010-015). Following removal of the kidney capsule and any surrounding fatty tissue, the kidneys were again washed in 1X PBS. Using tweezers to hold the kidney still, a disposable sterile scalpel (Swann-Morton; 0501) was used to cut one of the kidneys in half along the transverse plane. Either one or both halves of one of the kidneys were mounted directly to the centre of the jig of an Integraslice (Campden Instruments, UK; 7550 PSDS). A cylindrical tube was placed around the kidney before 1.8% UltraPure™ low melting point agarose (Invitrogen; 16520-050) in 1X PBS pH 7.4 was poured into the tube to fully embed the kidney portions. Once the agarose had solidified, the cylindrical tube was gently removed and the jig plus agarose-embedded kidney portions were screwed into the Integraslice chamber. 1X PBS (Invitrogen, 10010-015) at 4°C was poured into the chamber to the level of the top of the agarose. 200µm-thick slices were cut at a speed of 0.25mm/s with a left-right slicing amplitude of 1.5mm. The decision to make 200µm-thick sections was made based on previously published methods

(Crawford et al. 2012; Peppiatt-Wildman et al. 2012; Vickers et al. 2004). Thicker slices were excluded to prevent nutrient and oxygen starvation of the cells in the middle of the slices which could predispose them to apoptotic and/or necrotic cell death. Cut slices were removed from the slicing chamber using sterile tweezers and stored in a 12-well culture plate in 1X PBS on ice for up to 2 hours until all slices had been cut. Thereafter under sterile conditions in a laminar flow tissue culture hood (BIOQUELL, ABS1200CLS2-MK2), kidney slices were transferred to individual wells of a 12-well-plate containing control medium (Renal Epithelial Growth Medium; REGM; Lonza, CC3191) to acclimatise in a 5% CO_2 / 95% air humidified incubator at 37°C (SANYO, MCO-18AIC).

Determination of Rat Kidney Slice Viability Using an ATP Content Assay

Rat kidney slices were prepared as described above. After 0, 1, 4 and 24 hours in control medium or control medium containing the vehicle control (control medium) or 10µM cisplatin (Calbiochem; US; 232120), 10µM cyclosporin A (Sigma; 30024) or 30µM BEA (Sigma; B65705), slices were snap frozen in liquid nitrogen and stored at -80°C until all samples had been collected. One at a time, slices were removed from the -80°C freezer, weighed and homogenised in 120µl phenol-TE (phenol saturated with 10mM tris(hydroxymethyl)aminomethane (TRIS; Sigma; T1503) pH7.5 and 1mM diaminoethane tetra-acetic acid pH8 (EDTA). 100µl of this lysate was transferred to a 1.5ml Eppendorf containing 20µl chloroform (Fischer Scientific; UK; C/4960/17) and 15µl ddH_20, and kept on ice until all slices had been processed. When all slices were ready, they were all shaken vigorously by hand for 30 seconds before being centrifuged (Sigma Laboratory Centrifuge SK18; SciQuip; UK) at 10000*g* for 5 minutes at 4°C. The supernatants were collected and diluted 1:10 with ddH_20. 10µl of this solution was used to perform the ATP assay. According to the manufacturer's protocol, the ATP content of kidney slices was determined using The Molecular Probes ATP Determination Kit (Invitrogen; A22066) (a quantitative bioluminescence assay using recombinant firefly luciferase and its substrate D-luciferin). Briefly, ATP standards (10nM, 8nM, 6nM, 4nM, 2nM, 1.8nM, 1.6nM, 1.4nM, 1.2nM, 1nM, 0.8nM, 0.6nM, 0.4nM and 0.2nM) were prepared by diluting the supplied 5mM ATP stock solution in distilled water. 10µl of each standard or sample was then added to individual wells of a 96-well plate before 100µl of reaction solution (containing reaction buffer, firefly luciferase, D-luciferin and Dithiothreitol at the recommended

concentrations) was then also added. Luminescence at 560nm was detected using a Flouroskan Ascent FL™ Microplate Luminometer (Thermo Scientific; UK; 5210462). An ATP standard curve was created, and the ATP content of each kidney slice sample subsequently determined. This method of determining the ATP content of rat and human *ex vivo* kidney slices has been used previously (Vickers et al. 2004). To identify differences in the ATP content over time within each drug-treated group, one-way ANOVA and *post-hoc* Tukey tests were performed at the 5% significance level. Differences were deemed statistically significant when $p < 0.05$ (*). To identify differences in the ATP content between control and drug-treated groups after 1, 4 and 24 hours, a two-way ANOVA and *post-hoc* Tukey test was performed. Again, differences were deemed statistically significant when $p < 0.05$ *. N=3, n=3, for all time points and conditions.

Rat Kidney Slice H&E Staining

After 1 and 24 hours in renal epithelial growth medium (REGM; Lonza, CC3190), slices were removed from the humidified, 5% CO_2, 37°C incubator (SANYO, MCO-18AIC), fixed using 2% (w/v) paraformaldehyde (PFA; Sigma, 15,1812-7) in 1X PBS pH 7.4 at 4°C (1 hour), and then washed with 1X PBS pH 7.4 (10 minutes). Slices were stored in 1X PBS until processed in to paraffin blocks by Mr Derek Scarborough, Cardiff University. Four µm-thick kidney sections were cut and air-dried onto strongly adhesive slides (Leica, Germany). Slice sections were deparaffinised in xylene (Sigma, 534056) (2 x 5 minutes) and rehydrated to water using 100% (2 x 5 minutes), 95% (1 X 5 minutes) and 70% (1 x 2 minutes) ethanol (Sigma, 458600). Slice sections were incubated in haematoxylin (Sigma, HHS16) (1 minute), washed in running water (2 minutes), dipped in 0.2% acid water and then washed again in running water (2 minutes). Sections were incubated in eosin (Thermo Scientific, LAMB/100-D) (1 minute) and then dehydrated using 70% (1 X 5 minutes), 95% (1 X 5 minutes) and 100% ethanol (Sigma, 458600) (2 X 5 minutes) and then cleared in xylene (Sigma, 534056) (2 x 5 minutes). Coverslips were mounted on slides using histomount (TAAB Labs, Aldermaston, UK). Slides were scanned using a ScanScope Scanner and images captured of the kidney cortex region captured using ImageScope software (Aperio Technologies Incorporated, Vista, USA). Five random fields of view (snapshots) per kidney slice cortex were captured from which histopathological

assessments made. N=1, n=1 for control rat kidney slices. N=3, n=3 for *ex vivo* rat kidney slices after 1 hour and 24 hours in culture.

3.6 Results

Characterisation of *Ex Vivo* Kidney Slices

To determine the viability of *ex vivo* kidney slices over time, ATP content was assessed after 0, 1, 4 and 24 hours culture in control medium. In addition, the effect of treatment with medium containing 10µM cisplatin, 10µM cyclosporin A or 30µM BEA was also investigated on slice viability over time. To identify differences in the ATP content over time within each drug-treated group, individual one-way ANOVA and post-hoc Tukey tests were performed at the 5% significance level. Differences were deemed statistically significant when $p < 0.05$ (*). To identify differences in the ATP content between control and all drug-treated groups after 1, 4 and 24 hours, a two-way ANOVA and post-hoc Tukey test was performed. Again, differences were deemed statistically significant when $p < 0.05$ (*). All values are expressed as nmoles ATP/mg wet weight of slice (mean ± SEM; N=3, n=3).

ATP Content of *Ex Vivo* Control Slices over Time

The ATP content of control kidney slices at 0 hours (immediately after slicing) was 1.04 ± 0.07 nmoles ATP/mg wet weight. There was no statistical difference in ATP content after 1 hour (1.02 ± 0.05 nmoles ATP/mg wet weight) or 4 hours (0.85 ± 0.05 nmoles ATP/mg wet weight) compared to that at 0 hours. However after 24 hours, the ATP content of slices treated with control medium had significantly decreased to 0.57 ± 0.05 nmoles ATP/mg wet weight ($p < 0.01$ **) compared to that at 0 hours. These data are graphically plotted in Figure 3.2A.

ATP Content of *Ex Vivo* Slices treated with Cisplatin, Cyclosporin A and BEA over Time

The ATP content of kidney slices treated control medium containing 10µM cisplatin, 10µM cyclosporin A or 30µM BEA for 1, 4 and 24 hours were individually compared to the ATP content of control kidney slices immediately after slicing (*i.e.* at 0 hours). The ATP content of control *ex vivo* kidney slices at 0 hours was 1.04 ± 0.07 nmoles ATP/mg wet weight. There was no statistical difference in the ATP content of *ex vivo* kidney slices following 1 hour treatment with medium containing 10µM cisplatin (0.96 ± 0.03 nmoles ATP/mg wet weight; $p > 0.05$). However, after 4 hours (0.62 ± 0.05 nmoles ATP/mg wet

weight; $p < 0.01$ **) and 24 hours (0.46 ± 0.07 nmoles ATP/mg wet weight; $p < 0.001$ ***) the ATP content was significantly decreased compared to that at 0 hours. These data are graphically plotted in Figure 3.2B. The ATP content of control *ex vivo* kidney slices at 0 hours was 1.04 ± 0.07 nmoles ATP/mg wet weight. There was no statistical difference in the ATP content of *ex vivo* kidney slices following 1 hour (0.96 ± 0.06 nmoles ATP/mg wet weight; $P > 0.05$) or 4 hours (0.76 ± 0.07 nmoles ATP/mg wet weight; $p > 0.05$) treatment with medium containing 10µM cyclosporin. After 24 hours (0.48 ± 0.05 nmoles ATP/mg wet weight; $p < 0.01$ **), there was a significant decrease in ATP content of *ex vivo* kidney slices treated with medium containing 10µM cyclosporin A compared to the ATP content of kidney slices at 0 hours. These data are graphically plotted in Figure 3.2C. The ATP content of control *ex vivo* kidney slices at 0 hours (immediately after slicing) was 1.04 ± 0.07 nmoles ATP/mg wet weight. There was no statistical difference in the ATP content of *ex vivo* kidney slices following treatment with medium containing 30µM BEA for 1 hour (1.05 ± 0.06 nmoles ATP/mg wet weight; $P > 0.05$) or 4 hours (0.87 ± 0.05 nmoles ATP/mg wet weight; $p > 0.05$). After 24 hours (0.54 ± 0.05 nmoles ATP/mg wet weight; $p < 0.01$ **), there was a significant decrease in ATP content of *ex vivo* kidney slices treated with medium containing 30µM BEA compared control slices at 0 hours. These data are graphically plotted in Figure 3.2D.

Next, a two-way ANOVA and post-hoc Tukey test was used to identify differences in ATP content between control and drug-treated groups after 1, 4 and 24 hours. After 1 hour, no significant differences in the ATP content of control or drug treated *ex vivo* slices was identified ($p > 0.05$). After 4 hours, no significant difference was identified between control and cyclosporin A or BEA groups ($p > 0.05$), but a significant difference was seen between the control and the cisplatin group ($p < 0.05$, *). After 24 hours, there was no significant difference in the ATP content of the control or any of the drug groups. Apart from the significant decrease in ATP content of slices treated with control medium containing 10µM cisplatin after 4 hours compared to the time-matched ATP content of slices treated with control medium, no drug-induced decreases in ATP content were detected, indicating that the overall decrease in ATP content over time is independent of drug-treatment.

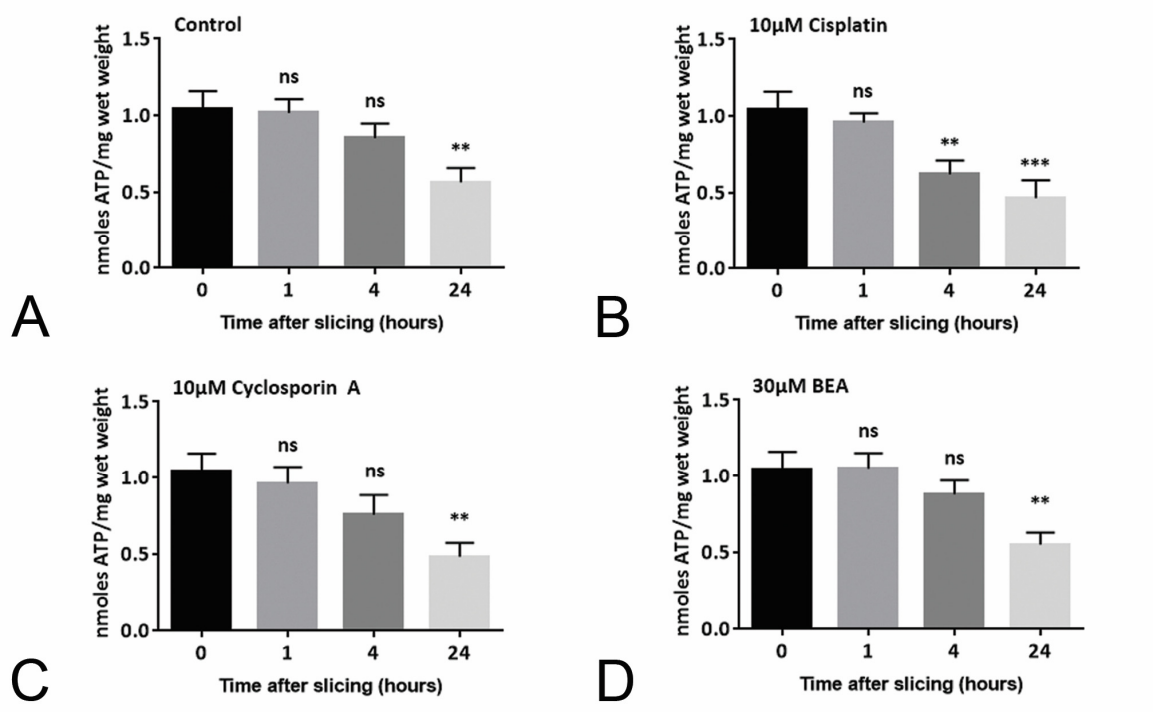

Figure 3.2. ATP content of *ex vivo* rat kidney slices under (A) control conditions, or in the presence of (B) 10µM cisplatin, (C) 10µM cyclosporin A or (D) 30µM BEA for 0, 1, 4 and 24 hours. (A) The ATP content of rat kidney slices was 1.04 ± 0.07 nmoles ATP/mg wet weight at the time of slicing (0 hours). No significant difference was detected in ATP content of slices cultured for 1 or 4 hours ($p > 0.05$; ns). However, a significant difference was detected 24 hours post-treatment (0.57 ± 0.05 nmoles ATP/mg wet weight; $p < 0.01$ **). (B) Decreases in ATP content were detected following 4 (0.62 ± 0.05 nmoles ATP/mg wet weight; $p < 0.01$ **) and 24 (0.46 ± 0.07 nmoles ATP/mg wet weight; $p < 0.001$ ***) hours treatment with cisplatin compared to that at time 0. (C) A decrease in ATP content was detected 24 hours exposure to medium containing cyclosporin A (0.48 ± 0.05 nmoles ATP/mg wet weight; $p < 0.01$ **) compared to that at time 0. (D) A decrease in ATP content was detected following 24 hours to medium containing BEA (0.54 ± 0.05 nmoles ATP/mg wet weight; $p < 0.01$ **) exposure compared to that at time 0. Significant differences were identified using a one-way ANOVA and post-hoc Tukey test. All values presented are mean ± SEM. N=3, n=3 for each condition and time point.

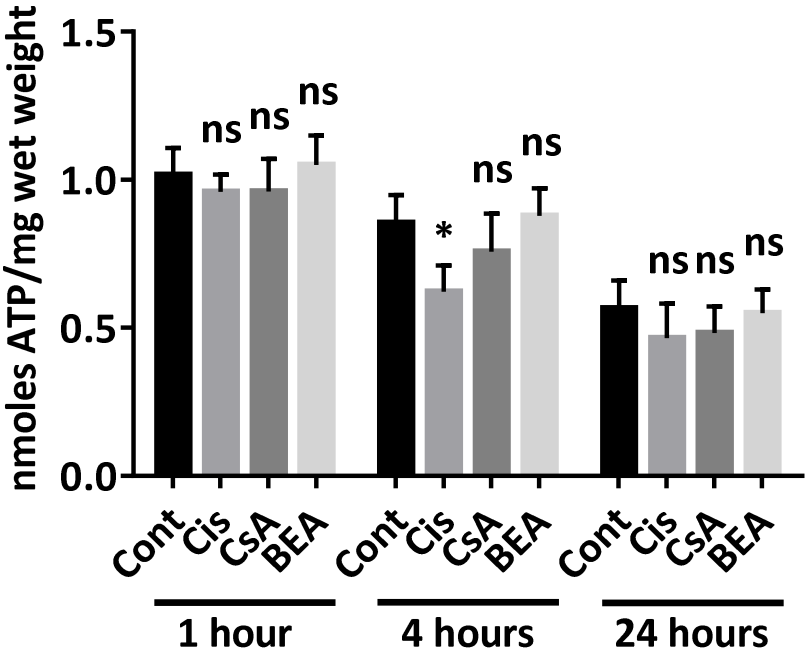

Figure 3.3. ATP content of *ex vivo* rat kidney slices under (A) control conditions, or in the presence of (B) 10µM cisplatin, (C) 10µM cyclosporin A or (D) 30µM BEA for 1, 4 and 24 hours. The ATP content of control rat kidney slices after 1 hour was 1.02 ± 0.05 nmoles ATP/mg wet weight. Compared to the time-matched control, no significant difference was detected in ATP content of slices also cultured for 1 hour in medium containing cisplatin (0.96 ± 0.03 nmoles ATP/mg wet weight; $p > 0.05$; ns), cyclosporin A (0.96 ± 0.06 nmoles ATP/mg wet weight; $P > 0.05$; ns) or BEA (1.05 ± 0.06 nmoles ATP/mg wet weight; $P > 0.05$; ns). The ATP content of control rat kidney slices after 4 hours was 0.85 ± 0.05 nmoles ATP/mg wet weight. Compared to the time-matched control, a significant difference was detected in ATP content of slices cultured for 4 hours in medium containing cisplatin (0.62 ± 0.05 nmoles ATP/mg wet weight; $p < 0.01$; **), but not cyclosporin A (0.76 ± 0.07 nmoles ATP/mg wet weight; $p > 0.05$; ns) or BEA (0.87 ± 0.05 nmoles ATP/mg wet weight; $p > 0.05$; ns). The ATP content of control rat kidney slices after 24 hours was 0.57 ± 0.05 nmoles ATP/mg wet weight. Compared to the time-matched control, no significant difference was detected in ATP content of slices also cultured for 24 hours in medium containing cisplatin (0.46 ± 0.07 nmoles ATP/mg wet weight; $p > 0.05$; ns), cyclosporin A (0.48 ± 0.05 nmoles ATP/mg wet weight; $P > 0.05$; ns) or BEA (0.54 ± 0.05 nmoles ATP/mg wet weight; $P > 0.05$; ns). Cont = control. Cis = cisplatin. CsA = cyclosporin A. BEA = bromoethylamine. Significant differences were identified using a two-way ANOVA and post-hoc Tukey test. All values presented are mean ± SEM. N=3, n=3 for each condition and time point.

Ex Vivo Kidney Slice Morphology

To further assess *ex vivo* kidney slice viability over time, histological assessment of slice morphology over time was performed. Representative haematoxylin and eosin (H&E) images of a formalin-fixed, paraffin-embedded control rat kidney and *ex vivo* rat kidney slices cultured under control conditions for 1 and 24 hours are shown in Figure 3.4. In control rat kidney cortex, nuclei appear uniform in size and shape and proximal tubule cells possess brush border membranes (Figure 3.4A). Following 1 hour in culture under control conditions, *ex vivo* rat kidney sections already show morphological features of injury; cell nuclei appear smaller and more condensed than control rat kidneys, with some cellular detachment from the tubule basement membrane (Figure 3.4B-D). When slices were kept in culture for 24 hours, clear morphological features of injury are apparent in all of the samples; cell nuclei appear small and condensed, there is loss of proximal tubule brush border membranes and sloughing epithelial cells into the tubule lumen is present (Figure 3.4E-G).

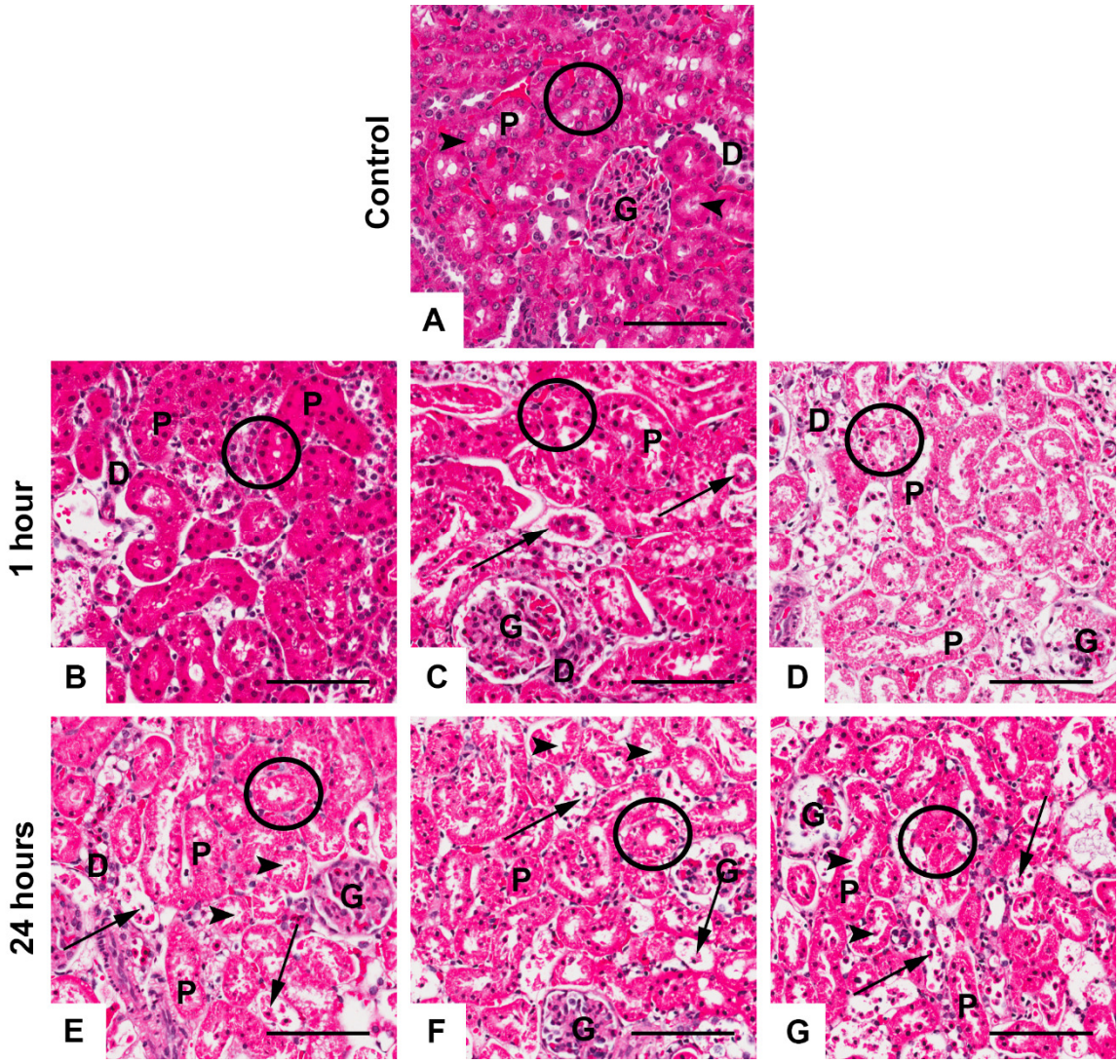

Figure 3.4. E*x vivo* rat kidney cortex slice morphology following culture for 1 (middle panels) and 24 (bottom panels) hours in control medium post-slicing. Representative H&E images showing the morphology of the cortex of (A) a control rat kidney section, (B-D) control *ex vivo* rat kidney slices cultured for 1 hour and (E-G) control *ex vivo* rat kidney slices cultured for 24 hours. (A) In control rat kidney sections nuclei appear uniform in size and shape (circled) and proximal tubules possess brush border membranes (arrow heads). (B-D) Following 1 hour in culture under control conditions, *ex vivo* rat kidney slices show morphological features of injury; cell nuclei appear smaller and more condensed (circled) with the cells of some tubules completely detaching from the basement membrane (arrows). (E-G) After 24 hours in culture, clear morphological features of injury are apparent in all kidney slice samples; cell nuclei appear very small and condensed (circled), there is loss of proximal tubule brush border membranes (arrow heads) and sloughing of epithelial cells into the tubular lumens is present (arrows). All images presented are representative of one section per individual sample, and are representative of 5 fields of view. N=1, n=1 for control rat kidney cortex. N=3, n=3 for control rat kidney *ex vivo* slices cultured for 1 hour and 24 hours. P = proximal tubule, D = distal tubule, G = glomerulus. Bars = 100µm. Slice culture and H&E performed by JG. Image analysis performed by RW.

In light of the clear deterioration of slice morphology (Figure 3.4) along with the significant decrease in slice ATP content indicative of cell death (Figure 3.2), the decision was made to focus on the characterisation of the *in vitro* renal cell model as a tool for studying drug-induced nephrotoxicity. A similar decrease in the ATP content of *ex vivo* kidney slices over time was also observed by another researcher, Mr Joao Graça, when slices were cultured in a similar manner. Together these data suggest that further optimisation of slice preparation and culture is required in order for meaningful toxicology testing data to be obtained.

Characterisation of *In Vitro* Primary Mouse Renal Cells

Proliferation and Apoptosis Assays

Proliferation and apoptosis assays were used to determine primary mouse renal cell viability under control culture conditions, for up to 15 days in culture. The incorporation of 5-bromo-2'-deoxyuridine (BrdU) into actively proliferating cell nuclei, and terminal deoxyribonucleotidyl transferase-mediated dUTP nick end labelling (TUNEL) of apoptotic cell nuclei, was used to assess the overall viability of renal cells in culture over time.

A representative immunofluorescent image of BrdU incorporation into new DNA within proliferating cell nuclei after 8 days in culture is shown in Figure 3.5A. The percentage of BrdU-positive cell nuclei was 81.31 ± 2.42% (mean ± SD; N=3, n=3) of total cell nuclei at day 5. By day 15, the percentage of BrdU-positive cell nuclei had significantly decreased to 26.22 ± 2.05% (mean ± SD; N=3, n=3; $p < 0.001$ ***) compared to that at day 5, as determined using a one-way ANOVA and a post-hoc Tukey test (Figure 3.5C).

A representative light microscopy image of apoptotic cell nuclei after 8 days in culture is shown in Figure 3.5B. The percentage of cells undergoing apoptosis was 4.22 ± 0.97% (mean ± SD; N=3, n=3) of total cells at day 5. By day 15, the percentage of total cells undergoing apoptosis had significantly decreased to 1.30 ± 0.32% (mean ± SD; N=3, n=3; $P < 0.01$ **) compared to that at day 5, as determined using a one-way ANOVA and a post-hoc Tukey test (Figure 3.5D).

Overall, cell viability over the culture time-course was high as determined by high proliferation and low apoptosis.

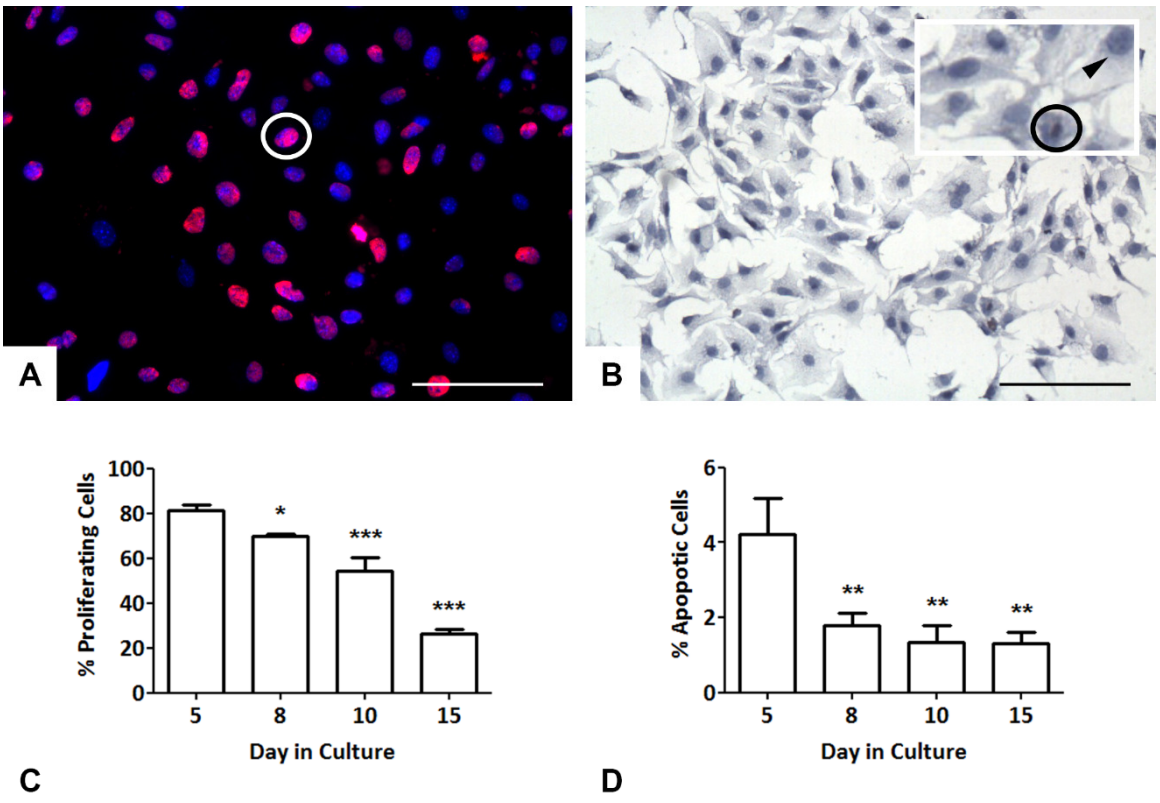

Figure 3.5. Assessment of primary mouse renal cell viability under control conditions over time using a BrdU-incorporation proliferation assay and a TUNEL apoptosis assay. (A) A representative image of proliferating cell nuclei after 8 days in culture. All cell nuclei are blue (Hoechst positive) and proliferating cell nuclei are red (BrdU positive). Bar = 100µm. (B) A representative image of apoptotic TUNEL cell nuclei after 8 days in culture. All cell nuclei are blue (haematoxylin positive) and apoptotic cell nuclei are brown (DAB positive). Bar = 100µm. (C) At day 5, 81.31 ± 2.42% (mean ± SD; N=3, n=3) of all nuclei were BrdU-positive. At day 8, there was a significant decrease in BrdU-positive nuclei (69.91 ± 1.13%; mean ± SD; N=3, n=3; $p < 0.05$ *) compared to that at day 5. Significant differences in BrdU-positive nuclei were also seen at day 10 (54.44 ± 6.00%; mean ± SD; N=3, n=3; $p < 0.001$ ***) and day 15 (26.22 ± 2.05; mean ± SD; N=3, n=3; $p < 0.001$ ***) compared to day 5. Significant differences were identified using a one-way ANOVA and a post-hoc Tukey test. Random snapshots were taken such that between 200 and 600 cell nuclei in total were counted at each time point. (D) At day 5, 4.22 ± 0.97% (mean ± SD; N=3, n=3) of cell nuclei were apoptotic. At day 8, there was a significant decrease in apoptotic nuclei (1.79 ± 0.34%; mean ± SD; N=3, n=3; $p < 0.01$ **) compared to that at day 5. Significant decreases in the percentage of apoptotic nuclei were also seen at day 10 (1.34 ± 0.46%; mean ± SD; N=3, n=3; $p < 0.01$ **) and day 15 (1.30 ± 0.32%; mean ± SD; N=3, n=3; $p < 0.01$ **) when compared to that at day 5. Random snapshots were taken such that a minimum of 100 total cell nuclei were counted at day 5, and between 200 and 600 cell nuclei at days 8, 10 and 15. Significant differences were identified using a one-way ANOVA and a post-hoc Tukey test.

Concentration-Dependent, Drug-Induced Apoptosis

Concentration-dependent drug-induced apoptosis in primary mouse renal cells was assessed using a TUNEL assay. Cells were grown for 7 days in control medium before 24 hour-treatment with control medium (vehicle control; medium), or medium containing cisplatin (1, 3, 5µM), cyclosporin A (1, 3, 5µM) or BEA (3, 10, 30µM). To identify differences in the percentage of apoptotic cells between control and drug treatments, individual one-way ANOVA and post-hoc Tukey tests was performed for each drug. All three drugs induced a concentration-dependent increase in the percentage of apoptotic cells compared to the control.

In the cisplatin group, 1.2 ± 0.4% (mean ± SD; N=3, n=3) of control cell nuclei were apoptotic. Compared to the control, no significant difference in the percentage of apoptotic nuclei was identified in cells treated with medium containing 1µM cisplatin (1.6 ± 0.5%; mean ± SD; N=3, n=3; $p > 0.05$ ns). However significant differences were identified in cells treated with medium containing 3µM cisplatin (3.9 ± 0.6%; mean ± SD; N=3, n=3; $p < 0.01$ **) and 5µM cisplatin (7.3 ± 6.7%; mean ± SD; N=3, n=3; $p < 0.001$ ***).

In the cyclosporin A group, 0.87 ± 0.57% (mean ± SD; N=3, n=3) of control cell nuclei were apoptotic. Compared to the control, no significant difference in the percentage of apoptotic nuclei was identified in cells treated with medium containing 1µM cyclosporin A (1.6 ± 0.6%; mean ± SD; N=3, n=3; $p > 0.05$ ns). However significant differences were identified in cells treated with medium containing 3µM cyclosporin A (4.1 ± 0.6%; mean ± SD; N=3, n=3; $p < 0.01$; **) and 5µM cyclosporin A (7.4 ± 1.0; mean ± SD; N=3, n=3; $p < 0.001$ ***).

In the BEA group, 1.0 ± 0.4% (mean ± SD; N=3, n=3) of control cell nuclei were apoptotic. Compared to the control, no significant difference in the percentage of apoptotic nuclei was identified in cells treated with medium containing 3µM BEA (1.5 ± 0.6%; mean ± SD; N=3, n=3; $p > 0.05$ ns) or 10µM BEA (1.4 ± 0.4%; mean ± SD; N=3, n=3; $p > 0.05$ ns). However significant differences were identified in cells treated with medium containing 30µM BEA (3.5 ± 0.3; mean ± SD; N=3, n=3; $p < 0.01$ **).

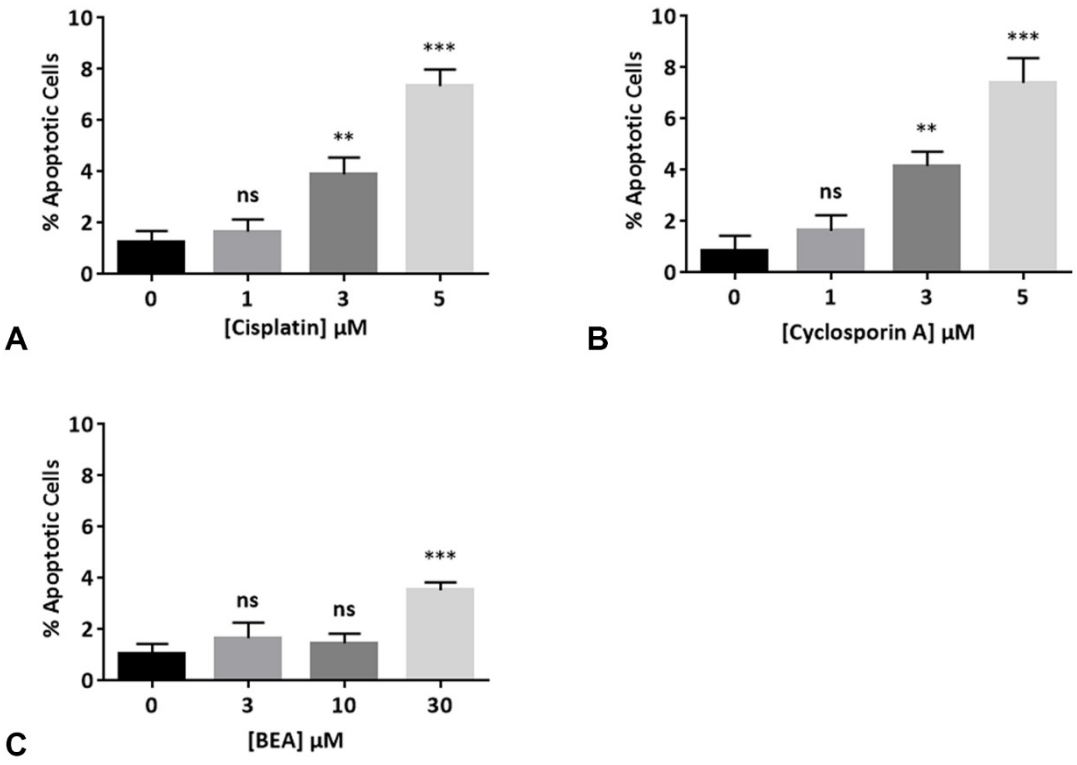

Figure 3.6. Percentage of apoptotic primary mouse renal cell nuclei following 24-hour treatment with medium containing (A) 0, 1, 3 and 5µM cisplatin, (B) 0, 1, 3 and 5µM cyclosporin A or (C) 0, 3, 10 and 30µM BEA. (A) 1.2 ± 0.4% (mean ± SD; N=3, n=3) of control cell nuclei were apoptotic. Compared to the control, no significant difference in the percentage of apoptotic nuclei was identified in cells treated with medium containing 1µM cisplatin (1.6 ± 0.5%; mean ± SD; N=3, n=3; $p > 0.05$ ns). However significant differences were identified in cells treated with medium containing 3µM cisplatin (3.9 ± 0.6%; mean ± SD; N=3, n=3; $p < 0.01$ **) and 5µM cisplatin (7.3 ± 6.7%; mean ± SD; N=3, n=3; $p < 0.001$ ***). (B) 0.87 ± 0.57% (mean ± SD; N=3, n=3) of control cell nuclei were apoptotic. Compared to the control, no significant difference in the percentage of apoptotic nuclei was identified in cells treated with medium containing 1µM cyclosporin A (1.6 ± 0.6%; mean ± SD; N=3, n=3; $p > 0.05$ ns). However significant differences were identified in cells treated with medium containing 3µM cyclosporin A (4.1 ± 0.6%; mean ± SD; N=3, n=3; $p < 0.01$; **) and 5µM cyclosporin A (7.4 ± 1.0; mean ± SD; N=3, n=3; $p < 0.001$ ***). (C) 1.0 ± 0.4% (mean ± SD; N=3, n=3) of control cell nuclei were apoptotic. Compared to the control, no significant difference in the percentage of apoptotic nuclei was identified in cells treated with medium containing 3µM BEA (1.5 ± 0.6%; mean ± SD; N=3, n=3; $p > 0.05$ ns) or 10µM BEA (1.4 ± 0.4%; mean ± SD; N=3, n=3; $p > 0.05$ ns). However significant differences were identified in cells treated with medium containing 30µM BEA (3.5 ± 0.3; mean ± SD; N=3, n=3; $p < 0.01$ **). Significant differences were identified using individual one-way ANOVA and post-hoc Tukey tests. Random snapshots were taken such that a between 100 and 150 total cells were counted for each drug and each concentration. Cell culture and assay performed by VP. Cell counts performed by VP. Statistical analysis performed by RW.

Concentration-Dependent, Drug-Induced Loss of Cell Adhesion

A concentration-dependent drug-induced effect on cell adhesion to the tissue culture plate was assessed by counting the number of detached (floating) cells in the culture medium following treatment. Cells were grown for 7 days in control medium before 24 hour-treatment with control medium (vehicle control; medium), or medium containing cisplatin (1, 3, 10µM), cyclosporin A (1, 3, 10µM) or BEA (1, 3, 30µM). At day 8 of culture, the number of floating cells in each of the treatment groups was calculated as a percentage of the total number of control cells (which included those floating in the control culture medium and those still attached to the control tissue culture plate). To identify significant differences between control and drug treatments, individual one-way ANOVA and post hoc Tukey tests were performed for each drug.

Figure 3.7 shows an increase in cell detachment from the tissue culture plate in response to treatment with medium containing cisplatin. The percentage of detached cells floating in control cell medium was 5.14 ± 1.39% (mean ± SD; N=3, n=3) of the total number of control cells. Treatment with medium containing 1µM cisplatin did not significantly increase the percentage of floating cells (12.63 ± 2.49%; mean ± SD; N=3, n=3; $p > 0.05$ ns) compared to the control. However, treatment with medium containing 3µM and 10µM cisplatin significantly increased the percentage of floating cells to 28.48 ± 10.72% (mean ± SD; N=3, n=3; $p < 0.05$ *) and 64.43 ± 6.92% (mean ± SD; N=3, n=3; $p < 0.001$ ***), respectively. Concentration-dependent increase in cell detachment from the tissue culture plate was visible by light microscopy (N=1, n=1); cells remaining attached to the tissue culture plate were visible beneath the floating cells in the medium prior to collection for counting cell counting.

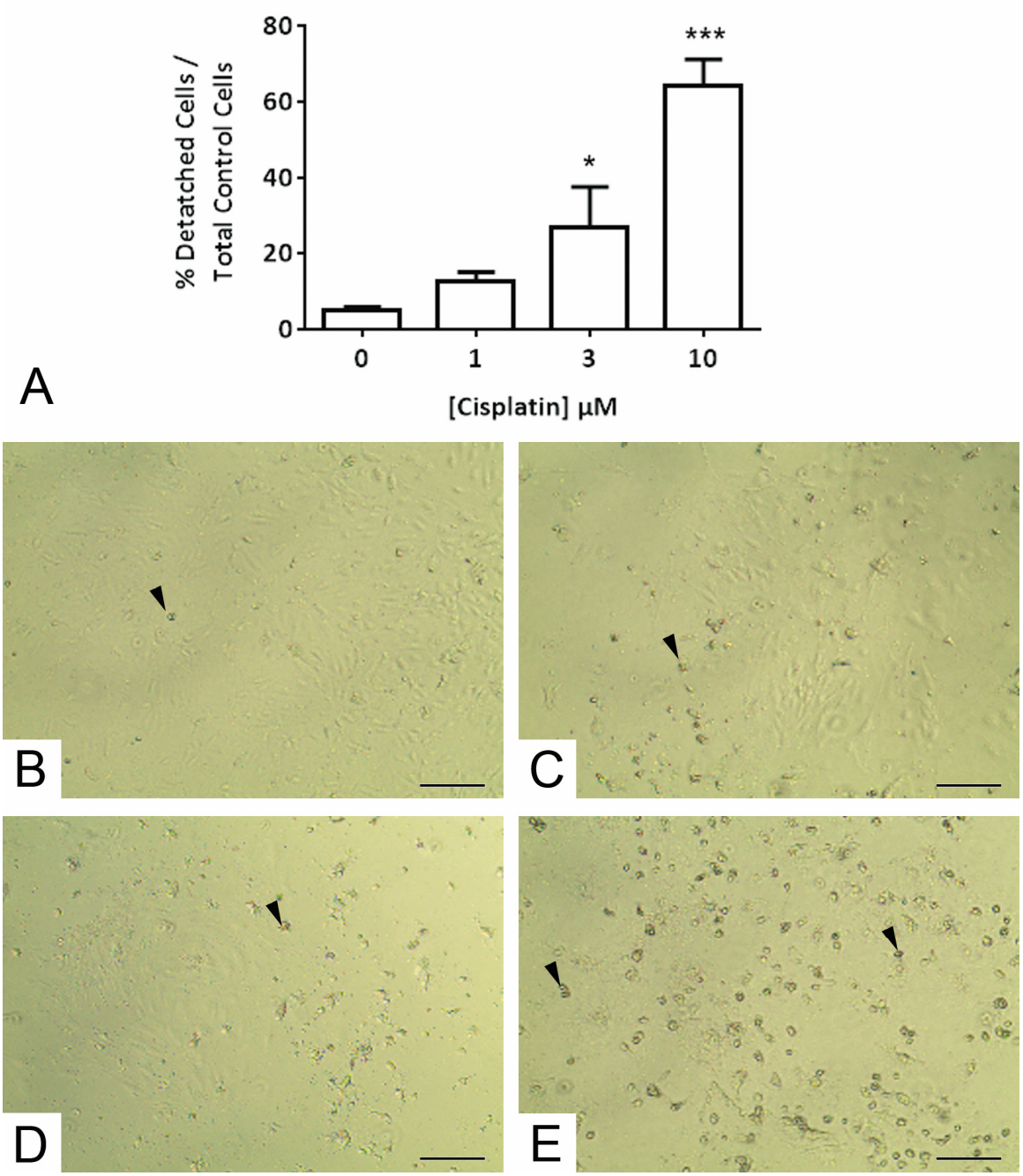

Figure 3.7. Cisplatin-induced detachment of primary mouse renal cells from the tissue culture plate. (A) The percentage of detached cells floating in control medium was 5.14 ± 1.39% (mean ± SD; N=3, n=3) of the total number of control cells. Treatment with medium containing 1µM cisplatin did not significantly increase the percentage of floating cells (12.63 ± 2.49%; mean ± SD; N=3, n=3; $p < 0.05$ ns) compared to the control. Treatment with medium containing 3µM and 10µM cisplatin significantly increased the percentage of floating cells to 28.48 ± 10.72% (mean ± SD; N=3, n=3; $p < 0.05$ *) and 64.43 ± 6.92% (mean ± SD; N=3, n=3; $p < 0.001$ ***), respectively. Significant differences were identified using a one-way ANOVA and a post-hoc Tukey test. Representative light microscopy images of the tissue culture plates following exposure to medium containing (B) 0, (C) 1, (D) 3 and (E) 10µM cisplatin (N=1, n=1). Cells remaining attached to the tissue culture plate are visible beneath the detached cells (arrow heads) floating in the culture medium. Bars = 200µm.

Figure 3.8 shows an increase in cell detachment from the tissue culture plate in response to treatment with medium containing cyclosporin A. The percentage of detached cells floating in control cell medium was 5.14 ± 1.39% (mean ± SD; N=3, n=3) of the total number of control cells. Treatment with medium containing 1µM cyclosporin A did not significantly increase the percentage of floating cells (10.55 ± 2.34%; mean ± SD; N=3, n=3; $p > 0.05$ ns) compared to the control. However, treatment with medium containing 3µM and 10µM cyclosporin A significantly increased the percentage of floating cells to 19.17 ± 4.68% (mean ± SD; N=3, n=3; $p < 0.01$ **) and 37.24 ± 5.17% (mean ± SD; N=3, n=3; $p < 0.001$ ***), respectively. Concentration-dependent increase in cell detachment from the tissue culture plate was visible by light microscopy (N=1, n=1); cells remaining attached to the tissue culture plate were visible beneath the floating cells in the medium prior to collection for counting cell counting.

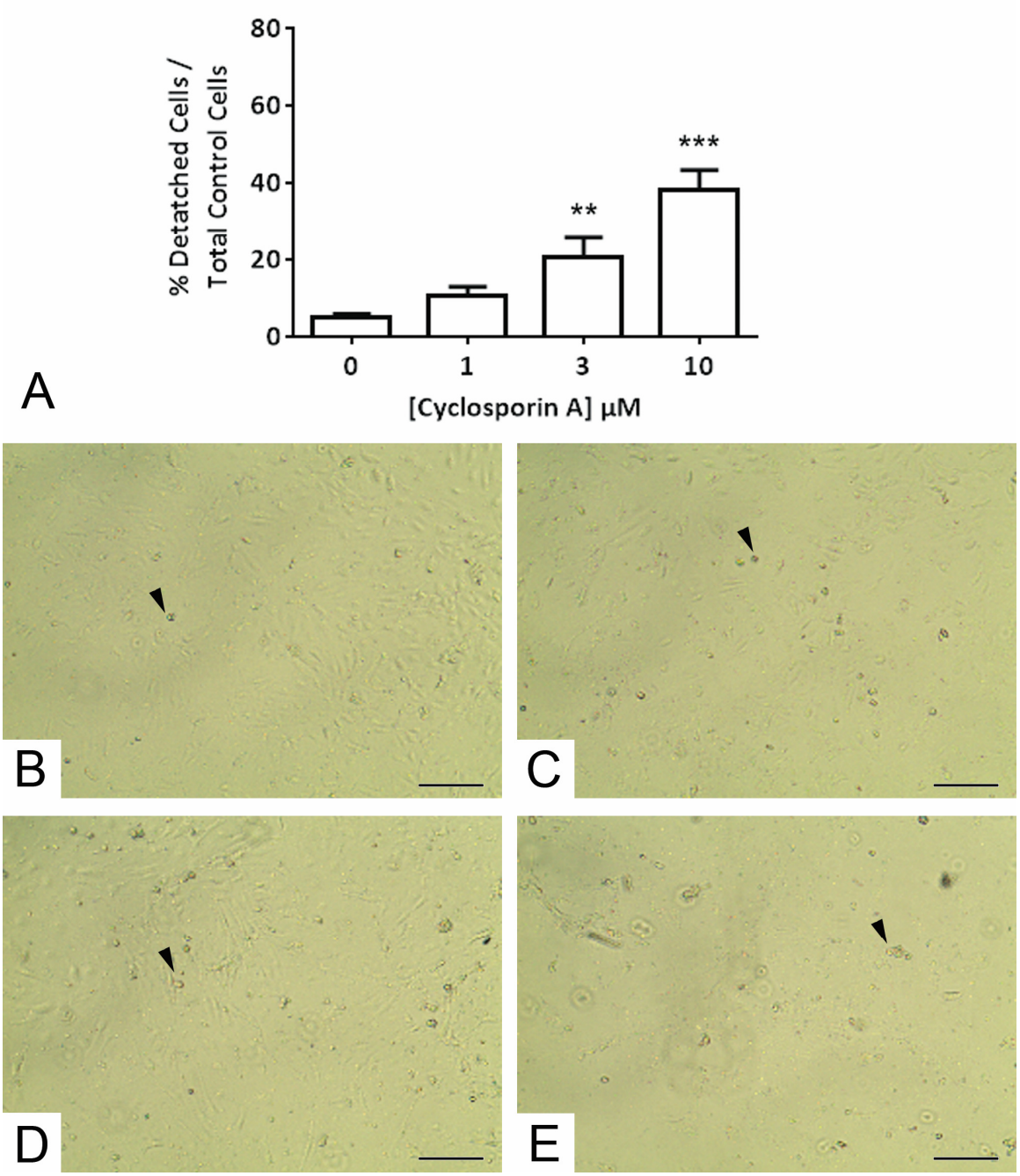

Figure 3.8. Cyclosporin A-induced detachment of primary mouse renal cells from the tissue culture plate. (A) The percentage of detached cells floating in control medium was 5.14 ± 1.39% (mean ± SD; N=3, n=3) of the total number of control cells. Treatment with medium containing 1µM cyclosporin A did not significantly increase the percentage of floating cells (10.55 ± 2.34%; mean ± SD; N=3, n=3; $p < 0.05$ ns) compared to the control. Treatment with medium containing 3µM and 10µM cyclosporin A significantly increased the percentage of floating cells to 19.17 ± 4.68% (mean ± SD; N=3, n=3; $p < 0.01$ **) and 37.24 ± 5.17% (mean ± SD; N=3, n=3; $p < 0.001$ ***), respectively. Significant differences were identified using a one-way ANOVA and a post-hoc Tukey test. Representative light microscopy images of the tissue culture plates following exposure to medium containing (B) 0, (C) 1, (D) 3 and (E) 10µM cyclosporin A (N=1, n=1). Cells remaining attached to the tissue culture plate are visible beneath the detached cells (arrow heads) floating in the culture medium. Bars = 200µm.

Figure 3.9 shows an increase in cell detachment from the tissue culture plate in response to treatment with medium containing BEA. The percentage of detached cells floating in control cell medium was 5.14 ± 1.39% (mean ± SD; N=3, n=3) of the total number of control cells. Treatment with medium containing 1µM BEA did not significantly increase the percentage of floating cells (8.22 ± 2.60%; mean ± SD; N=3, n=3; $p > 0.05$ ns) compared to the control. However, treatment with medium containing 3µM and 30µM BEA significantly increased the percentage of floating cells to 16.74 ± 3.33% (mean ± SD; N=3, n=3; $p < 0.001$ ***) and 25.35 ± 1.24% (mean ± SD; N=3, n=3; $p < 0.001$ ***), respectively. Concentration-dependent increase in cell detachment from the tissue culture plate was visible by light microscopy (N=1, n=1); cells remaining attached to the tissue culture plate were visible beneath the floating cells in the medium prior to collection for counting cell counting.

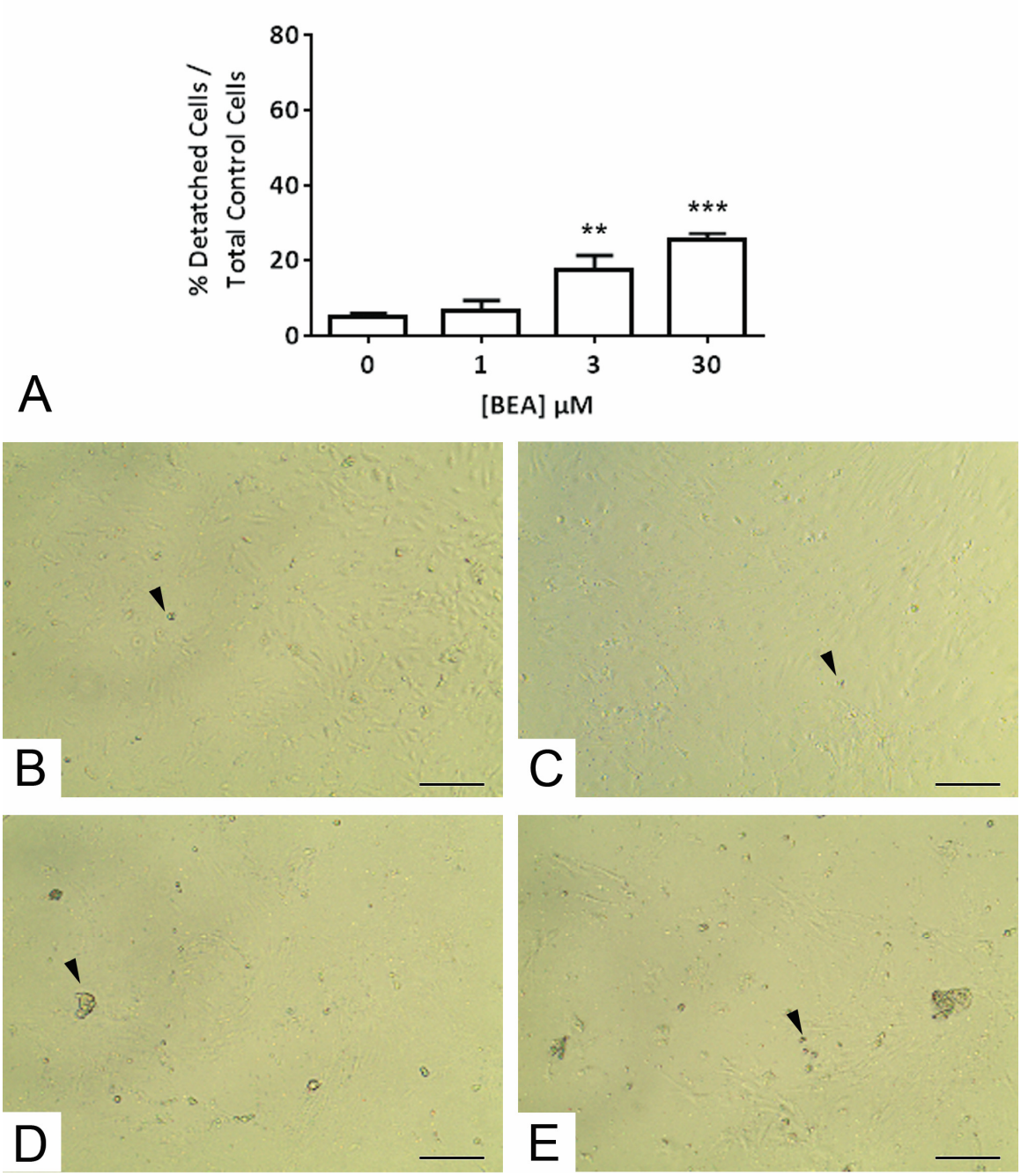

Figure 3.9. BEA-induced detachment of primary mouse renal cells from the tissue culture plate. (A) The percentage of detached cells floating in control medium was 5.14 ± 1.39% (mean ± SD; N=3, n=3) of the total number of control cells. Treatment with medium containing 1µM BEA did not significantly increase the percentage of floating cells (8.22 ± 2.60%; mean ± SD; N=3, n=3; $p > 0.05$ ns) compared to the control. Treatment with medium containing 3µM and 30µM BEA significantly increased the percentage of floating cells to 16.74 ± 3.33% (mean ± SD; N=3, n=3; $p < 0.001$ ***) and 25.35 ± 1.24% (mean ± SD; N=3, n=3; $p < 0.001$ ***), respectively. Significant differences were identified using a one-way ANOVA and a post-hoc Tukey test. Representative light microscopy images of the tissue culture plates following exposure to medium containing (B) 0, (C) 1, (D) 3 and (E) 30µM BEA (N=1, n=1). Cells remaining attached to the tissue culture plate are visible beneath the detached cells (arrow heads) floating in the culture medium. Bars = 200µm.

KIM-1 Immunoreactivity in Mouse Cells following Nephrotoxin Treatment

De novo expression of the kidney injury biomarker, kidney injury molecule-1 (KIM-1), was identified in primary mouse renal cells following 24-hour treatment with medium containing cisplatin, cyclosporin A and BEA (Figure 3.11 and 3.12). Representative images of KIM-1 immunoreactivity in each treatment group are presented in Figure 3.11. In all drug-treatment groups, KIM-1 was localised to cell membranes (arrow heads). Following treatment with control medium (vehicle control; medium), a small number of cells (3.24 ± 0.05% (mean ± SD; N=3, n=3)) displayed KIM-1 immunoreactivity (Figure 3.12). Following treatment with medium containing 10µM cisplatin, the percentage of cells expressing KIM-1 increased significantly (79.21 ± 5.68%; mean ± SD; N=3, n=3; $p < 0.001$ ***), compared to the control. Following treatment with medium containing 10µM cyclosporin A, the percentage of cells expressing KIM-1 increased significantly (44.02 ± 5.73%; mean ± SD; N=3, n=3; $p < 0.001$ ***), compared to the control. Following treatment with medium containing 30µM BEA, the percentage of cells expressing KIM-1 increased significantly (48.83 ± 4.89%; mean ± SD; N=3, n=3; $p < 0.001$ ***), compared to the control. Significant differences were identified using a one-way ANOVA and a post-hoc Tukey test.

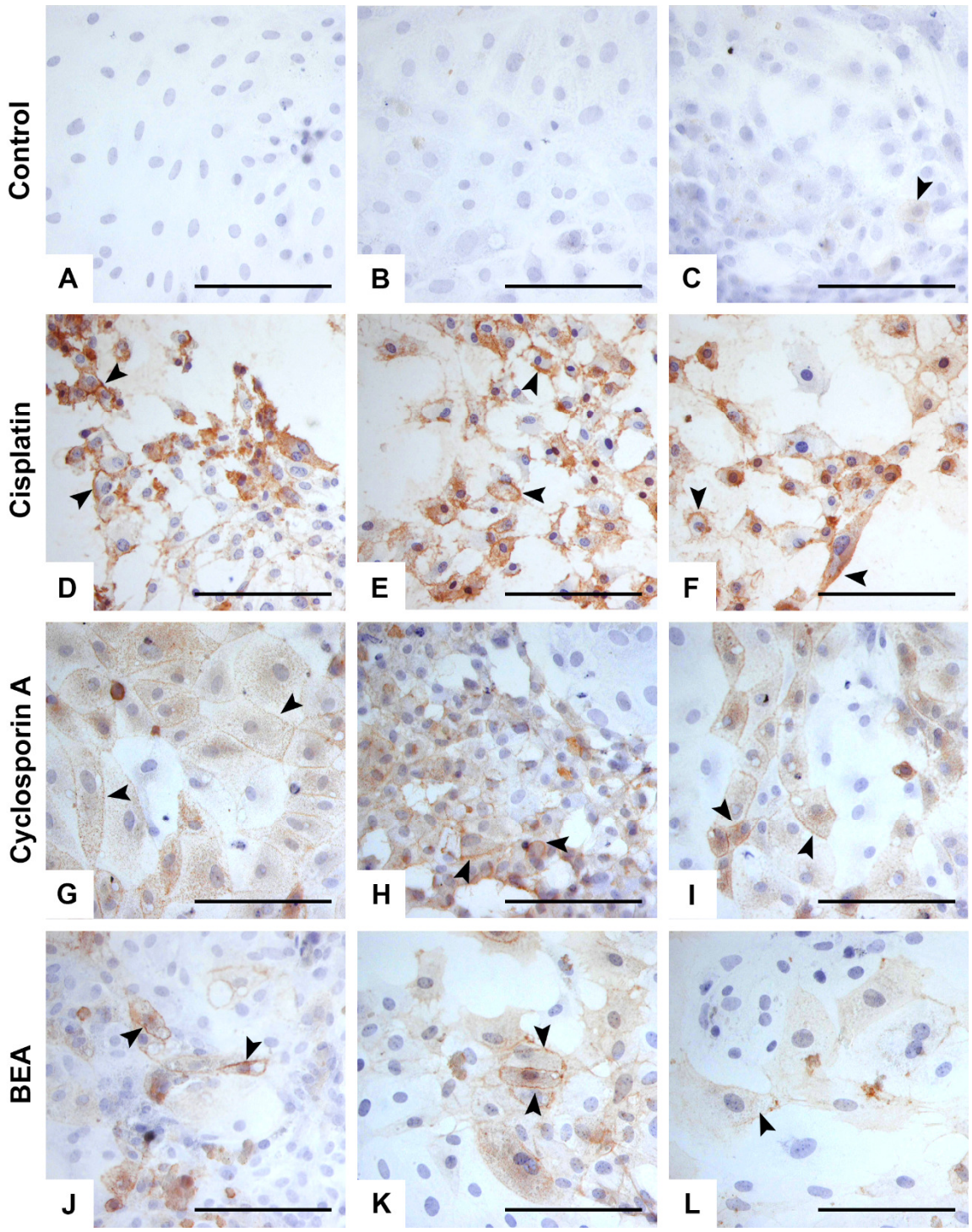

Figure 3.11. KIM-1 immunoreactivity in primary mouse renal cells cultured for 24 hours in (A-C) control medium or medium containing (D-F) 10µM cisplatin, (G-I) 10µM cyclosporin A and (J-L) 30µM BEA. (A-C) KIM-1 immunoreactivity was detected in a small number of cells cultured in control medium (vehicle control; medium) (arrow head). Treatment with medium containing (D-F) 10µM cisplatin, (G-I) 10µM cyclosporin A and (J-L) 30µM BEA increased the number of cells expressing KIM-1. Clear membrane expression was identified in drug-treatment groups (arrow heads). Images presented are representative of 5 fields of view per individual sample. KIM-1 immunoreactivity is brown, and the haematoxylin co-stain identifying nuclei is blue. N=3, n=3 for all groups. Bars = 100µm.

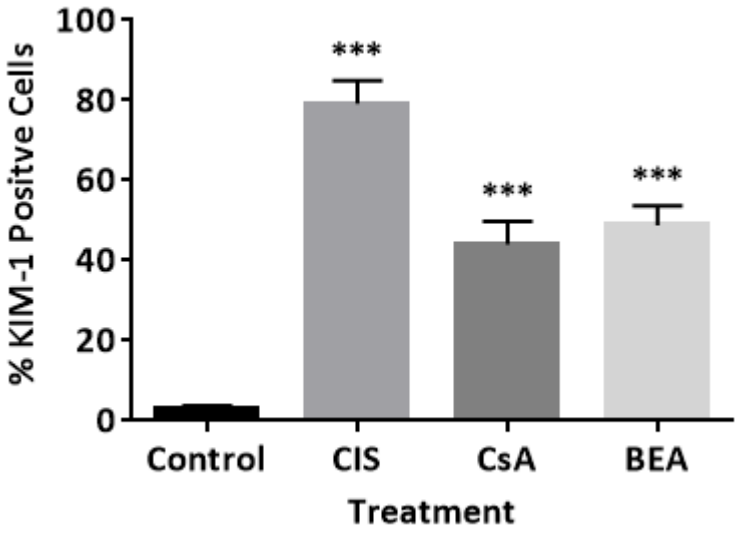

Figure 3.12. Percentage of primary mouse renal cells expressing KIM-1 following 24 hours treatment with control medium or medium containing 10µM cisplatin (CIS), 10µM cyclosporin A (CsA) or 30µM BEA Following treatment with control medium (vehicle control; medium), a small number of cells (3.24 ± 0.05% (mean ± SD; N=3, n=3)) displayed KIM-1 immunoreactivity. Following treatment with medium containing 10µM cisplatin, the percentage of cells expressing KIM-1 increased significantly (79.21 ± 5.68%; mean ± SD; N=3, n=3; $p < 0.001$ ***), compared to the control. Following treatment with medium containing 10µM cyclosporin A, the percentage of cells expressing KIM-1 increased significantly (44.02 ± 5.73%; mean ± SD; N=3, n=3; $p < 0.001$ ***), compared to the control. Following treatment with medium containing 30µM BEA, the percentage of cells expressing KIM-1 increased significantly (48.83 ± 4.89%; mean ± SD; N=3, n=3; $p < 0.001$ ***), compared to the control. To quantify the percentage of cells expressing KIM-1, snapshots of 5 random fields of view from each coverslip were taken, from which a minimum of 500 cells were assessed for biomarker expression. Significant differences were identified using a one-way ANOVA and a post-hoc Tukey test.

Osteopontin Immunoreactivity in Mouse Cells following Nephrotoxin Treatment

De novo expression of the kidney injury biomarker osteopontin was identified in primary mouse renal cells following 24-hour treatment with medium containing cisplatin, cyclosporin A and BEA (Figure 3.13 and 3.14). Representative images of osteopontin immunoreactivity in each treatment group are presented in Figure 3.13. In all groups, osteopontin was localised to cell cytoplasm (arrow heads). Following treatment with control medium (vehicle control; medium), 13.82 ± 2.28% (mean ± SD; N=3, n=3) of cells displayed osteopontin immunoreactivity (Figure 3.14). Following treatment with medium containing 10µM cisplatin, the percentage of cells expressing osteopontin increased significantly (71.91 ± 8.23%; mean ± SD; N=3, n=3; $p < 0.001$ ***), compared to the control. Following treatment with medium containing 10µM cyclosporin A, the percentage of cells expressing osteopontin increased significantly (41.76 ± 1.92%; mean ± SD; N=3, n=3; $p < 0.001$ ***), compared to the control. Following treatment with medium containing 30µM BEA, the percentage of cells expressing osteopontin increased significantly (35.14 ± 2.47%; mean ± SD; N=3, n=3; $p < 0.01$ **), compared to the control. Significant differences were identified using a one-way ANOVA and a post-hoc Tukey test.

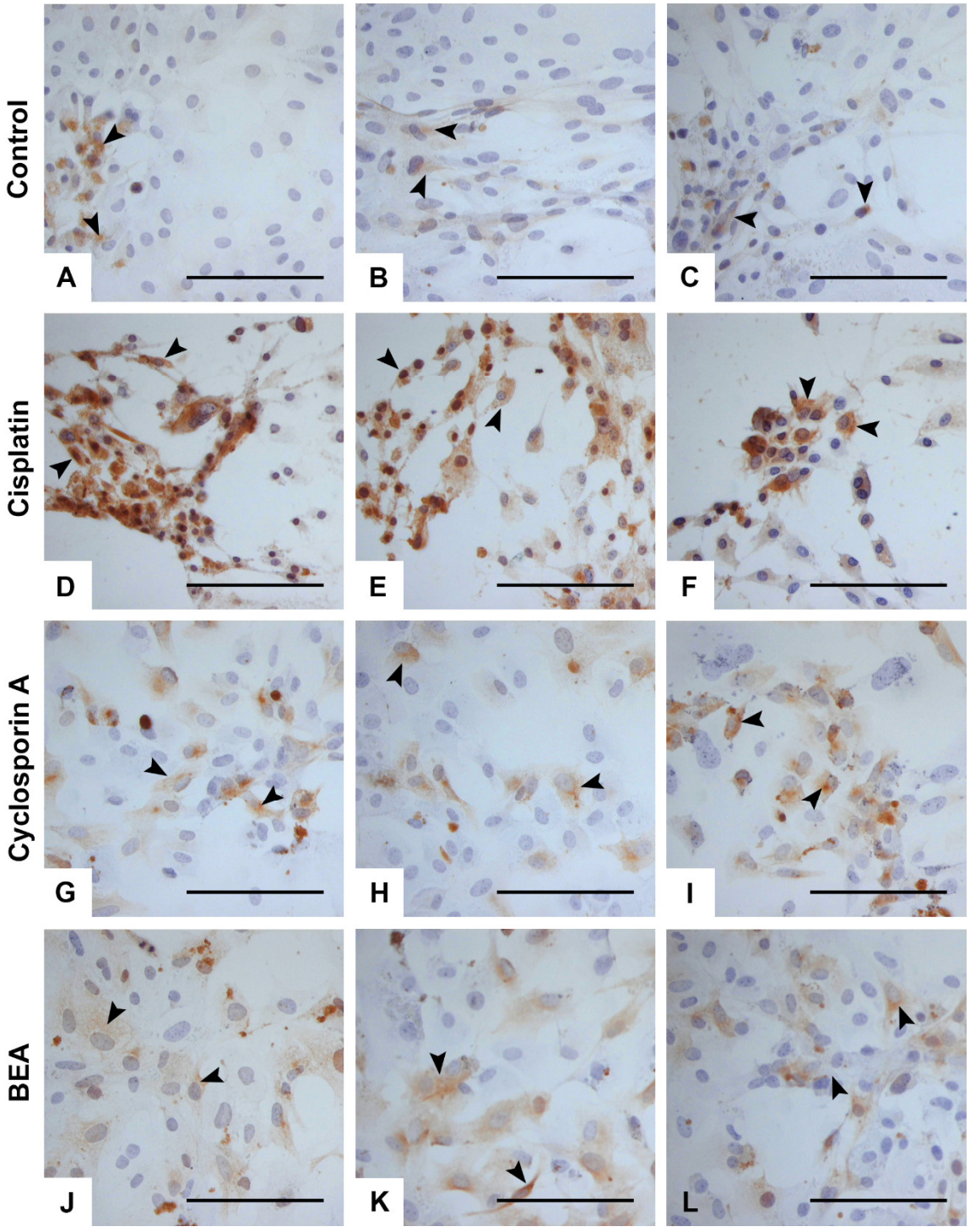

Figure 3.13. Osteopontin immunoreactivity in primary mouse renal cells cultured for 24 hours in (A-C) control medium or medium containing (D-F) 10µM cisplatin, (G-I) 10µM cyclosporin A and (J-L) 30µM BEA. (A-C) Osteopontin immunoreactivity was detected in a small number of cells cultured in control medium (vehicle control; medium) (arrow head). Treatment with medium containing (D-F) 10µM cisplatin, (G-I) 10µM cyclosporin A and (J-L) 30µM BEA increased the number of cells expressing osteopontin. In all groups, osteopontin immunoreactivity was localised to the cell cytoplasm (arrow heads). Images presented are representative of 5 fields of view per individual sample. Osteopontin immunoreactivity is brown, and the haematoxylin co-stain identifying nuclei is blue. N=3, n=3 for all groups. Bars = 100µm.

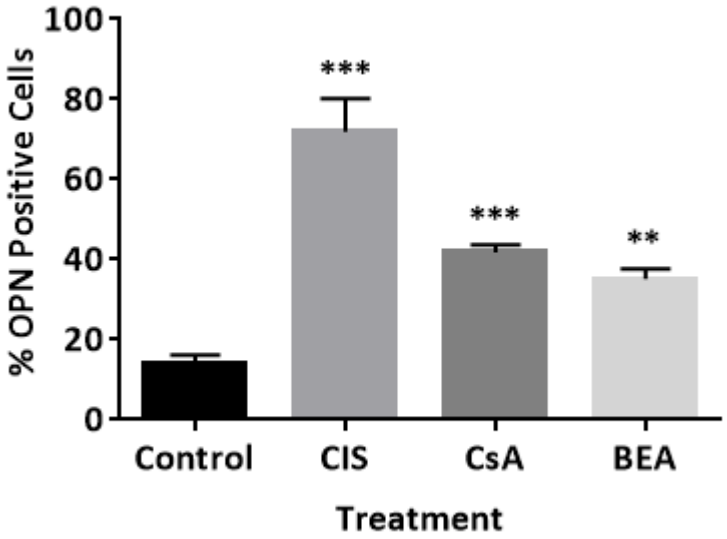

Figure 3.14. Percentage of primary mouse renal cells expressing osteopontin (OPN) following 24 hour-treatment with control medium or medium containing 10µM cisplatin (CIS), 10µM cyclosporin A (CsA) or 30µM BEA. Following treatment with control medium (vehicle control; medium), 13.82 ± 2.28% (mean ± SD; N=3, n=3) of cells displayed osteopontin immunoreactivity. Following treatment with medium containing 10µM cisplatin, the percentage of cells expressing osteopontin increased significantly (71.91 ± 8.23%; mean ± SD; N=3, n=3; $p < 0.001$ ***), compared to the control. Following treatment with medium containing 10µM cyclosporin A, the percentage of cells expressing osteopontin increased significantly (41.76 ± 1.92%; mean ± SD; N=3, n=3; $p < 0.001$ ***), compared to the control. Following treatment with medium containing 30µM BEA, the percentage of cells expressing osteopontin increased significantly (35.14 ± 2.47%; mean ± SD; N=3, n=3; $p < 0.01$ **), compared to the control. To quantify the percentage of cells expressing osteopontin, snapshots of 5 random fields of view from each coverslip were taken, from which a minimum of 500 cells were assessed for biomarker expression. Significant differences were identified using a one-way ANOVA and a post-hoc Tukey test.

Clusterin Immunoreactivity in Mouse Cells following Nephrotoxin Treatment

No expression of the kidney injury biomarker clusterin was detected in primary mouse renal cells following 24-hour treatment with control medium (vehicle control: medium) or medium containing 10µM cisplatin, 10µM cyclosporin A and 30µM BEA (Figure 3.15).

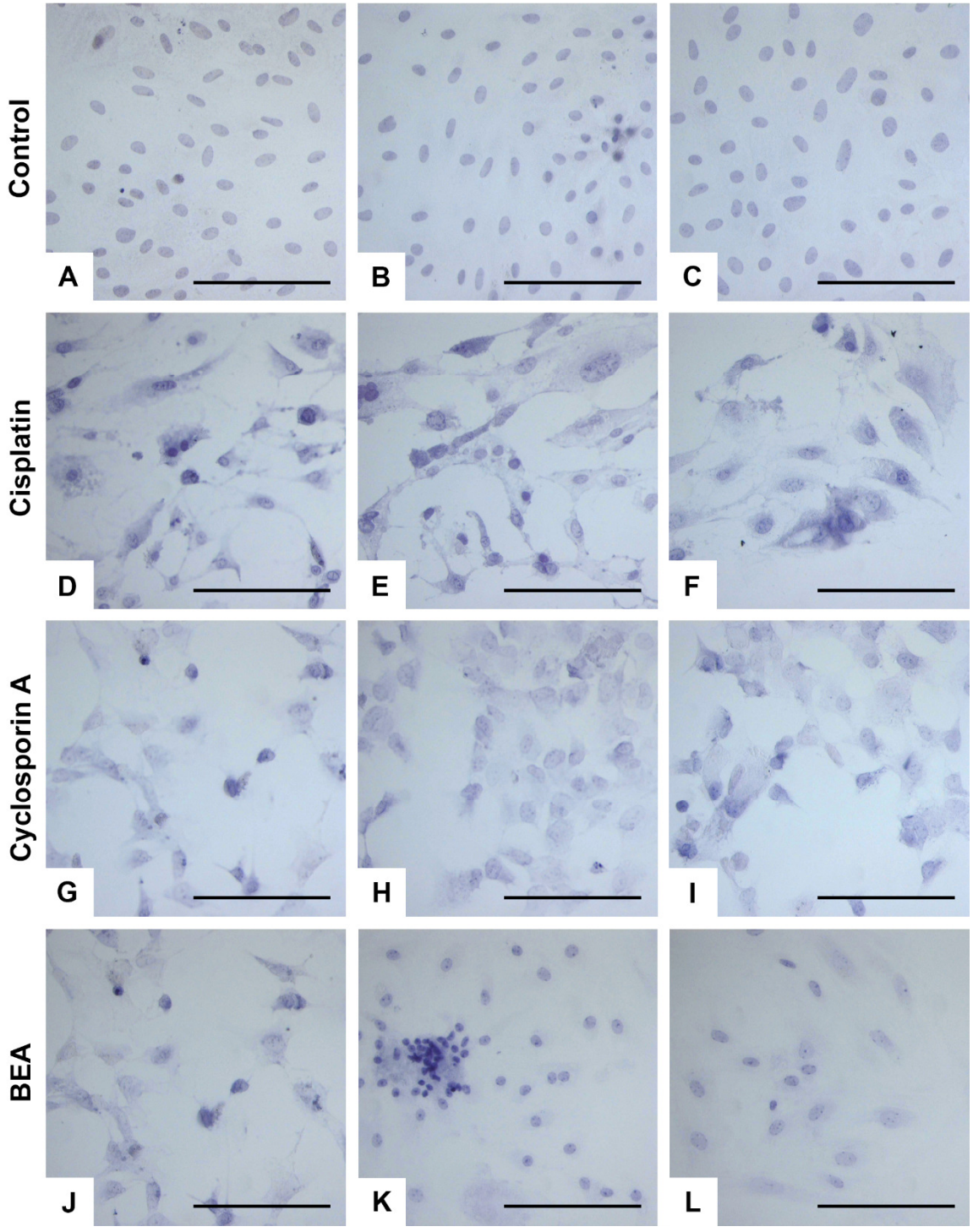

Figure 3.15. Clusterin immunoreactivity in primary mouse renal cells cultured for 24 hours in (A-C) control medium or medium containing (D-F) 10µM cisplatin, (G-I) 10µM cyclosporin A and (J-L) 30µM BEA. (A-C) No clusterin immunoreactivity was detected in cells cultured in control medium (vehicle control; medium) (arrow head). No clusterin immunoreactivity was detected following treatment with medium containing (D-F) 10µM cisplatin, (G-I) 10µM cyclosporin A and (J-L) 30µM BEA. Images presented are representative of 5 fields of view per individual sample. The haematoxylin co-stain identifying nuclei is blue. N=3, n=3 for all groups. Bars = 100µm.

Characterisation of *In Vitro* Primary Human Renal Cells

Previous studies using primary human renal cells as a tool for studying mineral ion homeostasis were performed using cells cultured for 8 days (see chapter 1 of this thesis). Cells at this time point are highly viable as determined using proliferation and apoptosis assays (see chapter 1 of this thesis). As such, characterisation of *in vitro* primary human renal cells as a model for studying drug-induced toxicity in this study, was also performed at this time point. Cells were grown for 7 days in control medium before 24-hour treatment with control medium (vehicle control; medium) or medium containing 25µM cisplatin. The effect of cisplatin-treatment on the expression of the kidney injury biomarkers, KIM-1, osteopontin and clusterin was assessed in cells that had then been in culture for 8 days.

Effect of Cisplatin on Kidney Injury Molecule-1 Expression in Human Cells

De novo expression of the kidney injury biomarker, kidney injury molecule-1 (KIM-1) was identified in primary human renal cells following treatment with the known nephrotoxin, cisplatin (Figure 3.16 and 3.19). No KIM-1 immunoreactivity was identified in cells treated for 24 hours with control medium (vehicle control; medium) (Figure 3.16 A, C, E). 0% of cells expressed KIM-1 (N=1, n=1) (Figure 3.19). However, 24-hour treatment with medium containing 25µM cisplatin, induced KIM-1 immunoreactivity in the cell cytoplasm (Figure 3.16 B, D, F). 98% of cells expressed KIM-1 (N=1, n=1) (Figure 3.19).

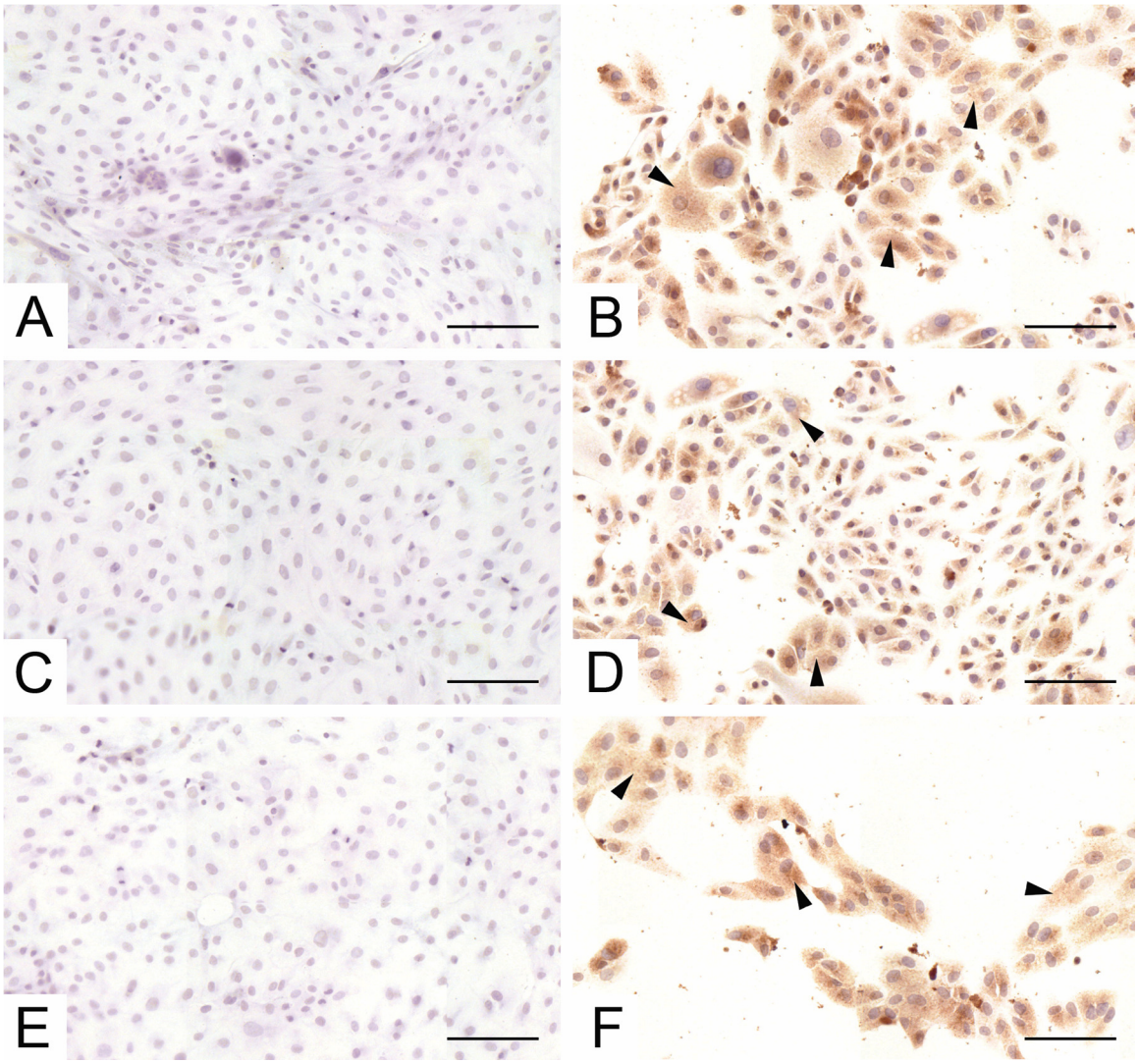

Figure 3.16. KIM-1 immunoreactivity in primary human renal cells cultured for 24 hours in (A, C, E) control medium or (B, D, F) medium containing 25µM cisplatin. No KIM-1 immunoreactivity was detected in cells treated with control medium (vehicle control; medium) (A, C, E). In cells treated with medium containing 25µM cisplatin, KIM-1 immunoreactivity was present in the cell cytoplasm (B, D, E) (arrows heads). KIM-1 immunoreactivity is brown, and the haematoxylin co-stain identifying individual cell nuclei is blue. Images presented are representative of 5 fields of view. A, C, & E are images taken from the same coverslip, and B, D, & F are images taken from the same coverslip; N=1, n=1 for each condition. Bars = 150µm.

Effect of Cisplatin on Osteopontin Expression in Human Cells

De novo expression of the osteopontin was identified in primary human renal cells following treatment with the known nephrotoxin, cisplatin (Figure 3.17 and 3.19). Osteopontin immunoreactivity in cells treated for 24 hours with control medium (vehicle control; medium) (Figure 3.17 A, C, E). 57% of cells expressed osteopontin (N=1, n=1) (Figure 3.19). However, 24-hour treatment with medium containing 25µM cisplatin, increased the number of cells displaying osteopontin immunoreactivity (Figure 3.17 B, D, F). 95% of cells expressed osteopontin (N=1, n=1) (Figure 3.19). Osteopontin was localised to the cell cytoplasm.

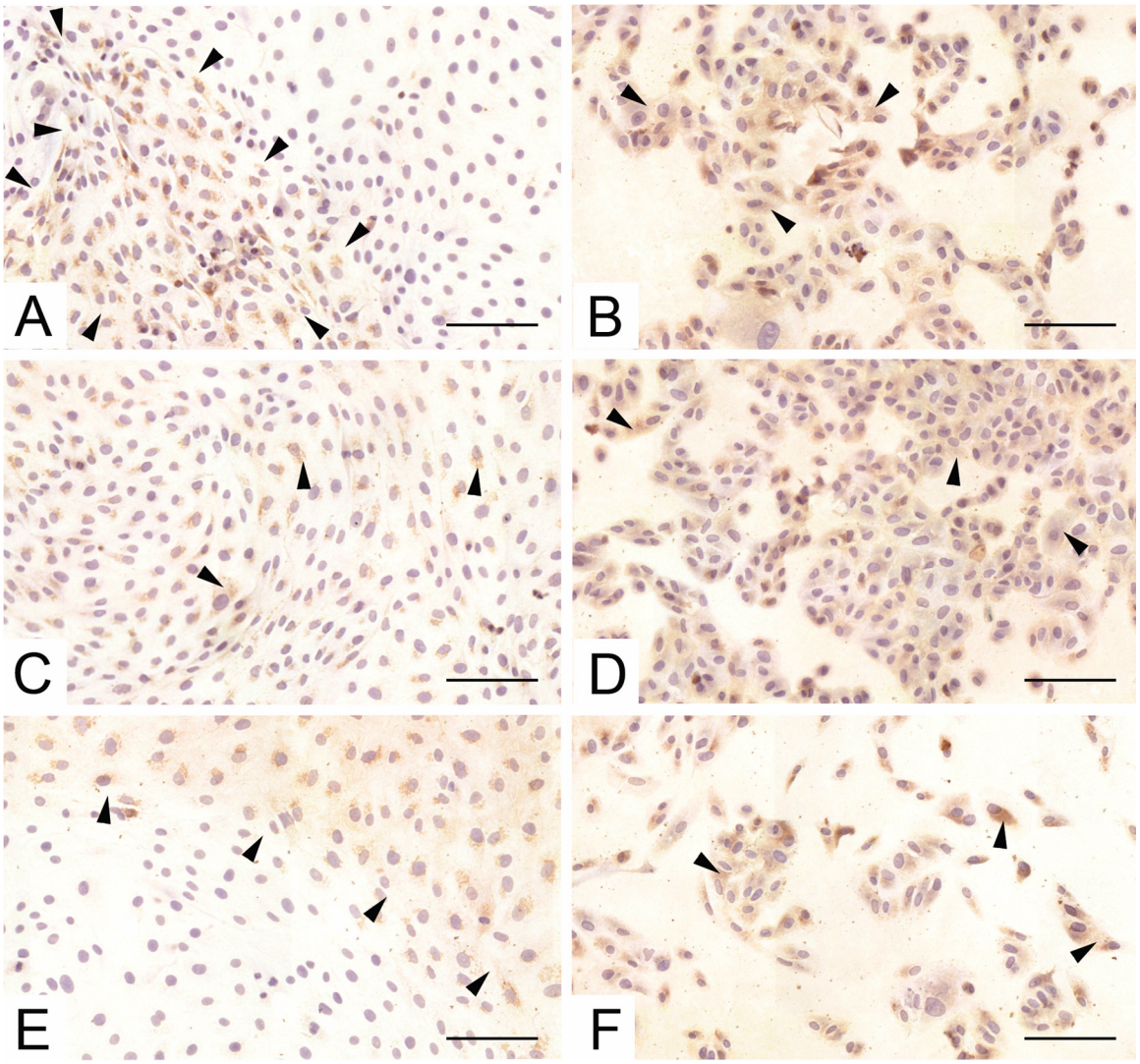

Figure 3.17. Osteopontin immunoreactivity in primary human renal cells cultured for 24 hours in (A, C, E) control medium or (B, D, F) medium containing 25µM cisplatin. Osteopontin immunoreactivity was detected in cells treated with control medium (vehicle control; medium) (A, C, E). In cells treated with medium containing 25µM cisplatin, the number of cells displaying osteopontin immunoreactivity increased. In both groups, osteopontin immunoreactivity was localised to the cell cytoplasm (B, D, E) (arrow heads). Osteopontin immunoreactivity is brown, and the haematoxylin co-stain identifying individual cell nuclei is blue. Images presented are representative of 5 fields of view. A, C, & E are images taken from the same coverslip, and B, D, & F are images taken from the same coverslip; N=1, n=1 for each condition. Bars = 150µm.

Effect of Cisplatin on Clusterin Expression in Human Cells

De novo expression of the kidney injury biomarker clusterin was identified in primary human renal cells following treatment with the known nephrotoxin, cisplatin (Figure 3.18 and 3.19). Clusterin immunoreactivity was detected in 4% (N=1, n=1) of cells treated for 24 hours with control medium (vehicle control; medium) (Figure 3.18 A, C, E, and Figure 3.19). However, 24-hour treatment with medium containing 25µM cisplatin, increased the number of cells displaying clusterin immunoreactivity (Figure 3.18 B, D, F). 41% of cells expressed clusterin (N=1, n=1) (Figure 3.19). Clusterin was localised to the cell cytoplasm with a small number of cells also displaying membrane localisation.

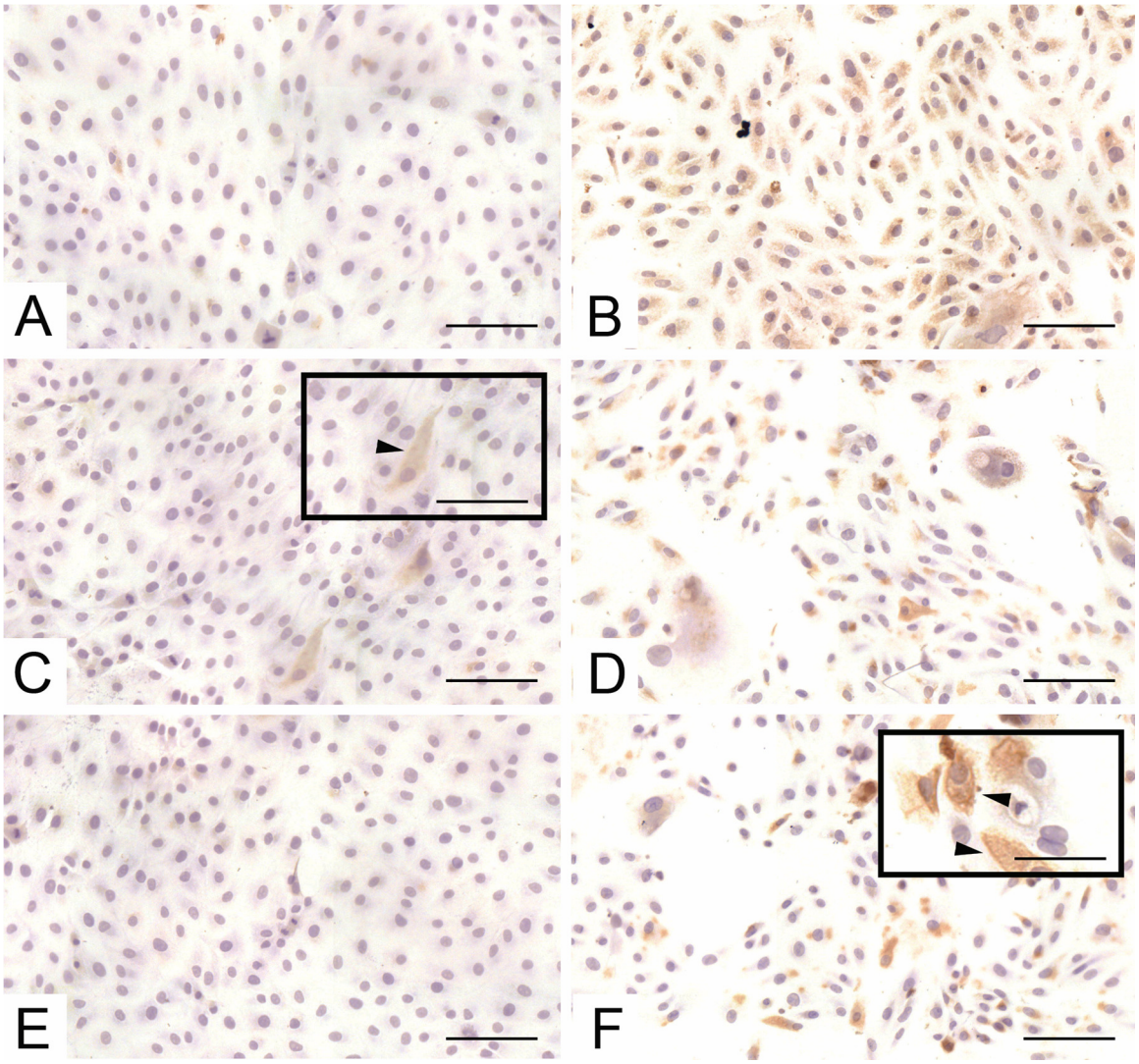

Figure 3.18. Clusterin immunoreactivity in primary human renal cells cultured for 24 hours in (A, C, E) control medium or (B, D, F) medium containing 25µM cisplatin. Clusterin immunoreactivity was detected in a small number of cells treated with control medium (vehicle control; medium) (A, C, E) (C insert image, arrow head). In cells treated with medium containing 25µM cisplatin, the number of cells displaying clusterin immunoreactivity increased. Clusterin was localised to the cell cytoplasm, although additional membrane expression was also seen in some cells (F, inset image, arrow heads). Clusterin immunoreactivity is brown, and the haematoxylin co-stain identifying individual cell nuclei is blue. Images presented are representative of 5 fields of view. A, C, & E are images taken from the same coverslip, and B, D, & F are images taken from the same coverslip; N=1, n=1 for each condition. Bars = 150µm; F inset bar = 50µm.

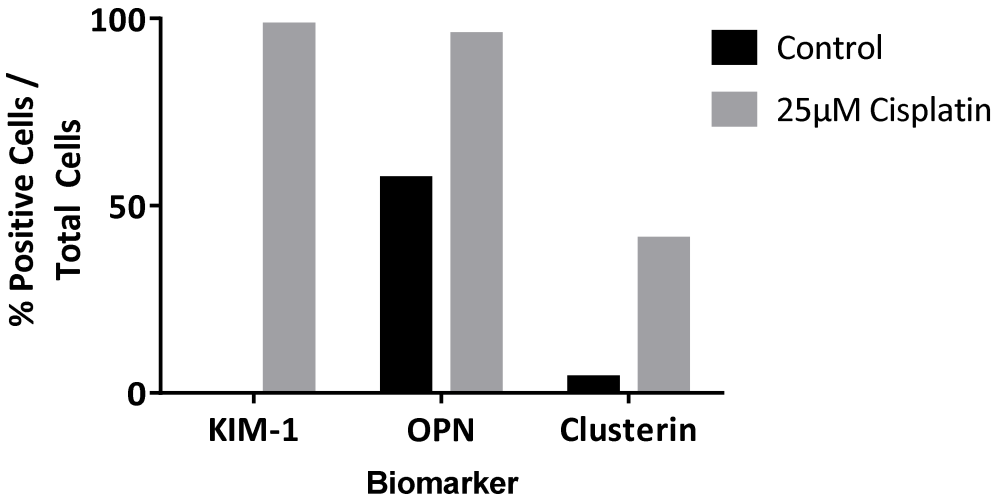

Figure 3.19. Percentage of primary human renal cells expressing KIM-1, osteopontin (OPN) and clusterin following 24-hour treatment with control medium or medium containing 25µM cisplatin. Following treatment with control medium (vehicle control; medium), 0% (N=1, n=1) of cells displayed KIM-1 immunoreactivity. Following treatment with medium containing 25µM cisplatin, the percentage of cells expressing KIM-1 increased to 98% (N=1, n=1). 57% (N=1, n=1) and 95% (N=1, n=1) of cells displayed osteopontin immunoreactivity following treatment with control medium or medium containing 25µM cisplatin, respectively. 4% (N=1, n=1) and 41% (N=1, n=1) of cells displayed osteopontin immunoreactivity following treatment with control medium or medium containing 25µM cisplatin, respectively. To quantify the percentage of cells expressing each of the biomarkers, snapshots of 5 random fields of view from each coverslip were taken, from which a minimum of 500 cells were assessed for biomarker expression.

3.7 Discussion

The kidney is a major organ of drug-induced toxicity (Bonventre et al. 2010), and as such, kidney injury is one of the most frequent adverse events reported during drug development (Jang et al. 2013). However, lack of fully characterised preclinical models for predicting nephrotoxicity specifically in humans means that it is often detected at late stages of drug development (Redfern et al. 2010). *In vitro* models capable of bridging-the-translational-gap between toxicity testing in animals and humans are required. As such, the aim of this study was to perform a characterisation of *ex vivo* kidney slices and *in vitro* primary renal cells as potential models to meet this need. Owing to limited access to human renal tissue/cells available in the present study, both models underwent initial characterisation using rodent tissue; rat tissue was chosen for the *ex vivo* tissue slice cultures, and mouse cells were chosen for the *in vitro* primary cell cultures. Characterisation of such models using both rodent and human tissue/cells to be used in parallel would improve translational drug development.

Ex vivo kidney slices

To begin characterisation of *ex vivo* rat kidney slices as a tool for studying drug-induced nephrotoxicity, a commercially available firefly luciferase ATP assay was used to determine slice viability immediately following slicing (*i.e.* at time 0 hours) and after 1, 4 and 24 hours in culture under control conditions. No significant difference was observed after 1 and 4 hours, but there was a significant difference in ATP content after 24 hours compared to immediately following slicing. As the presence of ATP is indicative of metabolically active cells, the decrease in ATP content over time is suggestive of cell death. This finding indicates that experiments using the slices be performed as soon as possible post preparation *i.e.* be very acute. The assay was also used to determine if the ATP content of slices was affected following exposure to the known nephrotoxic drugs cisplatin (a proximal tubule nephrotoxin), cyclosporin A (a distal tubule nephrotoxin) and BEA (a collecting duct nephrotoxin) over the same time course in culture. Such a readout would be useful for assessing drug-induced cell death. However, no significant differences in any of the drug treatments compared to the time-matched controls were observed, except for that of slices treated with medium containing 10µM cisplatin for 4 hours. The significant decrease in the ATP content of slices treated with medium

containing 10μM cisplatin for 4 hours compared to time-matched control slices suggests that cisplatin was able to induce cell death within this time frame. Cisplatin has been shown to induce cell death within a number of different cancer cell lines (HT-29, HCT-116, HepG2, and MCF-7) within 8 to 11 hours of treatment (Alborzinia et al. 2011), and as such it is possible that in the kidney, cisplatin can begin to induce cell death within a similar timeframe. These data suggest that using the ATP content of slices as a tool for assessing slice viability in response to nephrotoxins may be useful. However, it is also important to note that in this study the ATP content of control slices immediately after slicing (*i.e.* at time 0 hours) was less than half that previously reported under control conditions after 24 hours by another group using a similar model (Vickers et al. 2004). If this is indeed true, there are a number of improvements to the slicing protocol used in this study that could be made to improve the viability of the slices under control conditions. Firstly, the kidneys used in this study came from rats killed by CO_2 inhalation. CO_2 inhalation is thought to reduce the oxygen tension in the kidney leading to ischemia and is carried out over a prolonged period of time, usually about 10 minutes. As such, it would be preferable for future studies to use cervical dislocation in order euthanize rodents immediately such that the kidneys could be removed and placed in cold buffer before cells have the opportunity to become ischemic. This method of killing rats has been performed by others investigating *ex vivo* rat kidney sections (Peppiatt-Wildman et al. 2012). Secondly, instead of using 4°C PBS in which to prepare the slices, oxygenated, V7 preservation solution at 10°C could be used, as this has been used by others for *ex vivo* slice preparation (Vickers et al. 2004). Finally, rather than culturing the slices in a regular culture plate in a regular incubator, it would be wise to invest in a 'rocker' and 'roller' systems so that slices could be cultured in oxygenated medium on semi-permeable membranes and in metal cradles, respectively. In the Vickers et al. paper, they used oxygenated, V7 preservation solution at 10°C to prepare slices and a 'roller' system, and as such, it would be useful to obtain this equipment to enhance the viability of *ex vivo* tissue slices for future work.

In line with the decrease in ATP content over time in the current study, morphological changes indicative of cell death were also apparent by histological assessment. After just one hour in culture, evidence of nuclear condensation, and sloughing of cells into the

tubular lumen was observed. After 24 hours, there was also loss of proximal tubule brush border membranes in all samples assessed. Taken together therefore, the decrease in ATP content and morphological changes indicative of cell death over time indicate that improvements to the slice preparation/culture be made in order for the utility of this model to be fully assessed.

All that said, *ex vivo* kidney slices do still represent an exciting tool for studies of drug-induced toxicity. For preclinical drug safety assessment, for example, the use of *ex vivo* slices has many potential advantages. Firstly, many slices can be prepared from one kidney meaning that many drugs can be trialled simultaneously, or even the same drug can be trialled over a range of different concentrations. The observation of nephrotoxicity at a certain concentration, but not at a lower concentration, could guide drug dosing regimens in subsequent *in vivo* rodent studies. In essence, much more data could be generated that doing several *in vivo* studies, and as such, this would conform with the National Centre for the Replacement, Refinement and Reduction (NC3R) of animals in research guidelines. Additionally, the slices are thin enough such that mechanisms of toxicity (involving for example changes at the subcellular organelle level) could be studied using live cell imaging by confocal or 2-photon microscopy.

In vitro primary renal cells

Traditionally, rat is a species relevant to toxicology testing, and as such, *in vitro* cultures of primary rat renal cells have already undergone initial characterisation as a tool for studying drug-transporter and drug-drug interactions (Chung et al. 2013). Mouse is not a species traditionally associated with toxicology testing, and as such, *in vitro* cultures of primary mouse renal cells have not been characterised to the same extent. The decision in the present study to use mouse cells over rat cells was based on the fact that their characterisation could also be useful for elucidating molecular mechanisms of drug toxicity using cells obtained from mice that have undergone targeted gene deletion in future studies. That said, it would be useful for the same experiments carried out in the present study using mouse cells to be performed using rat cells, thereby building on the characterisation of the rat model developed by Chung et al. 2013.

Proliferation and apoptosis assays showed high cell viability as evidenced by high proliferation and low apoptosis of *in vitro* primary mouse renal cells for up to day 15 in

culture. *In vivo*, high renal cell proliferation occurs as a result of cell dedifferentiation and regeneration following ischemic or toxic insults (Bonventre 2003). However, it is unlikely that the high proliferation observed in this model was result of cell dedifferentiation induced by injury following removal from their natural environment. The reason for this, is that only a small number of mouse renal cells cultured for 8 days in control medium expressed (as determined by immunocytochemistry) KIM-1, a kidney biomarker massively upregulated in proliferating, dedifferentiated cells following injury (Ichimura et al. 1998; Ichimura et al. 2004). Instead, high proliferation rates are likely due to the addition of growth supplements to the culture medium. Indeed, previous studies support the fact that primary renal cell cultures do not undergo dedifferentiation. Brown et al. (2008), show that human primary renal cells maintain expression of both phenotypic proteins and morphological characteristics, whilst experiments performed in the host laboratory identified no increase in vimentin, a marker of cell dedifferentiation, over time in culture (see chapter 1 of this thesis). Strengthening the case for the use of primary renal cells over established cell lines such as HK2 as a tool for studying drug-induced toxicity, is the fact that extensive KIM-1 expression has been reported to be expressed in such cells (Han et al. 2002), suggesting they are already in a dedifferentiated state.

Concentration-dependent drug-induced apoptosis in primary mouse renal cells was quantified using a TUNEL assay. Compared to control cells, cells treated with medium containing increasing concentrations of cisplatin, cyclosporin A and BEA displayed an concentration-dependent apoptotic cell death. Future studies could also focus on quantifying drug-induced death using a lactate dehydrogenase assay (useful for when cell death is either apoptotic or necrotic) or caspase activation (useful when cell death is apoptotic).

In vivo, drug-induced nephrotoxicity is often associated with renal epithelial cell detachment from the basement membrane, and the sloughing of cells into the tubule lumen. This phenomenon gives rise to acute kidney injury. Cell sloughing well-documented *in vivo* phenomenon of treatment with the known nephrotoxin, cisplatin (Aleksunes et al. 2008; Huang et al. 2001; Wadey et al. 2013). As such, *in vitro* experiments using loss of cell adhesion/cell detachment from the tissue culture substrate (rather than the basement membrane) have previously been used as a drug-induced

effect by other groups (Del Bello et al. 2001; Imamdi et al. 2004; Kruidering et al. 1998; Mueller et al. 2003; P. Price et al. 2006; Slattery et al. 2005). Quantification of this drug-induced effect has previously been determined by counting the number of the floating versus attached cells (Kruidering et al. 1998). In the current study, primary mouse renal cells were treated with medium containing increasing concentrations of the nephrotoxins cisplatin, cyclosporin A and BEA, before the number of detached cells floating in the medium relative to the total number of control cells (floating plus attached), was quantified. All three nephrotoxins induced a concentration-dependent increase in cell detachment (*i.e.* loss of cell adhesion) from the tissue culture plate. Interestingly, *in vitro* studies using LLC-PK1 cells has shown that cisplatin disrupts cell-cell adhesion (giving rise to detached cells floating in the medium) in a PKC-dependent manner as evidenced by inhibition of the loss of cell adhesion in the presence of a PKC inhibitor (Imamdi et al. 2004).

The next assay was to assess the ability of the cells in the model to respond to nephrotoxin treatment with upregulation of the known biomarkers of drug-induced renal injury, KIM-1, osteopontin and clusterin. KIM-1 and osteopontin upregulation are well-documented responses to cisplatin treatment *in vivo* (Ichimura et al. 2004; Nan-Ya et al. 2014; Pinches et al. 2012b; Vinken et al. 2012; Wadey et al. 2013), and likewise, both are upregulated in the kidney following cyclosporin A treatment *in vivo* (Pichler et al. 1995; Pérez-Rojas et al. 2007). Confirming the utility of the cell model in the current study as a tool for studying drug-induced renal injury was the identification of the upregulation of KIM-1 and osteopontin following 24-hour treatment with medium containing cisplatin, cyclosporin A and BEA. While BEA is traditionally thought of as a collecting duct toxin, there are reports that it effects regions of the kidney other than the papilla in the literature (Delacruz et al. 1997), and hence why it can induce expression of KIM-1 and osteopontin in a cell culture consisting of proximal and distal tubule cells. The number of cells expressing clusterin did not increase following 24-hour treatment with medium containing any of the nephrotoxins. However, clusterin expression has been detected in cells treated for 24 hours with medium containing cisplatin and then cultured for a further 24 hours in control medium (Dr Valentina Peta, Cardiff University, unpublished observations). This is very interesting as in other models of renal injury, clusterin

expression has been shown to be upregulated during regeneration (Gobé et al. 1995) where it is thought to play a role in preventing apoptosis and enhancing cell attachment (Silkensen et al. 1997).

Future studies aim to investigate and quantify the presence of the biomarkers in the culture medium. If biomarker presence in the culture medium were to correlate with biomarker expression in cells, it would provide additional information as to whether a novel injury biomarker may have potential utility as a non-invasive kidney injury urinary biomarker *in vivo*. Such studies could be performed by Western blotting or ELIZA.

To validate my findings in mouse renal cells, a similar experiment carried out in primary, human, renal cells revealed an increase the number of cells expressing the kidney injury biomarkers KIM-1, osteopontin and clusterin following 24-hour treatment with medium containing cisplatin compared to time-matched control cells. Together, data from both mouse and human models indicate that *in vitro* primary renal cell cultures offer potential utility as a tool for studying drug-induced nephrotoxicity. Future studies to confirm these initial findings are ongoing. In addition, future studies aim to determine which cells are expressing injury biomarkers using co-stain protocol with a cell-type specific markers (for example, E- and N-Cadherin as markers of distal or proximal tubule cells respectively (Prozialeck et al. 2004)). This information would be useful in determining whether a drug is toxic to proximal or distal tubule cells, or both.

A major advantage of using *in vitro* primary renal cells as a tool for studying drug-induced nephrotoxicity during preclinical drug-safety assessment, is that several drugs, or indeed several concentrations of the same drug, could be screened for nephrotoxicity simultaneously. In this way, characterisation and validation of such models would conform to the National Centre for the Replacement, Refinement and Reduction of animals in research guidelines. In addition, the use of rodent and human models in parallel would improve translational drug safety assessment thereby reducing the rate of drug attrition during Phase III clinical trials and saving time, energy, investment, and risk to public health.

In summary, *ex vivo* tissue slices and *in vitro* primary cultures of renal cells represent two potential tools for screening novel drugs for their likelihood to induce nephrotoxicity

using biomarker expression as a readout. Under the conditions used in the current study, *in vitro* primary cells showed the most promising utility. Primary mouse renal cells displayed high viability and responded to 24-hour treatment with the known nephrotoxins cisplatin, cyclosporin and BEA with concentration-dependent increase in apoptosis and concentration-dependent loss of cell adhesion from the tissue culture plate. In addition, cells responded to 24-hour treatment with medium containing cisplatin, cyclosporin A and BEA with upregulation of the kidney injury biomarkers KIM-1 and osteopontin, but not that of clusterin. Primary human renal cells responded to 24-hour treatment with medium containing cisplatin with upregulation of KIM-1, osteopontin and clusterin. The difference in the expression of clusterin in response to nephrotoxin-treatment in human and mouse models not only highlights species differences, but reinforces the idea that use human models would not only improve studies of drug-induced toxicity specifically in humans, but when used alongside rodent models, would revolutionise preclinical, translational drug safety assessment.

Reference List

Alborzinia, H., et al. (2011), 'Real-time monitoring of cisplatin-induced cell death', *PLoS One,* 6 (5), e19714.

Aleksunes, L. M., et al. (2008), 'Renal xenobiotic transporters are differentially expressed in mice following cisplatin treatment', *Toxicology,* 250 (2-3), 82-8.

Almaden, Y., et al. (1996), 'Direct effect of phosphorus on PTH secretion from whole rat parathyroid glands in vitro', *J Bone Miner Res,* 11 (7), 970-6.

Andrukhova, O., et al. (2012), 'FGF23 acts directly on renal proximal tubules to induce phosphaturia through activation of the ERK1/2-SGK1 signaling pathway', *Bone,* 51 (3), 621-8.

Andrukhova, O., et al. (2014), 'FGF23 promotes renal calcium reabsorption through the TRPV5 channel', *EMBO J,* 33 (3), 229-46.

Aono, Y., et al. (2009), 'Therapeutic effects of anti-FGF23 antibodies in hypophosphatemic rickets/osteomalacia', *J Bone Miner Res,* 24 (11), 1879-88.

Arantes-Rodrigues, R., et al. (2013), 'Synergistic effect between cisplatin and sunitinib malate on human urinary bladder-cancer cell lines', *Biomed Res Int,* 2013, 791406.

Asplin, J. R., et al. (1998), 'Contribution of human uropontin to inhibition of calcium oxalate crystallization', *Kidney Int,* 53 (1), 194-9.

Astashkina, A., Mann, B., and Grainger, D. W. (2012), 'A critical evaluation of in vitro cell culture models for high-throughput drug screening and toxicity', *Pharmacol Ther,* 134 (1), 82-106.

Astor, B. C., et al. (2011), 'Trefoil factor 3 predicts incident chronic kidney disease: a case-control study nested within the Atherosclerosis Risk in Communities (ARIC) study', *Am J Nephrol,* 34 (4), 291-7.

Atta, M. G. and Whelton, A. (1997), 'Acute renal papillary necrosis induced by ibuprofen', *Am J Ther,* 4 (1), 55-60.

Bach, P. H., et al. (1983), 'Changes in medullary glycosaminoglycan histochemistry and microvascular filling during the development of 2-bromoethanamine hydrobromide-induced renal papillary necrosis', *Toxicol Appl Pharmacol,* 69 (3), 333-44.

Bailly, V., et al. (2002), 'Shedding of kidney injury molecule-1, a putative adhesion protein involved in renal regeneration', *J Biol Chem,* 277 (42), 39739-48.

Bandele, O., et al. (2013), 'Performance of urinary and gene expression biomarkers in detecting the nephrotoxic effects of melamine and cyanuric acid following diverse scenarios of co-exposure', *Food Chem Toxicol,* 51, 106-13.

Bauchet, A. L., et al. (2011), 'Immunohistochemical identification of kidney nephron segments in the dog, rat, mouse, and cynomolgus monkey', *Toxicol Pathol,* 39 (7), 1115-28.

Baum, M., et al. (2005), 'Effect of fibroblast growth factor-23 on phosphate transport in proximal tubules', *Kidney Int,* 68 (3), 1148-53.

Baxmann, A. C., et al. (2008), 'Influence of muscle mass and physical activity on serum and urinary creatinine and serum cystatin C', *Clin J Am Soc Nephrol,* 3 (2), 348-54.

Beenken, A. and Mohammadi, M. (2009), 'The FGF family: biology, pathophysiology and therapy', *Nat Rev Drug Discov,* 8 (3), 235-53.

Bellomo, R., Kellum, J., and Ronco, C. (2001), 'Acute renal failure: time for consensus', *Intensive Care Med,* 27 (11), 1685-8.

Bellomo, R., Kellum, J. A., and Ronco, C. (2012), 'Acute kidney injury', *Lancet,* 380 (9843), 756-66.

Bellomo, R., et al. (2004), 'Acute renal failure - definition, outcome measures, animal models, fluid therapy and information technology needs: the Second International Consensus Conference of the Acute Dialysis Quality Initiative (ADQI) Group', *Crit Care,* 8 (4), R204-12.

Ben-Dov, I. Z., et al. (2007), 'The parathyroid is a target organ for FGF23 in rats', *J Clin Invest,* 117 (12), 4003-8.

Benet-Pagès, A., et al. (2005), 'An FGF23 missense mutation causes familial tumoral calcinosis with hyperphosphatemia', *Hum Mol Genet,* 14 (3), 385-90.

Bergwitz, C. and Jüppner, H. (2010), 'Regulation of phosphate homeostasis by PTH, vitamin D, and FGF23', *Annu Rev Med,* 61, 91-104.

Bergwitz, C. and Jüppner, H. (2011), 'Phosphate sensing', *Adv Chronic Kidney Dis,* 18 (2), 132-44.

Bergwitz, C., et al. (2006), 'SLC34A3 mutations in patients with hereditary hypophosphatemic rickets with hypercalciuria predict a key role for the sodium-phosphate cotransporter NaPi-IIc in maintaining phosphate homeostasis', *Am J Hum Genet,* 78 (2), 179-92.

Betton, G. R., et al. (2012), 'Biomarkers of collecting duct injury in Han-Wistar and Sprague-Dawley rats treated with N-phenylanthranilic Acid', *Toxicol Pathol,* 40 (4), 682-94.

Biber, J., Brown, C. D., and Murer, H. (1983), 'Sodium-dependent transport of phosphate in LLC-PK1 cells', *Biochim Biophys Acta,* 735 (3), 325-30.

Biber, J., et al. (1996), 'Renal Na/Pi-cotransporters', *Kidney Int,* 49 (4), 981-5.

Blanchard, Elizabeth M (2012), 'Cisplatin and solid tumors: Still working, after all these years. ', (2; Journal of Solid Tumors), 26-33.

Bonewald, L. F. and Wacker, M. J. (2013), 'FGF23 production by osteocytes', *Pediatr Nephrol,* 28 (4), 563-8.

Bonventre, J. V. (2003), 'Dedifferentiation and proliferation of surviving epithelial cells in acute renal failure', *J Am Soc Nephrol,* 14 Suppl 1, S55-61.

Bonventre, J. V. and Yang, L. (2010), 'Kidney injury molecule-1', *Curr Opin Crit Care,* 16 (6), 556-61.

Bonventre, J. V., et al. (2010), 'Next-generation biomarkers for detecting kidney toxicity', *Nat Biotechnol,* 28 (5), 436-40.

Bourke, S., et al. (2005), 'Development of a lung slice preparation for recording ion channel activity in alveolar epithelial type I cells', *Respir Res,* 6, 40.

Branten, A. J., et al. (2000), 'Urinary excretion of glutathione S transferases alpha and pi in patients with proteinuria: reflection of the site of tubular injury', *Nephron,* 85 (2), 120-6.

Brix, A. E. (2002), 'Renal papillary necrosis', *Toxicol Pathol,* 30 (6), 672-4.

Brooks, A., Kilgour, E., and Smith, P. (2012), 'Molecular pathways: fibroblast growth factor signalling: a new therapeutic opportunity in caner', *Clin Cancer Res,* 18, 1855-62.

Brooks, C., et al. (2009), 'Regulation of mitochondrial dynamics in acute kidney injury in cell culture and rodent models', *J Clin Invest,* 119 (5), 1275-85.

Brown, C., et al. (2008), 'Characterisation of human tubular cell monolayers as a model of proximal tubular xenobiotic handling', *Toxicol Appl Pharmacol,* 233 (3), 428-38.

Brown, L., et al. (1992), 'Expression and distribution of osteopontin in human tissues: widespread association with luminal epithelial surfaces', *Mol Biol Cell,* 3 (10), 1169-80.

Busauschina, A., Schnuelle, P., and van der Woude, F. J. (2004), 'Cyclosporine nephrotoxicity', *Transplant Proc,* 36 (2 Suppl), 229S-33S.

Cancilla, B., et al. (2001), 'Fibroblast growth factor receptors and their ligands in the adult rat kidney', *Kidney Int,* 60 (1), 147-55.

Caverzasio, J., et al. (1984), 'Sodium-dependent inorganic phosphate (Pi) transport and adaptation to low Pi concentration medium in LLC-PK1 cells', *Prog Clin Biol Res,* 168, 315-8.

Charney, D. A., Singh, A., and Aron, N. (2005), 'A male nephrotic patient with rapid decline of renal function', *Nephrol Dial Transplant,* 20 (6), 1263-6.

Chertow, G. M., et al. (2005), 'Acute kidney injury, mortality, length of stay, and costs in hospitalized patients', *J Am Soc Nephrol,* 16 (11), 3365-70.

Chinery, R., et al. (1993), 'Expression and purification of a trefoil peptide motif in a beta-galactosidase fusion protein and its use to search for trefoil-binding sites', *Eur J Biochem,* 212 (2), 557-63.

Chiusolo, A., et al. (2010), 'Kidney injury molecule-1 expression in rat proximal tubule after treatment with segment-specific nephrotoxicants: a tool for early screening of potential kidney toxicity', *Toxicol Pathol,* 38 (3), 338-45.

Chong, W. H., et al. (2011), 'Tumor-induced osteomalacia', *Endocr Relat Cancer,* 18 (3), R53-77.

Chung, G., et al. (2013), 'Development and characterisation of rat primary proximal tubule cells', (Proceedings of The Physiological Society, 37th Congress of IUPS).

Ciarimboli, G., et al. (2005), 'Cisplatin nephrotoxicity is critically mediated via the human organic cation transporter 2', *Am J Pathol,* 167 (6), 1477-84.

Ciarimboli, G., et al. (2012), 'Proximal tubular secretion of creatinine by organic cation transporter OCT2 in cancer patients', *Clin Cancer Res,* 18 (4), 1101-8.

Cilenti, L., et al. (2005), 'Omi/HtrA2 protease mediates cisplatin-induced cell death in renal cells', *Am J Physiol Renal Physiol,* 288 (2), F371-9.

Clarke, B. L. (2011), 'FGF23 regulation of phosphorus homeostasis is dependent on PTH', *Endocrinology,* 152 (11), 4016-8.

Cook, N. R. (2010), 'Methods for evaluating novel biomarkers - a new paradigm', *Int J Clin Pract,* 64 (13), 1723-7.

Crawford, C., et al. (2012), 'An intact kidney slice model to investigate vasa recta properties and function in situ', *Nephron Physiol,* 120 (3), p17-31.

Daniele, G., et al. (2012), 'FGF receptor inhibitors: role in cancer therapy', *Curr Oncol Rep,* 14 (2), 111-9.

Davey, P. G. and Gosling, P. (1982), 'beta 2-Microglobulin instability in pathological urine', *Clin Chem,* 28 (6), 1330-3.

de Borst, M. H., et al. (2007), 'Induction of kidney injury molecule-1 in homozygous Ren2 rats is attenuated by blockade of the renin-angiotensin system or p38 MAP kinase', *Am J Physiol Renal Physiol,* 292 (1), F313-20.

de Geus, H. R., Betjes, M. G., and Bakker, J. (2012), 'Biomarkers for the prediction of acute kidney injury: a narrative review on current status and future challenges', *Clin Kidney J,* 5 (2), 102-08.

de Graaf, I. A., et al. (2010), 'Preparation and incubation of precision-cut liver and intestinal slices for application in drug metabolism and toxicity studies', *Nat Protoc,* 5 (9), 1540-51.

De Loor, J., et al. (2013), 'Urinary biomarkers for acute kidney injury in dogs', *J Vet Intern Med,* 27 (5), 998-1010.

Del Bello, B., et al. (2001), 'Cleavage of Bcl-2 in oxidant- and cisplatin-induced apoptosis of human melanoma cells', *Oncogene,* 20 (33), 4591-5.

Delacruz, L., et al. (1997), 'Urinary markers of nephrotoxicity following administration of 2 bromoethanamine hydrobromide a comparison with hexachlorobutadiene', *Biomarkers,* 2 (3), 169-74.

DeLong, E. R., DeLong, D. M., and Clarke-Pearson, D. L. (1988), 'Comparing the areas under two or more correlated receiver operating characteristic curves: a nonparametric approach', *Biometrics,* 44 (3), 837-45.

Demay, M. B., et al. (1992), 'Sequences in the human parathyroid hormone gene that bind the 1,25-dihydroxyvitamin D3 receptor and mediate transcriptional repression in response to 1,25-dihydroxyvitamin D3', *Proc Natl Acad Sci U S A,* 89 (17), 8097-101.

Denhardt, D. T. and Guo, X. (1993), 'Osteopontin: a protein with diverse functions', *FASEB J,* 7 (15), 1475-82.

Desjardins, L., et al. (2012), 'FGF23 is independently associated with vascular calcification but not bone mineral density in patients at various CKD stages', *Osteoporos Int,* 23 (7), 2017-25.

DesRochers, T. M., et al. (2013), 'Bioengineered 3D human kidney tissue, a platform for the determination of nephrotoxicity', *PLoS One,* 8 (3), e59219.

Diaz, D., et al. (2012), 'Phosphorous dysregulation induced by MEK small molecule inhibitors in the rat involves blockade of FGF-23 signaling in the kidney', *Toxicol Sci,* 125 (1), 187-95.

Dieci, M. V., et al. (2013), 'Fibroblast growth factor receptor inhibitors as a cancer treatment: from a biologic rationale to medical perspectives', *Cancer Discov,* 3 (3), 264-79.

Dienstmann, R., et al. (2014), 'Genomic aberrations in the FGFR pathway: opportunities for targeted therapies in solid tumors', *Ann Oncol,* 25 (3), 552-63.

Dieterle, F., et al. (2010a), 'Urinary clusterin, cystatin C, beta2-microglobulin and total protein as markers to detect drug-induced kidney injury', *Nat Biotechnol,* 28 (5), 463-9.

Dieterle, F., et al. (2010b), 'Renal biomarker qualification submission: a dialog between the FDA-EMEA and Predictive Safety Testing Consortium', *Nat Biotechnol,* 28 (5), 455-62.

Eddy, A. A. and Giachelli, C. M. (1995), 'Renal expression of genes that promote interstitial inflammation and fibrosis in rats with protein-overload proteinuria', *Kidney Int,* 47 (6), 1546-57.

Edelstein, C. L. (2008), 'Biomarkers of acute kidney injury', *Adv Chronic Kidney Dis,* 15 (3), 222-34.

EMA (2010), 'Consultation on the Qualification Opinion ILSI/HESI Submission of Novel Renal Biomarkers for Toxicity'.

Endre, Z. H. and Pickering, J. W. (2013), 'Biomarkers and creatinine in AKI: the trough of disillusionment or the slope of enlightenment?', *Kidney Int,* 84 (4), 644-7.

Estepa, J. C., et al. (1999), 'Effect of phosphate on parathyroid hormone secretion in vivo', *J Bone Miner Res,* 14 (11), 1848-54.

Eswarakumar, V. P., Lax, I., and Schlessinger, J. (2005), 'Cellular signaling by fibroblast growth factor receptors', *Cytokine Growth Factor Rev,* 16 (2), 139-49.

Farrow, E. G., et al. (2009), 'Initial FGF23-mediated signaling occurs in the distal convoluted tubule', *J Am Soc Nephrol,* 20 (5), 955-60.

Farrow, E. G., et al. (2010), 'Altered renal FGF23-mediated activity involving MAPK and Wnt: effects of the Hyp mutation', *J Endocrinol,* 207 (1), 67-75.

Faubel, S., et al. (2007), 'Cisplatin-induced acute renal failure is associated with an increase in the cytokines interleukin (IL)-1beta, IL-18, IL-6, and neutrophil infiltration in the kidney', *J Pharmacol Exp Ther,* 322 (1), 8-15.

Faul, C., et al. (2011), 'FGF23 induces left ventricular hypertrophy', *J Clin Invest,* 121 (11), 4393-408.

Ferguson, M. A., Vaidya, V. S., and Bonventre, J. V. (2008), 'Biomarkers of nephrotoxic acute kidney injury', *Toxicology,* 245 (3), 182-93.

Fliser, D., et al. (2007), 'Fibroblast growth factor 23 (FGF23) predicts progression of chronic kidney disease: the Mild to Moderate Kidney Disease (MMKD) Study', *J Am Soc Nephrol,* 18 (9), 2600-8.

Floege, J., et al. (1999), 'Localization of fibroblast growth factor-2 (basic FGF) and FGF receptor-1 in adult human kidney', *Kidney Int,* 56 (3), 883-97.

Fuhrmann, V., et al. (1999), 'Fibroblast growth factor receptor 4 (FGFR4) is expressed in adult rat and human retinal photoreceptors and neurons', *J Mol Neurosci,* 13 (1-2), 187-97.

Fukumoto, S (2012), 'FGF23 and tumor-induced osteomalacia', (29; Endocrine Abstracts).

Gammelager, H., et al. (2013), 'Five-year risk of end-stage renal disease among intensive care patients surviving dialysis-requiring acute kidney injury: a nationwide cohort study', *Crit Care,* 17 (4), R145.

Gaspari, F., et al. (2010), 'Predicting cisplatin-induced acute kidney injury by urinary neutrophil gelatinase-associated lipocalin excretion: a pilot prospective case-control study', *Nephron Clin Pract,* 115 (2), c154-60.

Gattineni, J., et al. (2009), 'FGF23 decreases renal NaPi-2a and NaPi-2c expression and induces hypophosphatemia in vivo predominantly via FGF receptor 1', *Am J Physiol Renal Physiol,* 297 (2), F282-91.

Gavine, P. R., et al. (2012), 'AZD4547: an orally bioavailable, potent, and selective inhibitor of the fibroblast growth factor receptor tyrosine kinase family', *Cancer Res,* 72 (8), 2045-56.

Gibson-D'Ambrosio, R. E., et al. (1987), 'Characteristics of long-term human epithelial cell cultures derived from normal human fetal kidney', *In Vitro Cell Dev Biol,* 23 (4), 279-87.

Glendenning, P., et al. (2000), 'Calcitriol upregulates expression and activity of the 1b isoform of the plasma membrane calcium pump in immortalized distal kidney tubular cells', *Arch Biochem Biophys,* 380 (1), 126-32.

Glube, N., et al. (2007), 'Caki-1 cells represent an in vitro model system for studying the human proximal tubule epithelium', *Nephron Exp Nephrol,* 107 (2), e47-56.

Gobé, G. C., et al. (1995), 'Clusterin expression and apoptosis in tissue remodeling associated with renal regeneration', *Kidney Int,* 47 (2), 411-20.

Goetz, R., et al. (2010), 'Isolated C-terminal tail of FGF23 alleviates hypophosphatemia by inhibiting FGF23-FGFR-Klotho complex formation', *Proc Natl Acad Sci U S A,* 107 (1), 407-12.

Group., Biomarkers Definitions Working (2001), 'Biomarkers and surrogate endpoints: preferred definitions and conceptual framework', *Clin Pharmacol Ther,* 69 (3), 89-95.

Guagnano, V., et al. (2011), 'Discovery of 3-(2,6-dichloro-3,5-dimethoxy-phenyl)-1-{6-[4-(4-ethyl-piperazin-1-yl)-phenylamino]-pyrimidin-4-yl}-1-methyl-urea (NVP-BGJ398), a potent and selective inhibitor of the fibroblast growth factor receptor family of receptor tyrosine kinase', *J Med Chem,* 54 (20), 7066-83.

Gutierrez, O., et al. (2005), 'Fibroblast growth factor-23 mitigates hyperphosphatemia but accentuates calcitriol deficiency in chronic kidney disease', *J Am Soc Nephrol,* 16 (7), 2205-15.

Hall, A. M., et al. (2008), 'Renal function and mitochondrial cytopathy (MC): more questions than answers?', *QJM,* 101 (10), 755-66.

Hallman, M. A., Zhuang, S., and Schnellmann, R. G. (2008), 'Regulation of dedifferentiation and redifferentiation in renal proximal tubular cells by the epidermal growth factor receptor', *J Pharmacol Exp Ther,* 325 (2), 520-8.

Han, W. K., et al. (2002), 'Kidney Injury Molecule-1 (KIM-1): a novel biomarker for human renal proximal tubule injury', *Kidney Int,* 62 (1), 237-44.

Harder, H. C. and Rosenberg, B. (1970), 'Inhibitory effects of anti-tumor platinum compounds on DNA, RNA and protein syntheses in mammalian cells in virtro', *Int J Cancer,* 6 (2), 207-16.

Harder, H. C., Smith, R. G., and Leroy, A. F. (1976), 'Template primer inactivation by cis- and trans-dichlorodiammine platinum for human DNA polymerase alpha, beta, and Rauscher murine leukemia virus reverse transcriptase, as a mechanism of cytotoxicity', *Cancer Res,* 36 (10), 3821-9.

Harris, K. and Stribling, B. (2007), 'Automated estimated GFR reporting: A new tool to promote safer prescribing in patients with chronic kidney disease?', *Ther Clin Risk Manag,* 3 (5), 969-72.

Hayes, J. D. and Pulford, D. J. (1995), 'The glutathione S-transferase supergene family: regulation of GST and the contribution of the isoenzymes to cancer chemoprotection and drug resistance', *Crit Rev Biochem Mol Biol,* 30 (6), 445-600.

Hayes, J. D., Flanagan, J. U., and Jowsey, I. R. (2005), 'Glutathione transferases', *Annu Rev Pharmacol Toxicol,* 45, 51-88.

Healy, E., et al. (1998), 'Apoptosis and necrosis: mechanisms of cell death induced by cyclosporine A in a renal proximal tubular cell line', *Kidney Int,* 54 (6), 1955-66.

Hedgepeth, R. C., et al. (2001), 'Expression of proteins that inhibit calcium oxalate crystallization in vitro in the urine of normal and stone-forming individuals', *Am J Kidney Dis,* 37 (1), 104-12.

Hildebrand, H., et al. (1999), 'Urinary antigens as markers of papillary toxicity. II: Application of monoclonal antibodies for the determination of papillary antigens in rat urine', *Arch Toxicol,* 73 (4-5), 233-45.

Hoenderop, J. G., et al. (1999), 'Molecular identification of the apical Ca2+ channel in 1, 25-dihydroxyvitamin D3-responsive epithelia', *J Biol Chem,* 274 (13), 8375-8.

Hoffmann, D., et al. (2010), 'Evaluation of a urinary kidney biomarker panel in rat models of acute and subchronic nephrotoxicity', *Toxicology,* 277 (1-3), 49-58.

Horlick, R. A., Stack, S. L., and Cooke, G. M. (1992), 'Cloning, expression and tissue distribution of the gene encoding rat fibroblast growth factor receptor subtype 4', *Gene,* 120 (2), 291-5.

Hoste, E. A., et al. (2006), 'RIFLE criteria for acute kidney injury are associated with hospital mortality in critically ill patients: a cohort analysis', *Crit Care,* 10 (3), R73.

Hu, M. C., Kuro-o, M., and Moe, O. W. (2012), 'Secreted klotho and chronic kidney disease', *Adv Exp Med Biol,* 728, 126-57.

Hu, M. C., et al. (2011), 'Klotho deficiency causes vascular calcification in chronic kidney disease', *J Am Soc Nephrol,* 22 (1), 124-36.

Hu, M. C., et al. (2010), 'Klotho: a novel phosphaturic substance acting as an autocrine enzyme in the renal proximal tubule', *FASEB J,* 24 (9), 3438-50.

Huang, Q., et al. (2001), 'Assessment of cisplatin-induced nephrotoxicity by microarray technology', *Toxicol Sci,* 63 (2), 196-207.

Hudkins, K. L., et al. (1999), 'Osteopontin expression in fetal and mature human kidney', *J Am Soc Nephrol,* 10 (3), 444-57.

Hughes, S. E. (1997), 'Differential expression of the fibroblast growth factor receptor (FGFR) multigene family in normal human adult tissues', *J Histochem Cytochem,* 45 (7), 1005-19.

Ichimura, T., et al. (2004), 'Kidney injury molecule-1: a tissue and urinary biomarker for nephrotoxicant-induced renal injury', *Am J Physiol Renal Physiol,* 286 (3), F552-63.

Ichimura, T., et al. (1998), 'Kidney injury molecule-1 (KIM-1), a putative epithelial cell adhesion molecule containing a novel immunoglobulin domain, is up-regulated in renal cells after injury', *J Biol Chem,* 273 (7), 4135-42.

Imamdi, R., de Graauw, M., and van de Water, B. (2004), 'Protein kinase C mediates cisplatin-induced loss of adherens junctions followed by apoptosis of renal proximal tubular epithelial cells', *J Pharmacol Exp Ther,* 311 (3), 892-903.

Inker, L. A., et al. (2012), 'Estimating glomerular filtration rate from serum creatinine and cystatin C', *N Engl J Med,* 367 (1), 20-9.

Isakova, T., Gutiérrez, O. M., and Wolf, M. (2009), 'A blueprint for randomized trials targeting phosphorus metabolism in chronic kidney disease', *Kidney Int,* 76 (7), 705-16.

Isakova, T., et al. (2011), 'Fibroblast growth factor 23 is elevated before parathyroid hormone and phosphate in chronic kidney disease', *Kidney Int,* 79 (12), 1370-8.

Ishida, S., et al. (2002), 'Uptake of the anticancer drug cisplatin mediated by the copper transporter Ctr1 in yeast and mammals', *Proc Natl Acad Sci U S A,* 99 (22), 14298-302.

Ishii, A., Sakai, Y., and Nakamura, A. (2007), 'Molecular pathological evaluation of clusterin in a rat model of unilateral ureteral obstruction as a possible biomarker of nephrotoxicity', *Toxicol Pathol,* 35 (3), 376-82.

Iwaki, T., et al. (2008), 'A missense mutation in the sodium phosphate co-transporter Slc34a1 impairs phosphate homeostasis', *J Am Soc Nephrol,* 19 (9), 1753-62.

Jang, K. J., et al. (2013), 'Human kidney proximal tubule-on-a-chip for drug transport and nephrotoxicity assessment', *Integr Biol (Camb),* 5 (9), 1119-29.

Jansen, J., et al. (2014), 'A morphological and functional comparison of proximal tubule cell lines established from human urine and kidney tissue', *Exp Cell Res,* 323 (1), 87-99.

Jenkinson, S. E., et al. (2012), 'The limitations of renal epithelial cell line HK-2 as a model of drug transporter expression and function in the proximal tubule', *Pflugers Arch,* 464 (6), 601-11.

Jin, Z. K., et al. (2013), 'Kidney injury molecule-1 and osteopontin: new markers for prediction of early kidney transplant rejection', *Mol Immunol,* 54 (3-4), 457-64.

Jones, S. E. and Jomary, C. (2002), 'Clusterin', *Int J Biochem Cell Biol,* 34 (5), 427-31.

Jüppner, Harald (2011), 'Phosphate and FGF-23', (79; Kidney International), S24-S27.

Kai, K., et al. (2013), 'Neutrophil gelatinase-associated lipocalin, a sensitive urinary biomarker of acute kidney injury in dogs receiving gentamicin', *J Toxicol Sci,* 38 (2), 269-77.

Kato, Y., et al. (2000), 'Establishment of the anti-Klotho monoclonal antibodies and detection of Klotho protein in kidneys', *Biochem Biophys Res Commun,* 267 (2), 597-602.

Kellum, J. A. (2008), 'Acute kidney injury', *Crit Care Med,* 36 (4 Suppl), S141-5.

Kellum, J. A., et al. (2002), 'Developing a consensus classification system for acute renal failure', *Curr Opin Crit Care,* 8 (6), 509-14.

Kempson, S. A., et al. (1995), 'Parathyroid hormone action on phosphate transporter mRNA and protein in rat renal proximal tubules', *Am J Physiol,* 268 (4 Pt 2), F784-91.

Kendrick, J., et al. (2011), 'FGF-23 associates with death, cardiovascular events, and initiation of chronic dialysis', *J Am Soc Nephrol,* 22 (10), 1913-22.

Keusch, I., et al. (1998), 'Parathyroid hormone and dietary phosphate provoke a lysosomal routing of the proximal tubular Na/Pi-cotransporter type II', *Kidney Int,* 54 (4), 1224-32.

Kharasch, E. D., et al. (1998), 'Role of the renal cysteine conjugate beta-lyase pathway in inhaled compound A nephrotoxicity in rats', *Anesthesiology,* 88 (6), 1624-33.

Kharasch, E.D., et al. (2006), 'Gene expression profiling of nephrotoxicity from the sevoflurane degradation product fluoromethyl-2,2-difluoro-1-(trifluoromethyl)vinyl ether ("compound A") in rats', *Toxicol Sci,* 90 (2), 419-31.

Khurana, I. (2005), *Textbook of Medical Physiology* (India: Elsevier).

Kim, S., et al. (2014), 'Identification of Noninvasive Biomarkers for Nephrotoxicity Using HK-2 Human Kidney Epithelial Cells', *Toxicol Sci*.

Kim, Y., et al. (2005), 'Role of ERK activation in cisplatin-induced apoptosis in OK renal epithelial cells', *J Appl Toxicol,* 25 (5), 374-82.

Kinoshita, Y., et al. (2005), '1,25-dihydroxyvitamin D suppresses circulating levels of parathyroid hormone in a patient with primary hyperparathyroidism and coexistent sarcoidosis', *J Clin Endocrinol Metab,* 90 (12), 6727-31.

Kirchner, S., et al. (2008), 'Luminal fructose inhibits rat intestinal sodium-phosphate cotransporter gene expression and phosphate uptake', *Am J Clin Nutr,* 87 (4), 1028-38.

Koh, N., et al. (2001), 'Severely reduced production of klotho in human chronic renal failure kidney', *Biochem Biophys Res Commun,* 280 (4), 1015-20.

Kola, I. and Landis, J. (2004), 'Can the pharmaceutical industry reduce attrition rates?', *Nat Rev Drug Discov,* 3 (8), 711-5.

Kruidering, M., et al. (1997), 'Cisplatin-induced nephrotoxicity in porcine proximal tubular cells: mitochondrial dysfunction by inhibition of complexes I to IV of the respiratory chain', *J Pharmacol Exp Ther,* 280 (2), 638-49.

Kruidering, M., et al. (1998), 'Cisplatin effects on F-actin and matrix proteins precede renal tubular cell detachment and apoptosis in vitro', *Cell Death Differ,* 5 (7), 601-14.

Kuro-o, M. (2010), 'Overview of the FGF23-Klotho axis', *Pediatr Nephrol,* 25 (4), 583-90.

Kuro-o, M., et al. (1997), 'Mutation of the mouse klotho gene leads to a syndrome resembling ageing', *Nature,* 390 (6655), 45-51.

Kurosu, H., et al. (2006), 'Regulation of fibroblast growth factor-23 signaling by klotho', *J Biol Chem,* 281 (10), 6120-3.

Lally, C., Healy, E., and Ryan, M. P. (1999), 'Cyclosporine A-induced cell cycle arrest and cell death in renal epithelial cells', *Kidney Int,* 56 (4), 1254-7.

Lammoglia, J. J. and Mericq, V. (2009), 'Familial tumoral calcinosis caused by a novel FGF23 mutation: response to induction of tubular renal acidosis with acetazolamide and the non-calcium phosphate binder sevelamer', *Horm Res,* 71 (3), 178-84.

Lamoureux, F., et al. (2012), 'Mapping cyclosporine-induced changes in protein secretion by renal cells using stable isotope labeling with amino acids in cell culture (SILAC)', *J Proteomics,* 75 (12), 3674-87.

Lanaspa, M. A., et al. (2013), 'Inorganic phosphate modulates the expression of the NaPi-2a transporter in the trans-Golgi network and the interaction with PIST in the proximal tubule', *Biomed Res Int,* 2013, 513932.

Lang, R., et al. (2013), 'Self-renewal and differentiation capacity of urine-derived stem cells after urine preservation for 24 hours', *PLoS One,* 8 (1), e53980.

Larsson, T., et al. (2003), 'Circulating concentration of FGF-23 increases as renal function declines in patients with chronic kidney disease, but does not change in response to variation in phosphate intake in healthy volunteers', *Kidney Int,* 64 (6), 2272-9.

Larsson, T., et al. (2004), 'Transgenic mice expressing fibroblast growth factor 23 under the control of the alpha1(I) collagen promoter exhibit growth retardation, osteomalacia, and disturbed phosphate homeostasis', *Endocrinology,* 145 (7), 3087-94.

Lash, L. H., Putt, D. A., and Cai, H. (2006), 'Membrane transport function in primary cultures of human proximal tubular cells', *Toxicology,* 228 (2-3), 200-18.

Lavi-Moshayoff, V., et al. (2010), 'PTH increases FGF23 gene expression and mediates the high-FGF23 levels of experimental kidney failure: a bone parathyroid feedback loop', *Am J Physiol Renal Physiol,* 299 (4), F882-9.

Legrand, M. and Payen, D. (2011), 'Understanding urine output in critically ill patients', *Ann Intensive Care,* 1 (1), 13.

Lepist, E. I., et al. (2014), 'Contribution of the organic anion transporter OAT2 to the renal active tubular secretion of creatinine and mechanism for serum creatinine elevations caused by cobicistat', *Kidney Int*.

Li, H., et al. (2011), 'Compound deletion of Fgfr3 and Fgfr4 partially rescues the Hyp mouse phenotype', *Am J Physiol Endocrinol Metab,* 300 (3), E508-17.

Li, S., et al. (2004), 'Immunohistochemical localization of Klotho protein in brain, kidney, and reproductive organs of mice', *Cell Struct Funct,* 29 (4), 91-9.

Li, Y., et al. (2014), 'Identification of Nephrotoxic Compounds with Embryonic Stem-Cell-Derived Human Renal Proximal Tubular-Like Cells', *Mol Pharm*.

Liebler, D. C. and Guengerich, F. P. (2005), 'Elucidating mechanisms of drug-induced toxicity', *Nat Rev Drug Discov,* 4 (5), 410-20.

Lin, X., et al. (2002), 'The copper transporter CTR1 regulates cisplatin uptake in Saccharomyces cerevisiae', *Mol Pharmacol,* 62 (5), 1154-9.

Lindberg, K., et al. (2014), 'The Kidney Is the Principal Organ Mediating Klotho Effects', *J Am Soc Nephrol*.

Liu, S., et al. (2008), 'FGFR3 and FGFR4 do not mediate renal effects of FGF23', *J Am Soc Nephrol,* 19 (12), 2342-50.

Liu, S., et al. (2006), 'Fibroblast growth factor 23 is a counter-regulatory phosphaturic hormone for vitamin D', *J Am Soc Nephrol,* 17 (5), 1305-15.

Lorenz-Depiereux, B., et al. (2006), 'Hereditary hypophosphatemic rickets with hypercalciuria is caused by mutations in the sodium-phosphate cotransporter gene SLC34A3', *Am J Hum Genet,* 78 (2), 193-201.

Loryan, I., Fridén, M., and Hammarlund-Udenaes, M. (2013), 'The brain slice method for studying drug distribution in the CNS', *Fluids Barriers CNS,* 10 (1), 6.

Ludwig, T., et al. (2004), 'Nephrotoxicity of platinum complexes is related to basolateral organic cation transport', *Kidney Int,* 66 (1), 196-202.

Madsen, J., et al. (2007), 'Tissue localization of human trefoil factors 1, 2, and 3', *J Histochem Cytochem,* 55 (5), 505-13.

Magyar, C. E., et al. (2002), 'Plasma membrane Ca2+-ATPase and NCX1 Na+/Ca2+ exchanger expression in distal convoluted tubule cells', *Am J Physiol Renal Physiol,* 283 (1), F29-40.

Marks, J., et al. (2006), 'Intestinal phosphate absorption and the effect of vitamin D: a comparison of rats with mice', *Exp Physiol,* 91 (3), 531-7.

Martignoni, M., Groothuis, G. M., and de Kanter, R. (2006), 'Species differences between mouse, rat, dog, monkey and human CYP-mediated drug metabolism, inhibition and induction', *Expert Opin Drug Metab Toxicol,* 2 (6), 875-94.

Matsumoto, N., et al. (2010), 'Immunohistochemical analyses of parathyroid hormone-dependent downregulation of renal type II Na-Pi cotransporters by cryobiopsy', *J Med Invest,* 57 (1-2), 138-45.

Mehling, M. and Tay, S. (2014), 'Microfluidic cell culture', *Curr Opin Biotechnol,* 25, 95-102.

Mehta, R. L., et al. (2007), 'Acute Kidney Injury Network: report of an initiative to improve outcomes in acute kidney injury', *Crit Care,* 11 (2), R31.

Miller, R. P., et al. (2010), 'Mechanisms of Cisplatin nephrotoxicity', *Toxins (Basel),* 2 (11), 2490-518.

Mirza, M. A., et al. (2009a), 'Circulating fibroblast growth factor-23 is associated with vascular dysfunction in the community', *Atherosclerosis,* 205 (2), 385-90.

Mirza, M. A., et al. (2009b), 'Relationship between circulating FGF23 and total body atherosclerosis in the community', *Nephrol Dial Transplant,* 24 (10), 3125-31.

Miyamoto, K., et al. (2005), 'Inhibition of intestinal sodium-dependent inorganic phosphate transport by fibroblast growth factor 23', *Ther Apher Dial,* 9 (4), 331-5.

Miyata, T., et al. (1998), 'Beta-2 microglobulin in renal disease', *J Am Soc Nephrol,* 9 (9), 1723-35.

Moallem, E., et al. (1998), 'RNA-Protein binding and post-transcriptional regulation of parathyroid hormone gene expression by calcium and phosphate', *J Biol Chem,* 273 (9), 5253-9.

Moe, O. and Kuro-O, M. (2014), 'Fibroblast growth factor 23 and uremic vascular calcification: is it time to escalate from biomarker status to pathogenic agent?', *Kidney Int,* 85 (5), 1022-3.

Moe, S. (2008), 'Disorders involving calcium, phosphorus, and magnesium', *Prim Care,* 35 (2), 215-37, v-vi.

Moe, S., et al. (2009), 'R-568 reduces ectopic calcification in a rat model of chronic kidney disease-mineral bone disorder (CKD-MBD)', *Nephrol Dial Transplant,* 24 (8), 2371-7.

Moe, S., et al. (2006), 'Definition, evaluation, and classification of renal osteodystrophy: a position statement from Kidney Disease: Improving Global Outcomes (KDIGO)', *Kidney Int,* 69 (11), 1945-53.

Mohammadi, M., Olsen, S. K., and Ibrahimi, O. A. (2005), 'Structural basis for fibroblast growth factor receptor activation', *Cytokine Growth Factor Rev,* 16 (2), 107-37.

Moscovitz, J. E. and Aleksunes, L. M. (2013), 'Establishment of metabolism and transport pathways in the rodent and human fetal liver', *Int J Mol Sci,* 14 (12), 23801-27.

Mueller, T., et al. (2003), 'Failure of activation of caspase-9 induces a higher threshold for apoptosis and cisplatin resistance in testicular cancer', *Cancer Res,* 63 (2), 513-21.

Murer, H., et al. (2003), 'Regulation of Na/Pi transporter in the proximal tubule', *Annu Rev Physiol,* 65, 531-42.

Musialik, D. (1989), 'Urinary excretion of beta-2-microglobulin in patients with active metabolic stone disease', *Int Urol Nephrol,* 21 (4), 381-7.

Mutsaers, H. A., et al. (2014), 'Switch in FGFR3 and -4 expression profile during human renal development may account for transient hypercalcemia in patients with Sotos syndrome due to 5q35 microdeletions', *J Clin Endocrinol Metab,* 99 (7), E1361-7.

Nakamura, T., et al. (2010), 'Disruption of multidrug and toxin extrusion MATE1 potentiates cisplatin-induced nephrotoxicity', *Biochem Pharmacol,* 80 (11), 1762-7.

Nakatani, T., et al. (2009), 'In vivo genetic evidence for klotho-dependent, fibroblast growth factor 23 (Fgf23) -mediated regulation of systemic phosphate homeostasis', *FASEB J,* 23 (2), 433-41.

Nan-Ya, K. I., et al. (2014), 'Usefulness of urinary kidney injury molecule-1 (Kim-1) as a biomarker for cisplatin-induced sub-chronic kidney injury', *J Appl Toxicol*.

Noiri, E., et al. (1999), 'Reduced tolerance to acute renal ischemia in mice with a targeted disruption of the osteopontin gene', *Kidney Int,* 56 (1), 74-82.

Olesen, P., et al. (2007), 'Calcification of human vascular smooth muscle cells: associations with osteoprotegerin expression and acceleration by high-dose insulin', *Am J Physiol Heart Circ Physiol,* 292 (2), H1058-64.

Oliveira, R. B., et al. (2010), 'Early control of PTH and FGF23 in normophosphatemic CKD patients: a new target in CKD-MBD therapy?', *Clin J Am Soc Nephrol,* 5 (2), 286-91.

Oliver, T. G., et al. (2010), 'Chronic cisplatin treatment promotes enhanced damage repair and tumor progression in a mouse model of lung cancer', *Genes Dev,* 24 (8), 837-52.

Olson, H., et al. (2000), 'Concordance of the toxicity of pharmaceuticals in humans and in animals', *Regul Toxicol Pharmacol,* 32 (1), 56-67.

Palm, C., Hartmann, K., and Weber, K. (2010), 'Expression and immunolocalization of calcium transport proteins in the canine duodenum, kidney, and pancreas', *Anat Rec (Hoboken),* 293 (5), 770-4.

Parikh, C. R. and Devarajan, P. (2008), 'New biomarkers of acute kidney injury', *Crit Care Med,* 36 (4 Suppl), S159-65.

Pavik, I., et al. (2013), 'Secreted Klotho and FGF23 in chronic kidney disease Stage 1 to 5: a sequence suggested from a cross-sectional study', *Nephrol Dial Transplant,* 28 (2), 352-9.

Peacock, M. (2010), 'Calcium metabolism in health and disease', *Clin J Am Soc Nephrol,* 5 Suppl 1, S23-30.

Peppiatt-Wildman, C. M., Crawford, C., and Hall, A. M. (2012), 'Fluorescence imaging of intracellular calcium signals in intact kidney tissue', *Nephron Exp Nephrol,* 121 (1-2), e49-58.

Pernet, C. R., Wilcox, R., and Rousselet, G. A. (2012), 'Robust correlation analyses: false positive and power validation using a new open source matlab toolbox', *Front Psychol,* 3, 606.

Persy, V. P., et al. (1999), 'Differences in osteopontin up-regulation between proximal and distal tubules after renal ischemia/reperfusion', *Kidney Int,* 56 (2), 601-11.

Pichler, R. H., et al. (1995), 'Pathogenesis of cyclosporine nephropathy: roles of angiotensin II and osteopontin', *J Am Soc Nephrol,* 6 (4), 1186-96.

Pinches, M., et al. (2012a), 'Evaluation of novel urinary renal biomarkers with a cisplatin model of kidney injury: effects of collection period', *Toxicol Pathol,* 40 (3), 534-40.

Pinches, M., et al. (2012b), 'Evaluation of novel renal biomarkers with a cisplatin model of kidney injury: gender and dosage differences', *Toxicol Pathol,* 40 (3), 522-33.

Pinches, M., et al. (2012c), 'Evaluation of novel urinary renal biomarkers: biological variation and reference change values', *Toxicol Pathol,* 40 (3), 541-9.

Pingle, S. C., et al. (2004), 'Osmotic diuretics induce adenosine A1 receptor expression and protect renal proximal tubular epithelial cells against cisplatin-mediated apoptosis', *J Biol Chem,* 279 (41), 43157-67.

Portale, A. A., et al. (2014), 'Disordered FGF23 and mineral metabolism in children with CKD', *Clin J Am Soc Nephrol,* 9 (2), 344-53.

Powell, C. J., et al. (1991), 'Haloalkylamine-induced renal papillary necrosis: a histopathological study of structure-activity relationships', *Int J Exp Pathol,* 72 (6), 631-46.

Powers, C. J., McLeskey, S. W., and Wellstein, A. (2000), 'Fibroblast growth factors, their receptors and signaling', *Endocr Relat Cancer,* 7 (3), 165-97.

Prasad, R., et al. (2005), 'Ectopic expression of alkaline phosphatase in proximal tubular brush border membrane of human renal cell carcinoma', *Biochim Biophys Acta,* 1741 (3), 240-5.

Price, P., et al. (2006), 'Dependence of cisplatin-induced cell death in vitro and in vivo on cyclin-dependent kinase 2', *J Am Soc Nephrol,* 17 (9), 2434-42.

Price, S. A., et al. (2010), 'Characterization of renal papillary antigen 1 (RPA-1), a biomarker of renal papillary necrosis', *Toxicol Pathol,* 38 (3), 346-58.

Prozialeck, W. C., Lamar, P. C., and Appelt, D. M. (2004), 'Differential expression of E-cadherin, N-cadherin and beta-catenin in proximal and distal segments of the rat nephron', *BMC Physiol,* 4, 10.

Prozialeck, W. C., et al. (2009), 'Preclinical evaluation of novel urinary biomarkers of cadmium nephrotoxicity', *Toxicol Appl Pharmacol,* 238 (3), 301-5.

Prozialeck, W., et al. (2007), 'Kidney injury molecule-1 is an early biomarker of cadmium nephrotoxicity', *Kidney Int,* 72 (8), 985-93.

Pérez-Rojas, J., et al. (2007), 'Mineralocorticoid receptor blockade confers renoprotection in preexisting chronic cyclosporine nephrotoxicity', *Am J Physiol Renal Physiol,* 292 (1), F131-9.

Qi, W., et al. (2007), 'Isolation, propagation and characterization of primary tubule cell culture from human kidney', *Nephrology (Carlton),* 12 (2), 155-9.

Qian, W., et al. (2005), 'Mitochondrial density determines the cellular sensitivity to cisplatin-induced cell death', *Am J Physiol Cell Physiol,* 289 (6), C1466-75.

Quabius, E. S., Murer, H., and Biber, J. (1996), 'Expression of proximal tubular Na-Pi and Na-SO4 cotransporters in MDCK and LLC-PK1 cells by transfection', *Am J Physiol,* 270 (1 Pt 2), F220-8.

Quarles, L. D. (2012), 'Role of FGF23 in vitamin D and phosphate metabolism: implications in chronic kidney disease', *Exp Cell Res,* 318 (9), 1040-8.

Rached, E., et al. (2008), 'Evaluation of putative biomarkers of nephrotoxicity after exposure to ochratoxin a in vivo and in vitro', *Toxicol Sci,* 103 (2), 371-81.

Rahmoune, H., et al. (2005), 'Glucose transporters in human renal proximal tubular cells isolated from the urine of patients with non-insulin-dependent diabetes', *Diabetes,* 54 (12), 3427-34.

Redfern, W, et al. (2010), 'Impact and frequency of different toxicities throughout the pharmaceutical life cycle', *49th Annual Meeting of The Society of Toxicology* (114(S1): 1081).

Riccardi, D., et al. (2000), 'Dietary phosphate and parathyroid hormone alter the expression of the calcium-sensing receptor (CaR) and the Na+-dependent Pi transporter (NaPi-2) in the rat proximal tubule', *Pflugers Arch,* 441 (2-3), 379-87.

Ritthaler, T., et al. (1999), 'Effects of phosphate intake on distribution of type II Na/Pi cotransporter mRNA in rat kidney', *Kidney Int,* 55 (3), 976-83.

Ryan, M. J., et al. (1994), 'HK-2: an immortalized proximal tubule epithelial cell line from normal adult human kidney', *Kidney Int,* 45 (1), 48-57.

Sakan, H., et al. (2014), 'Reduced renal α-Klotho expression in CKD patients and its effect on renal phosphate handling and vitamin D metabolism', *PLoS One,* 9 (1), e86301.

Schetz, M., et al. (2005), 'Drug-induced acute kidney injury', *Curr Opin Crit Care,* 11 (6), 555-65.

Searchfield, L., et al. (2011), 'Glutathione S-transferases as molecular markers of tumour progression and prognosis in renal cell carcinoma', *Histopathology,* 58 (2), 180-90.

Segawa, H., et al. (2009), 'Npt2a and Npt2c in mice play distinct and synergistic roles in inorganic phosphate metabolism and skeletal development', *Am J Physiol Renal Physiol,* 297 (3), F671-8.

Shalhoub, V., et al. (2011), 'Fibroblast growth factor 23 (FGF23) and alpha-klotho stimulate osteoblastic MC3T3.E1 cell proliferation and inhibit mineralization', *Calcif Tissue Int,* 89 (2), 140-50.

Shalhoub, V., et al. (2012), 'FGF23 neutralization improves chronic kidney disease-associated hyperparathyroidism yet increases mortality', *J Clin Invest,* 122 (7), 2543-53.

Shanahan, C. M., et al. (2011), 'Arterial calcification in chronic kidney disease: key roles for calcium and phosphate', *Circ Res,* 109 (6), 697-711.

Shaw, G., et al. (2002), 'Preferential transformation of human neuronal cells by human adenoviruses and the origin of HEK 293 cells', *FASEB J,* 16 (8), 869-71.

Shimada, T., et al. (2004a), 'Targeted ablation of Fgf23 demonstrates an essential physiological role of FGF23 in phosphate and vitamin D metabolism', *J Clin Invest,* 113 (4), 561-8.

Shimada, T., et al. (2001), 'Cloning and characterization of FGF23 as a causative factor of tumor-induced osteomalacia', *Proc Natl Acad Sci U S A,* 98 (11), 6500-5.

Shimada, T., et al. (2002), 'Mutant FGF-23 responsible for autosomal dominant hypophosphatemic rickets is resistant to proteolytic cleavage and causes hypophosphatemia in vivo', *Endocrinology,* 143 (8), 3179-82.

Shimada, T., et al. (2004b), 'FGF-23 is a potent regulator of vitamin D metabolism and phosphate homeostasis', *J Bone Miner Res,* 19 (3), 429-35.

Shimada, T., et al. (2004c), 'FGF-23 transgenic mice demonstrate hypophosphatemic rickets with reduced expression of sodium phosphate cotransporter type IIa', *Biochem Biophys Res Commun,* 314 (2), 409-14.

Shioi, A., et al. (1995), 'Beta-glycerophosphate accelerates calcification in cultured bovine vascular smooth muscle cells', *Arterioscler Thromb Vasc Biol,* 15 (11), 2003-9.

Siddik, Z. H. (2003), 'Cisplatin: mode of cytotoxic action and molecular basis of resistance', *Oncogene,* 22 (47), 7265-79.

Silkensen, J. R., et al. (1997), 'Temporal induction of clusterin in cisplatin nephrotoxicity', *J Am Soc Nephrol,* 8 (2), 302-5.

Sitara, D. (2007), 'Correlation among hyperphosphatemia, type II sodium phosphate transporter activity, and vitamin D metabolism in Fgf-23 null mice', *Ann N Y Acad Sci,* 1116, 485-93.

Sitara, D., et al. (2004), 'Homozygous ablation of fibroblast growth factor-23 results in hyperphosphatemia and impaired skeletogenesis, and reverses hypophosphatemia in Phex-deficient mice', *Matrix Biol,* 23 (7), 421-32.

Six, I., et al. (2014), 'Direct, acute effects of Klotho and FGF23 on vascular smooth muscle and endothelium', *PLoS One,* 9 (4), e93423.

Slattery, C., et al. (2005), 'Cyclosporine A-induced renal fibrosis: a role for epithelial-mesenchymal transition', *Am J Pathol,* 167 (2), 395-407.

Smith, R. C., et al. (2012), 'Circulating αKlotho influences phosphate handling by controlling FGF23 production', *J Clin Invest,* 122 (12), 4710-5.

Snedecor, C. W. and Cochran, W. G. (1989), 'Statistical Methods', (Wiley-Blackwell).

Sodek, J., Ganss, B., and McKee, M. D. (2000), 'Osteopontin', *Crit Rev Oral Biol Med,* 11 (3), 279-303.

Sohn, S. J., et al. (2013), 'In vitro evaluation of biomarkers for cisplatin-induced nephrotoxicity using HK-2 human kidney epithelial cells', *Toxicol Lett,* 217 (3), 235-42.

Star, R. A. (1998), 'Treatment of acute renal failure', *Kidney Int,* 54 (6), 1817-31.

Strom, T. M. and Jüppner, H. (2008), 'PHEX, FGF23, DMP1 and beyond', *Curr Opin Nephrol Hypertens,* 17 (4), 357-62.

Suemori, S., Lynch-Devaney, K., and Podolsky, D. K. (1991), 'Identification and characterization of rat intestinal trefoil factor: tissue- and cell-specific member of the trefoil protein family', *Proc Natl Acad Sci U S A,* 88 (24), 11017-21.

Svennevig, K., Prydz, K., and Kolset, S. O. (1995), 'Proteoglycans in polarized epithelial Madin-Darby canine kidney cells', *Biochem J,* 311 (Pt 3), 881-8.

Takeda, E., et al. (2004), 'Inorganic phosphate homeostasis and the role of dietary phosphorus', *J Cell Mol Med,* 8 (2), 191-200.

Thielemans, N., Lauwerys, R., and Bernard, A. (1994), 'Competition between albumin and low-molecular-weight proteins for renal tubular uptake in experimental nephropathies', *Nephron,* 66 (4), 453-8.

Tiong, H. Y., et al. (2014), 'Drug-Induced Nephrotoxicity: Clinical Impact and Preclinical in Vitro Models', *Mol Pharm*.

Tonomura, Y., et al. (2010), 'Evaluation of the usefulness of urinary biomarkers for nephrotoxicity in rats', *Toxicology,* 273 (1-3), 53-9.

Topala, C. N., et al. (2009), 'Activation of the Ca2+-sensing receptor stimulates the activity of the epithelial Ca2+ channel TRPV5', *Cell Calcium,* 45 (4), 331-9.

Townsend, D. M., et al. (2003), 'Metabolism of Cisplatin to a nephrotoxin in proximal tubule cells', *J Am Soc Nephrol,* 14 (1), 1-10.

Tsuruoka, S., et al. (2003), 'Nitric oxide production modulates cyclosporin A-induced distal renal tubular acidosis in the rat', *J Pharmacol Exp Ther,* 305 (3), 840-5.

Turner, N. and Grose, R. (2010), 'Fibroblast growth factor signalling: from development to cancer', *Nat Rev Cancer,* 10 (2), 116-29.

Urakami, Y., et al. (2004), 'Creatinine transport by basolateral organic cation transporter hOCT2 in the human kidney', *Pharm Res,* 21 (6), 976-81.

Urakawa, I., et al. (2006), 'Klotho converts canonical FGF receptor into a specific receptor for FGF23', *Nature,* 444 (7120), 770-4.

Vaidya, V. S., Ferguson, M. A., and Bonventre, J. V. (2008), 'Biomarkers of acute kidney injury', *Annu Rev Pharmacol Toxicol,* 48, 463-93.

Vaidya, V. S., et al. (2009), 'A rapid urine test for early detection of kidney injury', *Kidney Int,* 76 (1), 108-14.

Vaidya, V. S., et al. (2010), 'Kidney injury molecule-1 outperforms traditional biomarkers of kidney injury in preclinical biomarker qualification studies', *Nat Biotechnol,* 28 (5), 478-85.

Van Biesen, W., Vanholder, R., and Lameire, N. (2006), 'Defining acute renal failure: RIFLE and beyond', *Clin J Am Soc Nephrol,* 1 (6), 1314-9.

van Timmeren, M. M., et al. (2006), 'Tubular kidney injury molecule-1 in protein-overload nephropathy', *Am J Physiol Renal Physiol,* 291 (2), F456-64.

Verhulst, A., et al. (2008), 'Human proximal tubular epithelium actively secretes but does not retain rosuvastatin', *Mol Pharmacol,* 74 (4), 1084-91.

Verstrepen, W. A., et al. (2001), 'Renal osteopontin protein and mRNA upregulation during acute nephrotoxicity in the rat', *Nephrol Dial Transplant,* 16 (4), 712-24.

Vickers, A. E. and Fisher, R. L. (2004), 'Organ slices for the evaluation of human drug toxicity', *Chem Biol Interact,* 150 (1), 87-96.

Vickers, A. E., et al. (2004), 'Kidney slices of human and rat to characterize cisplatin-induced injury on cellular pathways and morphology', *Toxicol Pathol,* 32 (5), 577-90.

Villa-Bellosta, R., et al. (2009), 'The Na+-Pi cotransporter PiT-2 (SLC20A2) is expressed in the apical membrane of rat renal proximal tubules and regulated by dietary Pi', *Am J Physiol Renal Physiol,* 296 (4), F691-9.

Vinken, P., et al. (2012), 'Tissue Kim-1 and urinary clusterin as early indicators of cisplatin-induced acute kidney injury in rats', *Toxicol Pathol,* 40 (7), 1049-62.

Waanders, F., et al. (2010), 'Kidney injury molecule-1 in renal disease', *J Pathol,* 220 (1), 7-16.

Wadey, R. M., et al. (2013), 'Tissue Expression and Correlation of a Panel of Urinary Biomarkers Following Cisplatin-induced Kidney Injury', *Toxicol Pathol*.

Wahl, P. and Wolf, M. (2012), 'FGF23 in chronic kidney disease', *Adv Exp Med Biol,* 728, 107-25.

Waikar, S. S. and Bonventre, J. V. (2009), 'Creatinine kinetics and the definition of acute kidney injury', *J Am Soc Nephrol,* 20 (3), 672-9.

Wang, H., et al. (2012), 'Acute kidney injury and mortality in hospitalized patients', *Am J Nephrol,* 35 (4), 349-55.

Wang, P., et al. (2013), 'Tyrosol attenuates ischemia-reperfusion-induced kidney injury via inhibition of inducible nitric oxide synthase', *J Agric Food Chem,* 61 (15), 3669-75.

Warnock, D. G. and Peck, C. C. (2010), 'A roadmap for biomarker qualification', *Nat Biotechnol,* 28 (5), 444-5.

Weisbord, S. D., et al. (2006), 'Associations of increases in serum creatinine with mortality and length of hospital stay after coronary angiography', *J Am Soc Nephrol,* 17 (10), 2871-7.

Wesson, J. A., et al. (2003), 'Osteopontin is a critical inhibitor of calcium oxalate crystal formation and retention in renal tubules', *J Am Soc Nephrol,* 14 (1), 139-47.

White, KE, et al. (2001), 'Autosomal-dominant hypophosphatemic rickets (ADHR) mutations stabilize FGF-23', *Kidney Int,* 60 (6), 2079-86.

White, KE, et al. (2000), 'Autosomal dominant hypophosphatemic rickets is associated with mutations in FGF23 ', (26; Nature Genetics).

Wilmer, M. J., et al. (2010), 'Novel conditionally immortalized human proximal tubule cell line expressing functional influx and efflux transporters', *Cell Tissue Res,* 339 (2), 449-57.

Witteveen, J. E., et al. (2012), 'Increased circulating levels of FGF23: an adaptive response in primary hyperparathyroidism?', *Eur J Endocrinol,* 166 (1), 55-60.

Wolf, M. (2010), 'Forging forward with 10 burning questions on FGF23 in kidney disease', *J Am Soc Nephrol,* 21 (9), 1427-35.

Wyss, M. and Kaddurah-Daouk, R. (2000), 'Creatine and creatinine metabolism', *Physiol Rev,* 80 (3), 1107-213.

Wöhrle, S., et al. (2013), 'Pharmacological inhibition of fibroblast growth factor (FGF) receptor signaling ameliorates FGF23-mediated hypophosphatemic rickets', *J Bone Miner Res,* 28 (4), 899-911.

Xie, Y., et al. (2001a), 'Expression, roles, receptors, and regulation of osteopontin in the kidney', *Kidney Int,* 60 (5), 1645-57.

Xie, Y., et al. (2001b), 'Expression of osteopontin in gentamicin-induced acute tubular necrosis and its recovery process', *Kidney Int,* 59 (3), 959-74.

Yamazaki, M., et al. (2010), 'Both FGF23 and extracellular phosphate activate Raf/MEK/ERK pathway via FGF receptors in HEK293 cells', *J Cell Biochem,* 111 (5), 1210-21.

Yang, H. C., Zuo, Y., and Fogo, A. B. (2010), 'Models of chronic kidney disease', *Drug Discov Today Dis Models,* 7 (1-2), 13-19.

Yanochko, G. M., et al. (2013), 'Pan-FGFR inhibition leads to blockade of FGF23 signaling, soft tissue mineralization, and cardiovascular dysfunction', *Toxicol Sci,* 135 (2), 451-64.

Yao, X., et al. (2007), 'Cisplatin nephrotoxicity: a review', *Am J Med Sci,* 334 (2), 115-24.

Yu, Y., et al. (2010), 'Urinary biomarkers trefoil factor 3 and albumin enable early detection of kidney tubular injury', *Nat Biotechnol,* 28 (5), 470-7.

Zhang, J., et al. (2008), 'Immunolocalization of Kim-1, RPA-1, and RPA-2 in kidney of gentamicin-, mercury-, or chromium-treated rats: relationship to renal distributions of iNOS and nitrotyrosine', *Toxicol Pathol,* 36 (3), 397-409.

Zheng, W., et al. (2004), 'Critical role of calbindin-D28k in calcium homeostasis revealed by mice lacking both vitamin D receptor and calbindin-D28k', *J Biol Chem,* 279 (50), 52406-13.

Zhou, W., et al. (2010), 'Loss of clusterin expression worsens renal ischemia-reperfusion injury', *Am J Physiol Renal Physiol,* 298 (3), F568-78.

Zhou, Y., et al. (2008), 'Comparison of kidney injury molecule-1 and other nephrotoxicity biomarkers in urine and kidney following acute exposure to gentamicin, mercury, and chromium', *Toxicol Sci,* 101 (1), 159-70.